The Geochemistry of the Dykes in the Carletonville Goldfield

Alida Litthauer

Submitted in accordance with the requirements for the degree of Magister Scientiae in the Faculty of Natural and Agricultural Sciences, Department of Geology at the University of the Free State.

November 2009

Supervisor: Prof. W.A. van der Westhuizen
Co-supervisor: Prof.M. Tredoux

Declaration

I declare that the dissertation hereby handed in for the qualification Magister Scientiae at the University of the Free State, is my own independent work and that I have not previously submitted the same work for a qualification at/in another University/faculty.

Signed at Bloemfontein on the ____ day of _____2009.

_____
Alida Litthauer

Acknowledgements

The Author would like to thank the following:

- AngloGold Ashanti for the funding of the project.
- Mark Watts (Field Office), Rob Burnett, Katarien Deysel (Tau Tona) and Michelle Pienaar (Mponeng) for their assistance regarding sampling and the providing of information and mine plans.
- Hannes Moller, Tau Tona rock engineering.
- My supervisor, Professor Willem van der Westhuizen and co-supervisor, Professor Marian Tredoux for their support and guidance during the project.
- Professor Gerhard Beukes for his help with the mineralogical part of the study.
- Professor Anton le Roex, Fayrooza Rawoot and Christel Tinguely at UCT Department of Geology for their help with the REE analysis.
- Thandeka Klaas and Jonas Choane for their help with sample preparation for XRF analysis.
- Daniel Radikgomo for the preparation of thin sections.
- My parents for their constant help and support and for the proofreading of this thesis.
- My husband, Michael, for his unfailing support throughout the last 18 months.
- My friends and fellow musicians for much-needed distraction.

Finally, I want to thank the Lord, Jesus Christ for the ability to do research and the strength to complete this project.

Abstract

Numerous dykes traverse the Witwatersrand Supergroup rocks in the Carletonville Goldfield. The aim of this study was to investigate a classification system for the dykes.

Samples were obtained from Tau Tona and Mponeng mines as well as from AngloGold Ashanti's field office.

The mineralogical investigation revealed that most dykes, with the exception of the Brazil dyke, are altered. The most abundant minerals are chlorite, actinolite, epidote, quartz and albitised and/or saussuritised feldspar, corresponding to a greenschist metamorphic facies mineral composition. Veins are commonly filled with quartz, calcite, epidote and chlorite, with sulphides and Fe oxides occurring occasionally. However, mineralogical heterogeneity as a result of different degrees of alteration, were found between samples from the same dyke. This heterogeneity may be an important consideration where rock engineering is concerned as it could cause different sections of the same dyke to have different physical properties

Geochemical separation of the dykes into different groups was achieved by means of Bowen's (1984) TiO_2 v Zr and Zr/P v P/Ti plots as well as Linton's (1992) discriminant plot. These same plots were employed in order to classify the dykes according to geochemical data taken from literature for four igneous events, namely, the Ventersdorp Supergroup, Transvaal Supergroup, Bushveld Igneous Complex and Karoo Supergroup, as well as geochemical data for dykes from the East Rand Proprietary Mine. Rare Earth Element patterns from the dykes were compared to literature data for the above-named igneous events in order to obtain a better classification.

Table of Contents

List of Tables

List of Figures

Chapter 1: Introduction

1.1 The Purpose of the Study

The dykes in the Witwatersrand Basin pose numerous problems for the mining industry and are probably the greatest hazard associated with deep level mining. They are largely impermeable and create water compartments that can lead to the flooding of the mine when they are breached. However, the greatest concern is related to mining stability, as the dykes tend to cause seismic events when they are negotiated. These events, termed rock bursts, can cause major damage to mine property and injuries or fatalities to mining personnel, especially when such an event occurs during a shift. Lenhardt (1988) showed that the dykes in the Western Deep Levels mining area (now Tau Tona, Mponeng and Savuka Mines) are responsible for 82% of the high magnitude seismic events in that region. In many instances dykes intrude in a fault zone so that the displacement happens even before the dyke emplacement. These zones can stay active over a long time and can be reactivated. In some instances this requires a new establishment to be made on the other side of the dyke (pers. comm.: H. Moller, 2009). According to Greeff (1988b), a study of the relationship between the composition (geochemistry and mineralogy) of the dykes and their physical aspects, e.g. rock mechanics and porosity, would provide useful information for geologists and rock engineers at the mines. An investigation into the mineralogy of the dykes as well as their joints and veins could therefore be an aid in understanding the behaviour of these rocks. An attempt will be made to correlate the dykes with overlying lavas, where applicable, or with other stratigraphic units. A classification system, according to which individual dykes can be geochemically "finger-printed", will be investigated, as well as relationships between chemistry, mineralogy and rock mechanics properties.

1.2 The Study Area

The West Wits Line is situated on the north-western edge of the Witwatersrand Gold Field (Fig. 1.1), between the West Rand Fault in the east and the Potchefstroom Gap in the west (McCarthy, 2006). The West Wits Line is divided into two sections by the Bank Fault with the western section lying between Carletonville and Fochville (Robb, 2005). This section is sedimentologically distinct from the West Rand Gold

Field and is also referred to as the Carletonville Goldfield. Stratigraphically, the Carletonville Goldfield falls in the Central Rand Group (SACS, 2006). Folding that developed during Central Rand times, and before Ventersdorp times, indicates regional compression. However, this compressional regime was replaced by one of tension, resulting in block faulting during Middle Ventersdorp times (McCarthy, 2006).

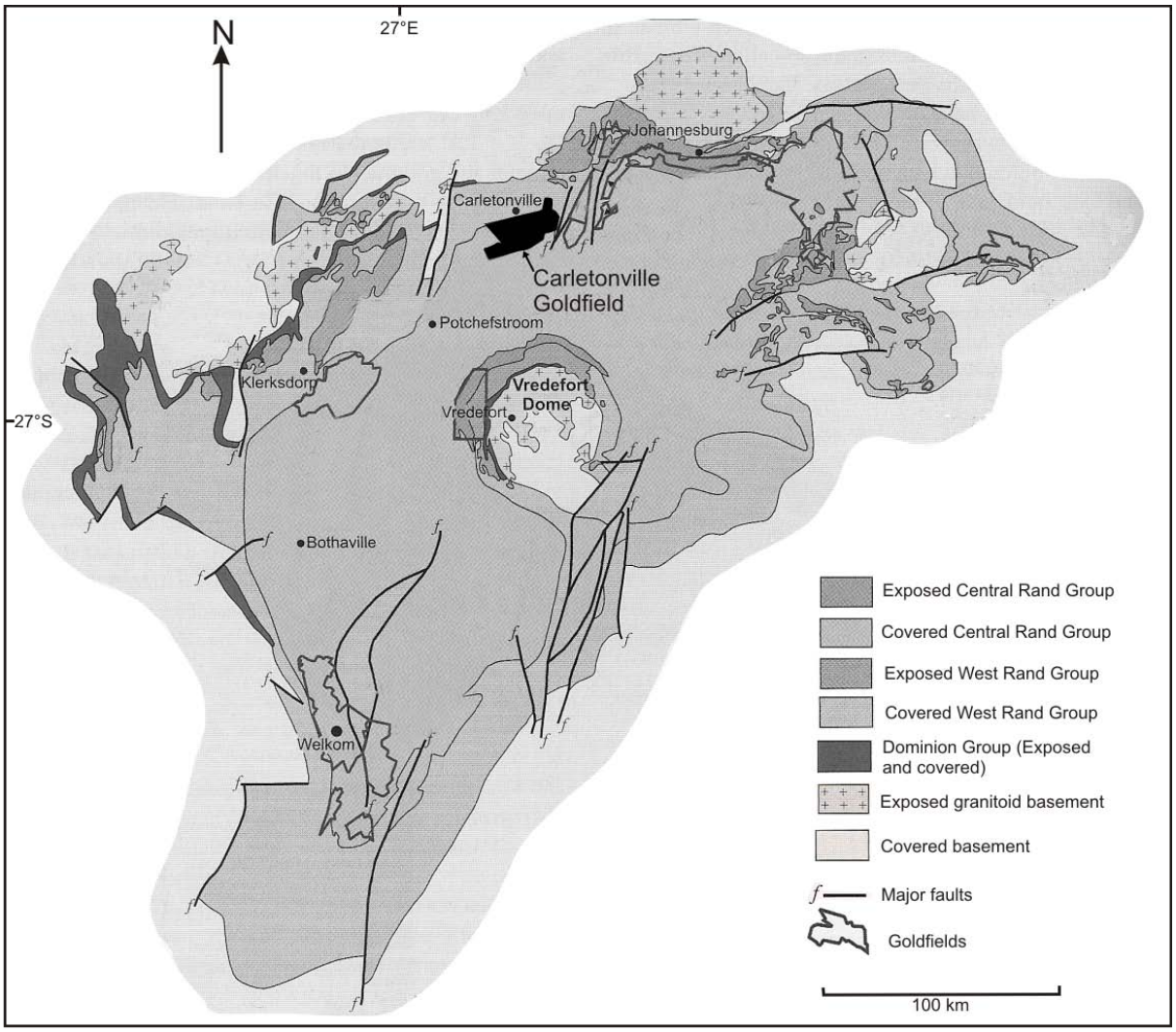

Figure 1.1. The Witwatersrand Basin with the location of the Carletonville Goldfield. Adapted from McCarthy (2006).

The entire Carletonville Goldfield was affected by pre-Ventersdorp erosion which was terminated by the outpouring of the lavas of the Ventersdorp Supergroup. The lower-most formation of the Ventersdorp Supergroup, the Venterspost Formation, is also known as the Ventersdorp Contact Reef (VCR), and is a major source of gold on many of the mines (McCarthy, 2006). It occurs in the Klerksdorp and

Carletonville Goldfields, the area north of the Loraine goldmine and, possibly, further east and northeast of the Central Rand Group Basin.

AngloGold Ashanti's West Wits operations are situated in the West Wits Line near Carletonville, and encompass the Tau Tona, Mponeng and Savuka mines (see fold-out map in Appendix A). Mponeng (formerly South Shaft or Shaft 1) is the youngest of the three former Western Deep Levels mines with its main shaft being completed in 1986 (www.mining-technology.com). Only two of the seven gold-bearing conglomerates in the lease area are economically viable and only one, the VCR, is currently being mined. The deepest operating stope is just over 3.3 km deep (www.anglogoldashanti.com).

Tau Tona mine started operations in 1962 (www.mining-technology.com). Two reef horizons, namely the VCR and the Carbon Leader Reef (CLR), are currently being mined. The vertical separation between the VCR and the CLR varies between 900 m and 1 200 m with the VCR stratigraphically at the top. Mining operations take place at depths ranging from 1.8 km to 3.9 km (www.anglogoldashanti.com).

1.3 Igneous Provinces with Possible Relevance to the Study Area

Apart from the Ventersdorp Supergroup, there are four other igneous provinces that could post date the Witwatersrand Supergroup. They are the Transvaal Supergroup, intrusives related to the Bushveld Igneous Complex, intrusives related to the Pilanesberg Alkaline Complex, and Karoo-age intrusives. However, Harris and Watkins (1990) exclude the Transvaal Supergroup from this list. No reason is given for this exclusion.

1.3.1 The Ventersdorp Supergroup

After the stabilisation of the Kaapvaal Craton, a series of four basins, namely the Dominion Group, the Witwatersrand and Ventersdorp Supergroups and the Transvaal Basin, developed on it between 3 000 and 2 100 Ma ago. The Ventersdorp Supergroup is the second last of these basins and was preceded by the Witwatersrand Supergroup, which it overlies. The Ventersdorp Supergroup covered most of the area of the older Dominion Group, as well as the Witwatersrand Supergroup, and its elliptical basin occupies an area of approximately 300 000 km^2

with a northeast axis of 750 km (Fig. 1.2). However, the true extent of the Ventersdorp Supergroup is difficult to determine due to poor exposures, as well as the presence of Transvaal and Karoo Supergroup cover. Borehole information indicates that the extent of the supergroup is much greater than indicated by its surface expression (Winter, 1976). A region around Bothaville, between the Klerksdorp and Welkom Gold fields, has been shown, by deep core drilling, to represent an area where a consistently recognised lithological succession is best developed. This region has been chosen as the type area of the Ventersdorp Supergroup (Winter, 1976).

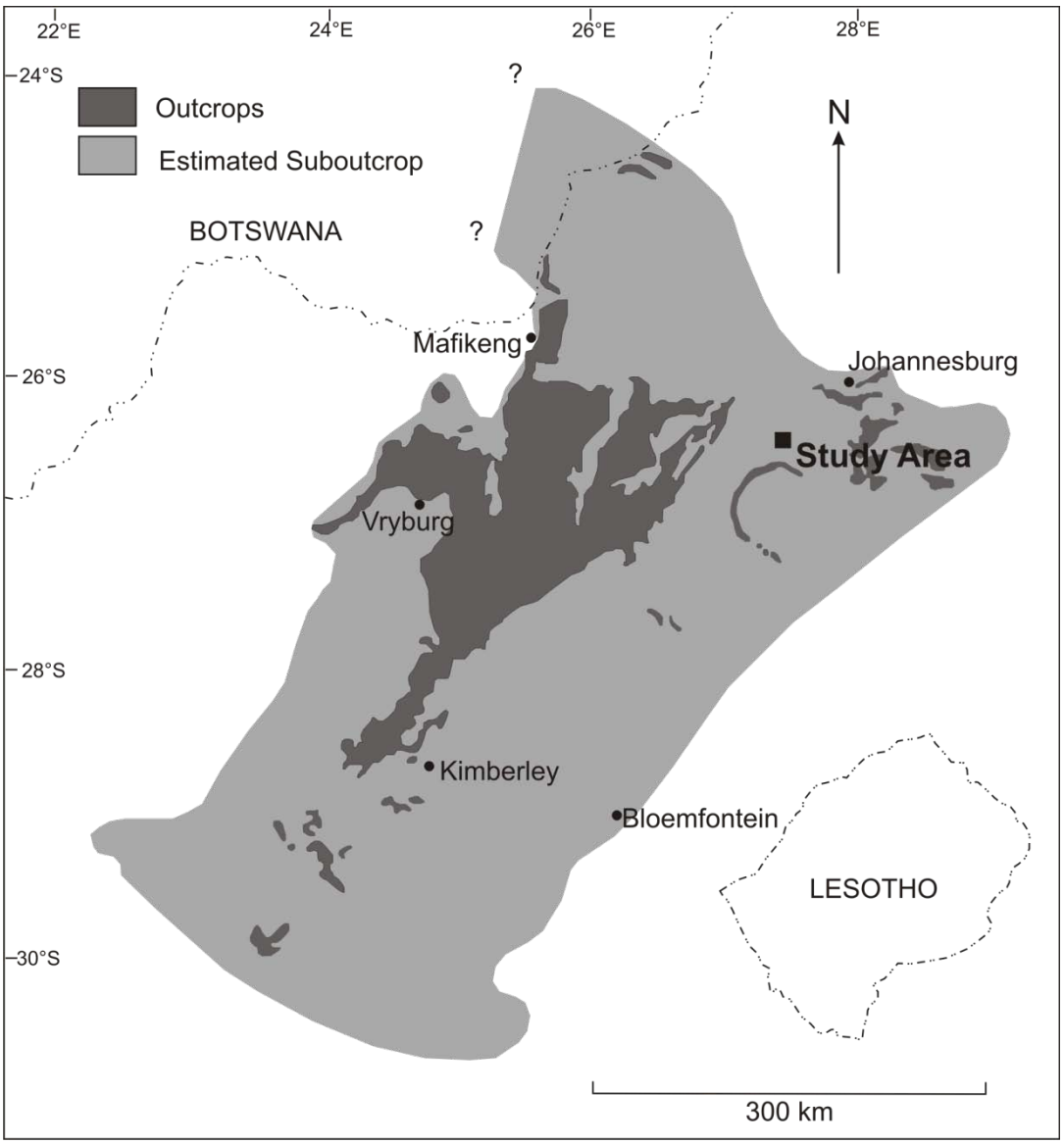

Figure 1.2. Outcrops and the estimated extent of the Ventersdorp Supergroup (adapted from Van der Westhuizen *et al*., 2006).

The Ventersdorp Supergroup (Fig. 1.3) comprises the Klipriviersberg Group at the base, followed by the Platberg Group, the sedimentary Bothaville Formation and the volcanic Allanridge Formation. The Klipriviersberg Group is essentially volcanic and represents a flood basalt sequence covering 100 000 km^2 and is, on average, between 1 500 and 2 000 m thick. It is further divided into the Venterspost Formation, Westonaria, Alberton, Orkney, Jeanette, Loraine and Edenville Formations. The Platberg Group is mostly absent from the northeastern part of the Ventersdorp depository and outcrops inconsistently over the rest of the area with varying thickness. The Platberg Group is subdivided into the sedimentary Kameeldoorns Formation, the intermediate to felsic volcanic rocks of the Goedgenoeg Formation, the Makwassie Formation quartz-feldspar porphyry, and the Rietgat Formation. The sedimentary Bothaville Formation has a greater lateral distribution than the Platberg Group. The volcanic Allanridge Formation forms the upper-most unit of the Ventersdorp Supergroup, and extruded over large areas. It covers the underlying rocks in the Northern Cape, Free State, and North West Provinces and outcrops extensively in the vicinity of Vryburg, Mafikeng, Warrenton, Bloemhof, the West Rand, west of Kimberley and along the Orange River close to Hopetown (Van der Westhuizen *et al*., 2006).

Some factors can influence the determination of age by changing the isotopic systems. Metamorphism, where rocks are subjected to high temperatures and the migration of fluids, tends to reset some of the isotopic systems. These factors cause the ages obtained to be younger than the true ages. Greenschist metamorphism affected the Rb-Sr ratios of the Ventersdorp Supergroup in such a way that it gives younger ages than other techniques. Whole-rock Pb-isotope studies yield well-constrained ages, but these probably reflect a metamorphic or hydrothermal event at about 2 370 Ma, which caused alteration of the rocks. The most accurate ages, around 2 700 Ma, are probably those obtained from U-Pb dating of zircons (Van der Westhuizen *et al*., 2006).

Ventersdorp Supergroup Rocks have undergone extensive alteration due to greenschist facies metamorphism. This has been attributed to autohydrothermal processes at low temperatures, which caused the formation of secondary minerals. The original igneous textures have been retained and give an indication of the original mineralogy, although the original minerals have been destroyed. Variations

in isotopic ratios can also be attributed to this alteration (Van der Westhuizen *et al*., 2006).

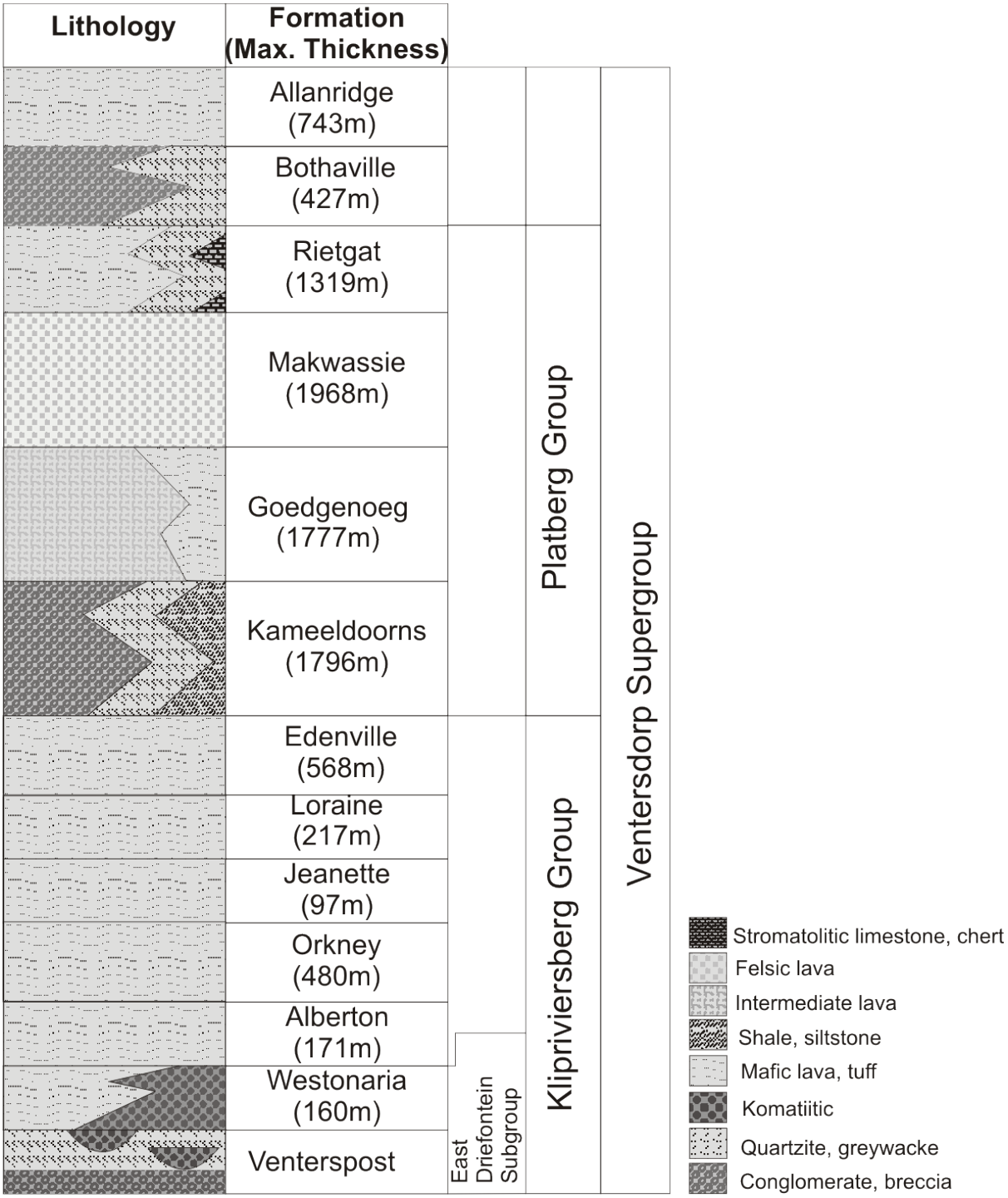

Figure 1.3. The stratigraphy of the Ventersdorp Supergroup (adapted from Van der Westhuizen *et al*., 2006).

1.3.2 The Transvaal Supergroup

The late Archaean/early Proterozoic Transvaal Supergroup is preserved in three structural basins, namely the Griqualand West Basin, Transvaal Basin (Fig. 1.4), and the Kanye Basin in Botswana. The Transvaal Basin is the most relevant to the study area and is subdivided into the Chuniespoort and Pretoria Groups. The Chuniespoort Group is purely sedimentary, but four units in the Pretoria Group consist completely or partially of lava. These units are the Bushy Bend Member of the Timeball Hill Formation, the Hekpoort Formation, The Machadodorp Member of the Silverton Formation and parts of the Rayton Formation. Of these the Bushy Bend lavas and Hekpoort Formation volcanics are the most relevant to the study area (Eriksson *et al.*, 2006).

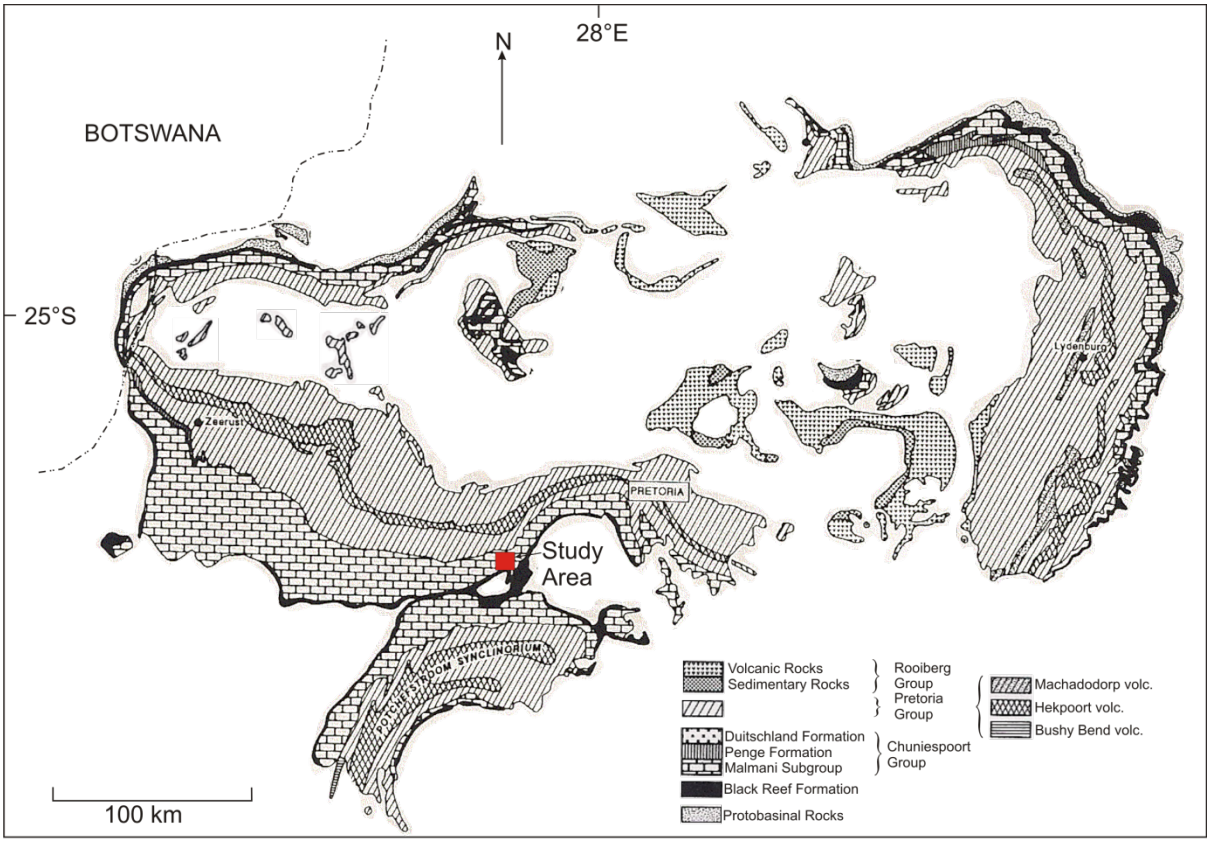

Figure 1.4. The Transvaal Basin of the Transvaal Supergroup (adapted from Eriksson *et al.,* 2006).

1.3.2.1 The Bushy Bend Lavas

The Busy Bend lavas were identified in 1993 by Eriksson *et al.* (1994). The lavas are situated approximately 10 km southeast of the town of Stilfontein and about 10 km northwest of the sharp bend in the Vaal River known as Bushy Bend (Fig. 1.5).

They have been identified over an area of approximately 30 km by 10 km, but a larger distribution is possible. The lavas are fine-crystalline to amygdaloidal, and it can be assumed that they erupted subaerially. The lava contains small plagioclase phenocrysts and former clinopyroxene in a fine-crystalline matrix consisting of the same material. The lava has undergone epidotisation and sericitisation, with pyroxenes having been altered to amphibole. Brecciated lava and veinlets of calcite and quartz occur throughout the succession, pointing to later hydrothermal activity, with the base of the succession being extensively epidotised. The lavas have a wide range of silica contents equivalent to that of picro-basalt to andesite. The wide range in concentrations of elements such as SiO_2, Fe_2O_3, and alkalis can be at least partly attributed to alteration (Eriksson *et al.* 1994). Unfortunately very little geochemical data are available for the Bushy Bend lavas.

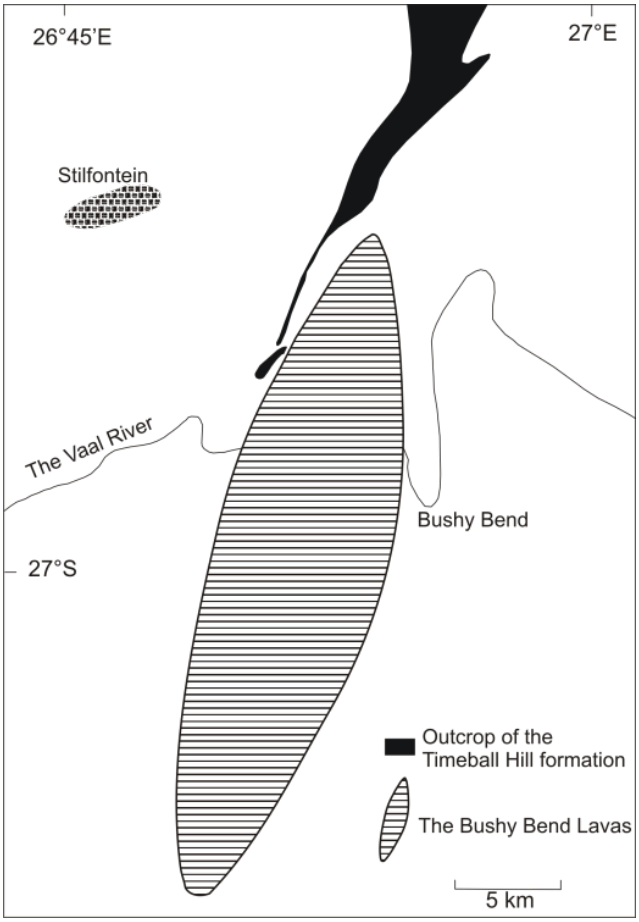

Figure 1.5. The Distribution of the Bushy Bend lavas (adapted from Eriksson *et al.,* 1994).

1.3.2.2 The Hekpoort Volcanics

The Hekpoort Formation has a thickness of up to 500 m in the Potchefstroom Basin and an average thickness of 300 m in the southern and middle parts of the main Transvaal Basin. Burger and Coertze (1973-1974) determined a Rb-Sr age of 2 224±21 Ma for the Hekpoort lavas. The formation consists of tuffs, pyroclastic material and microporphyritic to amygdaloidal lavas. The lavas consist of altered plagioclase and altered skeletal crystals of pyroxene and secondary minerals such as amphibole, chlorite, clinozoisite, epidote and quartz. Traces of biotite, cummingtonite, muscovite, iron oxides and sulphides are present locally. Secondary quartz veins are also present (Rezcko *et al.*, 1995). Oberholzer (1995) classified the lavas as tholeiitic, although he states that this result is probably due to the removal of alkalis. If the alkalis were present the lavas would probably be classified as calc-alkaline.

1.3.3 Bushveld-Age intrusives

1.3.3.1 The Losberg Complex

The Losberg Complex is considered to be coeval with the Rustenburg Layered Suite (Cawthorn *et al.,* 2006) and has a Rb-Sr age of 2 041±41 Ma (Anhaeusser, 2006). The subhorizontal layered mafic intrusive is situated 105 km south of Rustenburg and 70 km west of Johannesburg in the shale and quartzite of the Pretoria Group of the Transvaal Supergroup. The intrusive is approximately 130 m thick and has been divided into three units. The intrusive consists of a zone of harzburgite (18 m thick), consisting of orthopyroxene-olivine cumulate, at the base; a quartz norite zone (10 m thick), consisting of a plagioclase-orthopyroxene-clinopyroxene cumulate; and a quartz gabbro zone (102 m thick), consisting of a plagioclase-clinopyroxene cumulate. The rocks formed immediately below the roof of the complex include chill-phase gabbro and some late-phase augite granophyre (Anhaeusser, 2006).

1.3.3.2 Sills in the Fochville/Losberg and Vredefort Dome Areas

Numerous sills intruded below the cumulate rocks of the Bushveld Igneous Complex. It is generally accepted that more than one magma injection was responsible for the development of the Bushveld Complex and each magma injection may have its own

suite of associated sills. These sills occur throughout the Transvaal Supergroup surrounding the Bushveld Complex, and some might even have intruded at greater depth into the Witwatersrand Supergroup and the Vredefort Dome area (Cawthorn, *et al.* 1981), as discussed below. Cawthorn *et al.* (1981) investigated these sills in the area from Rustenburg to Fochville and identified six different types: metadolerites, hypersthene microgabbros, norites and pyroxenites, contaminated norites, quench-textured micropyroxenites and dolerites. In a hypersthene microgabbro sill close to the Losberg Complex just south of Fochville, hypershenes occur as prismatic blades and is occasionally rimmed by or intergrown with augite. Pleochroic hornblende occurs as a minor phase and was interpreted to be of igneous rather than metamorphic origin. The norite and pyroxenite sills are most common in the immediate vicinity of the Bushveld Complex; one such a sill is found near the northern margin of the granitic basement rocks exposed in the Vredefort Dome. One example of a quench-textured micropyroxenite is found below the Losberg Complex. This sill contains a few crystals of olivine that have been altered to serpentine. The other sill types are not represented in the immediate Fochville/Losberg area.

A number of Neoarchaean to Mesoproterozoic mafic and ultramafic intrusives were emplaced in the core and collar rocks of the Vredeford Dome (Anhaeusser, 2006). Many of these are tholeiitic and are regarded to be of Bushveld age (Coetzee *et al.* 2006). Most of these tholeiitic intrusives are found in the Witwatersrand rocks in the collar of the dome. The intrusives can be subdivided into three types, the Wittekopjes norite, Parsons Rust dolerite-norite and the Reebokkop dolerite on farms with similar names. All three these types show a negative correlation between Mg-numbers and Al_2O_3, TiO_2, CaO, Na_2O, P_2O_5, Zr, and Nb concentrations. This indicates a crystallisation of olivine and orthopyroxene at the expense of clinopyroxene and plagioclase and the concentration of incompatible elements in the melt during fractional crystallisation. The latter is further confirmed by a strong positive correlation between Zr and the concentration of other incompatible elements. The rocks also show a positive correlation between Mg-numbers and Cr concentrations, which is typical for mafic rocks. The Wittekopjes norite has a more primitive composition than the other two intrusives as it has a higher MgO content and Mg-number. The Wittekopjes norite has an interesting feature in that the

amount of silica decreases with a decrease in MgO and Cr concentration upwards in the sill. This phenomenon can possibly be ascribed to the crystallisation of large amounts of enstatite that depleted the magma of silica and is similar to that observed in the lowermost unit of the Bushveld Complex. The three intrusives show parallel REE patterns with an increase in REE concentrations with decreasing Mg-number. The intrusives are slightly enriched in LREE with HREE having an approximately chondritic abundance (Coetzee *et al.,* 2006). This pattern has been described as tholeiitic by Barker (1983).

The intrusives were compared with high-Mg noritic layered intrusives and dyke swarms prominent during the late Archaean and early Proterozoic. When comparison of major elements was done, the composition of the Wittekopjes norite is in-between that of the ultramafic and micropyroxenite sills of the Bushveld Complex. The Parsons Rust dolerite-norite and Reebokkop dolerite overlaps with the Bushveld's micropyroxenite sill and norite intrusives in the Witwatersrand Basin. When trace elements are compared, Ti/Zr ratios are similar to that of Bushveld sills, which is lower than that of modern tholeiitic rocks. REE patterns of the tholeiites do not show the same degree of LREE enrichment as the Bushveld micropyroxenite and ultramafic sills. It is possible that this flatter pattern was caused by the crystallisation of orthopyroxene from melts with highly fractionated REE patterns (Coetzee *et al.,* 2006*)*. Another reason could be that not all siliceous high-Mg basalts show a high degree of LREE enrichment (Sun *et al.,* 1989). A good correlation was also observed between the tholeiitic group and the ultramafic Bushveld sills, except for lower P_2O_5 and TiO_2 contents in the Bushveld sills (Coetzee *et al.,* 2006*)*.

1.3.4 The Pilanesberg Alkaline Province

Between 1 450 and 1 200 Ma ago widespread alkaline volcanic and plutonic activity took place during a period of relative tectonic stability on the Kaapvaal Craton. This event gave rise to the Pilanesberg Alkaline Province that consists of predominantly silica-undersaturated rocks, and probably ended with the eruption of the Premier group of kimberlite pipes. Alkali igneous complexes are roughly circular bodies in plan, only a few kilometres in diameter, and ideally consist of concentric rings or arcs of rocks such as nepheline syenite (foyaite), carbonatite, pyroxenite, ijolite and

syenite (Verwoerd, 2006). Alkali rocks contain Na and/or K in excess amounts necessary to form ordinary feldspar and pyroxene, due to a deficiency of silica. Peralkaline rocks contain alkalis in excess of alumina and are distinguished by non-aluminous alkaline minerals like aegirine and arfvedsonite. Carbonatite is the most silica deficient of the alkaline rocks and often intrudes at a late stage in the history of the complex. Carbonatites can also erupt from closely related fissures and diatremes. Many alkaline complexes contain volcanic and plutonic components. They represent either conduits or, in the case of layered bodies, relatively shallow magma chambers. The Pilanesberg in the North West Province is one of the largest and best-known alkaline ring complexes in the world. Smaller occurrences, dykes, necks, plugs, maars and volcanic complexes form part of the same petrogenetic province. Some of these smaller occurrences include dyke swarms, the Pienaars River Subprovince, the Goudini Complex, The Spitskop Complex, the Mogashoa Suite, the Glenover Complex, and the Stukpan Complex (Fig. 1.6) (Verwoerd, 2006). Of these, the dyke swarms and the Stukpan Complex are probably most relevant to the study.

The Pilanesberg Dyke Swarm is a set of northwest-trending dykes that cut through the northeastern half of the Pilanesberg Complex and extends over a distance of at least 350 km from Botswana to the Vaal River and fans out from a width of 40 km on the Botswana border to about 120 km south of Johannesburg. The dykes are considered to be part of the Pilanesberg Province on the basis of petrology and age. Many of these dykes are composite, with marginal zones of fine-grained dolerite intruded while still hot by slightly younger syenite and nepheline syenite in the centre.

The dykes have been traced magnetometrically in more detail north of the Pilanesberg than further south. Some of these dykes, like the Maanhaarrand near Magaliesburg, form prominent outcrops. Some other dykes that have been named are the Robinson, Venterspost and Gemspost dykes in the Witwatersrand gold mines, and the Pretoria dyke that runs through the Fountains valley and Wonderboompoort (Verwoerd, 2006).

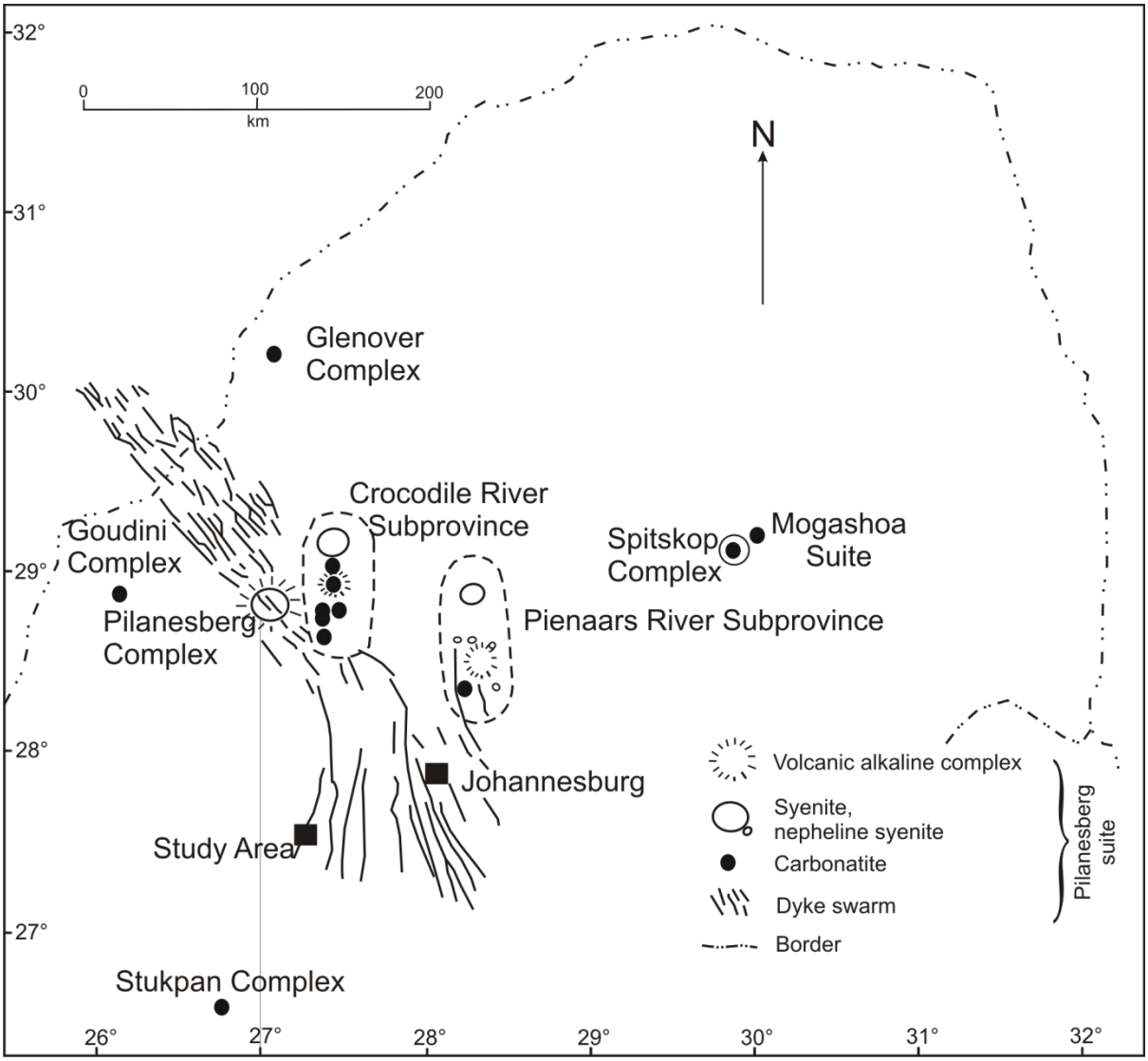

Figure 1.6. The Pilanesberg Alkali Province (adapted from Verwoerd, 2006).

The Stukpan Complex is situated in the Free State Goldfield 20 km east of Bothaville and about 180 km southwest of Johannesburg. It is overlain by Karoo strata and a dolerite sill approximately 200 m thick. The complex was discovered in 1982 when a prominent magnetic and gravity anomaly was tested by drilling. Geophysical modelling indicates that it could be the largest carbonatite occurrence in South Africa. The pipe penetrates Witwatersrand and Ventersdorp Supergroup rocks and has been dated at ~1 354 Ma. The only available samples are from drill core. These include Na-amphibole-rich calcite carbonatite, minor dolomite carbonatite and fenitised Ventersdorp lava and tuff. The carbonatite has a high Sr content but is extraordinarily poor in Ba, Nb, Zr, Y and REE (Verwoerd, 2006).

1.3.5 The Karoo Dolerite Suite

The Karoo Igneous Province is one of the world's classic continental flood basalt provinces. $^{40}Ar/^{39}Ar$ dating confirmed that the Karoo igneous event was short-lived, approximately 1 – 3 Ma, and indicates an age of 183±2 Ma for the Lebombo Group. The low-Ti basalts of the Central Area are slightly younger than the low-Ti basalts of the Lebombo Group (Fig. 1.7) (Duncan and Marsh, 2006).

The Karoo Dolerite Suite represents the feeder system to the flood basalt eruptions. It is best developed in the main Karoo Basin and occurs as a network of dykes, sills and saucer-shaped sheets. The sills range from a few metres to 200 m or more in thickness. The dykes are generally 2 – 10 m wide and 5 – 30 km long. The sheets and sills show some differentiation caused by processes such as flow differentiation and gravity settling, but the dykes are compositionally homogeneous and their geochemistry correlates well with that of the overlying lavas. Most of the dykes do not show strong systematic orientation, but there are two well developed linear dyke swarms, namely the Rooi Rand dyke swarm trending north-south in the southern Lebombo, and the Okavango dyke swarm trending east-southeast across northeastern Botswana (Duncan and Marsh, 2006).

Similar to other continental flood basalt provinces, the Karoo basalts are relatively siliceous, with SiO_2 contents in excess of 52%, and evolved in terms of their Mg-number. Basalts in equilibrium with normal mantle olivine would be expected to have a Mg number of ~70, whereas the Karoo mafic rocks have typical Mg-numbers of 50 – 60. This possibly indicates that the flood basalts were derived by fractionation from mantle-derived picritic precursors (Duncan and Marsh, 2006).

The vast majority of Karoo basaltic rocks can be classified as tholeiitic based on petrographic as well as geochemical characteristics. An important geochemical feature of the Karoo Igneous Province is the compositional provinciality amongst the basalt. The Karoo basalts and picrites in Zimbabwe can be distinguished from those in Lesotho and Swaziland (southern Lebombo mountains) by their K, Ti, P, Ba, Sr and Zr, with the former having unusually high concentrations of these elements compared to other tholeiites.

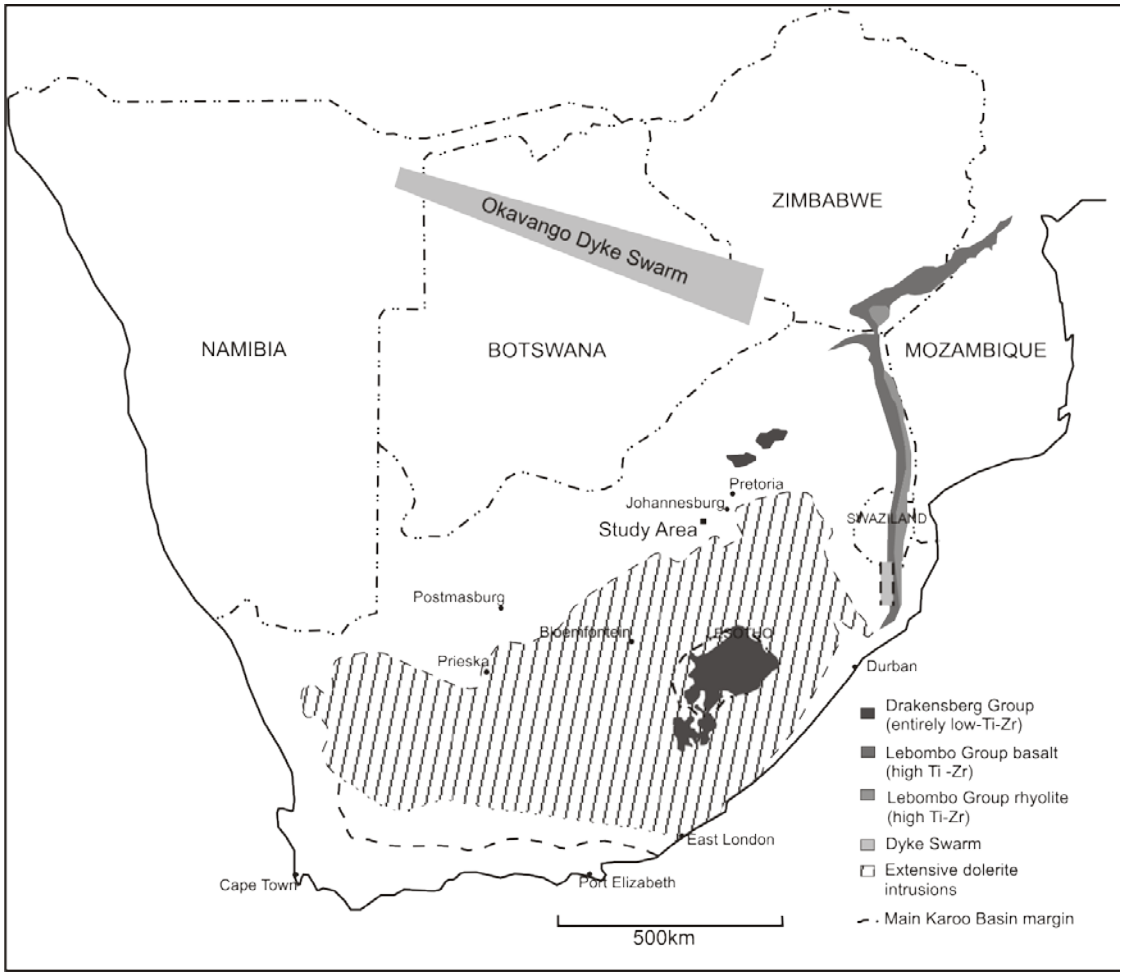

Figure 1.7. The location of Karoo basalts and dolerites relevant to the study area (adapted from Duncan and Marsh, 2006).

This observation gave rise to the concept of a northern high-Ti-Zr province and a southern low-Ti-Zr province. It is now recognised that these high-Ti basalts are not only confined to the northern part of the igneous province, but are also associated with the rift-related conditions of the Lebombo, Mwenezi-Save, Tuli, and Hwange-Victoria Falls areas. The Botswana dyke swarm also predominantly falls in this group. The Lesotho formation falls in the low-Ti-Zr group (Duncan and Marsh, 2006).

1.4 Previous Work

1.4.1 Dykes in the Witwatersrand Basin

McCarthy *et al.* (1990) used petrographic and geochemical techniques in order to identify feeder dykes to the Klipriviersberg Group volcanics on East Rand Proprietary Mines Ltd (ERPM), and to subdivide the dykes further into feeders of the different

Formations in this group. The orientation of the different feeder dykes were then used to determine changes in stress states along the northern margin of the Witwatersrand Basin, especially during Klipriviersberg times. In a detailed study of the intrusives on ERPM mine by Jeffery (1975) (in McCarthy *et al.*, 1990) and Fumerton (1975) (in McCarthy *et al.*, 1990), five major dyke events were recognised. These five events were confirmed by McCarthy *et al.* (1990) and are represented by the following rock types:

(1) Norite, occuring mainly on the western portions of the mine as shallow-dipping dykes and sills, consists of orthopyroxene, lesser clinopyroxene and plagioclase, and is considered, by the authors, to be of Bushveld age, similar to the sills described by Cawthorn *et al.* (1981).

(2) Ilmenite diabase, consisting of pyroxene and plagioclase that are variably altered to tremolite, chlorite and saussurite, with skeletal boxworks of ilmenite that has been altered to leucoxene. These rocks are considered to be pre-Transvaal in age, but Jeffery (1975) suggested that they could be of Bushveld age.

(3) Epidiorite, consisting almost entirely of actinolite in a ground mass of chlorite, calcite and minor opaque minerals. Cawthorn *et al.* (1981) considered them to be equivalents of the pre-Bushveld metadolerites that occur as sills in the Transvaal Supergroup.

(4) Aplitic dykes that, according to Jeffery (1975) (in McCarthy *et al.*, 1990), post-date Ventersdorp diabases.

(5) Ventersdorp diabases that are distinguished from all other intrusives by their greater degree of alteration, and are typically dark green to grey in colour, with some containing large feldspar phenocrysts. They consist almost entirely of extremely altered plagioclase and augite that is largely altered to amphibole, chlorite and serpentine. Sphene, apatite, secondary quartz, ilmenite and magnetite occur as secondary minerals.

McCarthy *et al.* (1990) found that the Alberton and Orkney Formation dykes have a strike direction of around 30°. The Jeanette and Loraine dykes show a more complex distribution and have strikes varying between 105° and 165°, as well as the 30° orientation. The ilmenite diabase dykes are commonly oriented in the 135°-160°

direction, but some exhibit the 30° strike. The epidiorite dykes show a 120° strike, parallel to some of the ilmenite diabase and Ventersdorp dykes. The epidiorite dykes are, however, not widely distributed. In order to correlate Klipriviersberg Group dykes with their respective Formations, the authors (McCarthy *et al.,* 1990) found discriminant anlysis using TiO_2, Zr, and Y to be the most useful. This is the same plot used by Linton (1992) which is discussed below.

Meier *et al.* (2009) studied the dykes in the Klerksdorp Goldfield, specifically in Kopanang Mine, in order to assess the possibility of metamorphic-hydrothermal ore formation in the Witwatersrand Basin. Their study included structural, mineralogical and geochemical investigations. The Vaal Reef, which is the main reef mined in Kopanang, is displaced by numerous dykes and faults. Sharp, unsheared dyke contacts indicate that magma emplacement occurred during or after reef displacement, and that magma intruded into active or pre-existing faults. Sigmoidal veins, containing chlorite and quartz in some dyke contacts, show that these contacts were subjected to partly ductile deformation during metamorphism. This confirms a premetamorphic emplacement of the dykes. This is similar to the conclusions drawn by Harris and Watkins (1990), who compared intrusives from Welkom, Klerksdorp, Evander and Carletonville mines, and compared them to a known Ventersdorp intrusive, the Conera Sill. All the dykes in their study were of the same metamorphic facies as the Conera Sill, and were therefore assumed to be of the same age. The authors subsequently assumed that metamorphism and alteration affected the intrusives and country rock as a single package. The mineralogical investigations of the two studies yielded approximately the same results, but Meier *et al.* (2009) noted that some samples were almost completely replaced by carbonates. This indicates that significant amounts of CO_2 were present in the hydrothermal fluid responsible for the alteration of the rocks.

Meier *et al.* (2009) compared the chemistry of dykes with that of overlying lava flows from the Klipriviersberg Group. By comparing immobile elements, including REEs, they showed that the dykes believed to be of Ventersdorp age are on a single fractionation trend which overlaps the Jeanette and Loraine-Edenville Formations of the Klipriviersberg Group. Younger dykes from elsewhere in the Witwatersrand Basin, such as the ilmenite diabase and epidiorite dykes, as well as Bushveld aged

intrusives, showed distinct geochemical differences from Klipriviersberg dykes and lavas.

1.4.2 The Ventersdorp Supergroup

Bowen (1984a) classified the volcanic rocks of the Witwatersrand Triad (i.e. the Dominion Group, Witwatersrand Supergroup and Ventersdorp Supergroup) as primarily subalkaline tholeiitic rocks. She distinguished geochemically between the Klipriviersberg Group, the Platberg Group and the Pniel sequence, as well as their smaller subdivisions. Three chemically distinct units were identified in the Klipriviersberg Group, namely the Alberton Formation, Orkney Formation, and the Loraine and Edenville Formations together. In the Platberg Group, the Goedgenoeg Formation, at the base of the group, and the Rietgat Formation, at the top, are chemically similar, but are separated by the chemically distinct Makwassie Formation.

Due to the subjection of the rocks to low grade greenschist metamorphism, some elements, namely Na, K, Mn, Ba and Rb, cannot be used to make any petrogenetic deductions as they are too mobile in metamorphic processes. Ti, P, Nd, Zr, Y and the light REEs were found to have been little affected by these processes (Bowen, 1984a) and are therefore much more useful.

Bowen (1984a) used several techniques to distinguish between the different rock units. The simplest of these was orthogonal discrimination which assesses the range of each major and trace element, as well as that for each interelement ratio for every geochemical unit. The element ranges of each formation are then compared with those of every other formation. If the ranges of an element from two different units do not overlap it means that this element could possibly be used to discriminate between the two units. The significance of the difference in ranges is determined by calculating the so-called “orthogonal discriminator” (OD). The OD is obtained by dividing the difference between the minimum value of the highest range and the maximum value of the lowest range (i.e. the separation between the ranges) by the minimum value of the highest range. A value between 0 and 1 is obtained. A value of 0 indicates that the ranges are immediately adjacent to one another. The greater the separation between ranges, the closer the OD will be to 1, with a value of 1 only being reached if a particular element is absent from one of the formations.

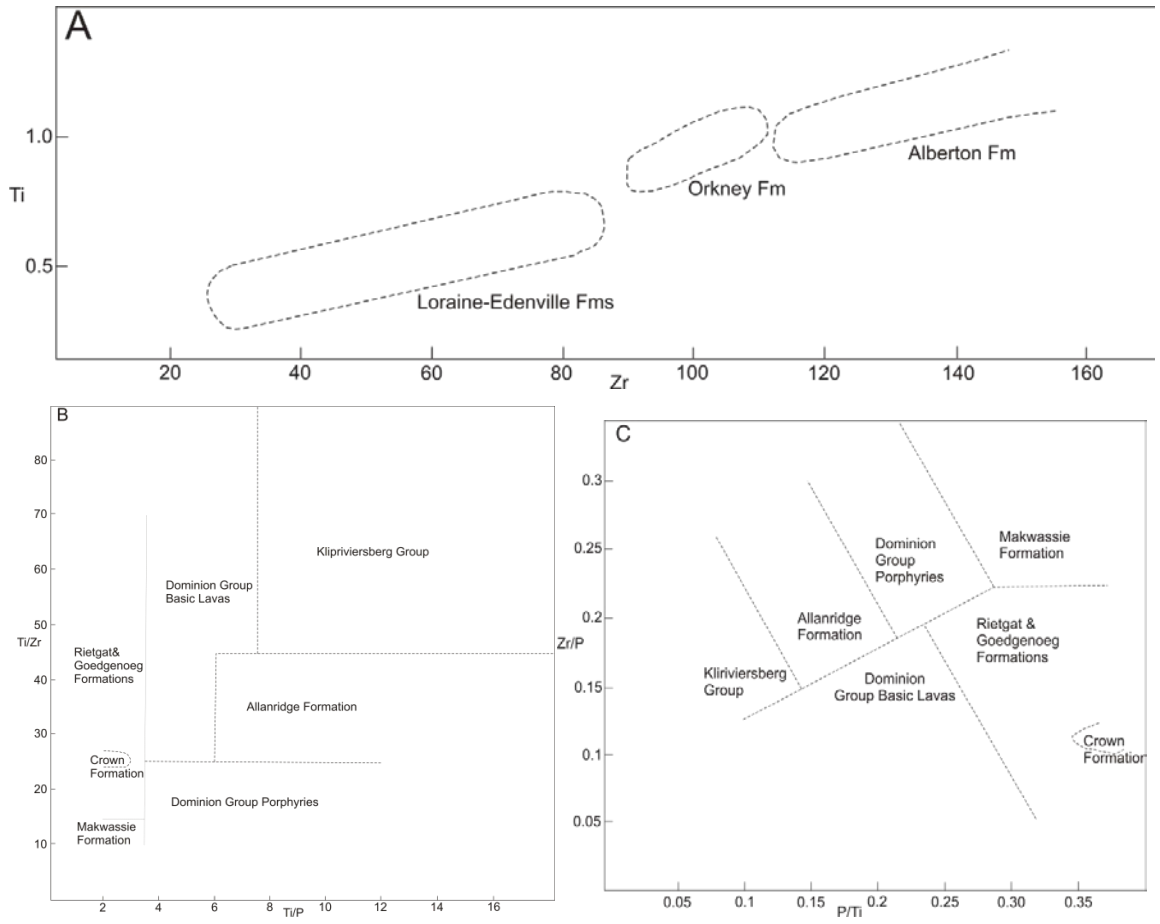

Figure 1.8. A: Ti v Zr, B: Ti/Zr v Ti/P, C: Zr/P v P/Ti plots used by Bowen (1984a) to distinguish between different formations.

A more detailed explanation of orthogonal discrimination can be found in Bowen (1984a). This method was successful in distinguishing all stratigraphic units geochemically from one another, except the Dominion Group basalts from those of the Allanridge, Loraine-Edenville, Orkney and Loraine Formations. The use of three discrimination plots, Ti/Zr vs Ti/P, Zr/P vs P/Ti and TiO_2 vs Zr, (Figure 1.8 A, B, and C) could separate all the units from one another.

The third technique was discriminant analysis. This method could assess the success of the parameters defining the groups and could classify unknown samples (Bowen, 1984a).

The conclusions of Bowen (1984b), who investigated the petrogenesis of these same rocks, are summarized below:

The Loraine-Edenville rocks are the most primitive of the Klipriviersberg Group succession and are classified as magnesian tholeiites to tholeiitic andesites. The lavas probably evolved from the fractional crystallisation of Mg-rich orthopyroxene, possibly accompanied by a small amount of chromite. This was followed by the crystallisation of an augite dominated extract from the residual liquid. The Alberton and Orkney Formations are more evolved than the Loraine-Edenville Formation, with the Orkney Formation being intermediate between the other two. The three groups are probably consanguineous, but they do not form a continuous differentiation sequence. Enrichment in siderophile elements in the Orkney Formation requires that the Alberton and Orkney Formations' fractionation paths diverged after reaching evolved Loraine-Edenville compositions. This enrichment could be due to variable roles of oxides or minerals such as plagioclase, which tend to exclude siderophile elements, in the late stages of differentiation. These two groups either formed independently from a common parent, or by varying degrees of partial melting of the same source which was progressively more depleted in incompatible elements. Concerning the Platberg Group, Bowen (1984b) suggested that the Makwassie Formation was derived from a crustal melt, and that the chemically indistinguishable Goedgenoeg and Rietgat Formations formed due to a mixing of this crustal melt with an unrepresented basic magma. The Allanridge Formation lavas seem to have evolved independently from both the Platberg and Klipriviersberg Groups. The idea that the Allanridge lavas represent a separate magmatic episode is supported by the fact that it is separated from both the other two formations by the mature, flat-lying sediments of the Bothaville Formation. The Allanridge lavas are also more evolved than both the Platberg and Klipriviersberg Groups, although it is possible that the lavas were derived by the fractional crystallisation of Klipriviersberg type magma. However, Bowen (1984b) considered source heterogeneity with the Allanridge lavas evolving along a similar path, although independently, to be a more feasible explanation.

Linton (1992) compared Klipriviersberg Group samples with mid-ocean ridge basalts, continental arc basalts, island arc basalts, Archaean basalts, ocean island basalts, continental rift basalts, and continental flood basalts. The lavas proved to be chemically similar to Archean basalts. TiO_2, Al_2O_3, Fe_2O_3+FeO_2, MnO, P_2O_5 and Y are similar in content. Cr displays similar values and depletion in Archaean Basalt

and Ni displays similar values and enrichment in Archaean Basalt. The Klipriviersberg lavas also display affinities to MORB, CRB, and CFB. Linton (1992) also managed to distinguish between the different units of the Klipriviersberg Group by means of discriminant function analysis (D.F.A), using the incompatible elements TiO_2, Y, and Zr. In Fig. 1.9 some of Bowen's data (1984a) was plotted using Linton's D.F.A. functions (Fn1= 0.01720*Y-0.06078*Zr+20.8084*TiO2.11.4636 Fn2= 0.24892*Y+0.16017*Zr-11.7088*TiO2-0.07079). All samples plotted correctly except for one Rietgat Formation sample that was misclassified as a Makwassie Formation sample.

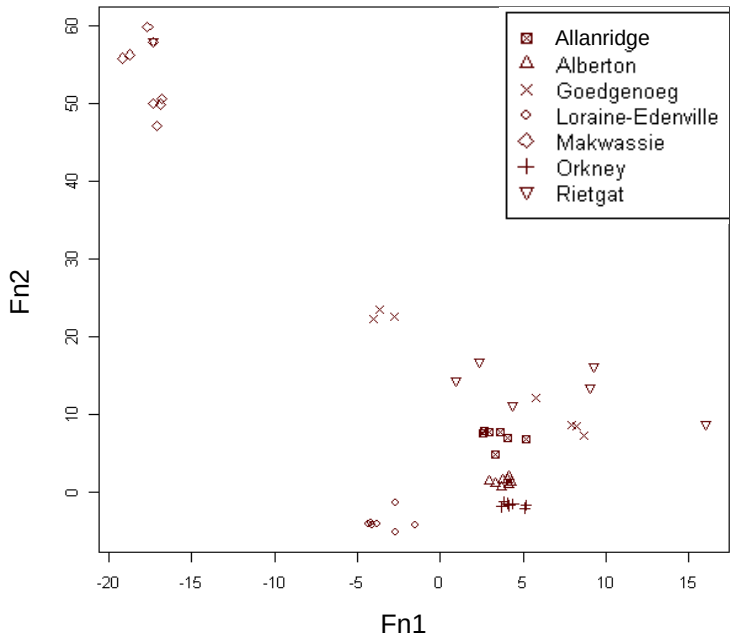

Figure 1.9. Distinguishing between different formations in the Klipriviersberg Group with Fn2 v Fn1. Discriminant functions from Linton (1992) and data from Bowen (1984a)

Winter (1995) investigated the stratigraphy and geochemistry of the Alberton Formation. The Alberton Formation overlies the Venterspost Formation. The lava is aphanitic and severely altered, more so than the other Klipriviersberg lavas, with none of the original minerals or textures being preserved, and has a grey-green colour. The Edenville Formation lavas are similarly altered. Both the Alberton and Edenville Formations are in direct contact with sedimentary formations, namely Venterspost Formation sediments and the Kameeldoorns Formation respectively. Winter (1995) states this as the reason why these two lava formations are the most altered. The mineral assemblage, epidote, chlorite, albite, and sulphides, is characteristic of propylitic alteration, with some areas showing excessive silicification

(lighter areas) or chloritisation and epidotisation (darker areas). The original composition of Alberton Formation feldspars has been destroyed and their current composition is Ab_{95} – Ab_{97}, indicating that the rocks have undergone sodium metasomatism (Winter, 1995). Ca-plagioclase has been completely altered to Na-plagioclase, epidote-bearing assemblages and chlorite. Pyroxene has been altered to chlorite and actinolite, consistent with greenschist facies metamorphism. The presence of actinolite and carbonates and the absence of prehnite and pumpellyite suggest the metamorphic fluids responsible for the alteration had a high CO_2 content (Winter, 1995).

Winter (1995) proposed that, in most cases, the chemical state of the lavas still reflects original magmatic compositions, except in the lower Alberton, which has been subjected to more intense hydrothermal alteration. Using various techniques, Winter (1995) determined that Zr, Y, Nb, V, Ni, Cr, Co, Zn, Al_2O_3, TiO_2, Fe_2O_3 and MgO were least to moderately mobile during alteration.

Winter (1995) classified the rocks of the Alberton and lower Orkney Formations as tholeiitic basaltic-andesites with a calc-alkaline affinity. However, some trends between elements, such as Ti and Zr, are not consistent with a strictly calc-alkaline provenance. Winter (1995) also determined that the lavas were erupted in a within-plate tectonic environment.

1.4.3 Transvaal Supergroup

1.4.3.1 Hekpoort Volcanics

Oberholzer (1995) classified the Hekpoort lavas using mainly Ti, Zr, Nb, Y and REEs by means of the classification systems of Winchester and Floyd (1977) and Jensen (1976). According to the Winchester and Floyd system the lavas were classified as andesitic, while the Jensen system classified them as calc-alkaline. However, the Irvine and Baragar (1971) AFM diagram classifies the lavas as tholeiitic. Oberholzer (1995) also compared the geochemistry of the Hekpoort Formation with that of other similar deposits. These include the Ventersdorp mafic volcanics. The Hekpoort lavas were found to have a higher SiO_2 and MgO content than the Ventersdorp lavas, with the exception of the Loraine-Edenville Formation that has a higher MgO content. However, the most notable difference lies in the much lower alkali content of the Hekpoort lavas. The low alkali content of the Hekpoort lavas can be attributed

to the high degree of alteration to which the rocks were submitted. Only the Loraine-Edenville Formation has higher Cr and Ni contents than the Hekpoort lavas.

Data from some of the studies discussed will be used in subsequent chapters in order to find a geochemical classification system for the dykes in the Carletonville Goldfields.

Chapter 2: Sampling and Analytical Techniques

2.1 Sampling

A total of 94 samples were obtained from Tau Tona and Mponeng. 85 samples were taken from the core yards of Tau Tona and Mponeng and the remaining five were taken underground on 104 level in Tau Tona (Appendix A). Where possible, the chill zones and central zones of dykes were sampled. In some cases chill zones were visibly contaminated with country rock. These were not sampled. Care was also taken to take samples with minimal veining. It is important to note that the nature of the study area imposes limits on sampling methods as well as the number of samples that could be taken. As it is only possible to sample very few dykes underground, most of the sampling relies on the availability of dykes in drill core. For this reason some dykes will be represented by more samples than others, and in some cases only one sample per dyke was available. Mine plans and locality maps were obtained from the geology offices at the respective mines (Fold-out maps in Appendix A).

2.2 Sample Preparation and Analytical Techniques

Thin sections for petrographic study were made from 45 samples. Powder X-ray diffraction was excecuted on 31 samples on a Siemens D5000 XRD (Appendix B). XRD films were used in cases where single mineral identification was required. These were made on a Phillips PW1051 X-ray diffractometer using a Debye-Scherrer camera.

Samples were crushed in a jaw crusher and pulverised in a carbon steel mill. The powdered samples were then used in geochemical analyses as well as for mineralogical investigation. For major element analysis, fusion discs were made according to the method developed by Norrish and Hutton (1969). According to this method approximately 3 g of sample is dried overnight at 100°C in a porcelain crucible, after which the sample is weighed, ignited at 1 000°C and weighed again. 0.28 g of this sample is then mixed with 0.02 g of $NaNO_3$ and 1.5 g of Spectroflux ($Li_2B_4O_7$ = 47%, Li_2CO_3 = 36.7%, La_2O_3 = 16.3%). The mixture is then melted in platinum crucibles at 950°C and formed into a fusion disc. Analyses for trace elements and sodium were executed on pressed powder briquettes that were made

by compressing a mixture of 8 g of powdered sample and 3 g of Hoechst Wax Micro powder at 20 tons. Major and trace element geochemistry was affected by means of X-ray fluorescence spectrometry (XRF) on a Panalytical Axios X-ray spectrometer using SuperQ software. The standards used for calibration include certified reference materials as well as in-house standards.

Rare Earth Element analysis was carried out by means of ICP-MS at the Department of Geology at the University of Cape Town. For REE analysis 50 mg of pulverised samples were digested in Teflon beakers using 4 ml of a concentrated 4:1 HF/HNO_3 solution at 50-60°C for at least 24 hours. After digestion the samples were dried in the beakers at ±75°C. Once dry, 2 ml HNO_3 was pipetted into the beakers and once again left to dry. The last step was then repeated. 4 ml of the internal standard solution (ISS) was added to each sample and the samples were treated by ultra sound for 1 hour. The ISS consists of 10ppb In, Re, Rh and Bi in 5% HNO_3. Each sample was diluted to 50 ml with ISS and weighed. 1 ml of this solution was weighed, diluted further to 10 ml and weighed again, ultimately reaching a 10 000 times dilution. The whole procedure was also followed with the external standard (BHVO2) as well as a total procedural blank (tpb) to which no sample was added.

All results are included in Appendix C. A list of the standards is included in Appendix D.

Chapter 3: Mineralogy

3.1 Introduction

A mineralogical investigation of some of the dykes in Tau Tona was conducted by Greeff (1988a) as part of an investigation of the dykes after seismic events originating at the Peggy Dyke. He examined a large number of thin sections of different dykes, including the Bank, Speckled, Twin, Peggy and CLA dykes as well as Ventersdorp lava samples.

In this study, at least one thin section per dyke was made and X-ray powder diffraction was carried out, mostly on the same samples from which thin sections were made. The XRD patterns are included in Appendix B.

The thin sections themselves were electronically scanned and are included, as it often provides a better idea of features such as the rock textures and veining. Thin sections have dimensions of 44 mm x 25 mm, but some of the images have been cropped in the length. Where applicable, results from this study are compared to those from Greeff (1988a). For each set of photomicrographs, A was taken in plane polarized light, and B with crossed nicols. The modal compositions were estimated using XRD peak sizes in conjunction with thin section observations (Appendix B), as point counting is problematic due to the intergrown nature of minerals. Minerals were labelled where possible and abbreviations are given in the captions.

3.2 Petrographic Study

3.2.1 The Peggy Dyke

Figure 3.1. PEG1.

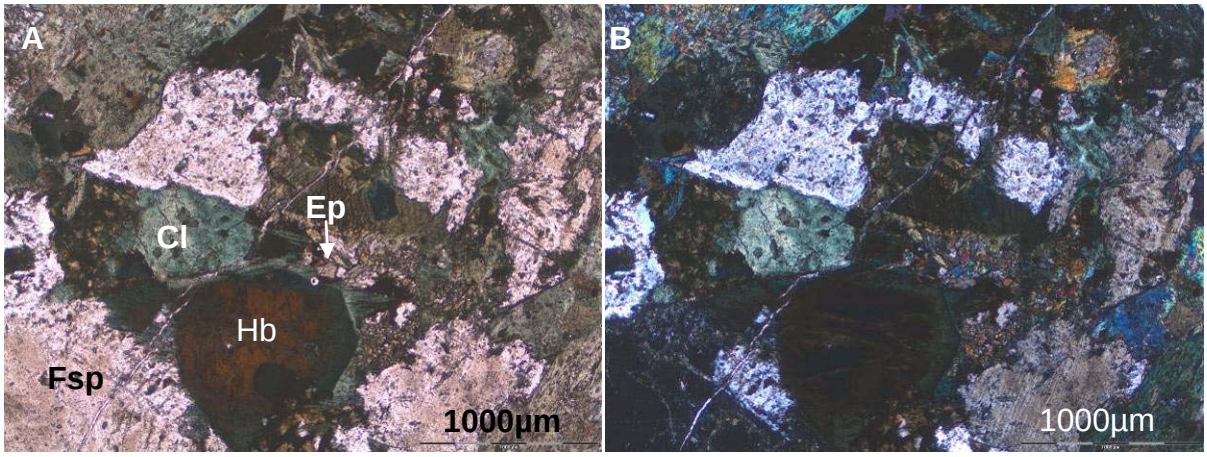

Figure 3.2. PEG1, showing altered plagioclase, chlorite, epidote and hornblende with an altered rim. Hb=Hornblende, Fsp=Feldspar, Cl=Chlorite, Ep=Epidote.

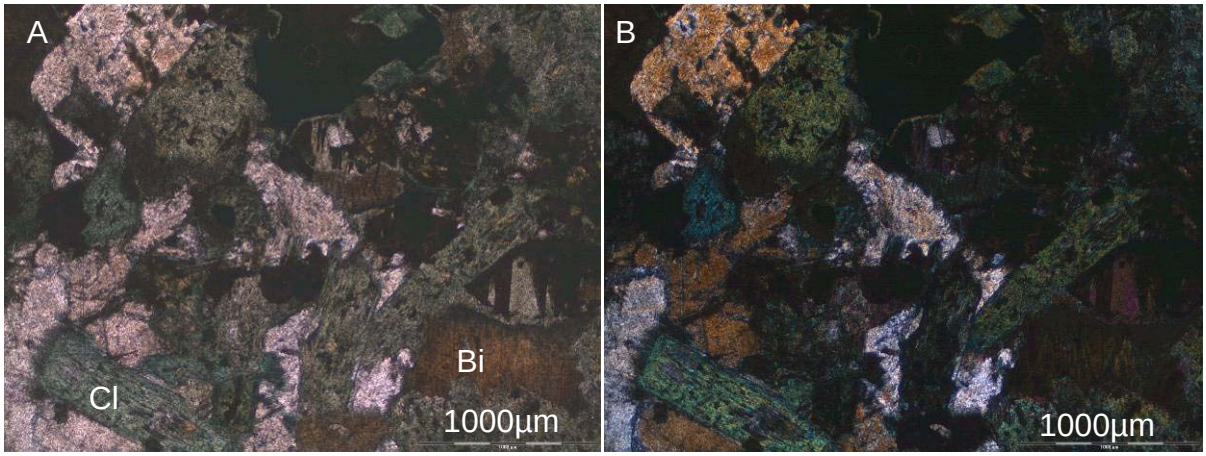

Figure 3.3. PEG1 with chlorite, altered plagioclase and remnants of unaltered biotite. Bi=Biotite.

PEG1 (Fig. 3.1) is a medium to coarse crystalline rock. It contains chlorite, epidote, remnants of biotite that are in the process of being chloritised, saussuritised feldspar which was identified as albite by means of XRD, sphene, some actinolite and a few crystals of brown hornblende (Fig. 3.2 and 3.3). The large hornblende crystal at bottom centre of Fig. 3.2 is in the process of being chloritised at the rim. This particular sample is cut by a vein of approximately 2 – 3 mm wide. The vein consists of chlorite, small quartz crystals and larger patches of calcite.

Figure 3.4. PEG2.

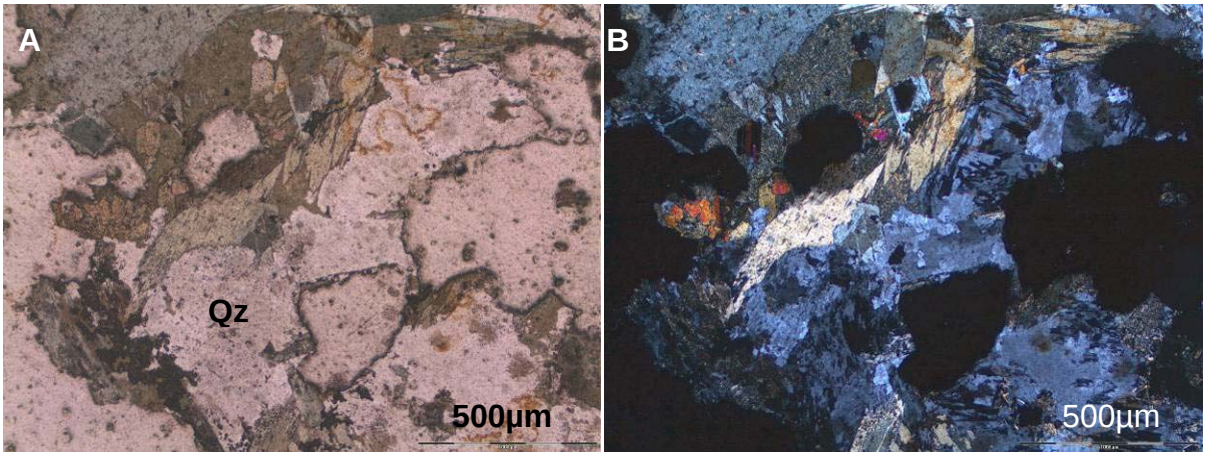

Figure 3.5. PEG2 with large amounts of quartz and smaller amounts of chlorite and epidote. The large black areas are holes in the thin section. Qz=Quartz.

PEG2 (Fig. 3.4) is more coarse crystalline than PEG1 and contains less dark minerals. The sample contains far more quartz, which in PEG1 was restricted to veins. PEG2 contains remnants of biotite being chloritised, as well as epidote and some iron oxide staining (Fig. 3.5), albite, and illite-montmorillonite.

Figure 3.6. PEG5.

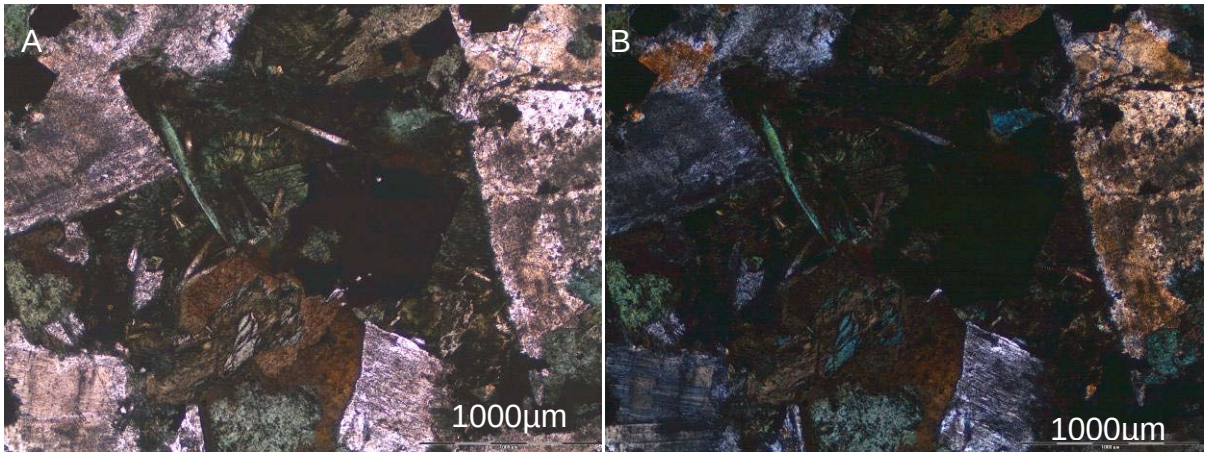

Figure 3.7. PEG5 with large euhedral plagioclase crystals, chlorite and biotite.

PEG5 (Fig. 3.6) is medium to coarse crystalline. Euhedral, saussuritised plagioclase is present, along with chlorite, biotite, hornblende and epidote (Figs. 3.7 and 3.8). Albite twinning is still visible in the plagioclase crystals, but these are too altered to identify specifically by optical means. XRD analysis indicated albite.

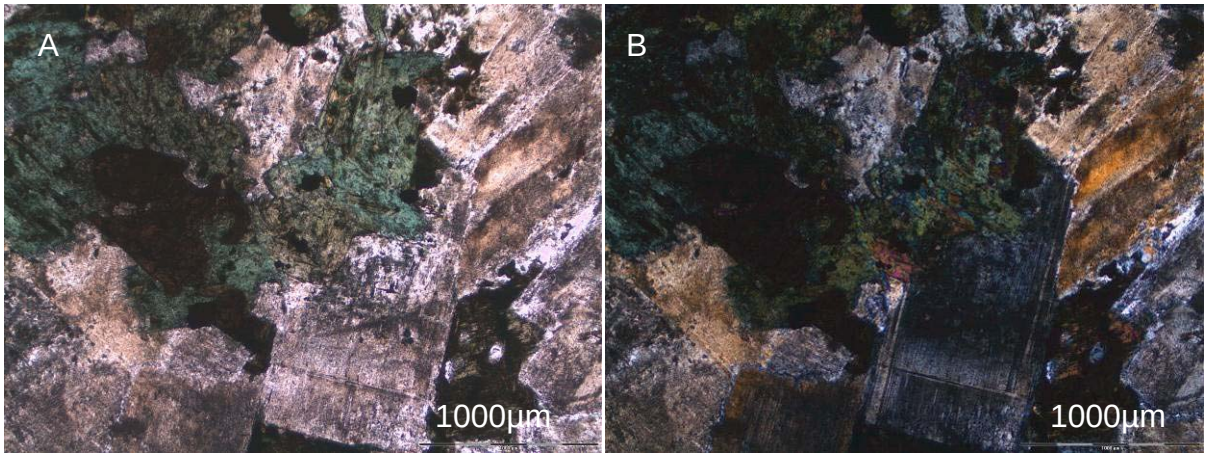

Figure 3.8. PEG5 with plagioclase, chlorite and epidote.

Greeff (1988a) included two Peggy dyke samples in his petrographic study of the dykes. He makes no mention of epidote, biotite, sphene or amphiboles. He does, however, mention rutile in one sample, which was not found in any of the samples in this study. He also makes no mention of albite, or any other plagioclase. One of Greeff's samples contains large patches of calcite, whereas all calcite in the Peggy dyke samples from this study is located in veins. It is clear from both studies, as

well as from a comparison of the two, that the Peggy dyke is mineralogically rather heterogeneous, with all the samples being medium to coarse crystalline.

3.2.2 The Georgette Dyke

Figure 3.9. GEOR1.

GEOR1 (Fig. 3.9) contains microphenocrysts of feldspar that have been almost completely altered to chlorite. The sample also contains quartz, epidote, actinolite and altered sphene (Fig. 3.10).

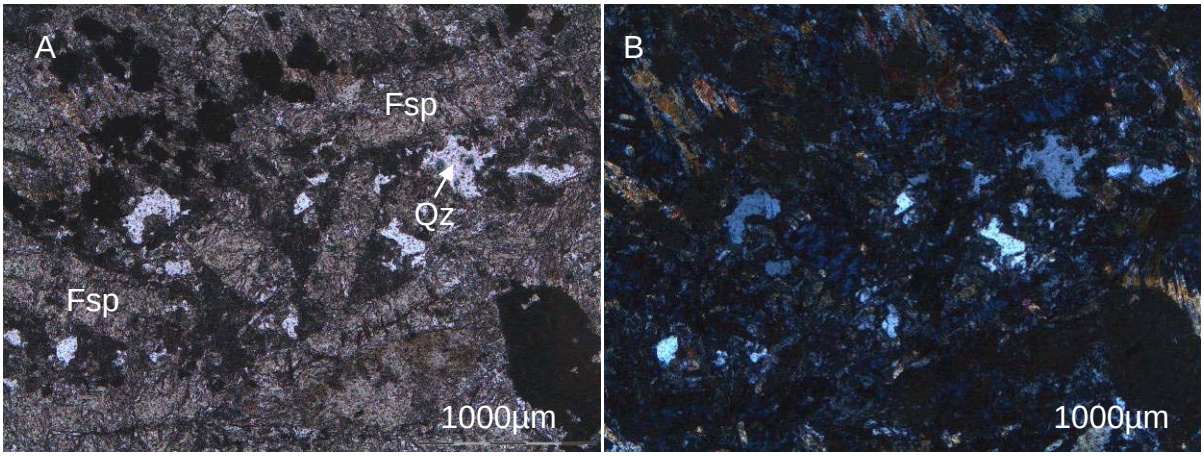

Figure 3.10. GEOR2 with quartz, altered feldspar and some opaques.

3.2.3 The Skelm Dyke

Figure 3.11. SKE1.

The Skelm dyke (Fig. 3.11) is medium crystalline and consists of epidote, chlorite, actinolite, altered albite and illite-montmorillonite, and quartz both in small veins and in the rock itself. Altered sphene and pyrite are present and the difference can be seen in Fig. 3.12. The rock is fractured in places with the bulk of the epidote being situated in the fractures (Fig. 3.13). Some of the fractures contain iron oxides and opaque minerals (Fig. 3.14).

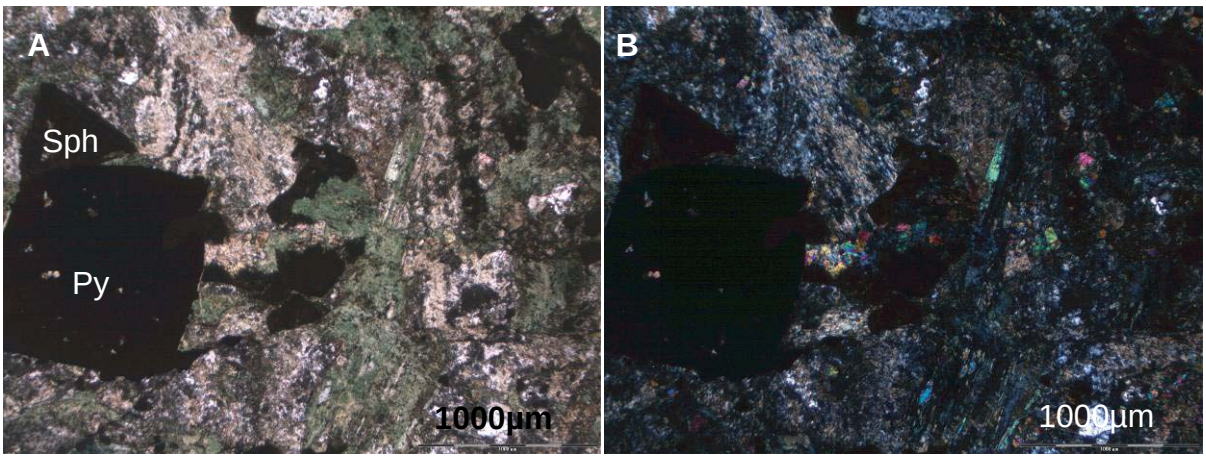

Figure 3.12. SKE1 showing pyrite (square crystal) and altered sphene (higher relief and not quite as dark in B). Py=Pyrite, Sph=Sphene.

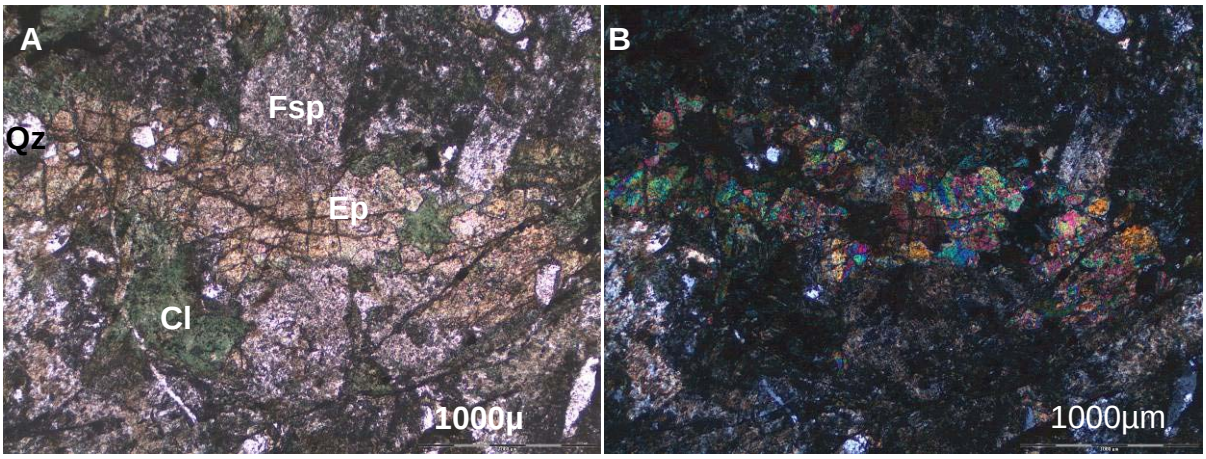

Figure 3.13. An epidote vein in SKE1.

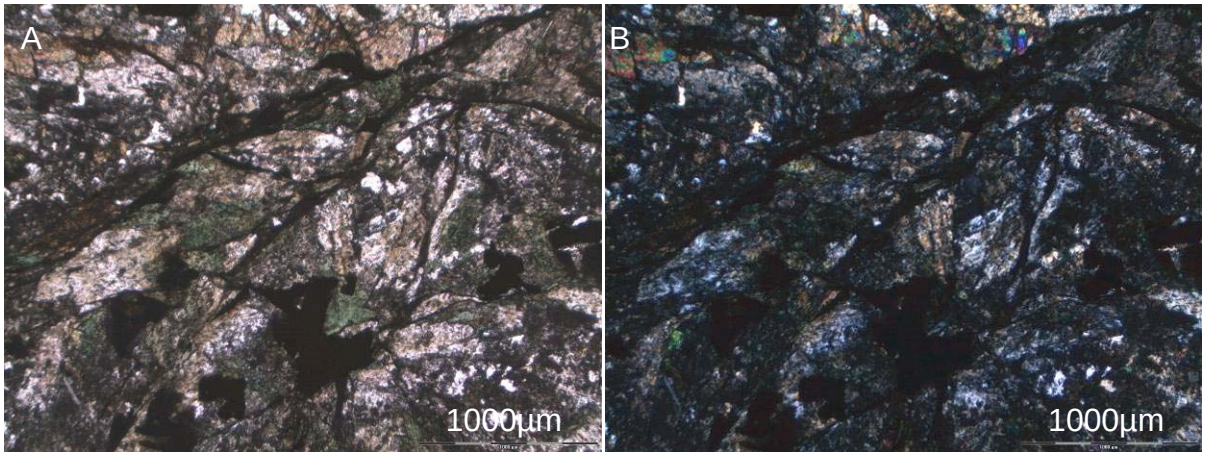

Figure 3.14. Darker veins iron oxide in SKE1.

Figure 3.15. SKE3.

SKE3 (Fig. 3.18) is very similar to SKE1 in that both are fine to medium crystalline and both contain epidote-filled veins. In SKE3 (Fig. 3.19) some quartz is also present in the veins, but epidote remains volumetrically dominant. Chlorite, epidote and sphene are present along with altered plagioclase, of which the twinning is still visible.

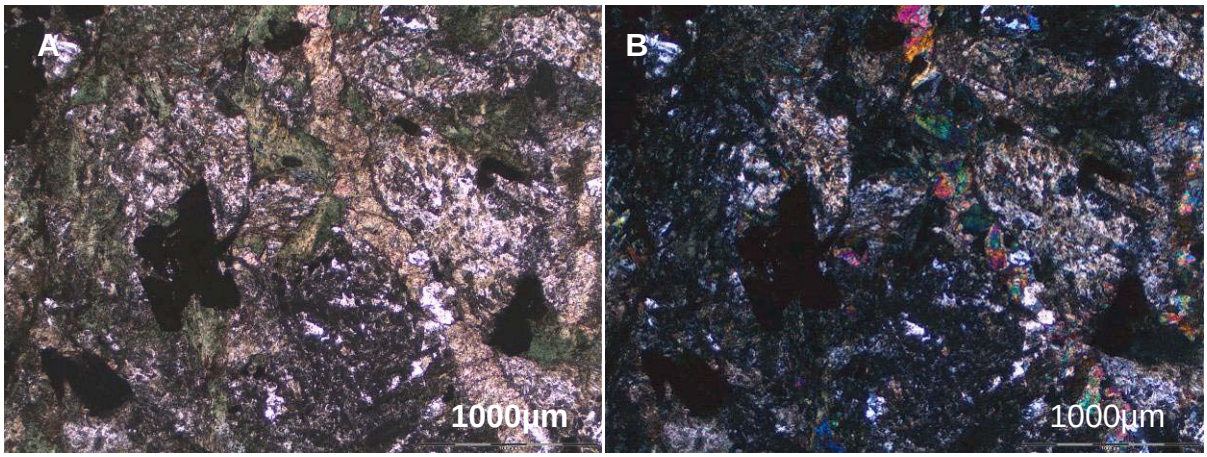

Figure 3.16. An epidote vein in SKE3. Albite twinning in the plagioclase crystals is still visible.

Figure 3.17. SKE5.

SKE5 is medium to fine crystalline (Fig. 3.15). It contains altered plagioclase, intergrown chlorite and epidote, quartz, some iron oxide staining and opaque minerals (Fig. 3.16). Nodules consisting entirely of chlorite are also present. These chlorite nodules are suspected to be altered pyroxene phenocrysts (Fig. 3.17).

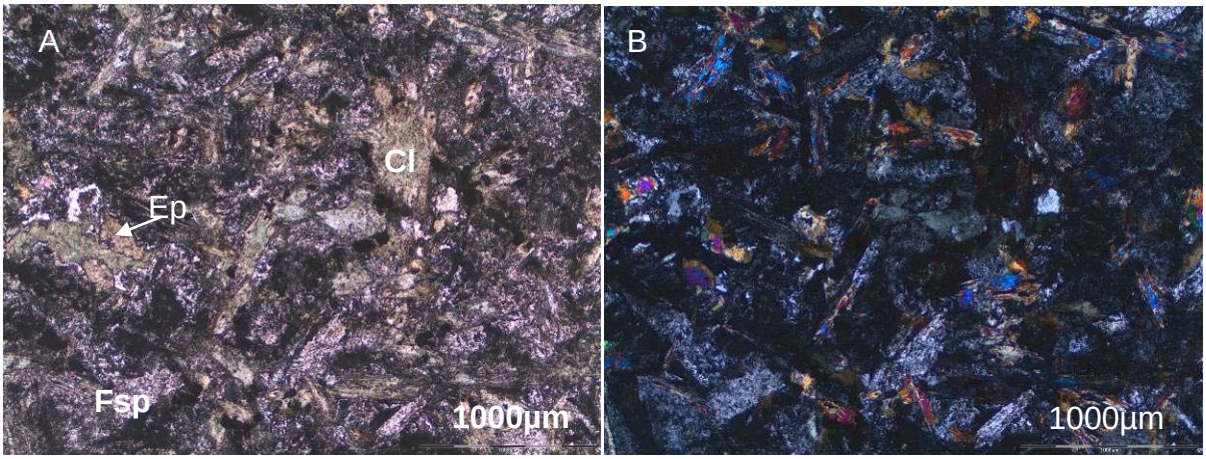

Figure 3.18. SKE5 consisting of intergrown chlorite and epidote.

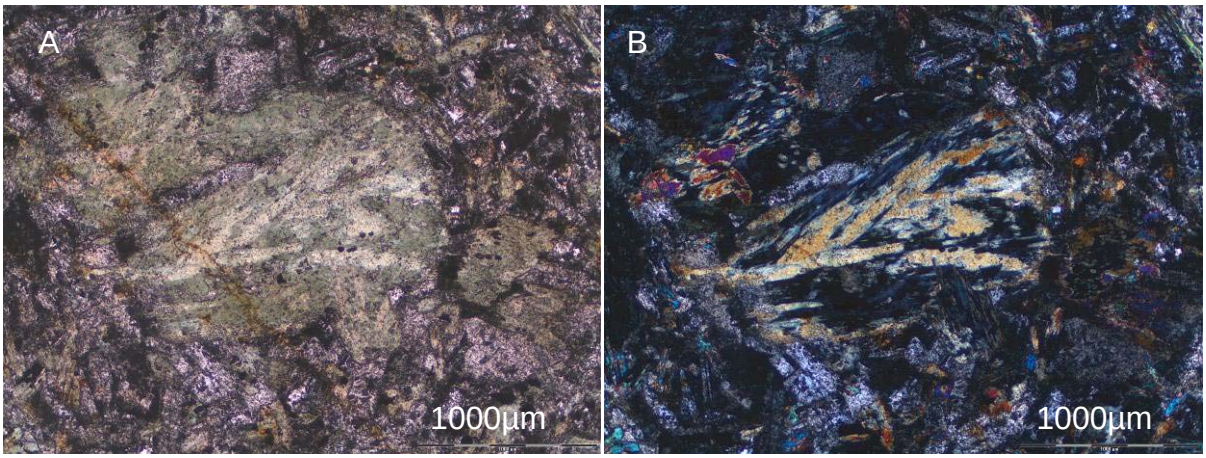

Figure 3.19. The chlorite nodule in SKE5.

3.2.4 The Soll Dyke

Figure 3.20. SOL2.

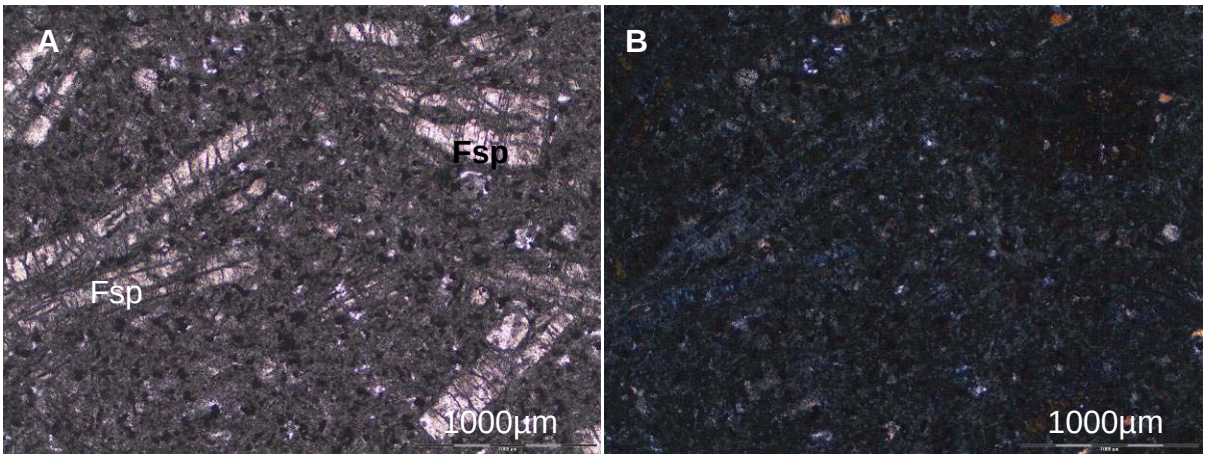

Figure 3.21. Euhedral plagioclase microphenocrysts in a fine matrix.

SOL2 (Fig. 3.20) is fine crystalline and contains euhedral microphenocrysts as well as finer crystals of plagioclase. Both types have been altered almost completely, and albite twinning is no longer visible (Fig. 3.21). The matrix is fine crystalline and consists mostly of chlorite. Small quartz crystals are also present together with opaque minerals.

Figure 3.22. SOL3.

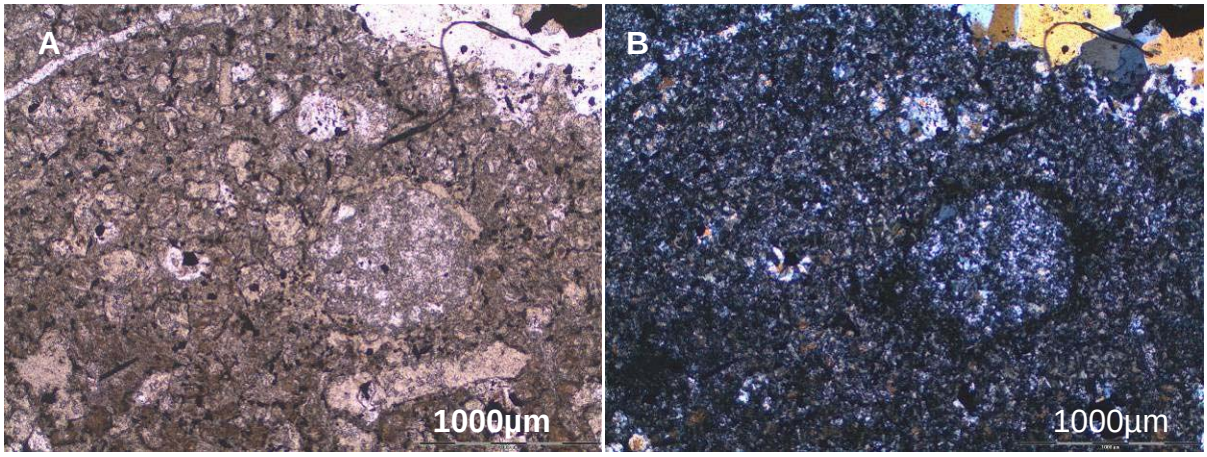

Figure 3.23. Alteration in SOL3.

SOL3 (Fig. 3.22) is altered and consists mostly of chlorite and quartz with small amounts of epidote being present together with opaque minerals (Fig. 3.23). The veins consist of quartz, chlorite and sulphides (Fig. 3.24). Sulphides are mostly confined to the veins.

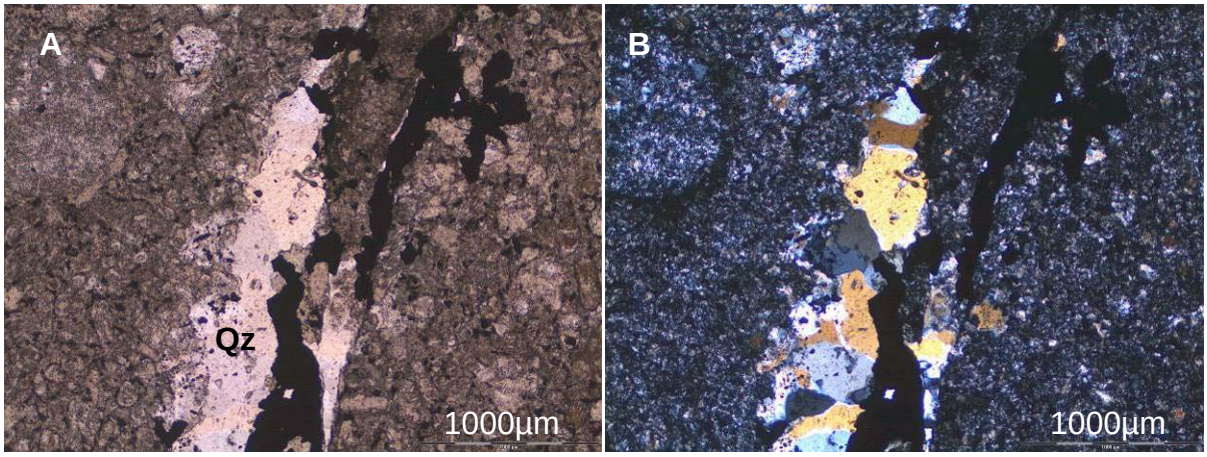

Figure 3.24. Vein consisting of quartz, chlorite and sulphides.

3.2.5 The Kudu Dyke

Figure 3.25. KUD1.

KUD1 (Fig. 3.25) is fine crystalline and consists of albite, chlorite, epidote and quartz with microphenocrysts that have been altered to chlorite and smaller amounts of epidote (Fig. 3.26). Few small crystals of opaque minerals are present. Veins are filled with either epidote and quartz or calcite and quartz, the latter being the younger.

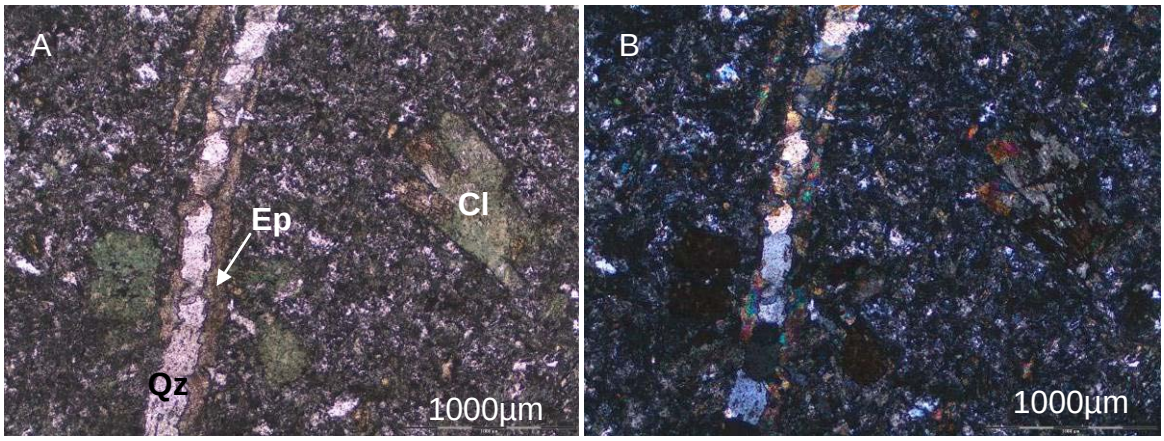

Figure 3.26. KUD1 with chlorite nodules and an epidote-quartz vein.

3.2.6 The Sill

Figure 3.27. SIL1.

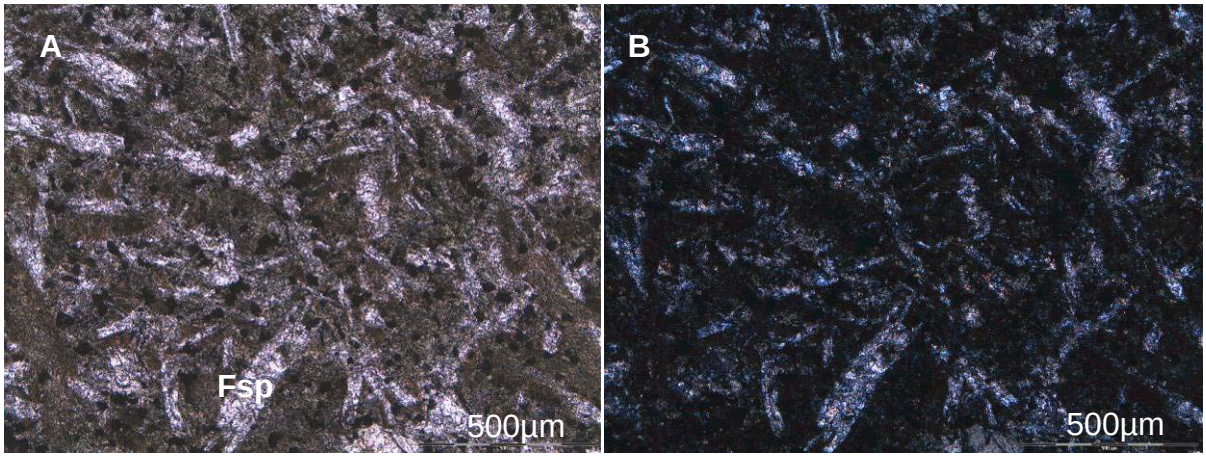

Figure 3.28. Scattered needle-like plagioclase crystals in SIL1.

SIL1 (Fig. 3.27) is fine crystalline and consists of scattered needle-like altered plagioclase crystals in a matrix of chlorite and opaque minerals (Fig. 3.28). The vein consists of calcite.

3.2.7 The Jeans Dyke

Figure 3.29. JEA1.

JEA1 (Fig. 3.29) contains chlorite as the dominant mineral. The chlorite is dark green in places, indicating a high iron content (Nesse, 2004). Epidote is also present along with sphene, quartz and some opaque minerals (Fig. 3.30). Large calcite crystals are also present. Veins are filled with chlorite. One extremely altered nodule, consisting of clay minerals with sulphide minerals on its rim is present.

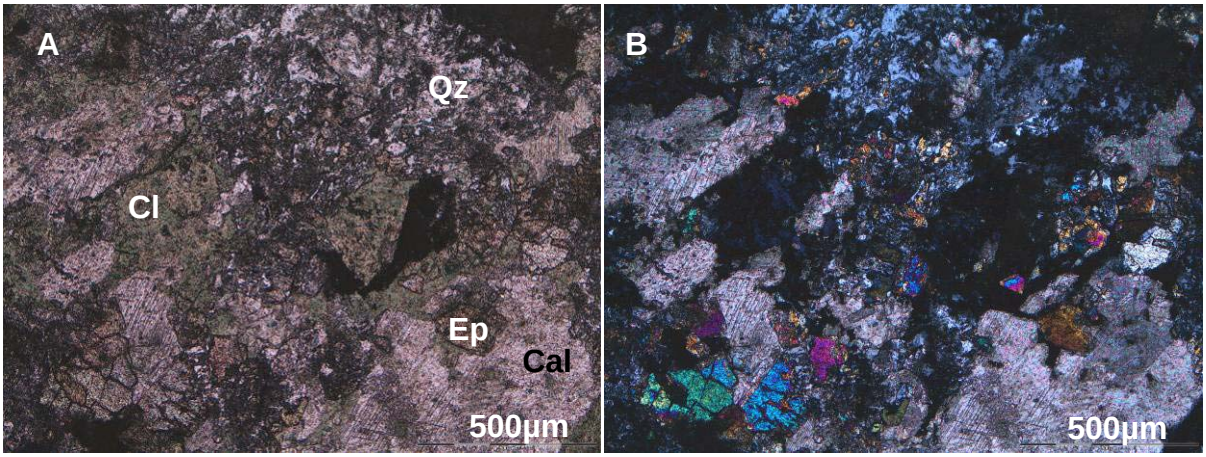

Figure 3.30. Epidote, quartz and altered plagioclase in JEA1. Cal=Calcite.

3.2.8 The Friday Dyke

Figure 3.31. FRI1.

FRI1 (Fig. 3.31) consists of intergrown chlorite and epidote as well as quartz, sphene, and prehnite (Figs. 3.32 and 3.33).

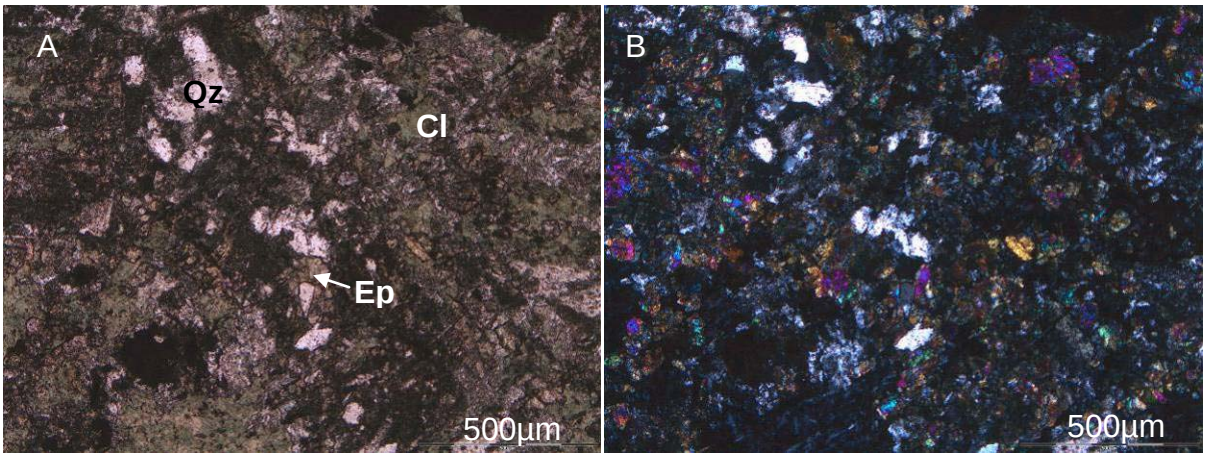

Figure 3.32. Intergrown epidote and chlorite along with quartz in FRI1.

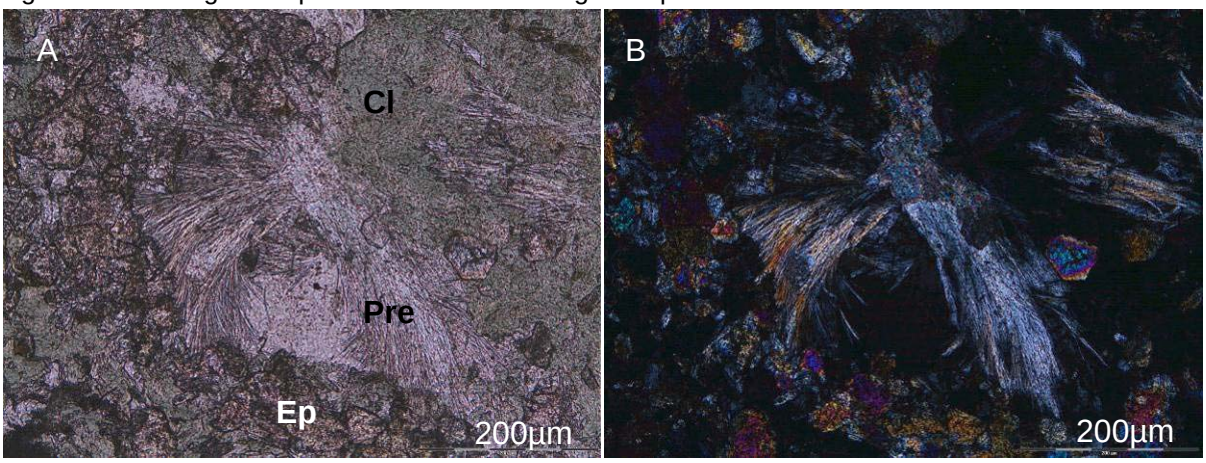

Figure 3.33. Prehnite in FRI1. Pre=Prenite.

Figure 3.34. FRI4.

FRI4 (Fig. 3.34) is medium crystalline and consists of chlorite, epidote, altered plagioclase, small amounts of quartz and sphene (Fig. 3.35).

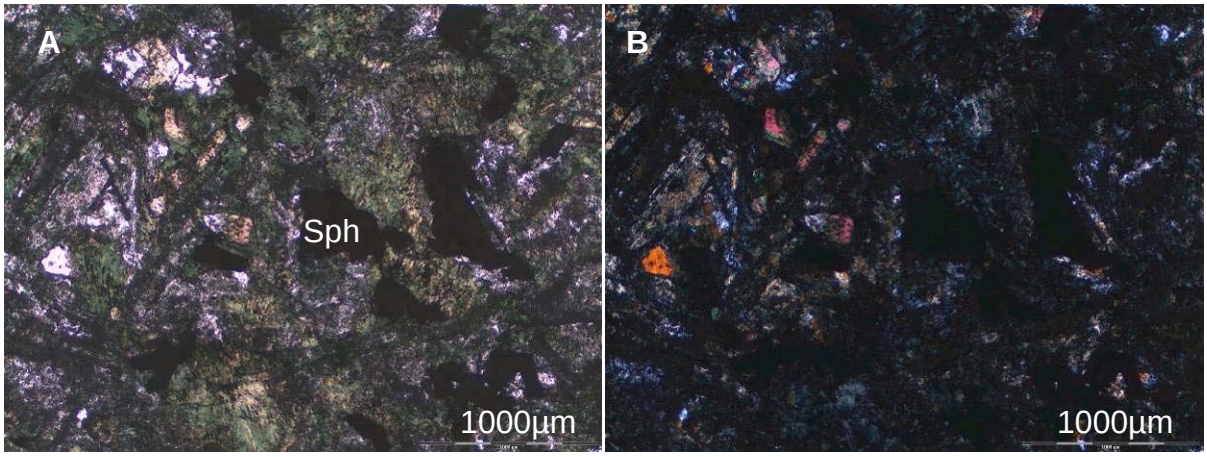

Figure 3.35. Chlorite, epidote, quartz and sphene in FRI4.

Figure 3.36. FRI7.

FRI7 (Fig. 3.36) is more fine crystalline than FRI 1 and 4 and consists of intergrown chlorite and epidote as well as some actinolite, quartz sphene and saussuritised feldspar (Fig. 3.37).

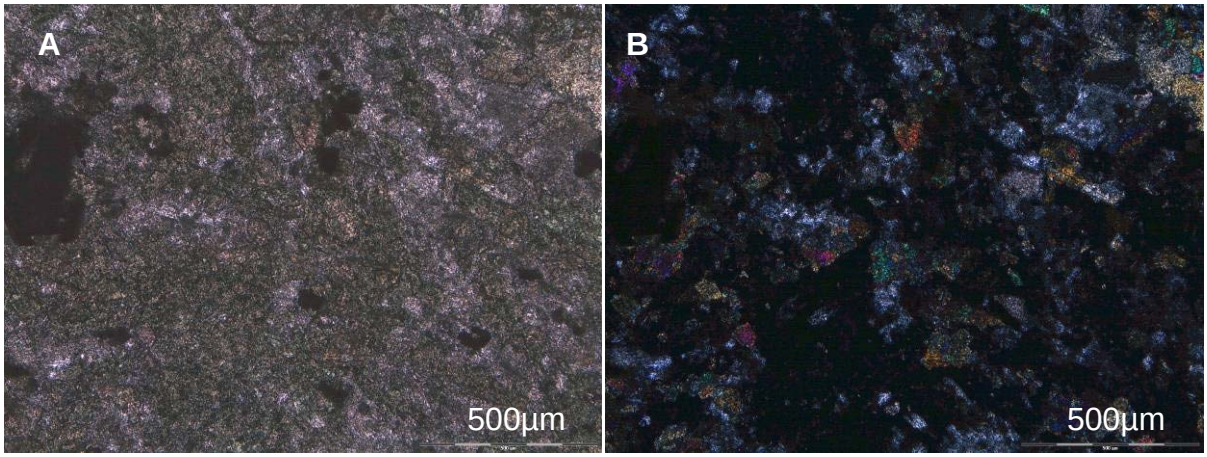

Figure 3.37. Intergrown epidote and chlorite, quartz and sphene.

3.2.9 The Lib Dyke

Figure 3.38. LIB1.

LIB1 (Fig. 3.38) is medium to fine crystalline and consists mostly of chlorite, but albite and small amounts of quartz are also present, along with some opaque minerals (Fig. 3.39).

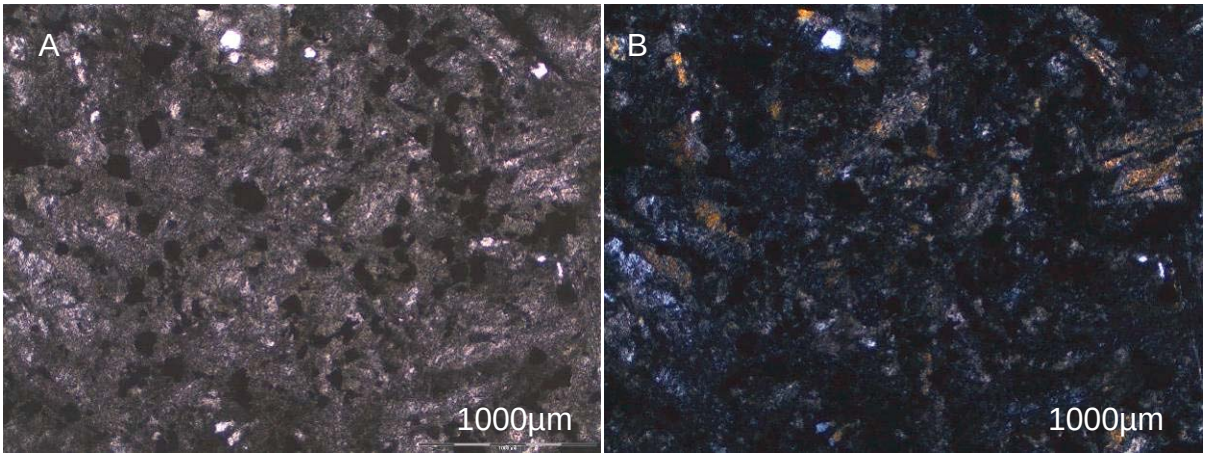

Figure 3.39. LIB1 consists mostly of chlorite. Albite and small amounts of quartz are present along with a large percentage of opaque minerals.

3.2.10 The Little Tumi Dyke

Figure 3.40. LIT1.

LIT1 (Fig. 3.40) is medium to coarse crystalline with large albite crystals. Chlorite, epidote, actinolite, small amounts of quartz and opaque minerals can be identified optically (Fig. 3.41). Illite-montmorillonite was identified by means of XRD.

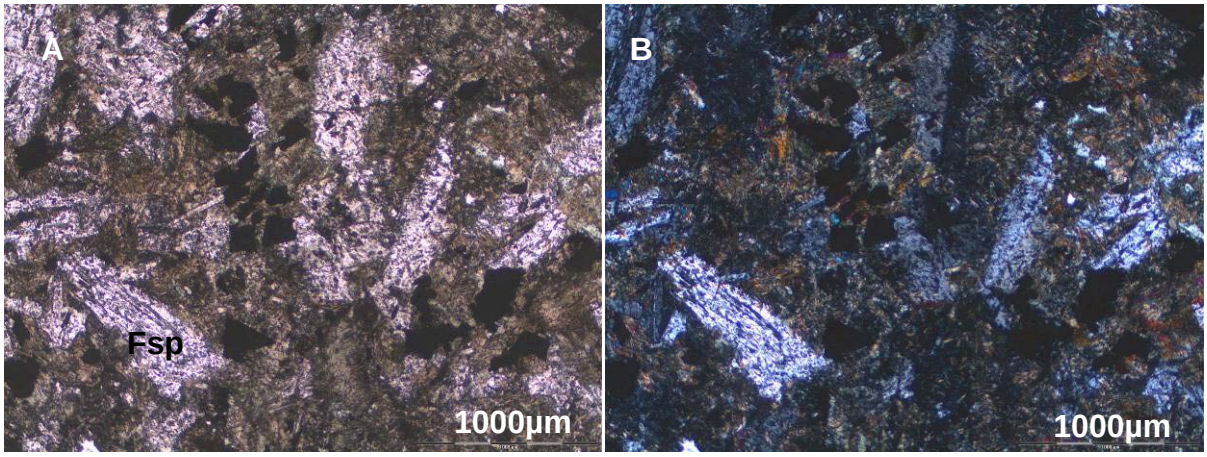

Figure 3.41. Large albite crystals in LIT1.

3.2.11 The PE Dyke

Figure 3.42. PE1.

PE1 (Fig. 3.42) is medium crystalline and consists of chlorite, small amounts of epidote, actinolite, altered sphene, large amounts of quartz (Fig. 3.43), and lath-like crystals of what is suspected to have been plagioclase, but is now completely chloritised.

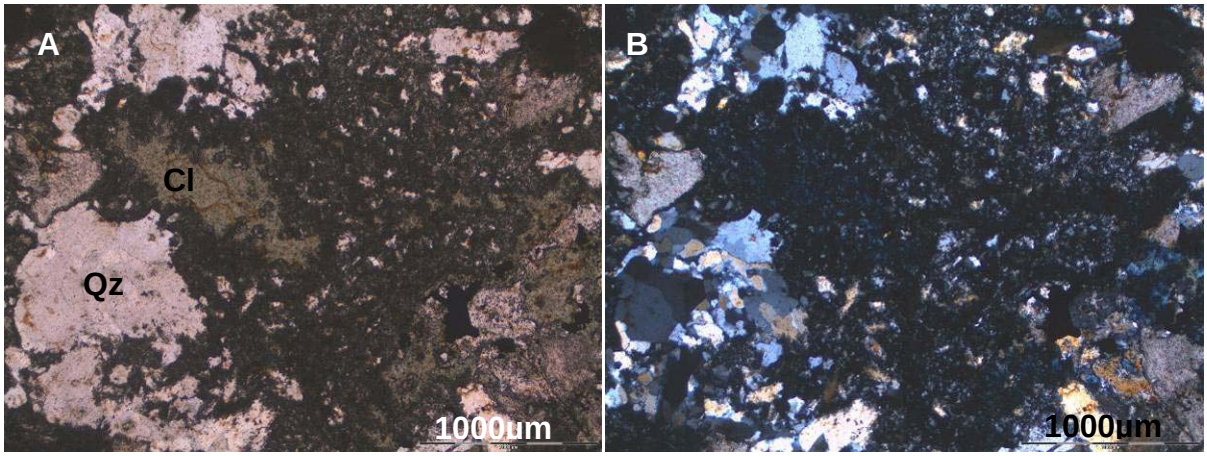

Figure 3.43. Large amounts of quartz and chlorite in PE1.

3.2.12 Ventersdorp Lava

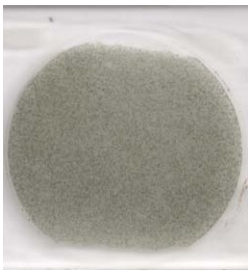

Figure 3.44. LAV1.

The lava sample (Fig. 3.44) is fine crystalline and consists of large amounts of chlorite intergrown with some epidote and actinolite (Fig. 3.45). Albite is also present along with some iron oxides. Hydrobiotite (sericite) was identified by means of XRD.

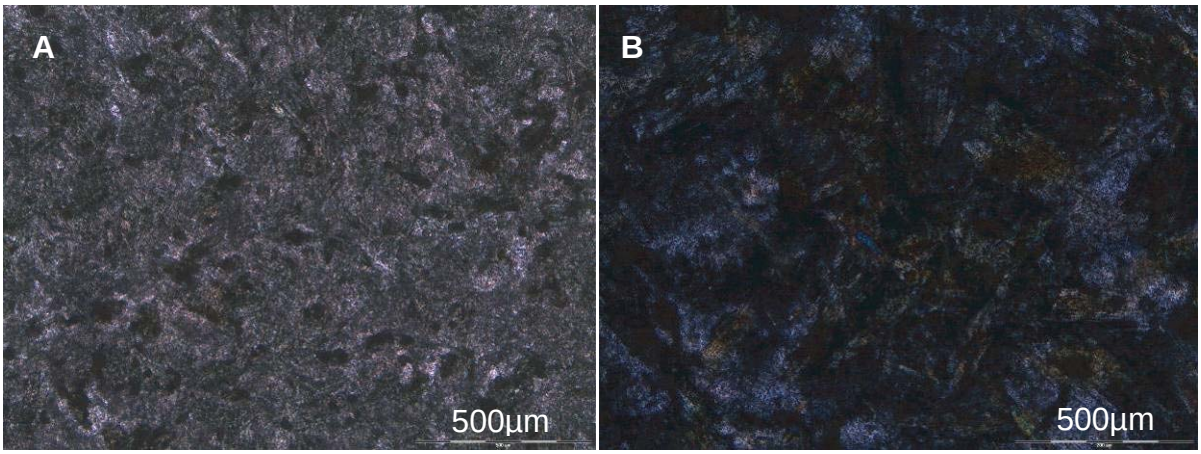

Figure 3.45. Fine crystalline Ventersdorp lava with visisble albite and epidote.

Greeff (1988a) studied numerous Ventersdorp lava samples. They differed greatly in both mineralogy and texture. All samples containd plagioclase, chlorite, epidote, quartz and opaque minerals. Minerals that are present in some samples are actinolite, calcite, pyroxene, rutile, sphene and remnants of biotite. One occurrence of zeolite and a few of apatite are found. Greeff never specifies from which units of the Ventersdorp Supergroup his samples were obtained, therefore the heterogeneity in mineralogy and texture could be the result of the sampling of different flows or even different stratigraphic units. However, the Alberton Formation is the hanging wall for Ventersdorp Contact reef and it would be fair to assume that Greeff's samples are from this formation. The mineralogical and textural descriptions given

by Greeff support this assumption. Winter (1995) found that, with the exception of the Alberton Formation, it is very difficult to recognise specific stratigraphic units of the Klipriviersberg group by means of petrography alone.

Winter (1995) divided the Alberton Formation into three units. The lower units (1 and 2) are highly altered with very little of the original mineralogy or textures being preserved. The rocks consist of microcrystalline quartz, chlorite, actinolite, feldspar (ranging from albite to orthoclase), sericite, and carbonates. The degree of alteration decreases with increase in distance from the Ventersdorp-Witwatersrand contact. Winter found that the rocks of Unit 3 are considerably better preserved than in units 1 and 2. Plagioclase and clinopyroxene exist as major minerals along with minor secondary phases of actinolite, chlorite, epidote, carbonate, sericite, rutile and sulphides. Plagioclase and pyroxene exist, both as phenocrysts and in the matrix.

3.2.13 The Amigo Dyke

Figure 3.46. AMI3.

AMI3 (Fig. 3.46) is medium crystalline and consists of altered plagioclase, chlorite, iron oxides and opaque minerals. A small quartz vein cuts the sample (Fig. 3.47). XRD analysis was conducted on AMI1 and only chlorite and quartz were detected.

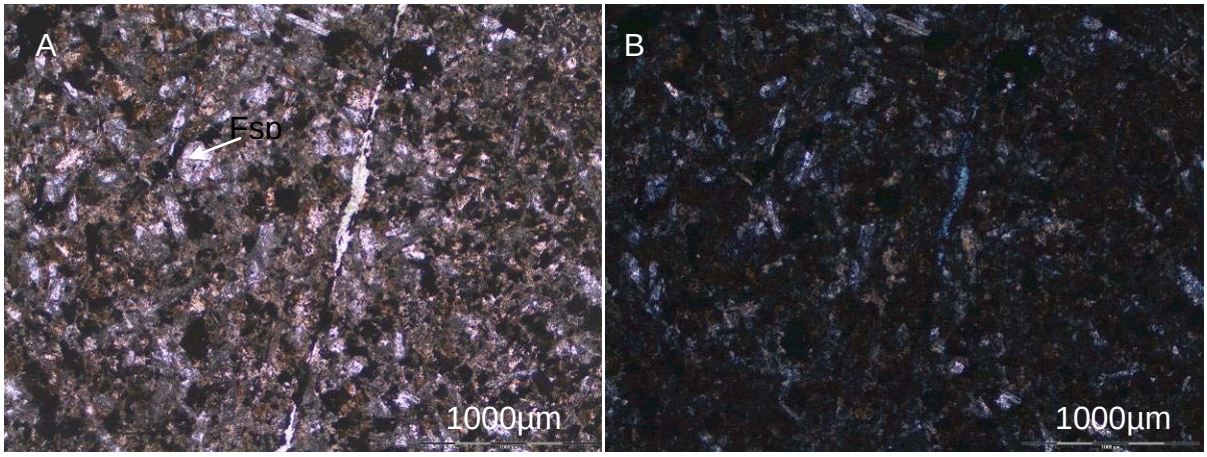

Figure 3.47. Altered plagioclase, chlorite, iron oxides and opaque minerals in AMI3. A small quartz vein is present.

AMI5 (Fig. 3.48) consists of a fine mass intergrown chlorite and epidote along with some opaque minerals. Scattered throughout the sample are clusters of pyroxene crystals (Fig. 3.49). Remnants of plagioclase crystals are also present as well as large pyrite nodules. Some plagioclase remnants are contained within these nodules (Fig. 3.48).

Figure 3.48. AMI5.

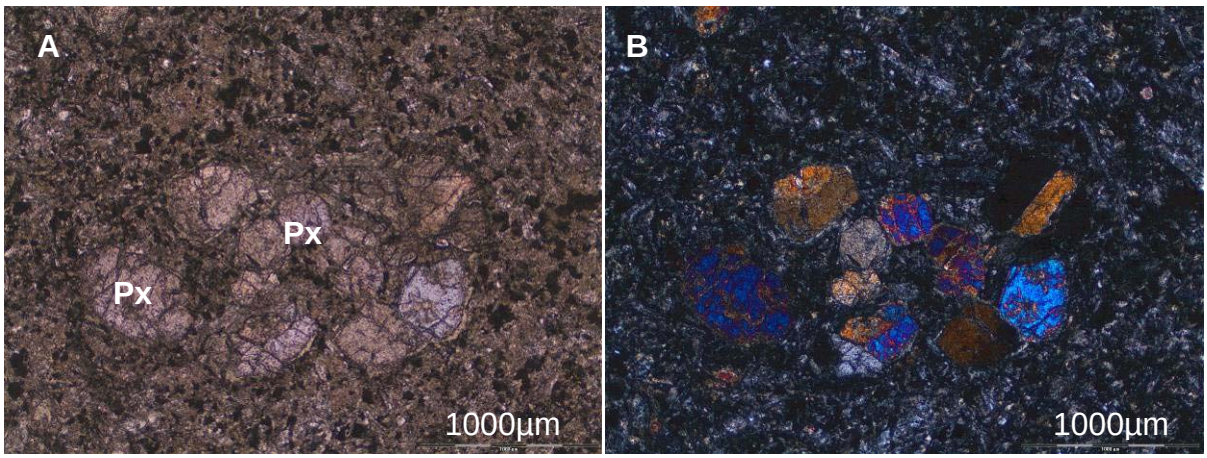

Figure 3.49. A pyroxene cluster in a matrix of chlorite and opaque minerals in AMI5. Px=Pyroxene.

3.2.14 The Bank Dyke

Figure 3.50. BAN1.

BAN1 (Fig. 3. 50) is medium to coarse crystalline and consists of altered plagioclase and some less altered pyroxene although some pyroxenes have been chloritised (Fig. 3.51). Some quartz is also present along with opaque minerals and epidote. Actinolite and sericite were both detected by means of XRD in BAN2.

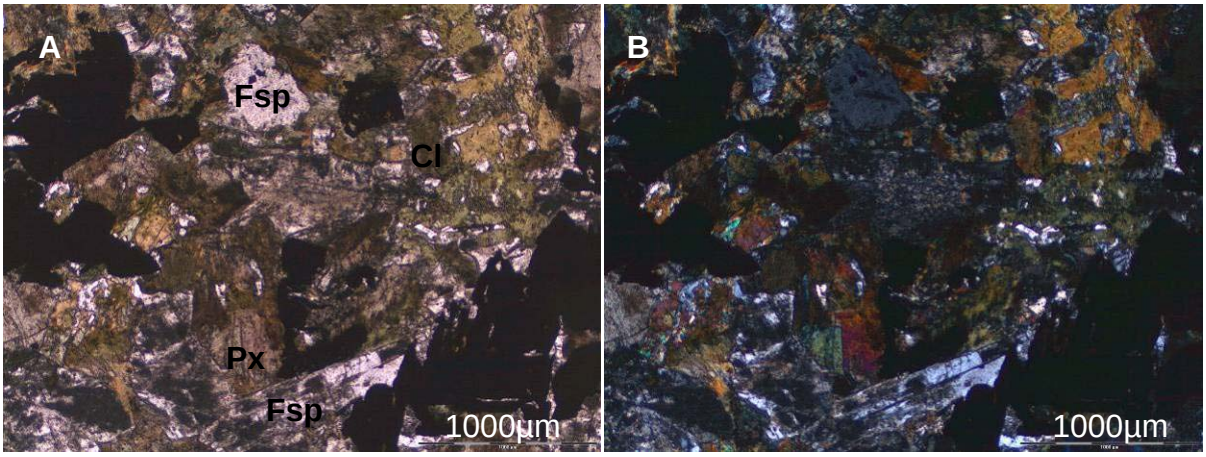

Figure 3.51. Saussuritised plagioclase, large opaque crystals, chlorite and remnants of unaltered pyroxene in BAN1.

Greeff's (1988a) description of the Bank dyke is very similar to what was found in this study. He did detect hornblende, and, in one sample, biotite, which were not found in this study. Opaque minerals in both studies were found to be large and skeletal. Greeff found that they are associated with pyroxenes.

3.2.15 The Speckled Dyke

Figure 3.52. SPE1.

The SPE1 sample (Fig. 3.52) consists of large altered remnants of plagioclase in a fine matrix of chlorite, opaque minerals and quartz (Fig. 3.53). A network of calcite and quartz veins is present (Fig. 3.52). The calcite veins appear to be the youngest. Greeff's study (1988a) of the Speckled dyke is in many ways similar to this study. He did, however, find pyroxene and biotite in some of his samples. Opaque minerals vary in size from tiny specks to large crystals. His findings indicate a somewhat heterogenous mineralogy, with some samples containing no feldspar. This heterogeneity is probably due to differences in degrees of alteration in the dyke. The dyke originally contained large amounts of euhedral plagioclase, and their skeletal remains can still be observed, even though the feldspars are now occasionally absent.

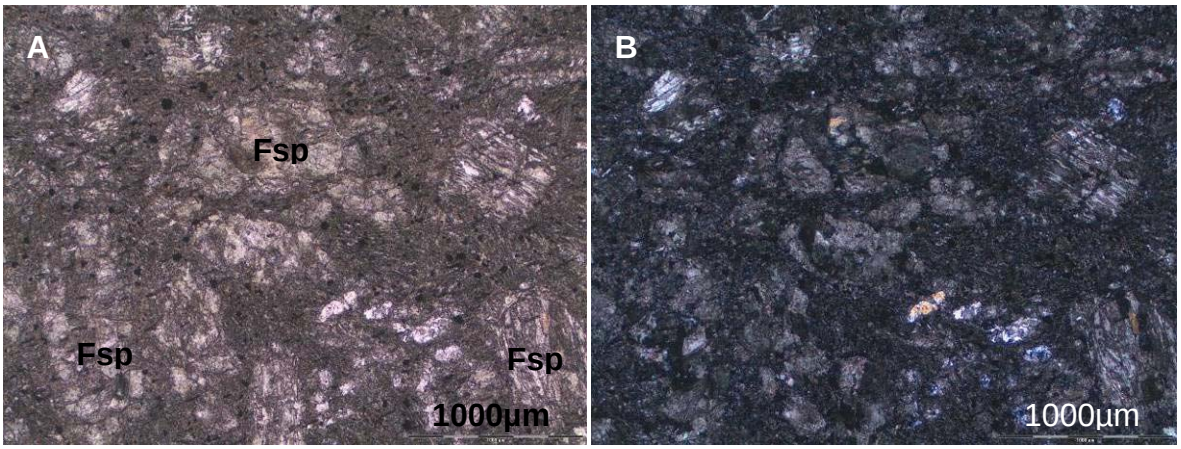

Figure 3.53. Large altered remains of plagioclase in fine matrix in SPE1.

3.2.16 The Twin Dyke

Figure 3.54. TWI1.

TWI1 (Fig. 3.54) is fine-crystalline and consists of quartz, chlorite, opaque minerals and illite (detected by means of XRD). Veins are filled with dark minerals (Fig. 3.54), possibly iron oxides or stringer-like and filled with quartz (Fig. 3.55), with the dark veins being the oldest. Quartz nodules containing sulphides are present,

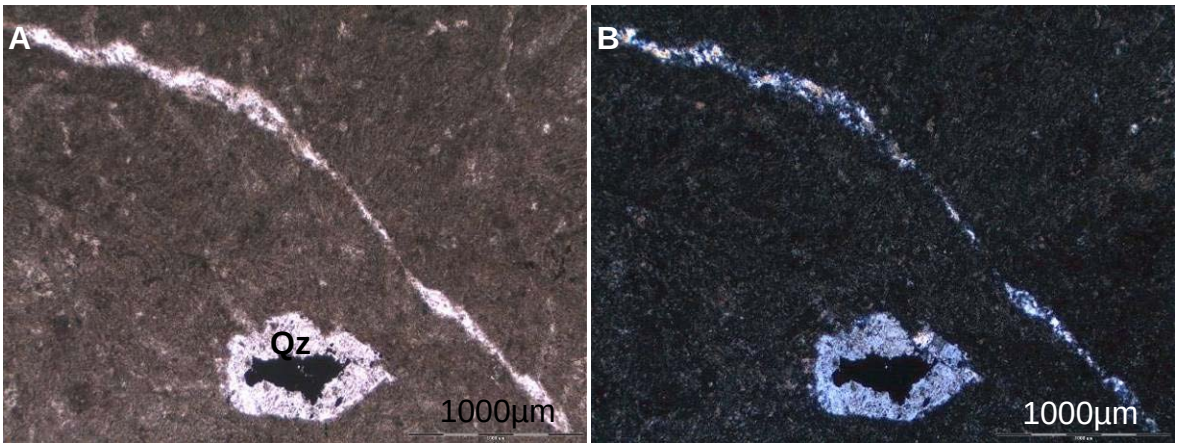

Figure 3.55. TWI1 containing a stringer-like quartz vein and a quartz and sulphide nodule.

Greeff (1988a) studied only one Twin dyke sample. He found biotite and rutile in addition to the minerals found in this study.

3.2.17 The Brazil Dyke

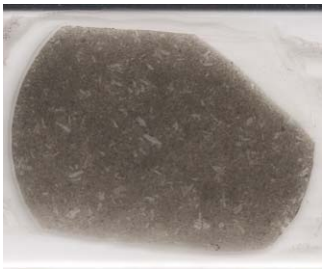

Figure 3.56. BRA2.

BRA2 (Fig. 3.56) is relatively unaltered, with some chloritisation being present in the smaller crystals of the matrix. The plagioclase crystals are fresh enough for their compositions to be determined by means of the Michel-Lévy method, and were found to have a labradoritic composition ($An_{50} – An_{70}$). Clinopyroxene is present as microphenocrysts and are also largely unaltered (Fig. 3.57). Smaller unaltered plagioclase crystals are present in the matrix along with chlorite and sulphides. Quartz, albite and a small amount of actinolite was identified by means of XRD.

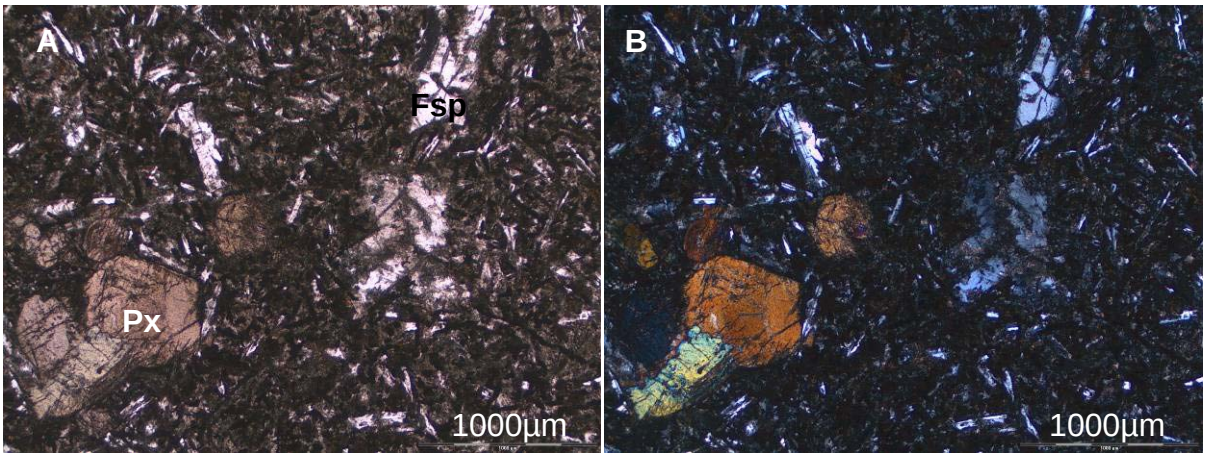

Figure 3.57. The relatively unaltered BRA2 with microphenocrysts of pyroxene in a medium to fine matrix of plagioclase, pyroxene, chlorite and opaque minerals.

Figure 3.58. BRA3.

BRA3 (Fig. 3.58) is from the chill zone of the Brazil dyke. It contains clinopyroxene and slightly altered plagioclase microphenocrysts in a matrix of slightly altered plagioclase and chlorite (Fig. 3.59). Large sulphide nodules are also present. The sample also contains a large altered patch, consisting of chlorite, albite and pyrophyllite, and is cut by a quartz vein (Fig. 3.56). Albite and pyrophyllite were identified by means of XRD (film technique).

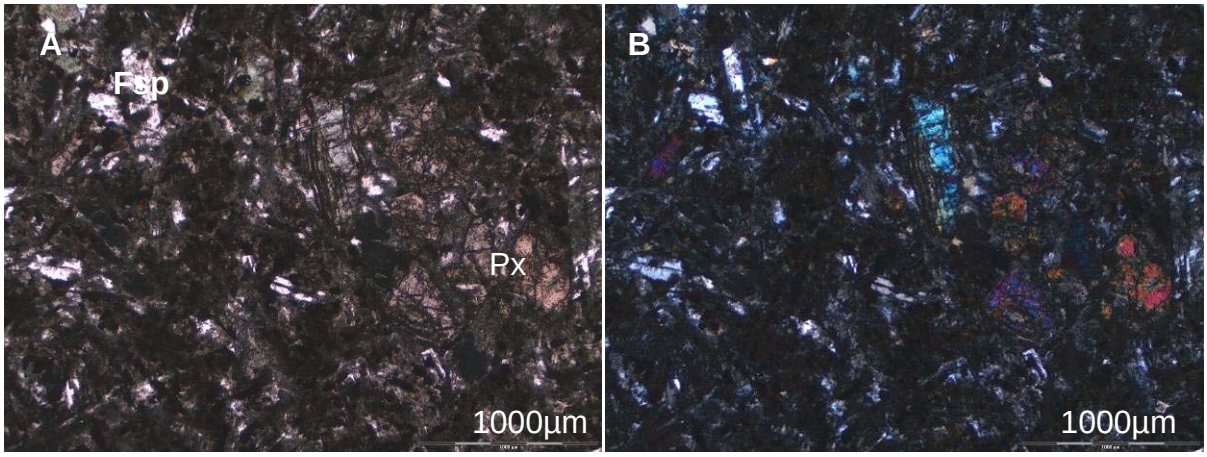

Figure 3.59. Slightly altered plagioclase and pyroxene in BRA3.

Figure 3.60. BRA4.

BRA4 (Fig. 3.60) is medium crystalline with only minor alteration. Clinopyroxene is present along with plagioclase, which was once again identified as labradorite, and small amounts of quartz (Fig. 3.61). Large volumes, up to ±10%, of sulphide minerals are present. BRA4 can be classified mineralogically as a dolerite.

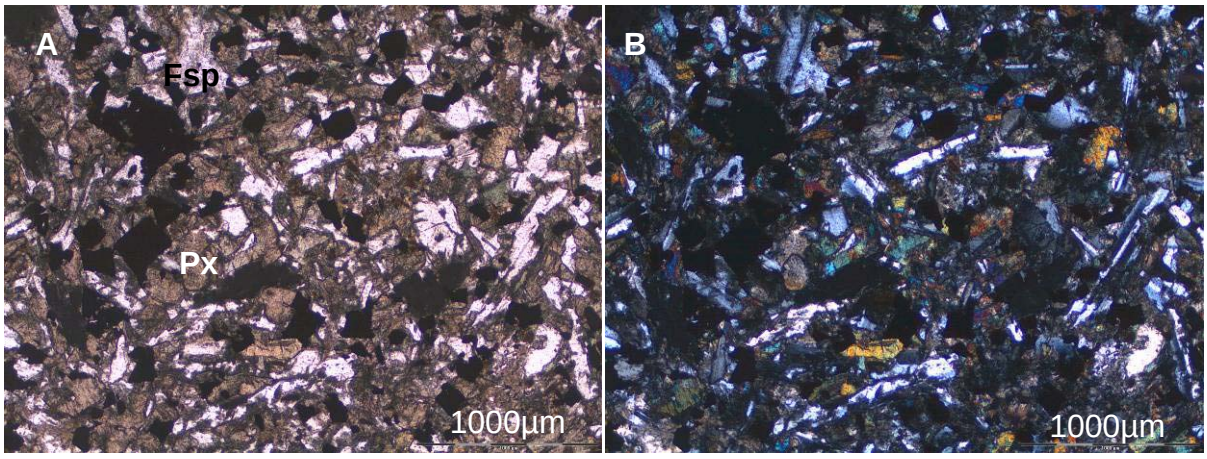

Figure 3.61. The unaltered BRA4. Large volumes of sulphides are present.

3.2.18 The CLA Dyke

Figure 3.62. CLA3.

CLA3 (Fig. 3.62) is medium crystalline and consists of altered remnants of plagioclase, chlorite, epidote, quartz and some altered sphene (Fig. 3.63). Calcite is present in veins.

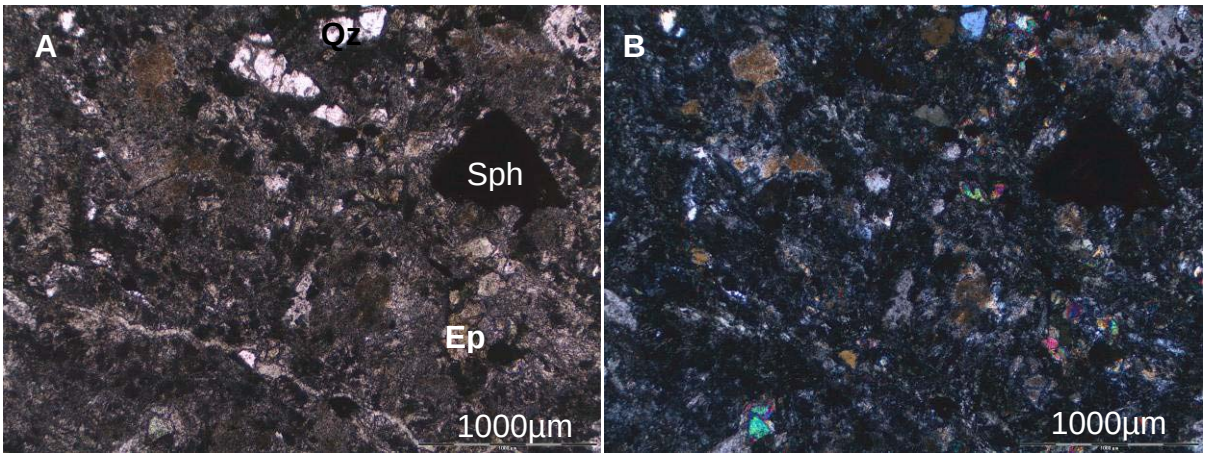

Figure 3.63. A large altered sphene crystal in CLA3. Other minerals are chlorite, epidote and quartz. Calcite is found in veins.

CLA4 (Fig. 3.64) consists of saussuritised feldspar, chlorite, epidote, altered sphene, quartz, and some sulphides. Small remnants of pyroxene are present (Fig. 3.65).

Figure 3.64. CLA4.

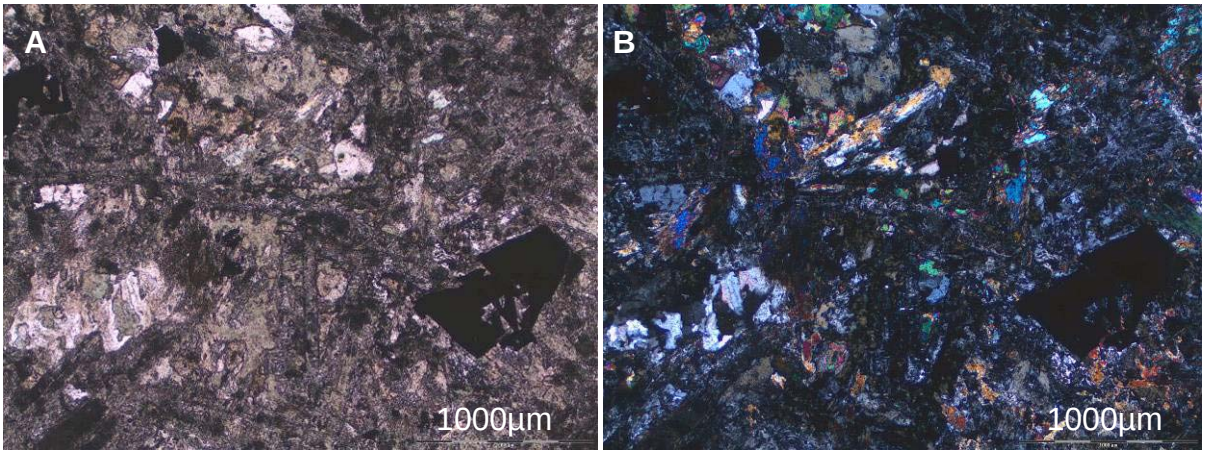

Figure 3.65. Chlorite, quartz, epidote and remnants of unaltered pyroxene in CLA4.

CLA7 consists of altered plagioclase chlorite and epidote, quartz, large opaque mineral crystals and remnants of original pyroxenes (Fig. 3.66).

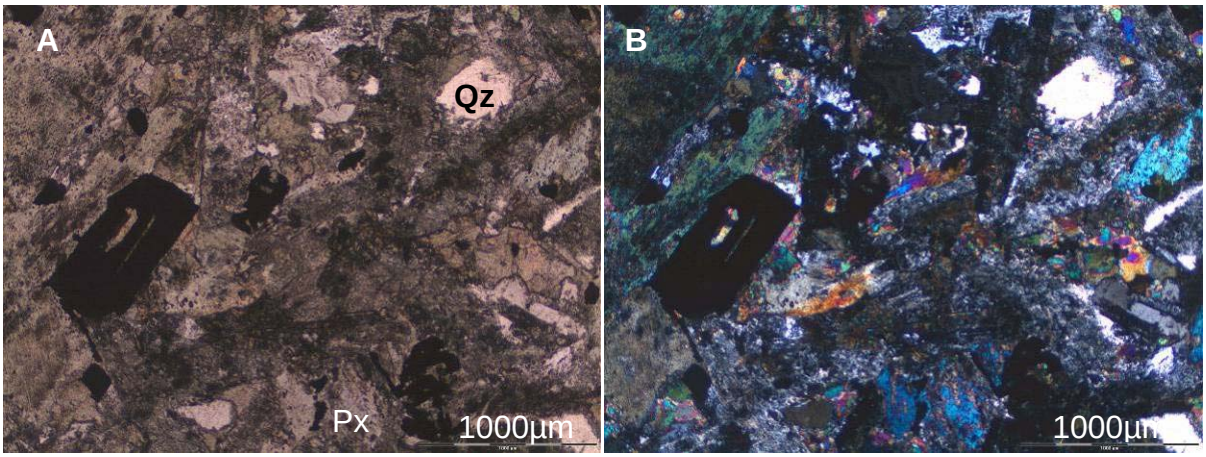

Figure 3.66. A large opaque mineral in along with chlorite, quartz and remnants of pyroxenes in CLA7.

Greeff (1988a) studied one CLA dyke sample. In addition to the minerals found in this study Greeff also found biotite and apatite. Sphene and pyroxene were absent from his sample. All the CLA dyke samples were found to be highly altered.

3.2.19 The KEN Dyke

Figure 3.67. KEN1.

KEN1 (Fig. 3.67) is extremely altered so that only skeletal remains of plagioclase are visible. The sample consists mostly of chlorite and quartz with smaller amounts of iron oxides and opaque minerals (Fig. 3.68).

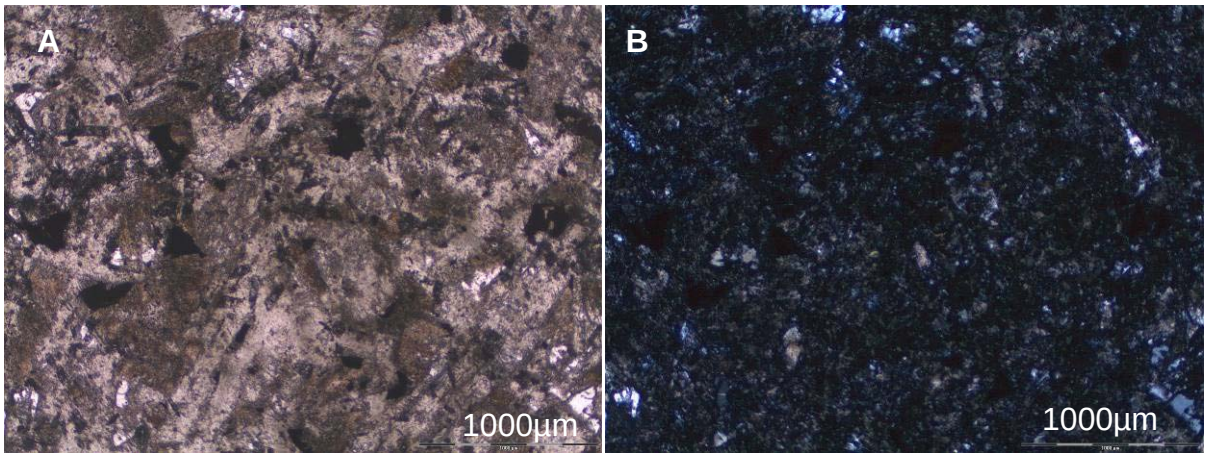

Figure 3.68. Alteration in KEN1. Chlorite and quartz are identifiable optically.

KEN2 (Fig. 3.69) consists of saussuritised plagioclase with some slightly chloritised clinopyroxene clusters occurring. Small amounts of chlorite are present along with some opaque minerals and a quartz vein (Fig. 3.70).

Figure 3.69. KEN2.

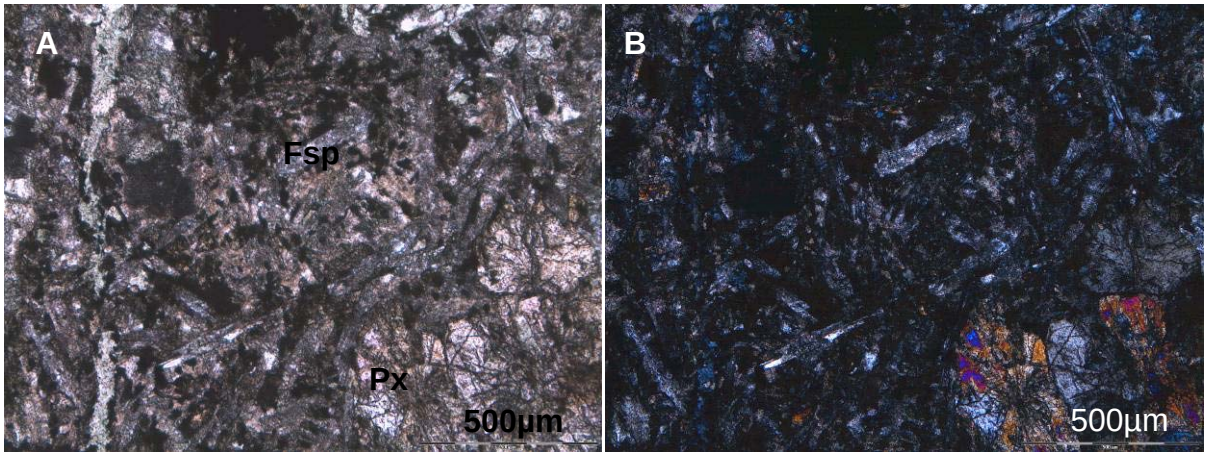

Figure 3.70. A chloritised pyroxene cluster in saussuritised plagioclase and opaque minerals in KEN2.

3.2.20 The Swannie Dyke

Figure 3.71. SWA2.

SWA2 (Fig. 3.71) is medium crystalline and consists of chlorite, epidote, actinolite, quartz, calcite and altered sphene (Fig. 3.72). Feldspar is almost completely absent and opaque minerals make up less than 1% of the total rock volume.

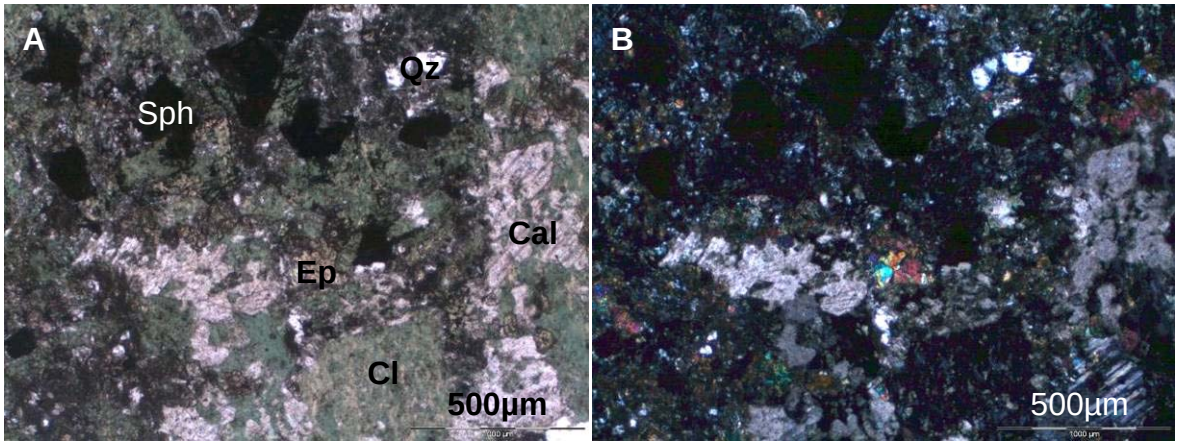

Figure 3.72. Chlorite, quartz, calcite, sphene, epidote and opaque minerals in SWA2

3.2.21 The "Unknown" Samples

Figure 3.73. UNK1.

UNK1 (Fig. 3.73) is medium to fine crystalline and consists of chlorite, both scattered and in nodules, and quartz with some iron oxide staining (Fig. 3.74). Veins are filled with quartz and calcite.

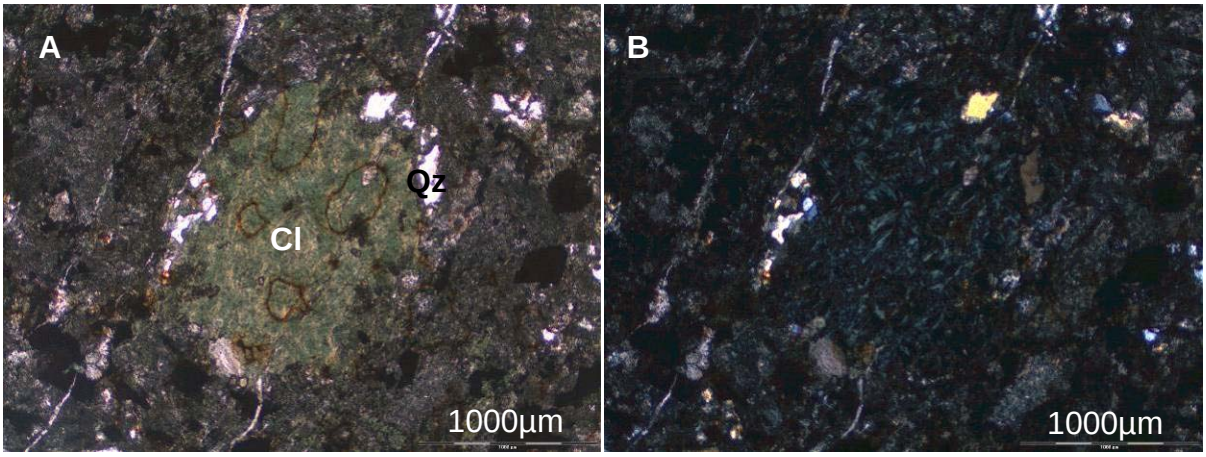

Figure 3.74. One of the chlorite nodules rimmed by quartz and stained by iron oxide in UNK1.

UNK2 consists of large completely altered plagioclase crystals, chlorite, small amounts of epidote and large crystals of opaque minerals (Fig. 3.75). Veins are filled with calcite.

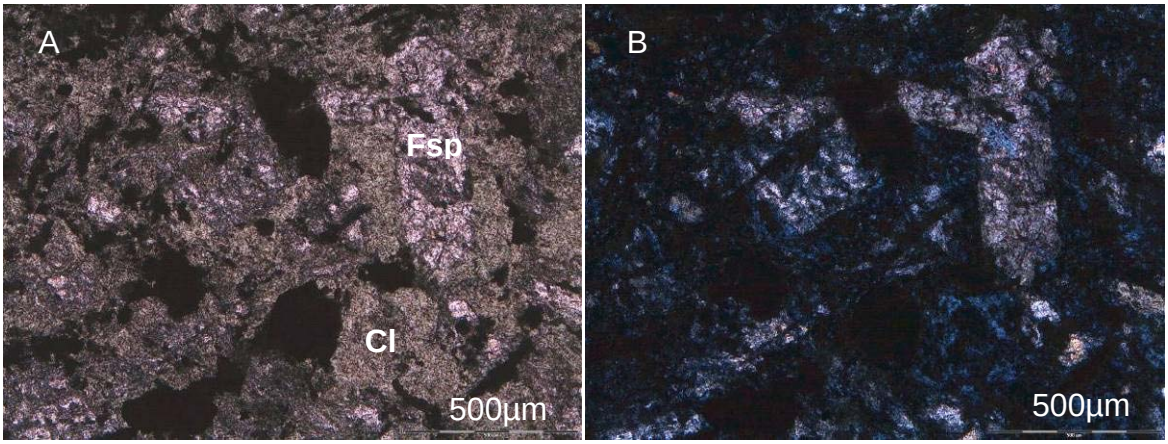

Figure 3.75. Highly altered plagioclase and chlorite and opaque minerals in UNK2.

UNK4A (Fig. 3.76) is fine crystalline and consists of chlorite, albite, epidote and quartz with a vein containing chlorite, quartz, calcite and opaque minerals (Fig. 3.77).

Figure 3.76. UNK4A.

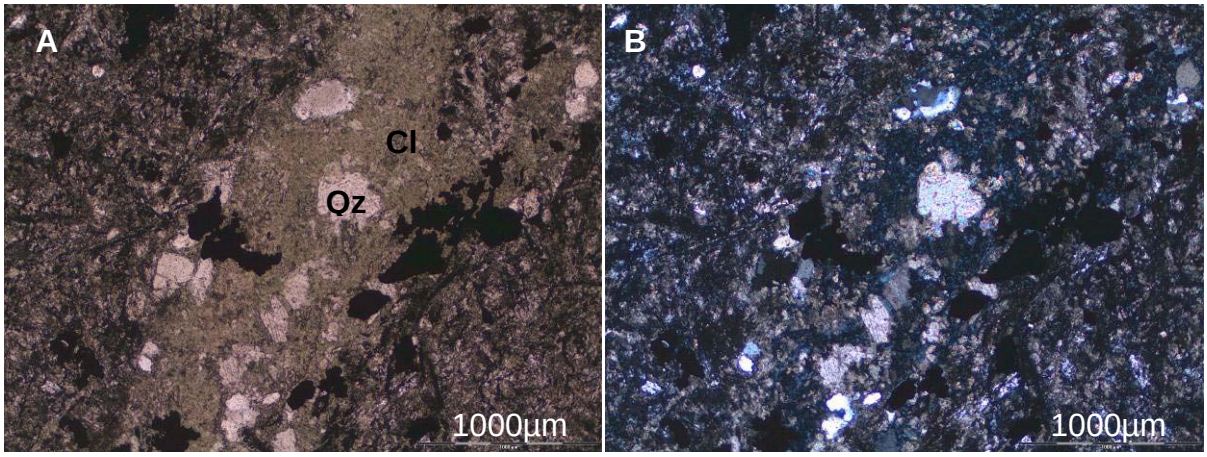

Figure 3.77. Vein containing chlorite, quartz and opaque minerals in UNK4A.

UNK6 (Fig. 3.78) is medium to fine crystalline. The altered remains of plagioclase are still present along with chlorite, quartz and some calcite (Fig. 3.79). Sulphide nodules surrounded by quartz also occur.

Figure 3.78. UNK6.

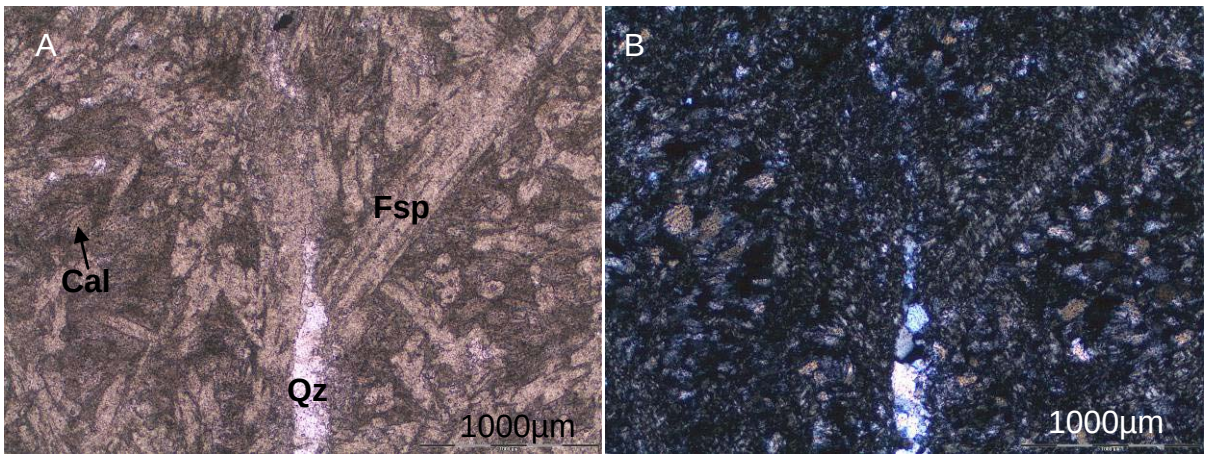

Figure 3.79. Altered remains of plagioclase in a fine matrix of chlorite, along with quartz and calcite in UNK6.

UNK7 (Fig. 3.80) is medium to coarse crystalline and contains chlorite, large saussuritised plagioclase crystals (Fig. 3.81), small remnants of altered pyroxene and biotite, large calcite crystals and some opaque minerals (Fig.3.82) as well as illite-montmorillonite. UNK7 is mineralogically very similar to the Peggy dyke samples.

Figure 3.80. UNK7.

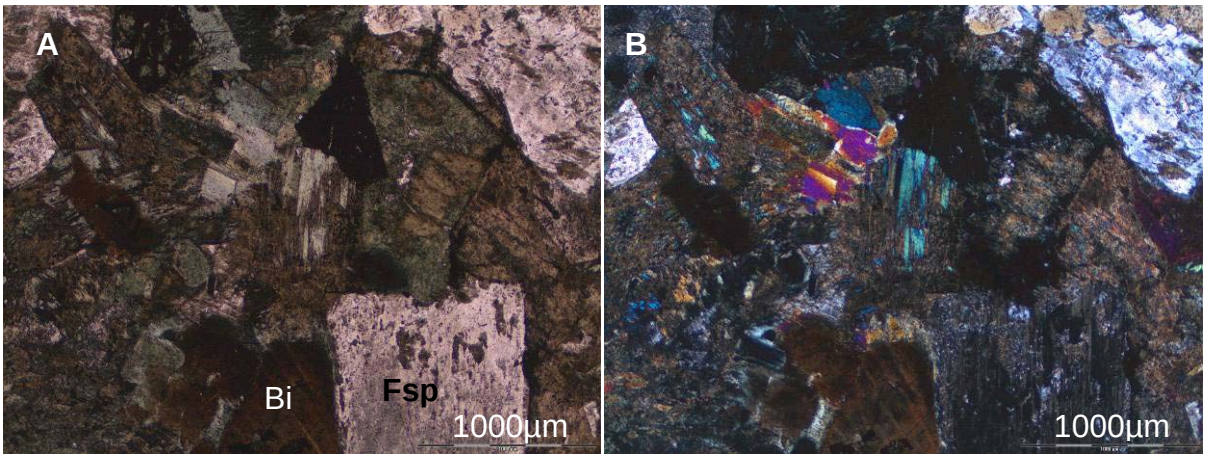

Figure 3.81. Large saussuritised euhedral plagioclase crystals, remnants of biotite, and chlorite.

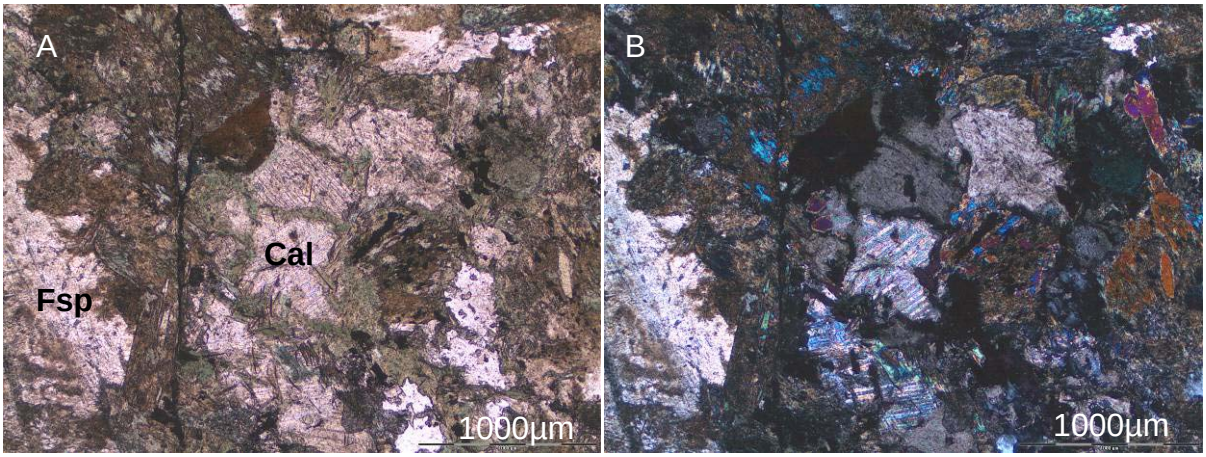

Figure 3.82. Large patches of calcite along with plagioclase and remnants of pyroxene.

Figure 3.83. 120A2 from Unknown 8.

120A2 (Fig. 3.83) is one of three samples that belong to a previously unknown dyke labelled Unknown 8 in this study. It consists predominantly of saussuritised feldspar, chlorite intergrown with actinolite, and smaller amounts of quartz and epidote (Fig. 3.84). Muscovite and small sphene crystals are found in lesser amounts. The sample is cut by a quartz vein. XRD analysis indicates the presence of montmorillonite.

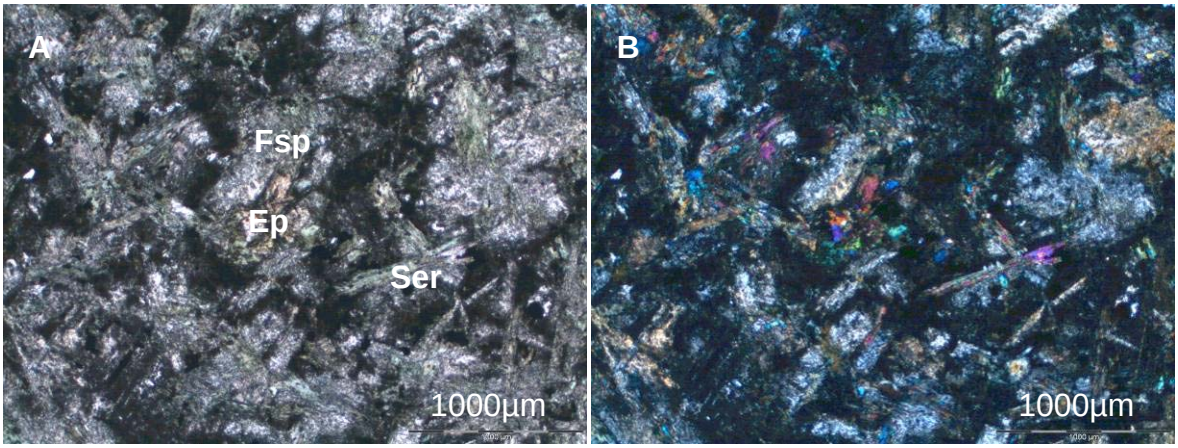

Figure 3.84. Altered feldspar, chlorite, epidote and sericite in 120A2. Ser=Sericite.

Figure 3.85. 120B2 from Unknown 9.

120B2 (Fig. 3.85) is from the dyke labelled Unknown 9 in this study. It is medium to fine crystalline and consists predominantly of completely altered feldspar, chlorite

and quartz. Small opaque minerals, possibly chalcopyrite, are present and fractures are filled with chlorite and iron oxides/hydroxides (Fig. 3.86).

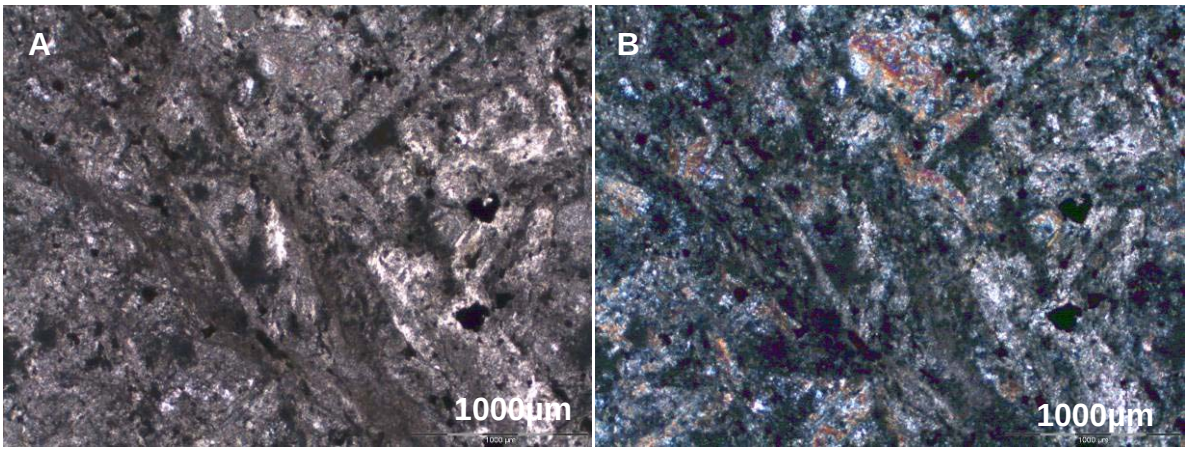

Figure 3.86. Altered feldspar, and chlorite in 120B2. The fracture is filled with chlorite and iron oxides/ hydroxides.

3.3 Discussion

The chlorite + actinolite + epidote + albite + quartz mineral assemblage is characteristic of greenschist facies metamorphism in metabasites, but either chlorite or actinolite may be absent. Greenschist facies metamorphism has a lower temperature limit of 400°C. However, it is possible for greenschist facies assemblages to form at lower temperatures in the presence of CO_2-rich fluids, with laumontite, prehnite and pumpellyite reacting with CO_2 to form calcite, epidote, quartz and chlorite (Yardley, 1989). Sphene is the most common Ti-rich mineral in metabasites in the greenschist facies, but ilmenite and rutile can occur instead. The formation of the different minerals depends on the bulk-rock geochemistry as well as CO_2 potential. Sphene is stable when the mole fraction of CO_2 is less than 0.1 (Miyashiro, 1994).

In constrast to higher-grade metamorphism, the principal effect during low-grade metamorphism is the hydration of anhydrous minerals (Robinson and Bevins, 1999). According to Schiffman and Day (1999) low-grade metamorphic rocks such as metabasites can display compositional heterogeneity that can be visible in outcrop, hand specimen, or even on thin section scale. Such “meta-domains” occur as a result of original heterogeneity being enhanced by fluid-rock interaction, which is

controlled by the porosity and permeability of the rock. For example, fractured sections of metabasite dykes may become enriched in calcium due to the filling of voids. This process can clearly be seen in many of the dykes where veins have become calcite-filled.

Compositional heterogeneity can clearly be seen in dykes such as the Peggy and Speckled dykes. Similar heterogeneity is found in the Alberton Formation according to Winter (1995), and can also be seen in the "Ventersdorp lava" samples studied by Greeff (1988b). The heterogeneity usually occurs as a result of variable degrees of alteration. Good examples would be the Peggy dyke, where some samples contain hornblende and biotite and others do not, and the CLA dyke where remnants of pyroxenes were found in this study, but not in Greeff's study. The composition of the primary minerals of mafic rocks determines which secondary minerals will form during low-grade metamorphism, e.g. olivine and orthopyroxenes are pseudomorphed by Mg-smectite, serpentine and talc. The absence of serpentine and talc in all samples indicate that no olivine was present.

Ca and Al are released from plagioclase and contribute towards the formation of calcite, prehnite, pumpellyite, epidote, and sphene, causing these minerals to form in veins, vesicles and within the primary plagioclase itself. The removal of Ca from the plagioclase means that the resulting plagioclase has an albitic composition. The replacement of clinopyroxene by actinolite and lesser chlorite (uralitisation) is characteristic of greenschist metamorphism. The formation of actinolite requires, at least in part, the decomposition of significant amounts of chlorite, and forms after chlorite, albite, epidote and quartz have formed. Primary ilmenite and magnetite can be pseudomorphed by low Ti-magnetite or sphene, which is able to form as a result of aluminium being released in the process of albitisation (Schiffman and Day, 1999).

3.4 Normative Mineralogy

CIPW norms were calculated in GCDkit (Janousek *et al.*, 2007) using major element data (See Appendix C), and averages for each dyke are given in Table 3.1. The major element concentrations were recalculated to 100% volatile free. FeO and Fe_2O_3 were calculated from total Fe (given as Fe_2O_3 in Appendix C) using a

Fe_2O_3/FeO ratio of 0.15 (Middlemost, 1989). The normative mineralogy for each sample is included in Appendix B. It should be kept in mind that CIPW norms assume the absence of water, and therefore no biotite or hornblende is calculated. This is clearly not an accurate reflection of many of the rocks, as primary biotite and hornblende is visible, e.g. in the Peggy dyke. The fact that some elements have probably been mobilised during greenschist metamorphism will also have an influence on the normative mineralogy.

The observed plagioclase contents of the samples correlate reasonably well with the calculated norm, although all anorthite has been converted to albite (one of the constituents of saussurite (Nesse, 2004)). In the case of the Jeans dyke (JEA1), plagioclase has been converted to calcite. Samples with large amounts of modal chlorite do not necessarily have high normative pyroxene percentages. However, pyroxene is not the only source of chlorite during alteration, and biotite and hornblende can also be altered to chlorite. The presence of normative corundum is likely due to the apparent enrichment of aluminium as a result of the depletion of elements such as Na, K and Ca.

Table 3.1. Average CIPW norms for the dykes. Major element data taken from Table C.1. n = number of analyses.

	Peggy n=6	Georgette n=3	Skelm n=5	Soll n=3	Kudu n=1	Sill n=2	Jeans n=3	Friday n=9
Quartz	1.65	27.19	11.82	34.31	20.44	23.02	14.62	17.04
Corundum	0	2.15	0.00	9.07	0	5.67	4.01	5.66
Orthoclase	7.92	0.06	0.33	0	0.06	0.62	0	0
Albite	35.94	7.36	14.05	5.50	16.75	5.37	5.64	1.29
Anorthite	11.15	21.39	29.44	7.76	30.54	15.90	25.07	22.04
Diopside	18.11	3.75	9.69	0.00	2.7	8.97	4.54	3.91
Hypersthene	19.70	34.52	26.90	37.13	25.44	33.54	37.11	38.94
Olivine	0	0	0	0	0	0	0	0
Magnetite	2.47	1.95	2.90	2.94	2.00	2.68	3.02	3.74
Ilmenite	2.61	1.52	4.02	2.98	1.69	3.41	4.66	5.83
Apatite	0.48	0.19	0.93	0.44	0.38	0.96	1.40	1.73

Table 3.1. (continued).

	Lib n=1	Lit. Tumi n=1	PE n=2	Lava n=1	Amigo n=4	Bank n=7	Speckled n=5	Twin n=2
Quartz	16.73	7.54	11.94	5.13	23.53	5.81	32.87	43.62
Corundum	0	0	0.65	0.55	8.90	0.08	9.15	14.26
Orthoclase	0	4.08	0	6.62	0.03	1.98	0	11.85
Albite	10.32	21.15	6.81	34.61	6.33	16.22	0	1.27
Anorthite	29.94	22.16	31.50	24.97	13.18	28.81	7.16	0.21
Diopside	1.28	8.36	2.51	0	0	10.79	0	0
Hypersthene	30.78	26.66	35.31	23.96	37.44	27.99	47.35	25.40
Olivine	0	0	0	0	0	0	0	0
Magnetite	3.38	3.28	3.35	1.87	3.14	3.03	2.57	2.02
Ilmenite	5.21	4.85	6.08	1.96	6.14	5.42	0.92	1.22
Apatite	2.04	1.99	1.93	0.36	1.44	0.81	0.14	0.20

Table 3.1. (continued).

	Brazil n=8	CLA n=9	Ken n=7	Swannie n=3	UNK1 n=1	UNK2 n=1	UNK3 n=1	UNK4 n=2
Quartz	9.98	15.63	7.21	20.40	7.66	2.301	20.62	16.74
Corundum	1.62	6.85	2.07	9.21	0	0.405	0	1.68
Orthoclase	1.00	0	0.33	0	0	0	5.73	0
Albite	14.20	4.23	13.61	0	8.12	4.739	14.47	12.06
Anorthite	25.28	22.07	26.28	11.87	31.41	37.611	33.14	27.75
Diopside	8.35	3.81	9.30	3.36	12.87	0	8.29	6.30
Hypersthene	29.66	41.71	33.31	43.39	28.97	42.028	11.81	26.28
Olivine	0	0	0	0	0	0	0	0
Magnetite	3.15	3.06	3.12	4.15	3.34	4.132	0.96	2.75
Ilmenite	5.70	2.39	4.71	5.97	5.97	6.84	1.92	4.24
Apatite	0.87	0.31	0.72	1.84	1.80	2.084	0.43	0.79

Table 3.1. (continued).

	UNK6 n=1	UNK7 n=1	UNK8 n=3	UNK9 n=3
Quartz	3.98	5.73	17.33	24.84
Corundum	9.22	0	0.90	4.58
Orthoclase	0	4.61	4.49	7.21
Albite	31.56	32.24	19.26	6.88
Anorthite	0.19	11.29	24.57	21.90
Diopside	0	10.08	9.23	0
Hypersthene	54.73	29.55	20.24	30.30
Olivine	0	0	0	0
Magnetite	3.18	2.71	1.87	2.12
Ilmenite	1.16	2.57	1.75	1.81
Apatite	0.17	0.45	0.39	0.340

Silica concentrations show the same apparent increase, but some silica may also have been added to the system in the form of veins, resulting in normative quartz. No modal rutile was observed.

3.5 Conclusion

The petrographic study of the dykes revealed that all the dykes, with the exception of the Brazil dyke, have undergone low-grade metamorphism. Primary mafic minerals such as pyroxenes have mostly been converted to chlorite, actinolite and epidote, and feldspars have been albitised. In some instances, remnants of the original minerals can still be seen, e.g. in the Peggy dyke where hornblende and biotite are still present, the Amigo Dyke where clusters of largely intact clinopyroxene phenocrysts occur, and in the CLA dyke where small amounts of pyroxene remain unaltered. In comparing dyke samples from this study with each other and with those from Greeff (1988a) it becomes clear that compositional heterogeneity exists within the dykes themselves. The heterogeneity is likely the result of differences in the degree of alteration along dykes, but original heterogeneity could have made a significant contribution. Veins are a common feature in most of the dykes and are mostly filled with calcite and quartz, but some include epidote, chlorite, iron oxides and sulphides in veins. An interesting case is the Skelm dyke, where veins are filled almost exclusively with epidote.

The Brazil dyke is unusual in the sense that it shows much less alteration than any of the other dykes, and, apart from small amounts of chloritisation, displays an almost intact primary mineralogy. The Friday dyke is the only case where prehnite was identified, and the Jeans dyke, as well as Unknown 7, contains large patches of calcite outside veins and in the rock itself. Apart from these few “odd” characteristics it would be very difficult to identify most of the dykes by using petrographic methods alone. It would be advisable to compile a library of petrographic data including numerous samples from each dyke in order to obtain a clearer picture of the petrographic characteristics of each dyke. This could in turn lead to a better understanding of the mechanisms involved in their alteration and, possibly, to an identification system based on mineralogy.

Chapter 4: Geochemistry I

4.1. Major and Trace Element Statistics

4.1.1 Major Element Oxides

In a study on the dykes in the Central Welkom Goldfield, Rompel (1995) found that very little chemical variation is present within a specific dyke, and that dykes can be traced according to their chemical composition along their strike. Therefore, if chemical variation does occur, it may indicate that the elements have been mobilised by low-grade metamorphism to varying degrees. Rompel (1995) also found that individual dykes could be fingerprinted according to their chemistry, and therefore, large variation, especially in those elements that are regarded as immobile, would indicate different origins for samples.

Box and whisker diagrams, such as those plotted in Figs. 4.1 to 4.5, are very useful when examining the element variations within and between dykes. The plot represents the median as the solid black rectangle in the box. In cases where only one sample is present (e.g. Ventersdorp lava), this rectangle is the only feature plotted. The dashed lines ("whiskers") indicate the maximum and minimum, non-outlier, values in the range. According to convention, the whiskers can be no longer than 1.5 times the length of the box, and any data values that are not contained in this range are seen as outliers, and marked as circles. The box represents the range between the upper and lower quartiles of the data. The quartiles are values halfway between the maximum/minimum values and the median (Verzani, 2005). The box plots were constructed using GCDkit (Janousek *et al.,* 2007), an R-based geochemistry software package.

The most notable feature in the box plots is the extreme range in SiO_2, TiO_2, MgO, and CaO concentrations in the Sill (Figs. 4.1, 4.3 and 4.4). This may indicate that, what was assumed to be a single intrusive is in reality two different intrusives. This possibility will be investigated further in Chapter 5. At first glance there seems to be great variation in P_2O_5 concentrations, but this is due to the large scale of the plot (Fig. 4.4). CaO (Fig. 4.4), Na_2O and K_2O (Fig. 4.5) show large ranges in almost all the dykes. These large ranges are probably due to the mobilisation of the elements in question during metamorphism, a possibility that is further strengthened by the

absence of K_2O in eight of the dykes. However, the heterogeneous nature of alteration, as well as the fact that not all dykes are equally altered may cause elements such as K_2O to be removed from some dykes or even from some sections of the dykes and not from other. This possibility will be investigated further in a following section.

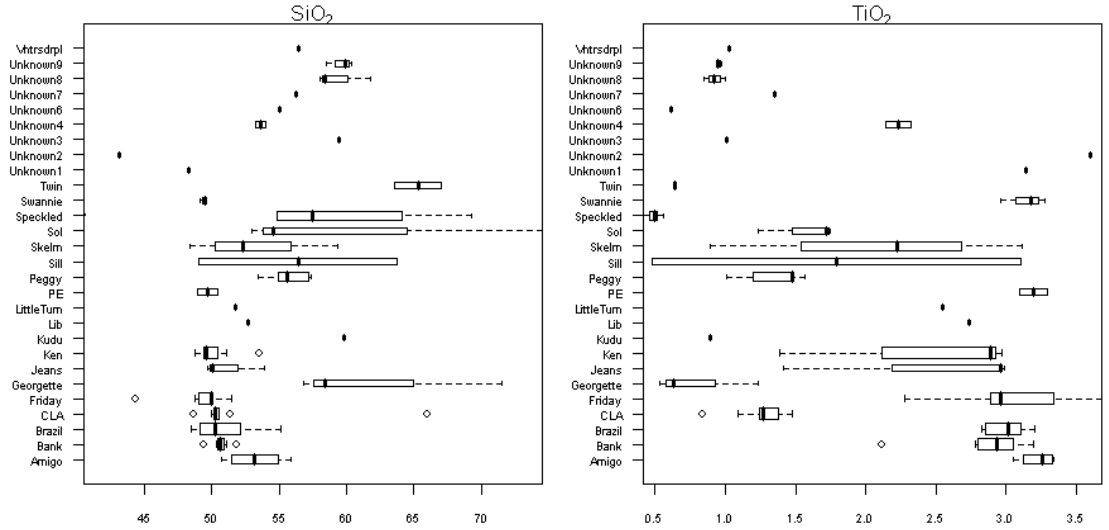

Figure 4.1. Box plots for SiO_2 and TiO_2, showing small SiO_2 ranges in most of the dykes, but large ranges for SiO_2 and TiO_2 in the Sill. Concentrations in wt%.

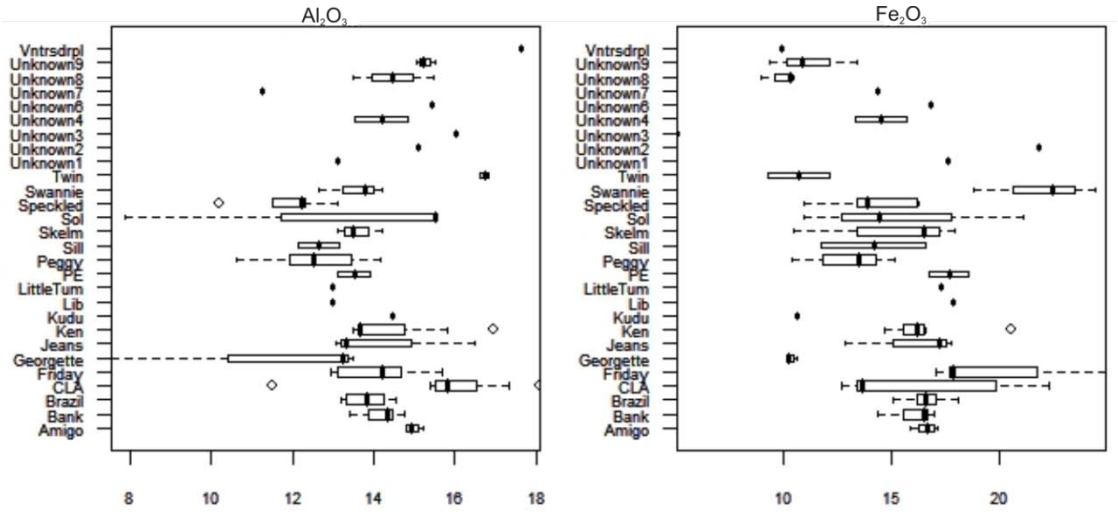

Figure 4.2. Box plots for Al_2O_3 and total Fe_2O_3 showing some variation for both oxides. Concentrations in wt%.

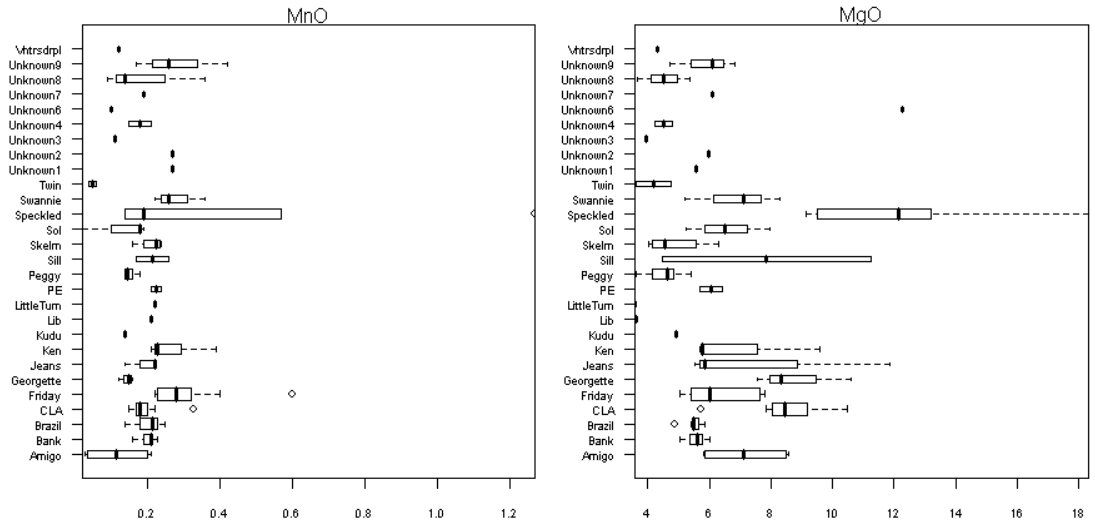

Figure 4.3. Box plots showing little variation in MnO and more variation in MgO. Concentrations in wt%.

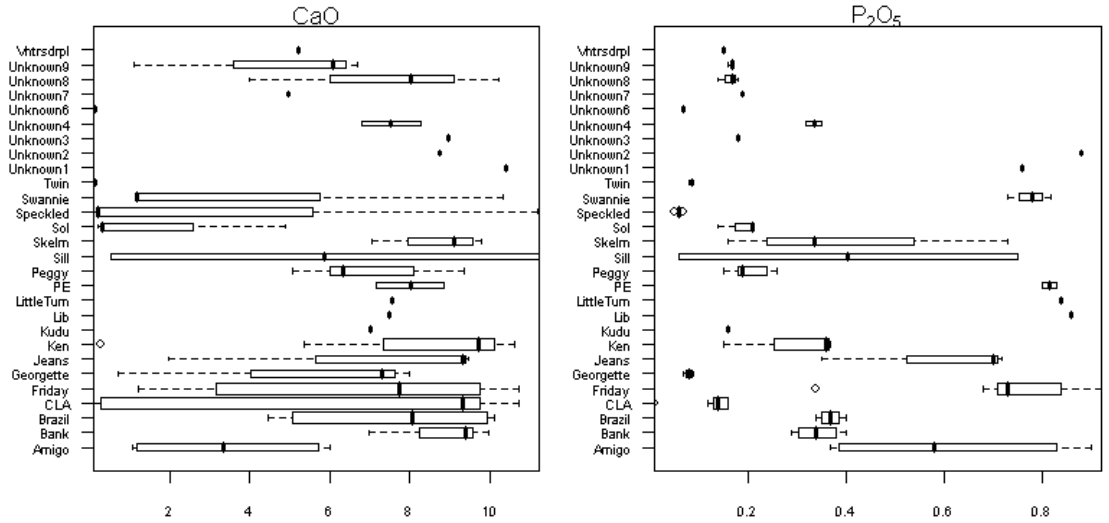

Figure 4.4. Box plots for CaO and P_2O_5, showing large CaO ranges for all dykes, but small differences in P_2O_5 concentrations. Concentrations in wt%.

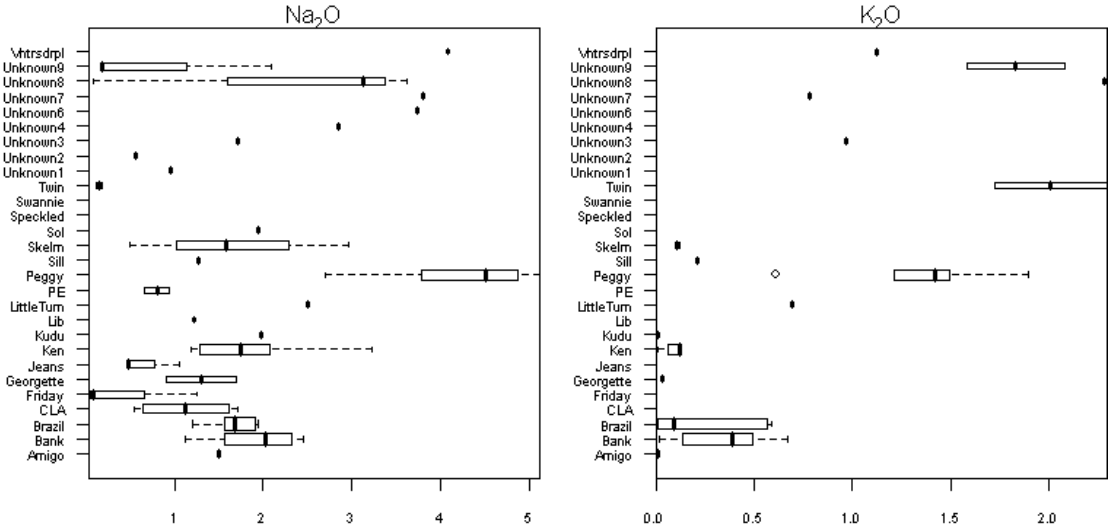

Figure 4.5. Box plots showing large variation in Na_2O K_2O concentrations. Concentrations in wt%.

4.1.2 Trace Elements

Of the trace elements, only Cr, Ni, Sr, Rb, Zr and Y (concentrations given in ppm) are included in the statistical investigation because they are used in subsequent geochemical classifications. Cr contents for all the dykes fall in a relatively small range (Fig. 4.6). Two exceptions are the Sill and the Speckled dyke, with the Speckled dyke having not only a much wider range of Cr concentrations, but also much higher Cr concentrations than any of the other dykes. In the CLA dyke CLA5 plots as an outlier with a much higher Cr content than the other CLA samples. The dykes' Ni contents (Fig. 4.6) are much more varied than the Cr contents. The Sill, Soll, Georgette and Jeans dykes have very large Ni ranges and CLA5 is once again an outlier, indicating either the presence of a cumulate effect or the sampling of a different intrusive.

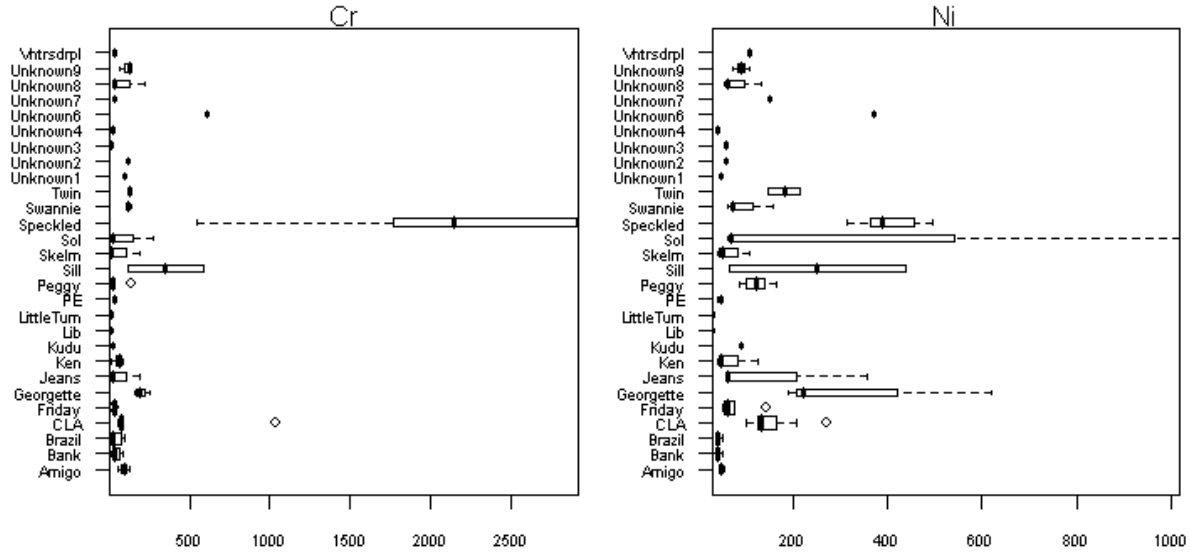

Figure 4.6. Box plots showing little variation in Cr contents, but some variation in Ni contents.

Sr concentrations vary greatly within dykes, and similar variation is found in Rb concentrations (Fig. 4.7). Sr and Rb largely mirror the behaviour of Ca and K respectively, due to their chemical similarity to these elements (White, 2007). This is reflected in the box plots. Y and Zr display very similar trends (Fig. 4.8): The largest ranges in both elements are in the Sill, but large ranges of both elements are present in the Amigo and Skelm dykes as well. The Little Tumi and Lib dykes have the highest Zr concentrations, exceeding 450 ppm.

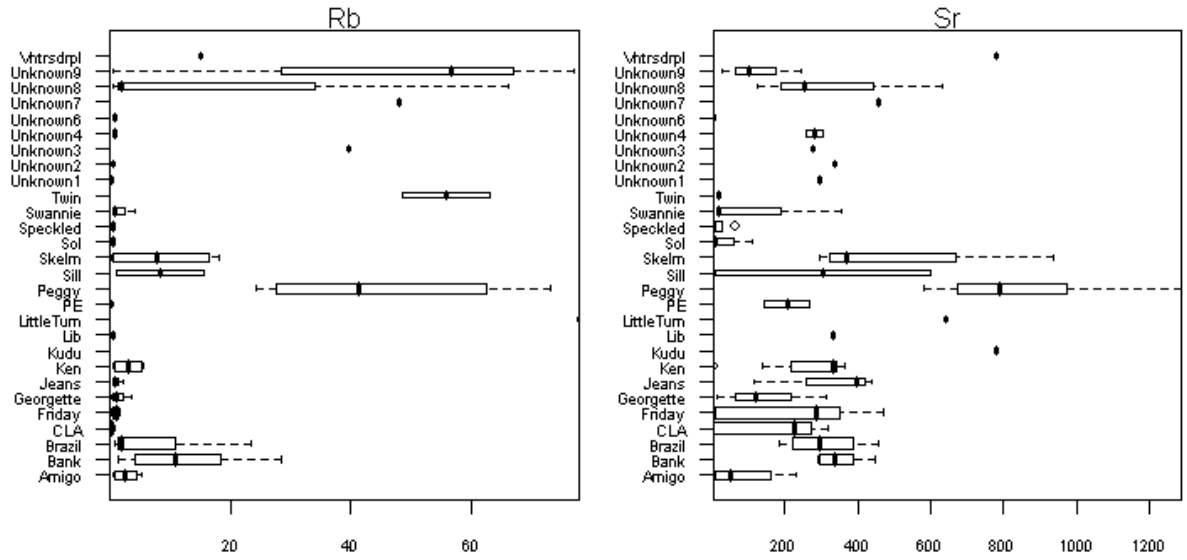

Figure 4.7. Box plots showing large variation in both Rb and Sr concentrations.

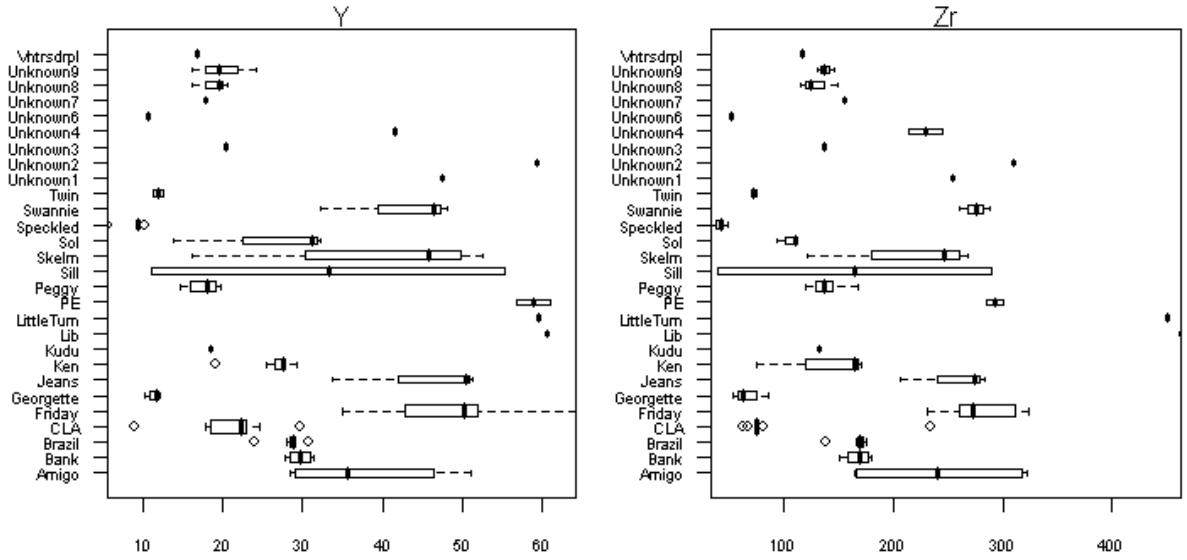

Figure 4.8. Box plots showing some variation for both Y and Zr.

4.2 Element Mobility

Since most of the dykes have undergone greenschist metamorphism it is likely that certain elements have been redistributed. Bowen (1984a) noted that K, Na, Mn, Rb and Ba were extremely mobile in the Ventersdorp lavas and cannot be used to make any deductions on their geochemistry. In his study on the geochemistry of the Klipriviersberg group, Linton (1992) used the following technique, first introduced by Palmer *et al.* (1986) (in Linton, 1992), to test element mobility: An immobile element is selected as the divisor for element ratios. A second immobile element is used as the numerator for the x-axis. The unknown element is used as the y-axis

numerator. Zr (as divisor) and Ti (as x-axis numerator) are popular choices as their analytical precision is good and both are regarded as being immobile. In addition, both are highly incompatible in basalts and fractionation does not produce dramatic fluctuations in their concentrations (Linton, 1992). In order to take the possible influence of fractionation and partial melting into account, Linton (1992) divided his lava samples into three groups based on their Mg content. This technique was also applied to the samples in this study. If the element in question was immobile, samples from the different MgO groups should plot more or less together. On the other hand, if vertical scatter occurs in the plots it would indicate mobility of the element.

In Linton's study (1992), samples in the same Mg range clustered together to form three distinct groups, a trend which was not observed in this study where the distinction is more complex. This can be ascribed to the fact that the dyke samples are more than likely related to different stratigraphic units. The plots (Fig. 4.9 A to M) indicate that the mobility of an element appears to be related to its Mg content. SiO_2 (A), Fe_2O_3 (B), MnO (C), CaO (E), Na_2O (F) and Y (M) show the most scatter in the >9% MgO range. Al_2O_3 (D) and K_2O (H) are most scattered in the <6% MgO range, and Cr and Ni being the most scattered in the intermediate range MgO. K_2O is completely absent from the 6 – 9% MgO range. This may indicate that the intermediate MgO rocks are older than the rocks with higher and lower MgO contents, and that they have therefore been subjected to longer periods of metamorphism. TiO_2 and Zr mobility is impossible to determine in the ratio plots, but if the box plots show similar variation for these elements as for Y, and it is therefore likely that they have also been mobilised (Fig 4.1 and 4.8) and that using their ratios as x-axis values may lead to misleading conclusions. The mobility of these elements will be discussed in Chapter 5.

When the ratio plot patterns from this study are compared with those done by Linton it would seem that the dyke chemistry has been changed far more than that of the Ventersdorp lavas studied by Linton. However, this is possibly an unwarranted conclusion to make as it is not known to what extent the different possible origins of the dykes can influence the plots, even though most primary magmatic effects have been compensated for by separating groups on the grounds of MgO content. In some plots, notably in the SiO_2 and Al_2O_3 ones (Fig. 4.10), smaller groups form

within larger groups; these smaller groups are mostly made up of samples from the same dykes.

In a study such as this where individual intrusives are investigated it probably makes more sense to use box plots to determine which elements have been mobilised. The reasoning behind this is that the ratio plots give a generalised view of which elements were mobile, but the box plots give an indication of which elements were mobile in individual dykes. The ratio plot also can mask effects of Ti and Zr mobility because they may not be as immobile as normally assumed. Another advantage of the box plots is that they show where outliers are present e.g. in CLA dyke (Fig. 4.1, 4.3 and 4.6). An outlier may indicate that multiple sampling of supposedly the same intrusive has resulted in the sampling of an unrelated intrusive which is in close proximity.

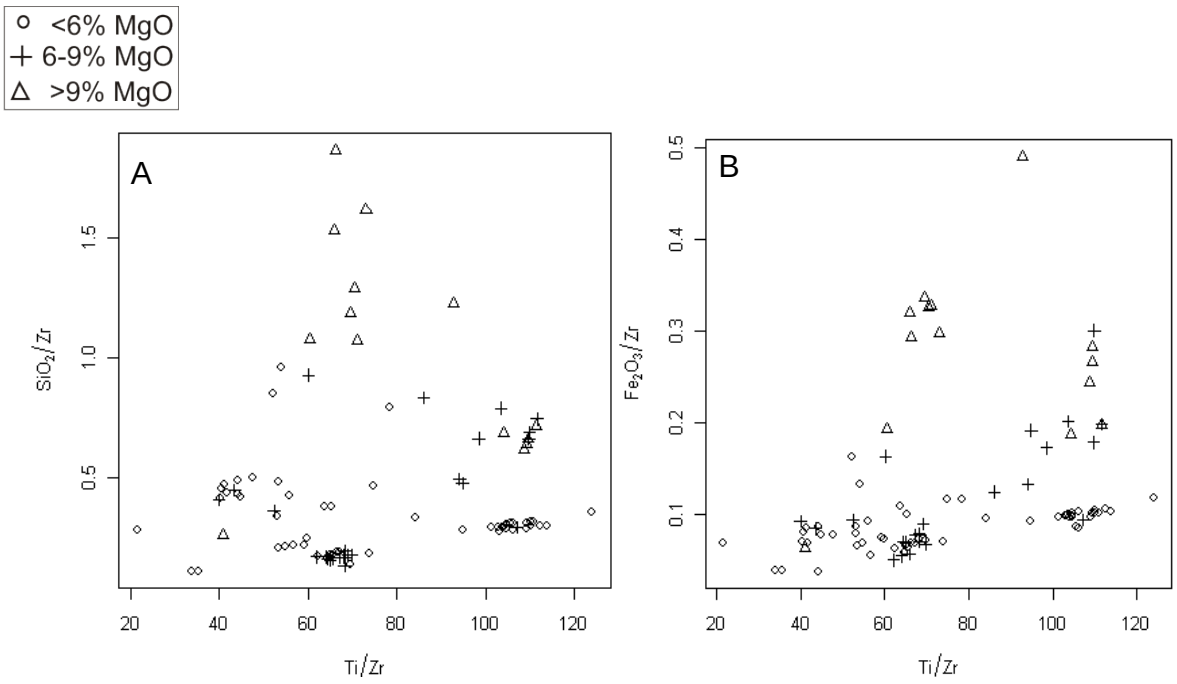

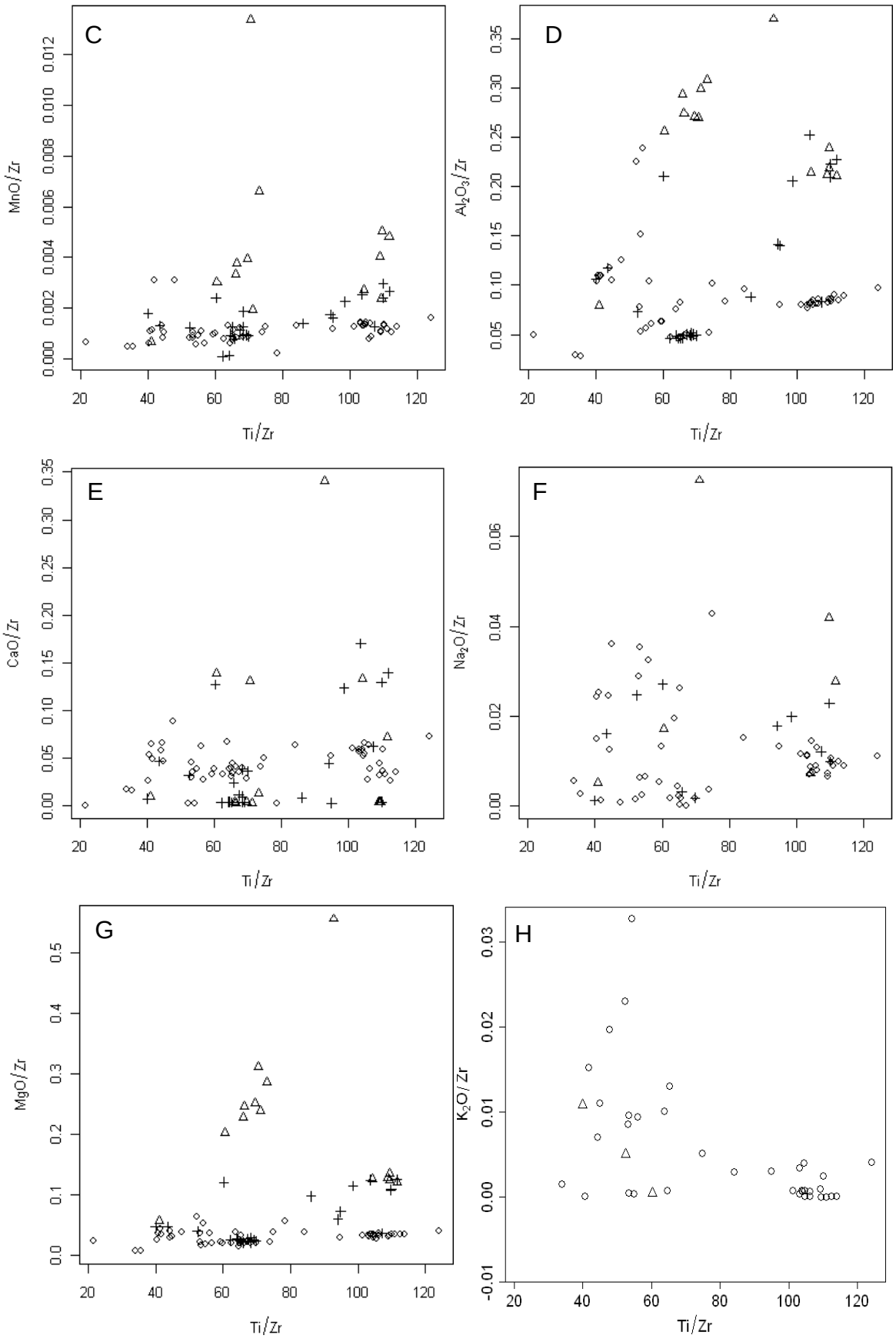
C
MnO/Zr
0.000
0.002
0.004
0.006
0.008
0.010
0.012
20
40
60
80
100
120
Ti/Zr
D
Al_2O_3/Zr
0.05
0.10
0.15
0.20
0.25
0.30
0.35
Ti/Zr
E
CaO/Zr
0.00
0.05
0.10
0.15
0.20
0.25
0.30
0.35
Ti/Zr
F
Na_2O/Zr
0.00
0.02
0.04
0.06
Ti/Zr
G
MgO/Zr
0.0
0.1
0.2
0.3
0.4
0.5
Ti/Zr
H
K_2O/Zr
-0.01
0.00
0.01
0.02
0.03
Ti/Zr

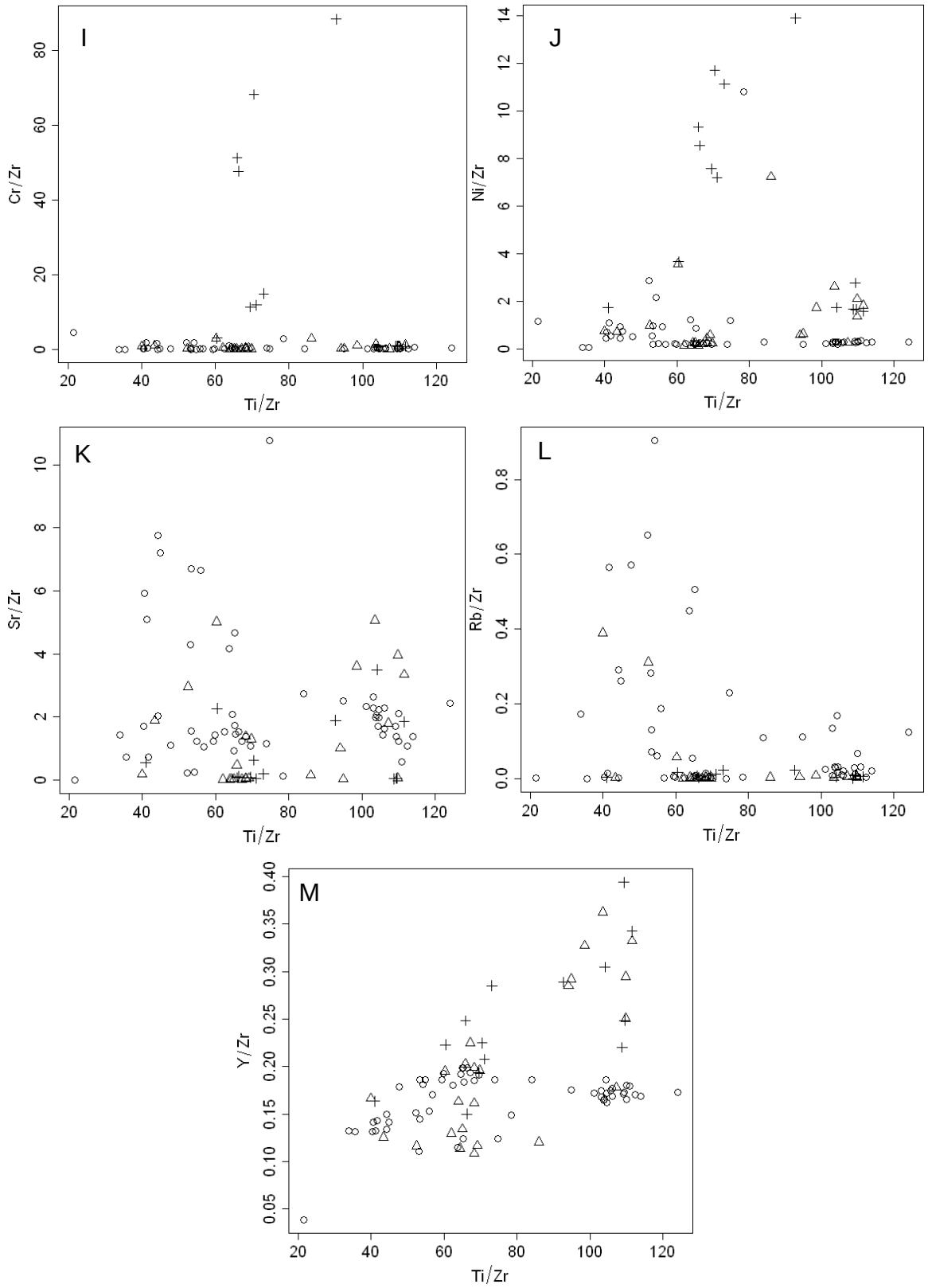

Figure 4.9. Plots used to determine element mobility. All samples were included and separated according to their MgO content.

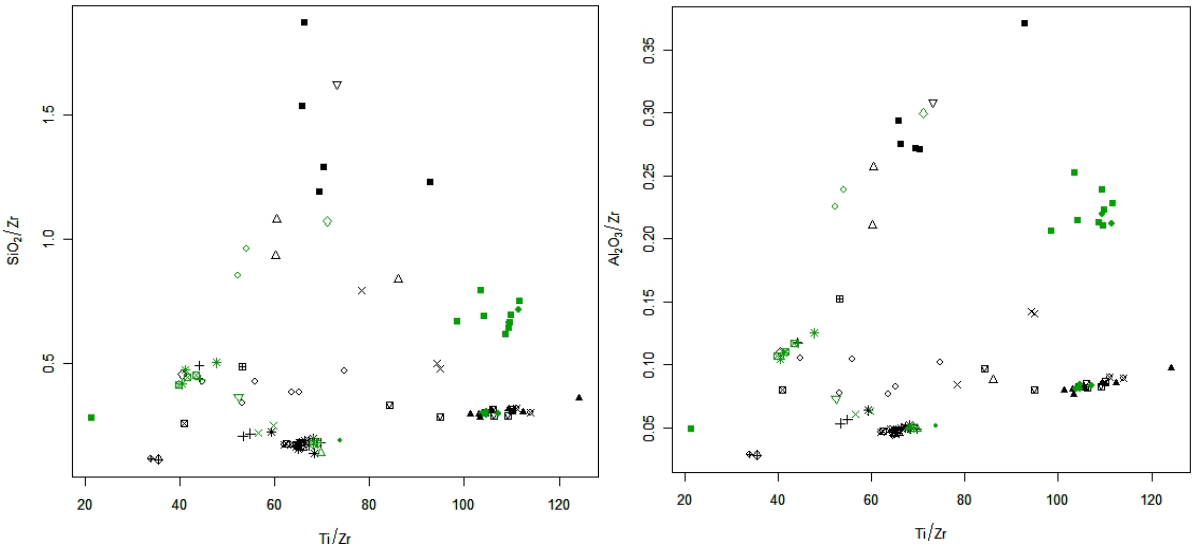

Figure 4.10. SiO_2 and Al_2O_3 mobility plots showing the smaller groups made by samples from the same dykes.

4.3 Chemical Variation between Chill and Central Zones of Dykes

The chill zones of intrusives are regarded to have a geochemistry that is equivalent to that of the unfractionated magma due to a quick cooling rate which 'locks in' the original chemistry. However, it is more likely that fractionation of mantle-compatible elements into the chill zone will occur with its formation. In this study there are 10 cases where both chill zones of the dykes and central zones were sampled, making it possible to compare the chemistry of the different zones. It is most useful to compare the concentrations of compatible elements especially since many incompatible elements are present in concentrations that would make comparison statistically meaningless, or were below the detection limit of the XRF spectrometer.

If fractionation did occur, the chill zones will have a higher compatible element concentration than the central zones, as these elements, especially Ni and Cr tend to partition into olivine and early pyroxenes (Rollinson, 1993). MgO, CaO, Cr and Ni were used in the comparison, as well as SiO_2 which should display an opposite trend to those of the above-mentioned compatible elements. The expected trends are clearly seen in the Bank dyke, especially in the samples from borehole DPH3885 (Fig. 4.11) where all compatible elements have higher concentrations in the chill zones than in the centre. The samples from DPH3880 (Fig. 4.12) show the same trend, where the fractionation of both Ni and Cr are even more pronounced. Approximately the same trend with the fractionation of compatible elements into chill

zones is seen in the Brazil (Fig. 4.13 and 4.14), CLA (Fig. 4.15), Friday (Fig. 4.16) and Swannie (Fig.4.18) dykes, although Ni and Cr do not show the same tendency in the Brazil 1 (DPH3881) and Brazil 2 (DPH3884) dykes respectively.

The Speckled dyke (Fig. 4.17) displays exactly the opposite trend with the central zone being more enriched in incompatible elements than the chill zones. The same trend is seen in Unknown 8 (Fig. 4.19), especially in Ni and Cr concentrations. Unknown 9 (Fig. 4.20) does not conform perfectly to either scenario, but has a centre that is slightly enriched in Cr and slightly depleted in SiO_2. In the other dykes SiO_2 does not always display a trend opposite to that of the compatible elements, but does so in the Brazil 2, CLA, Speckled and Unknown 9. Possible reasons for this will be discussed below.

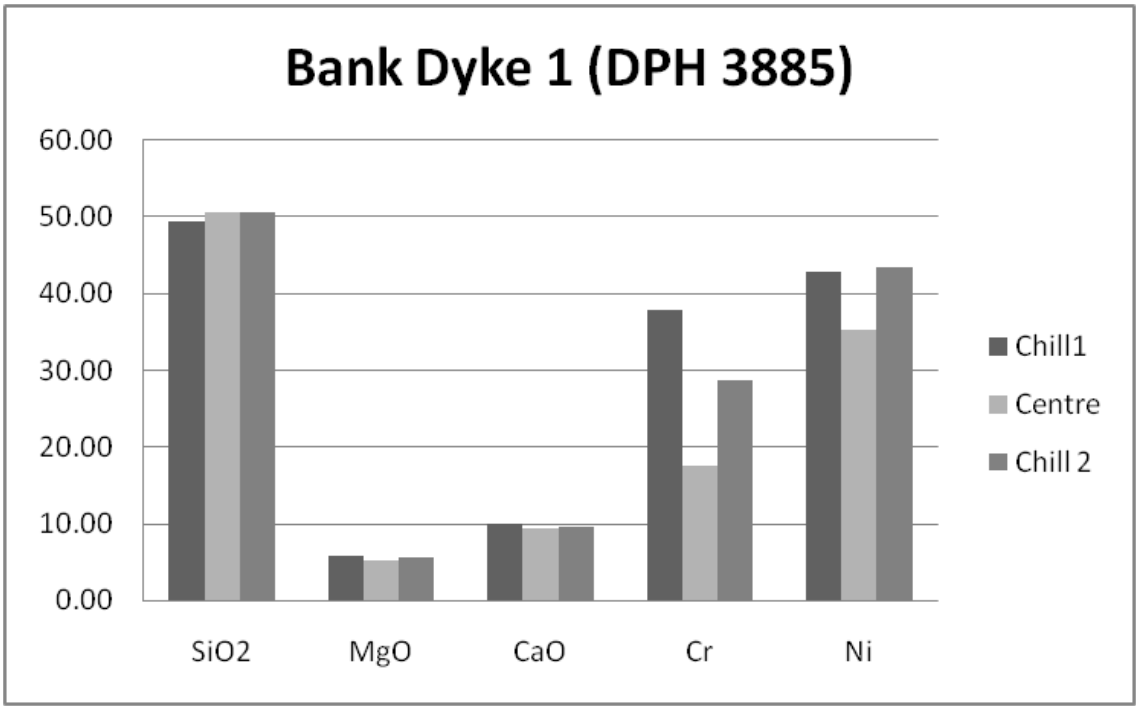

Figure 4.11. Element concentrations in the chill zones and central zone of the Bank dyke in borehole number DPH 3885, showing enrichment of compatible elements in the chill zones. The unit for the major element oxides is wt% and for Cr and Ni, ppm.

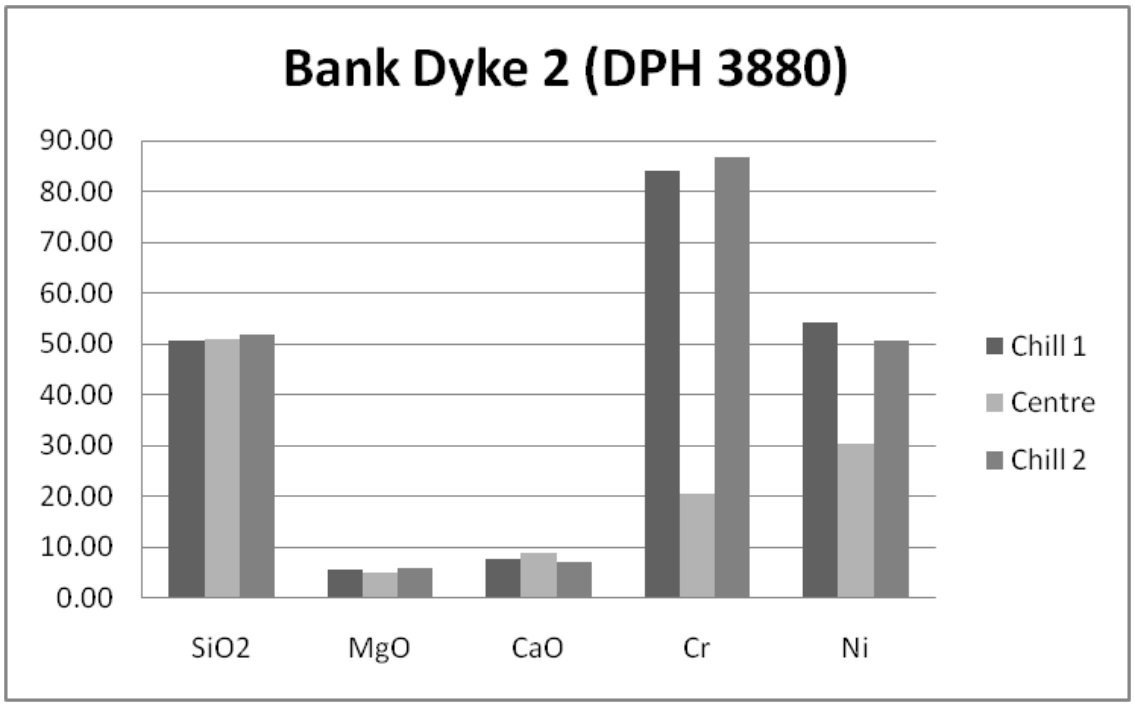

Figure 4.12. Element concentrations in the chill zones and central zone of the Bank dyke in borehole number DPH 3880 showing enrichment of Cr and Ni in the chill zones. The unit for the major element oxides is wt% and for Cr and Ni, ppm.

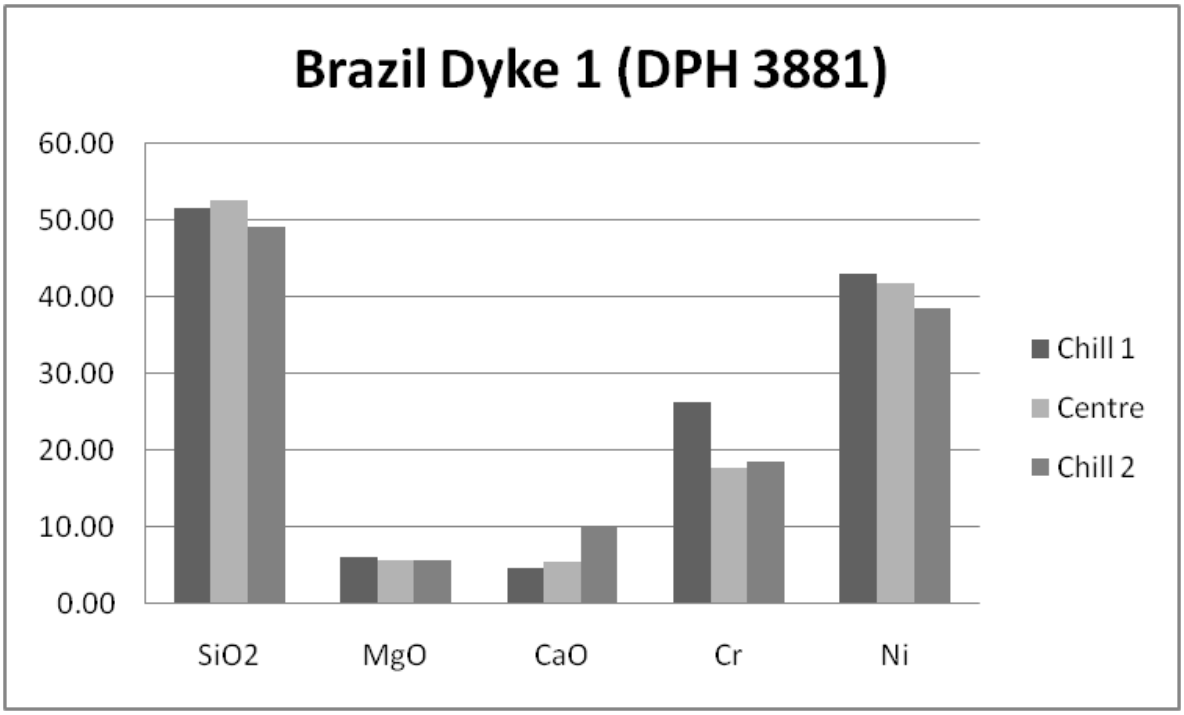

Figure 4.13. Element concentrations in the chill zones and central zone of the Brazil dyke in borehole number DPH 3881, showing Cr enrichment in the chill zones and Ni enrichment in chill zone 1. The unit for the major element oxides is wt% and for Cr and Ni, ppm.

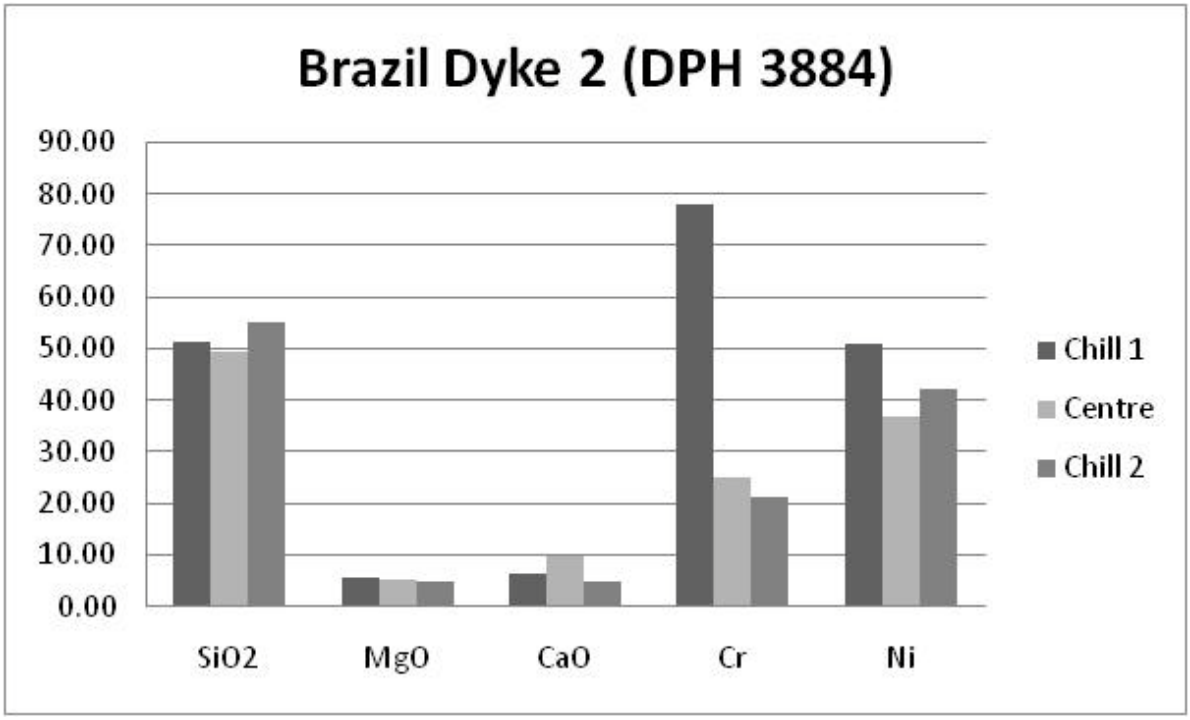

Figure 4.14. Element concentrations in the chill zones and central zone of the Brazil dyke in borehole number DPH 3884, showing Cr enrichment in chill zone 1 and Ni enrichment in both chill zones. The unit for the major element oxides is wt% and for Cr and Ni, ppm.

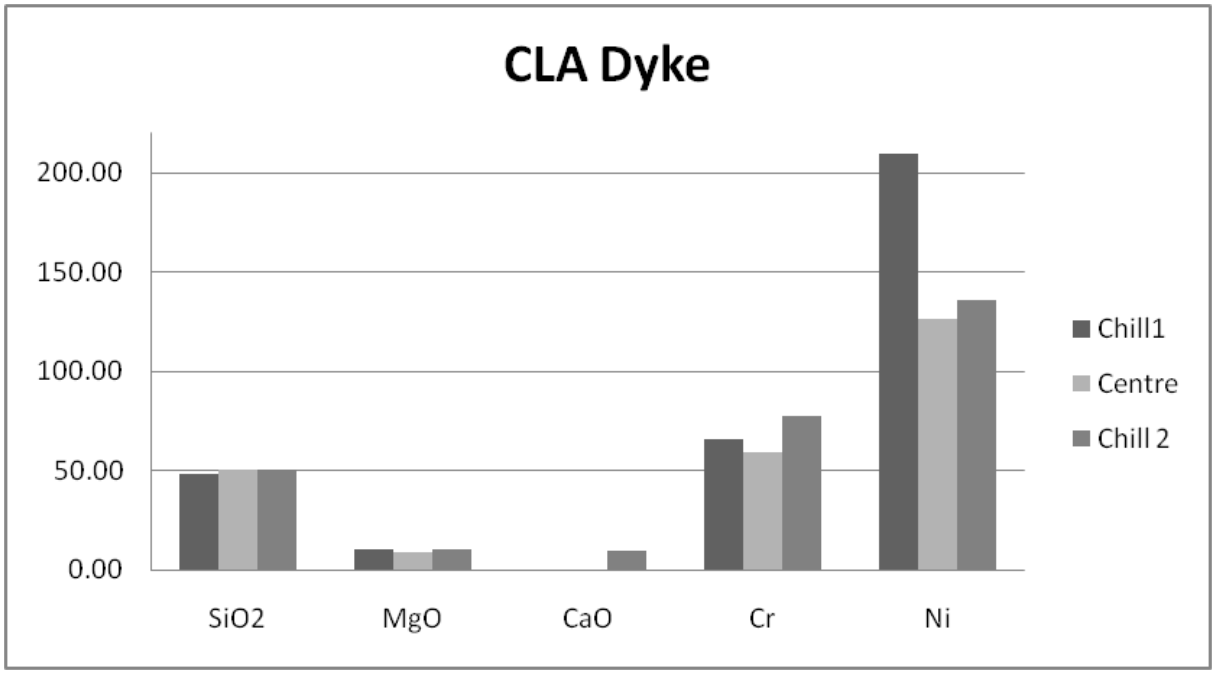

Figure 4.15. Element concentrations in the chill zones and central zone of the CLA, showing enrichment of compatible elements in the chill zones. The unit for the major element oxides is wt% and for Cr and Ni, ppm.

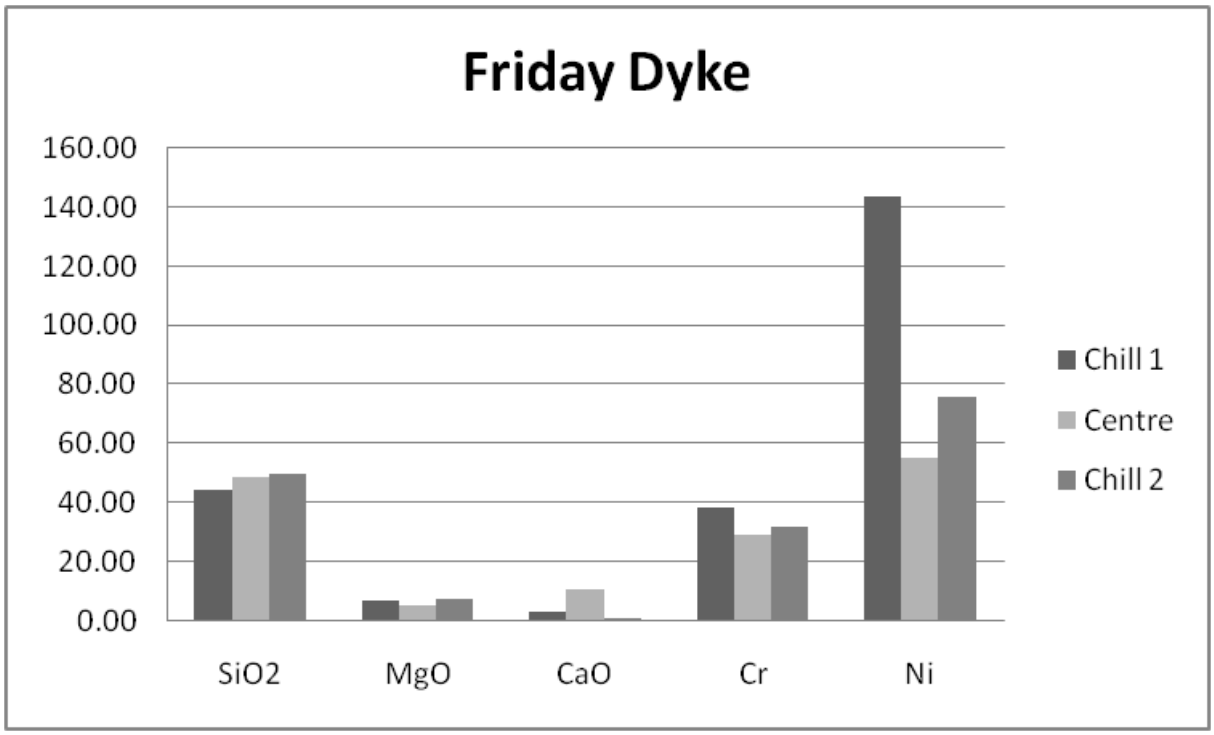

Figure 4.16. Element concentrations in the chill zones and central zone of the Friday dyke, showing enrichment in MgO, Cr and Ni. The unit for the major element oxides is wt% and for Cr and Ni, ppm.

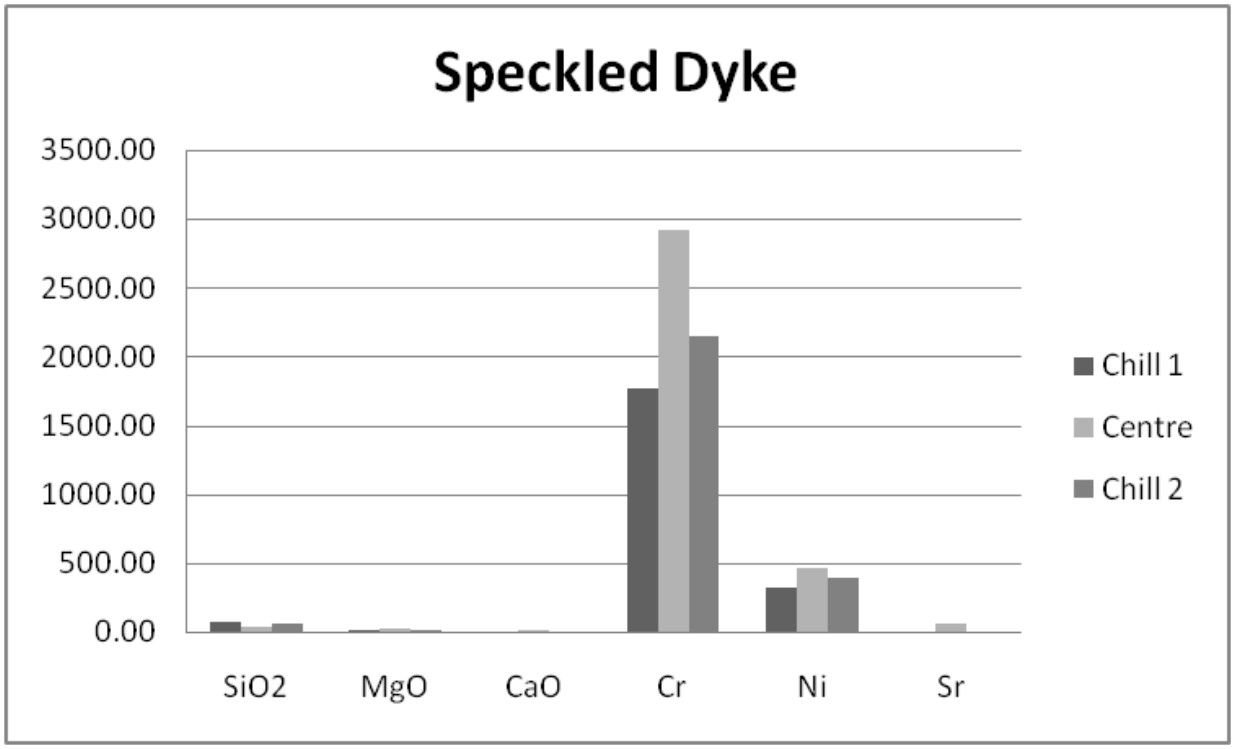

Figure 4.17. Element concentrations in the chill zones and central zone of the Speckled dyke, showing an enrichment Cr, Ni and Sr in the central zone. The unit for the major element oxides is wt% and for Cr, Ni and Sr, ppm.

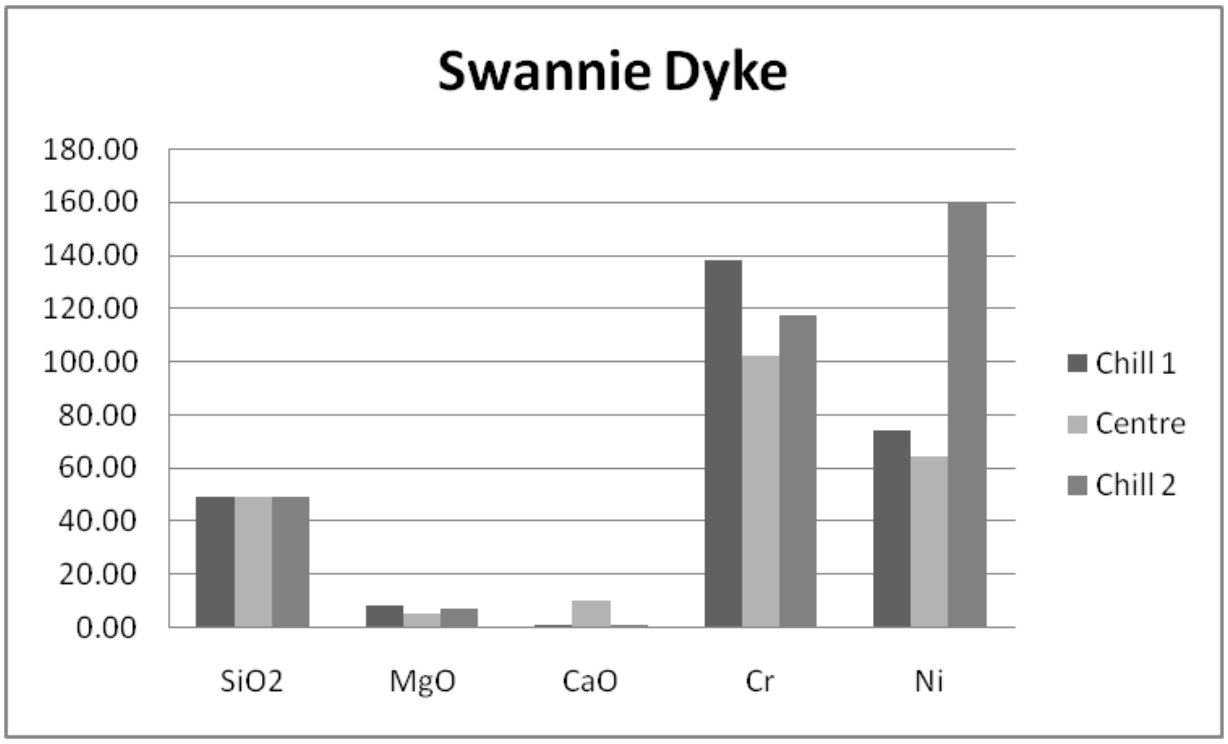

Figure 4.18. Element concentrations in the chill zones and central zone of the Swannie dyke, showing enrichment of Cr and Ni in the chill zones. The unit for the major element oxides is wt% and for Cr and Ni, ppm.

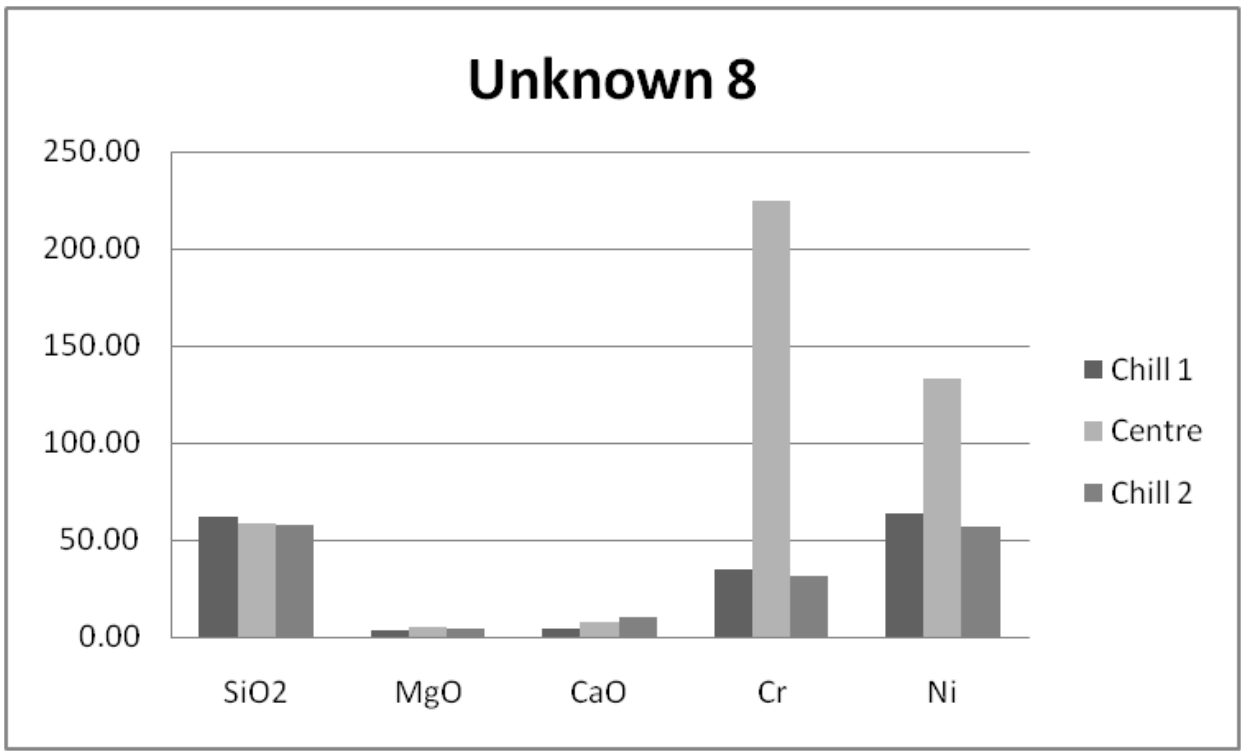

Figure 4.19. Element concentrations in the chill zones and central zone of the "Unknown 8" dyke, showing enrichment of Cr and Ni in the central zone. The unit for the major element oxides is wt% and for Cr and Ni, ppm.

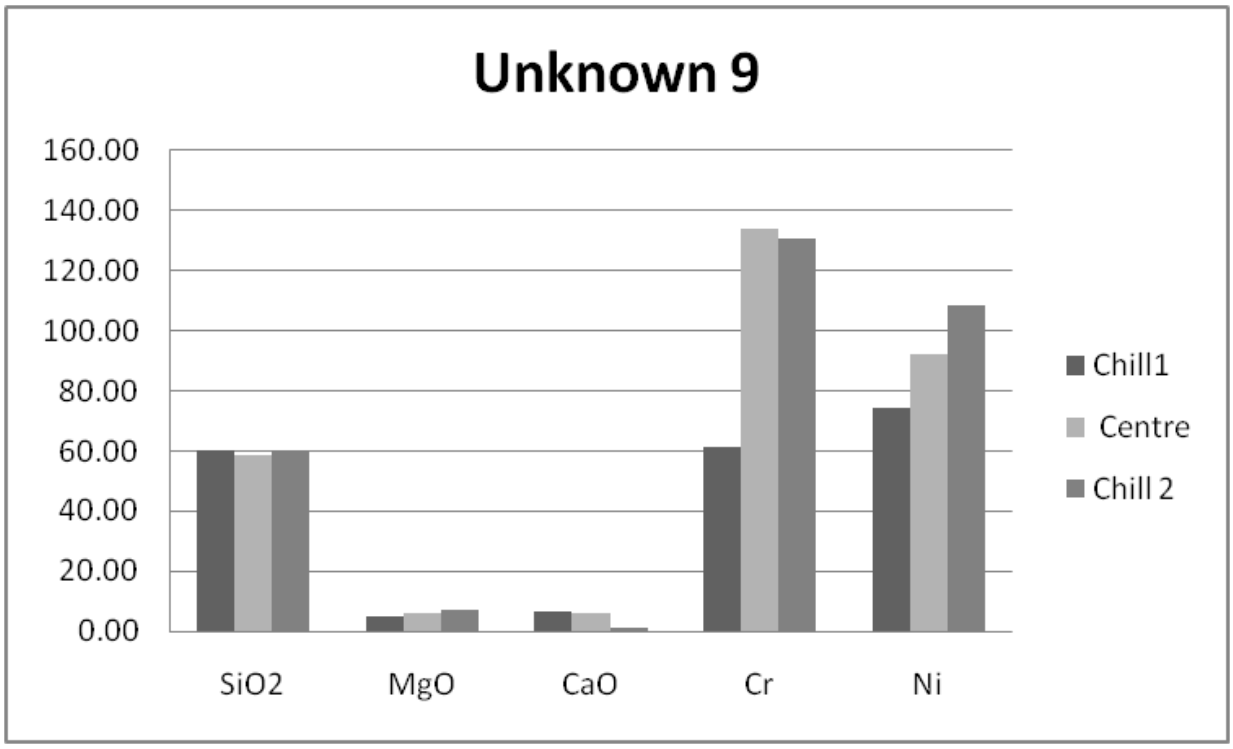

Figure 4.20. Element concentrations in the chill zones and central zone of the "Unknown 9" dyke, showing Cr and Ni enrichment in the central zone and chill zone 2. The unit for the major element oxides is wt% and for Cr and Ni, ppm.

A possible explanation for this "inverse" trend in chemistry in the Speckled dyke and to a certain extent in Unknown 9 can be found in a study executed on a lava flow near the Katse dam in Lesotho (De Bruiyn, *et al.* 2000). Both the top and bottom sections of the flow have a tholeiitic composition, but the central zone is picritic. Some olivine crystals in this zone contain microscopic melt inclusions that probably represent quenched parental liquid, which was apparently intermediate in composition between those of the contact zones and the central part. Geochemical modelling indicated that approximately 28% olivine had to be separated from the parental magma in order to yield the tholeiitic base and top zones.

The separation of the olivine was likely achieved by means of flow differentiation. When a fluid containing suspended particles flows though a conduit, the particles will migrate toward the region with the highest flow rate, i.e. away from the walls of the conduit. Bhattacharji (1967) was first to apply this principle, which was originally observed in blood vessels, to magmas. His experimental work showed that early minerals would concentrate in the centre of dykes and sills in which high flow rates are present, but would settle once the rate decreases. This means that the mantle-

compatible element-rich pyroxenes and, possibly, olivines would move from the chill zone into the central zone of the intrusive. If this principle is used to explain the "inverse" chemistry of the Speckled and Unknown 8 dykes it would mean that these dykes had higher flow rates than the dykes with compatible elements concentrated in their chill zones. This trend may be useful as an identification tool for these two dykes, however, there may be other dykes in the study are which were not included in this study, that display the same trend. An interesting feature of Unknown 9 is the concentration of Cr and Ni in only one chill zone. This concentration of mantle-compatible elements may lead one to suspect the presence of a cumulate layer of early minerals. However, the dyke is almost perfectly vertical (pers. comm. K. Deysel, 2009) which eliminates the possibility of gravitational settling of early minerals to the chill zone. Two likely explanations exist, the first is that the dyke changed from slow flowing to fast flowing as different magma pulses intruded, and the second involves different cooling rates for the two sides of the dyke, resulting in the partitioning of compatible elements in the chill zone with the quicker cooling rate. However, a more detailed study of this dyke is required in order to obtain any definite answers.

4.3 Rock Classification

Since any mineralogical classification is made impossible by the severe alteration of the primary igneous minerals to chlorite actinolite and other clay minerals, a logical next step would be to classify the dykes with existing geochemical plots. Both classifications for rock names and for tectonic settings were used. These plots are ideally used with unaltered rocks, and the fact that the dykes are altered may cause some misclassification. It could, however, still give a preliminary idea of which dykes are related to which igneous event.

The Irvine and Baragar (1971) AFM diagram (Fig. 4.21) distinguishes between calc-alkaline and tholeiitic rocks. The Ventersdorp lava sample, Unknown 3 and PEG3 and 6 plot in the Calc-alkaline series and PEG2, 4 and 5 plot on the line between the two series. All other samples plot in the tholeiite field.

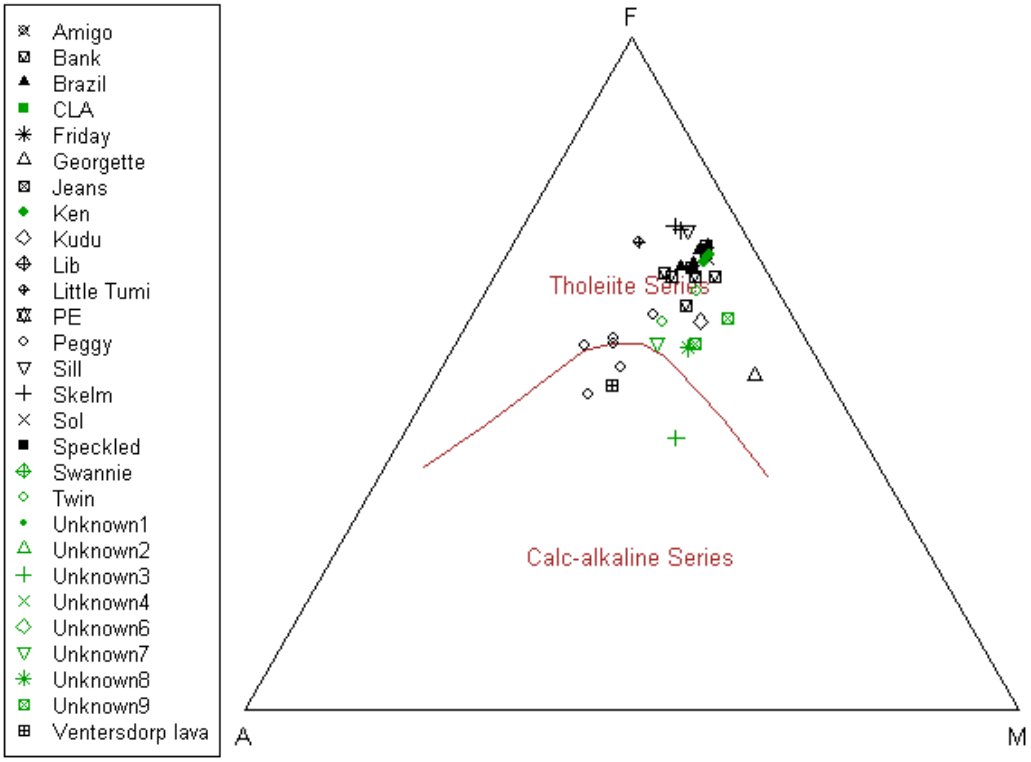

Figure 4.21. AFM classification diagram (Irvine and Baragar, 1971), dividing igneous rocks into tholeiitic and calc.alkaline series. The majority of the dyke samples are classified as tholeiitic.

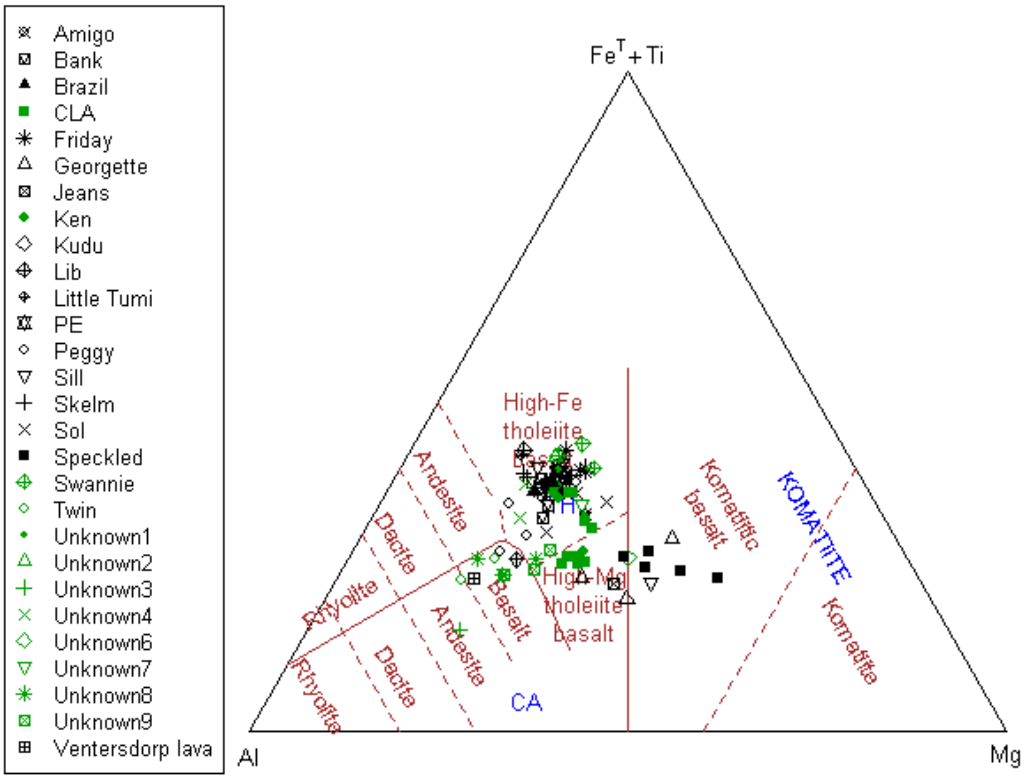

Figure 4.22. Jensen cation plot (1976) classifies most samples as high-Fe tholeiite basalts. The Speckled dyke is classified as a komatiitic basalt.

In the Jensen (1976) cation plot most of the samples plot in the high-Fe tholeiite basalt field, with a few exceptions (Fig. 4.22). The Speckled dyke, SIL1 and GEOR3 plot in the komatiitic field. The CLA, KEN1, and other two Georgette samples are classified as High-Mg tholeiite basalts. The Ventersdorp lava sample, Twin dyke, Unknown 8, Lib dyke and PEG6 are classified as basalts, although TWI2 plots more in the andesite field. Unknown 3 is classified as an andesite. A few samples plot on the boundaries between fields. The remainder of the samples are classified as high-Fe tholeiite basalt.

According to the Winchester and Floyd (1977) Zr/TiO_2 vs. Nb/Y system most samples are classified as subalkaline basalt (Fig. 4.23). PEG 1-5, SOL3, GEOR 3 and UNK7 plot in the alkaline basalt field, with CLA9 being classified as a trachy-andesite. While most of the Friday dyke samples are classified as subalkaline basalts FRI4 and 5 encroach slightly into the andesite/basalt field. Unknown 1 and 2, the Skelm dyke, JEA 1 and 3 and Unknown 8 also fall in this field. Unknown 9, JEA2, the Kudu dyke, Lib and Little Tumi dykes are classified as andesites.

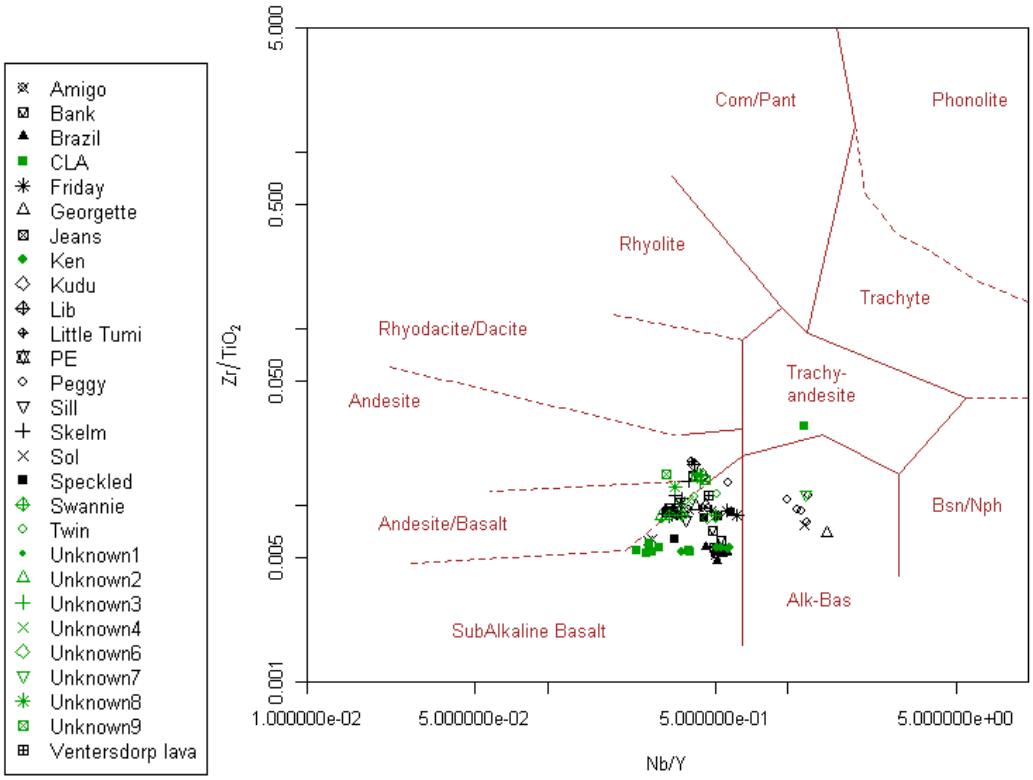

Figure 4.23. Winchester and Floyd's Zr/TiO_2 v Nb/Y diagram (1977) classifies the majority of samples as sub.alkaline basalt to andesite. The Peggy dyke is classified as alkali basalt.

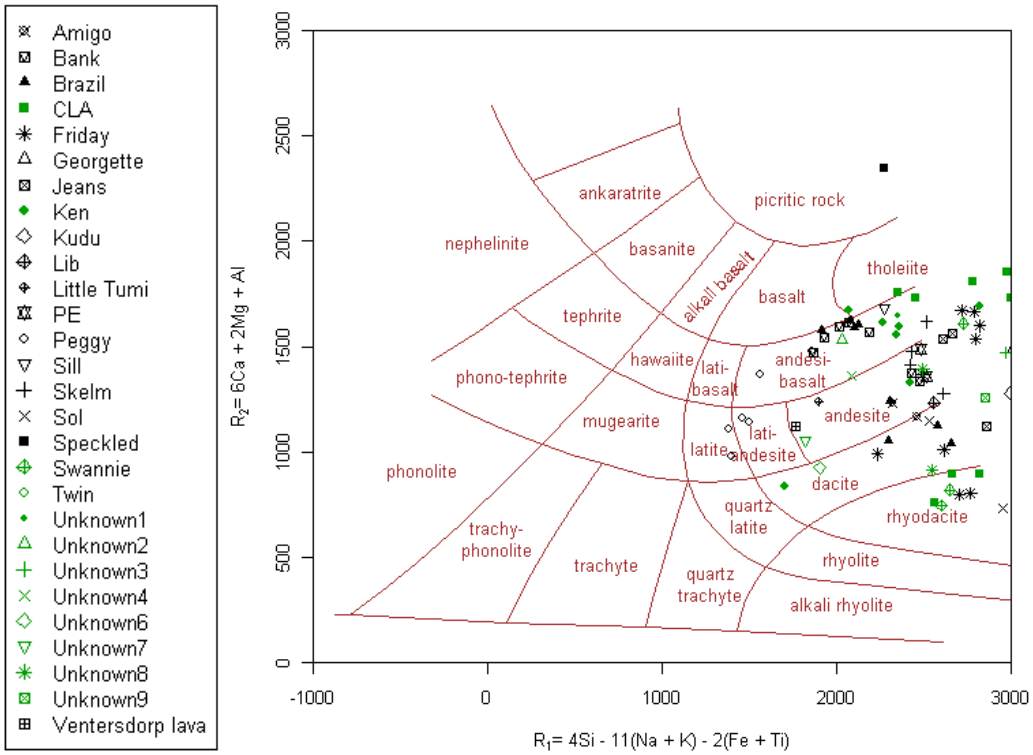

Figure 4.24. The R1-R2 diagram by De la Roche et al. (1980) gives a more felsic classification than the other plots. Some samples, including the Speckled dyke, are not plotted due to the absence of alkalis, causing a shift to the right on the x-axis.

When the classification system by De la Roche *et al.* (1980) (Fig. 4.24) is used, there is a general shift towards more felsic classifications with samples from the CLA, Friday and Swannie dykes as well as SOL1 being classified as rhyodacites. This plot also tends to separate samples from the same dyke into widely different groups, e.g. The Friday (andesi-basalt and dacite), CLA (andesi-basalt and rhyodacite) and Brazil (andesi-basalt and dacite). The Peggy dyke plots towards the more alkaline part of the plot.

4.4 Geotectonic Classification

In the Ti – Zr – Y diagram (Fig. 4.25) most of the samples, including the Ventersdorp lava sample are classified as “within plate basalt”. Most CLA and some Speckled dyke samples fall in the MORB – island arc basalt – low alkali tholeiite field, and one CLA sample plots outside any field. In the Ti- Zr diagram (Fig. 4.26) many samples, including the Brazil dyke, cannot be classified due to excessively high Ti or Zr concentrations. While most of the classified samples plot either as calc-alkaline basalts (Unknown 8 and 9, Kudu dyke and Ventersdorp lava) or low alkali tholeiites (Speckled and Georgette dykes and Unknown 6) the CLA, Peggy and Soll dykes plot

as MORB. This may be an indication that these dykes are related to the Ventersdorp lavas as Linton (1992) classified some Ventersdorp rocks as MORB.

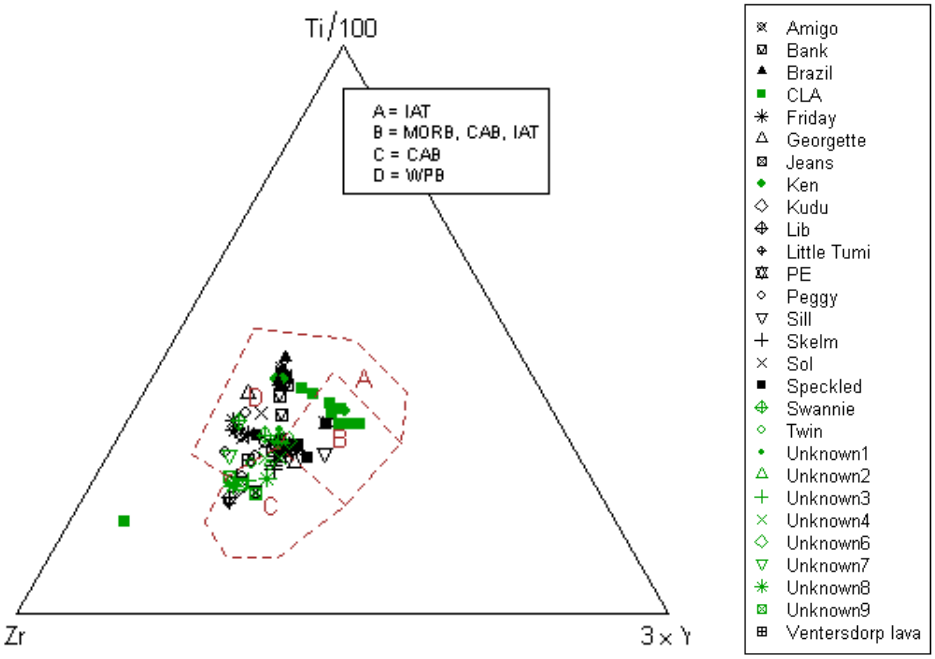

Figure 4.25. Ti – Zr – Y diagram for tectonic classification (after Pearce and Cann, 1973). LAT=Low K tholeiites, MORB=Ocean floor basalts, WPB=within plate basalts.

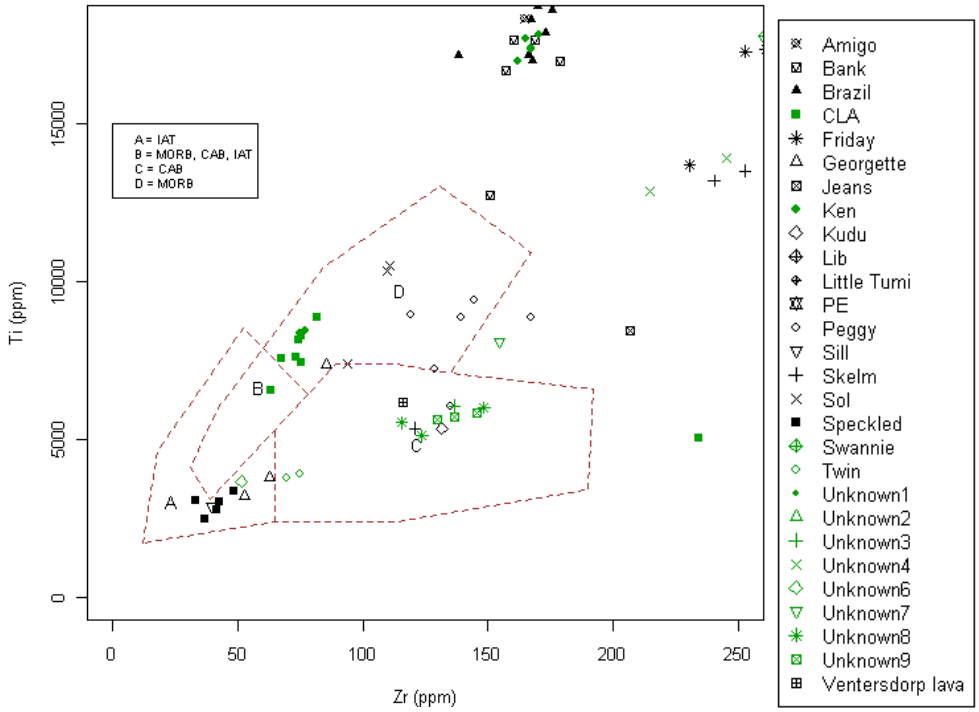

Figure 4.26. Ti – Zr (after Pearce and Cann, 1973). Acronyms are the same as for the previous figure.

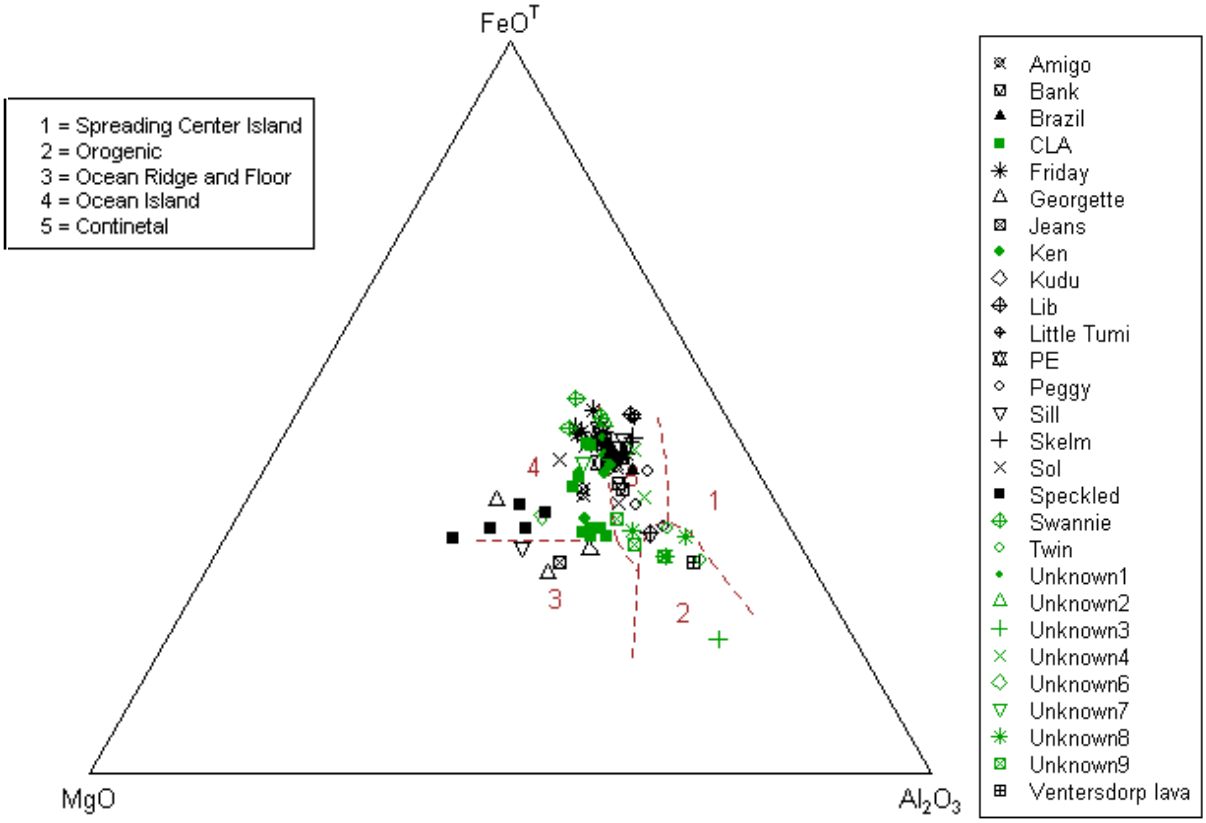

Figure 4.27. Total Fe – MgO – Al_2O_3 (after Pearce *et al.*, 1977) classifies the majority of the dykes as having a continental origin.

The FeO^t – MgO – Al_2O_3 diagram (Fig. 4.27) can be used for rocks with a SiO_2 range of 51 – 56%. Most of the dyke samples fall in this range, but there are a few exceptions. One limiting factor of this diagram is that it was drawn up using analyses from relatively modern rocks. Caution should therefore be exercised when using this diagram on older rocks as in the case in this study. Most samples plot as continental flood basalts. GEOR1 and 2, SIL1 and JEA2 plot as ocean ridge and ocean floor basalts. Unknown 3, the Ventersdorp lava sample, Unknown9 and Unknown 8A, PEG6, TWI1 and the Lib dyke are classified as orogenic basalts. The Speckled dyke, Swannie, Amigo, CLA and Ken dykes and SIL2 are classified as ocean island basalts.

4.5 Conclusions

Box plots show large variations in certain elements in some of the dykes. The most remarkable of these is the Sill, with large ranges in SiO_2, TiO_2, MgO, CaO, Ni and Cr, possibly indicating different and maybe unrelated origins for the two samples. Another significant observation is that CLA9 plots as an outlier with regard to most of the elements, and may have a different origin from the other CLA samples.

Variation in element concentrations can be attributed to these elements becoming mobile during greenschist metamorphism. A test for mobility, where the element in question over Zr is plotted against Ti/Zr, indicates that CaO, K_2O, Na_2O, Rb and Sr were the most mobile, as one would expect from their known geochemistry. MgO, Ni and Cr seem to have been the least affected by greenchist metamorphism. When these plots are compared to those from Linton (1992), it seems that the dykes' chemistry have been more affected by alteration than the lavas studied by Linton. The fact that samples from the same dykes often group together in the plots could indicate that the scatter of the plots are influenced by the fact that the dykes are most probably from different stratigraphic units.

Some elemental variations occur between the central and chill zones of dykes. When compatible element concentrations are compared in chill and central zones, the chill zones mostly have higher concentrations of compatible elements than the central zones. The opposite trend is seen in the Speckled dyke and in Unknown 8 and to a certain extent in Unknown 9. This "inverse" chemistry is possibly as a result of fast-flowing magma in the dyke, causing the first-formed crystals to migrate to the centre of the dyke.

The results of the geochemical classifications are best summarised in table form (Table 4.1).

Geotectonic plots seem to be very susceptible to the alteration of the rocks plotted. Some samples, notably the CLA, Peggy and Soll dykes to be classified as mid-ocean ridge basalts, which may indicate that they are related to the Ventersdorp lavas as Linton's study (1992) classified some Ventersdorp rocks as MORB. It is possible that these geotectonic plots only serve to show even further how altered

these rocks are and that any plots, such as those used in geochemical and tectonic classification should be treated with circumspection.

Table 4.1. A summary of the classifications of the dykes according to four plots.

	AFM	Jensen Cation	Zr/TiO_2 v Nb/Y	R1-R2
Peggy	Calc-alkaline	High-Fe tholeiite basalt	Alkali basalt	Latite/lati-andesite/andesi-basalt
Georgette	Tholeiite	Komatiitic basalt/High-Mg tholeiite basalt	Alkali basalt/Sub-alkaline basalt	NC
Skelm	Tholeiite	High-Fe tholeiite basalt	Andesite/Basalt	Andesite
Bank	Tholeiite	High-Fe tholeiite basalt	Sub-alkaline basalt	andesi-basalt/andesite
CLA	Tholeiite	High-Mg tholeiite basalt	Sub-alkaline basalt	rhyodacite/andesi-basalt
Brazil	Tholeiite	High-Fe tholeiite basalt	Sub-alkaline basalt	andesi-basalt/dacite
Speckled	Tholeiite	Komatiitic basalt	Sub-alkaline basalt	NC
Twin	Tholeiite	Basalt	Sub-alkaline basalt	NC
Kudu	Tholeiite	High-Fe tholeiite basalt	Andesite/Basalt	NC
Friday	Tholeiite	High-Fe tholeiite basalt	Sub-alkaline basalt	dacite/andesite
Jeans	Tholeiite	High-Fe tholeiite basalt	Andesite/Basalt	andesite
Soll	Tholeiite	High-Fe tholeiite basalt	Sub-alkaline basalt	andesite

Sill	Tholeiite	Komatiitic basalt/High-Fe tholeiite basalt	Sub-alkaline basalt	andesi-basalt/NC
Ken	Tholeiite	High-Fe tholeiite basalt	Sub-alkaline basalt	andesi-basalt
Swannie	Tholeiite	High-Fe tholeiite basalt	Andesite	rhyodacite
Amigo	Tholeiite	High-Fe tholeiite basalt	Sub-alkaline basalt	dacite
LIB	Tholeiite	Basalt	Andesite	andesite
Little Tumi	Tholeiite	High-Fe tholeiite basalt	Andesite	andesite
PE	Tholeiite	High-Fe tholeiite basalt	Andesite/Basalt	andesite
Ventersdorp Lava	Calc-alkaline	Basalt	Sub-alkaline basalt	andesite

Chapter 5: Geochemistry II

5.1 Grouping of Dykes According to Their Geochemistry

Dykes sharing the same origin should have approximately the same geochemistry and it is theoretically possible to divide them into groups according to their geochemistry. In order to be considered viable for use in the geochemical investigation of the dykes, the element in question must have been immobile and unaffected by primary magmatic processes such as fractionation in basaltic magma. The merits of Ti and Zr in this regard have already been discussed in the previous chapter. Y has similar behaviour, with regards mobility and primary magmatic processes, to that of Ti and Zr as all three are High Field Strength Elements (HFSEs), i.e. they form small, highly charged cations (Rollinson, 1993). As previously mentioned, Bowen (1984a) successfully separated the rocks of the Witwatersrand Triad by means of TiO_2 v Zr, Zr/P v P/Ti plots and the discriminant plot devised by Linton (1992) gave a good geochemical separation of the Klipriviersberg Group rocks. These three plots were employed in the separation of the dykes into chemically distinct groups.

In the TiO_2 v Zr plot (Fig. 5.1), all CLA dyke samples, except CLA9, group together along with one Georgette sample (GEOR3) and SOL3 from the Soll dyke. All Peggy samples, as well as Unknown 7, plot together except PEG6 which is slightly removed from the other Peggy samples and plots in the same group as Unknowns 3, 8 and 9, the Kudu dyke, and the Ventersdorp lava. The two Sill samples plot in completely different groups, one with the Speckled dyke and the other in the Friday dyke group on PE dyke sample PE1. SOL1 and SOL2 plot close together, but SOL3 plots closer to the CLA group. The Brazil dyke samples plot together along with most of the Ken and Bank dyke samples and the two Amigo dyke samples AMI3 and AMI5. Only BAN1 of the Bank dyke plots outside this field. The Friday, PE, Swannie, Unknown 1 and Unknown 2 dykes, as well as two Amigo samples (AMI1 and AMI2) and two Jeans samples (JEA1 and JEA3) plot in one field along with Skelm dyke sample SKE2 and SIL2. Skelm dyke samples 1 and 3 plot in the same field as the two Unknown4 samples and Friday dyke sample FRI4. The Speckled, Unknown6, and Twin dykes, along with Georgette samples GEOR1 and GEOR2 as well as SIL1

plot in the field with the lowest TiO_2 and Zr values. The Lib and Little Tumi dykes plot together away from any of the other fields. These two dyke samples are distinguished from the other dykes by their high Zr content.

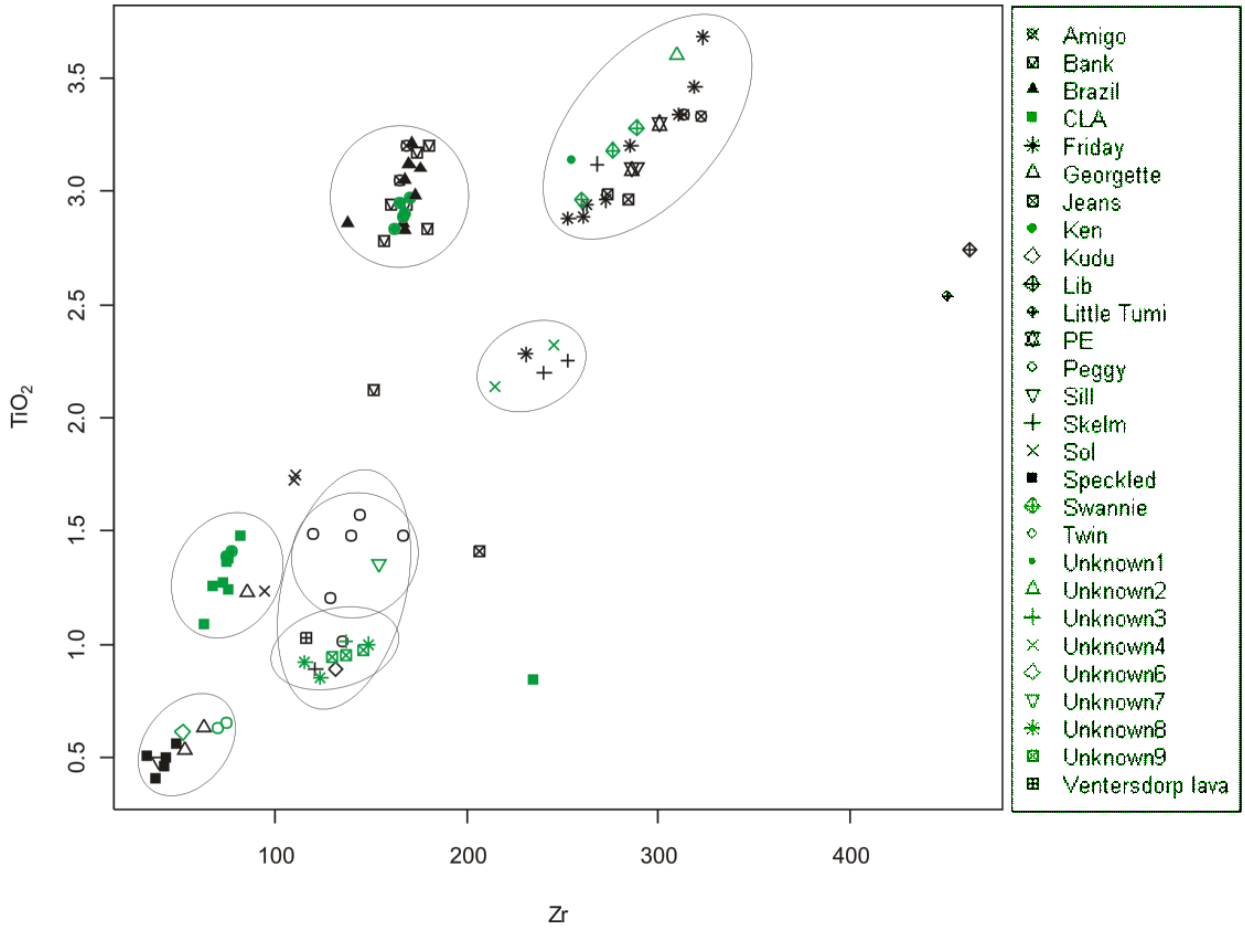

Figure 5.1. Dyke samples on a plot of TiO_2 (wt%) v Zr (ppm) (after Bowen, 1984a) showing the grouping of dykes.

When the Zr/P v P/Ti plot is used (Fig. 5.2), the dyke samples plot into three groups with only five outliers (PEG1, JEA2, GEOR3, LIT1 and LIB1) that do not plot in any of the fields. The CLA9 sample was omitted from the plot as it has a Zr/P ratio >5 due to a high Zr content and low P content. The Peggy, Speckled, Twin, Skelm, Georgette, Kudu, Unknown3, Unknown4, Unknown6, Unknown7, Unknown 8 and Unknown 9 and the Ventersdorp lava group together. Included in this group are also SIL1, FRI4, and SOL3. The CLA, Brazil, Ken, Soll, and Bank dykes plot in the group below, along with Amigo dykes samples AMI3 and AMI5 and SPE4 from the Speckled dyke. The Friday, Jeans, Swannie, Unknown1, Unknown2 and PE dykes plot in the field with the highest P/Ti and lowest Zr/P ratios. The Amigo dyke

samples AMI1 and AMI2, Skelm dyke sample SKE2 and SIL2 are also in this field. The Lib and Little Tumi dykes once again plot together in their own field.

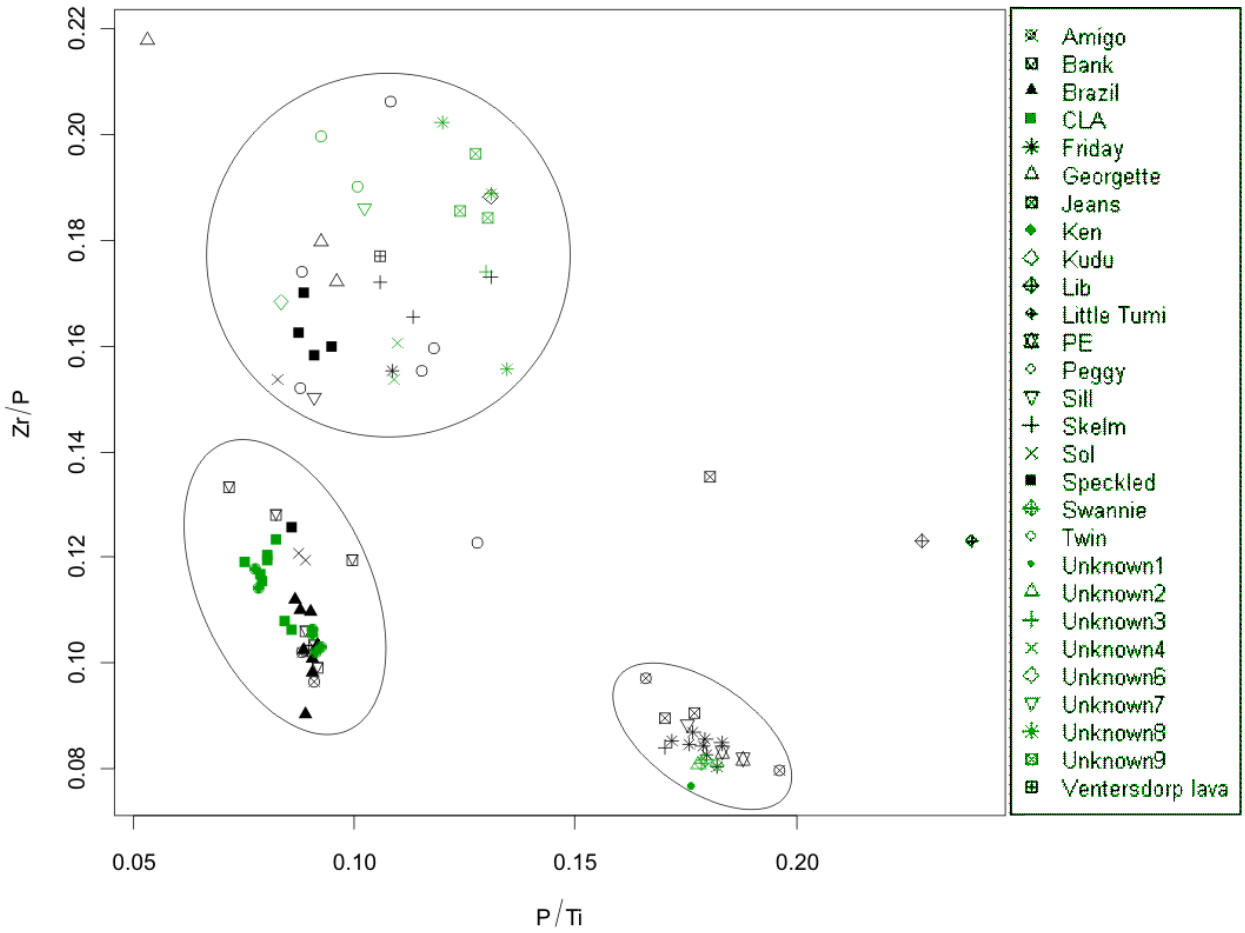

Figure 5.2. Dyke samples on a plot of Zr/P v P/Ti (after Bowen, 1984a) showing the division of dykes into three groups.

When the samples are plotted on Linton's discriminant plot (Fig. 5.3) they form essentially the same groups as in the TiO_2 v Zr plot. The CLA samples (excluding CLA9) group together with KEN 1 and 4, and the Speckled, Georgette and Twin dykes group together with SIL1 and UNK6. Unknown 8 and 9 group together with the Peggy dyke, Ventersdorp lava, the Kudu dyke, SKE5, GEOR3 and SOL3, Unknown3 and Unknown7. SKE1 and 3, Unknown 4 and FRI4 form a group. The Bank, Brazil and Amigo dykes group together with the Ken dyke, and the Friday and Swannie dykes, SKE2, SIL2, AMI1 and 2, and Unknown 2 group together.

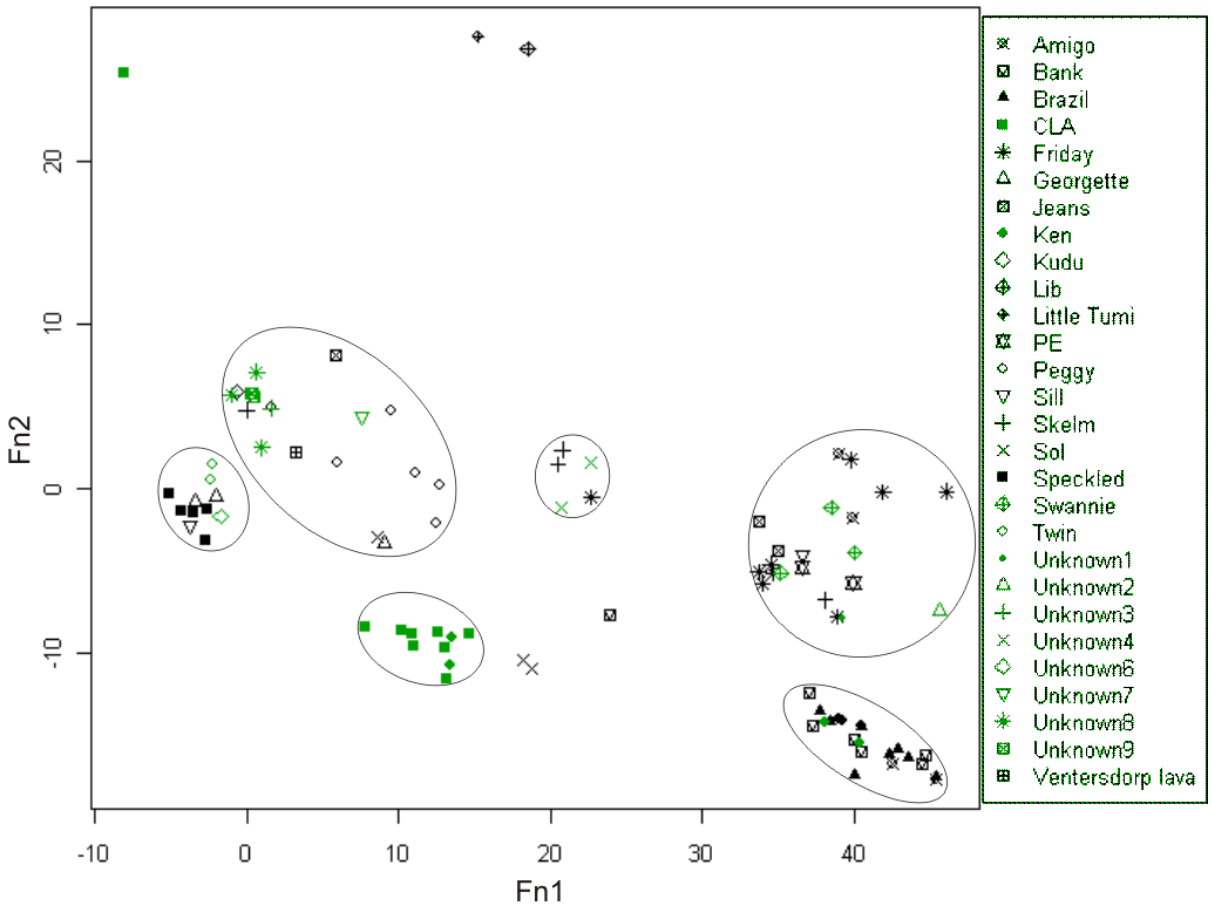

Figure 5.3. The grouping of dyke samples on the discriminant plot developed by Linton (1992). Fn1=0.0172Y-0.06078Zr+20.8084TiO_2-11.4636; Fn2=-0.24892Y+0.16017Zr-11.7088TiO_2-0.07079.

When the dyke samples are plotted onto these immobile, High Field Strength Element (HFSE) plots, samples from the same dyke mostly plot together. The Soll, Peggy, Amigo, Jeans, Georgette and Skelm dykes as well as the Sill, are exceptions, although to a lesser extent in the case of the Peggy dyke. It may be that the HFSEs are not entirely immobile, but mobility of these elements would likely not cause large variation between samples. On the other hand, large variations in geochemistry, such as that between the two Sill samples, probably indicate that the samples actually represent two different intrusives. Intrusives are mapped mostly by using data derived from drill core, and to some extent, by means of underground mapping. If very little data is available for an area it is more difficult to make correct deductions, and mine plans are constantly updated as more data becomes available. Thus, before any conclusions regarding sample scatter due to element mobility can be made, one should first look at the sample localities to determine whether any samples have been misnamed:

- FRI4 always plots away from the rest of the Friday dyke samples and groups with two Skelm dyke and the two UNK4 samples (Figs. 5.1, 5.2 and 5.3). When one refers to Fig. 2.2 it is clear that FRI4 really belongs to the Skelm dyke.
- KEN1 and 4 plot with the CLA dyke samples (Figs. 5.1 and 5.3), but on the locality map they are very close to KEN2 and 3 and not near the CLA dyke (Fig. 2.4).
- Similarly, CLA9 is completely removed from all the other samples on the plots (Figs. 5.1 and 5.3), but it was sampled very close to CLA4 and 5 (Fig. 2.4).
- Skelm dyke samples SKE1 and 3 were sampled close to each other (Fig. 2.4), but SKE5 (Fig. 2.2) was sampled a few hundred meters away. SKE2 is not indicated on the map. The physical distance between SKE5 and SKE1 and 3 is reflected in their chemistry where SKE1 and 3 plot together, but SKE 2 and 5 plot in different groups (Figs. 5.1 and 5.3). This difference in chemistry may indicate the sampling of two different intrusives, and that SKE2 is from the same dyke as SKE5.
- Similar situations as in the Skelm dyke can be observed in the Jeans dyke (Fig. 5.1 and 5.3). JEA1 and 3 were sampled in Tau Tona in the Pretorius Fault (Fig. 2.4) and JEA2 was sampled a considerable distance away in Mponeng (Fig. 2.9). This once again raises the possibility of the sampling of two different dykes.
- Likewise, GEOR3 (Fig. 2.12) was sampled a considerable distance away from GEOR1 and 2 (Fig. 2.8) and has a completely different geochemistry (Figs 5.1 and 5.3). It should be noted, however that there are three Georgette dykes that cut each other, often hampering the accuracy of labelling.
- According to the maps (Figs. 2.9 and 2.13), UNK2 and 3 seem likely to be from the Jeans dyke in Mponeng. UNK2 and 3 are chemically similar to JEA2 (Fig 5.3). This confirms that the three samples are from the same source.
- The Soll dyke samples were taken close to each other (Fig. 2.3), but the chemically distinct SOL3 (Figs. 5.1 and 5.3) was taken in a fault cutting the Soll dyke. The possible local influence of the fault on the geochemistry of the dyke will be discussed in a later section.

- UNK1 (Fig. 2.2) seems to be a Peggy dyke sample according to the map, but not according to the geochemistry (Figs. 5.1, 5.2 and 5.3).
- The UNK4 samples are known to be from an unnamed dyke in Mponeng (Fig. 2.10).
- UNK6 and 7 are not indicated on the maps, but, according to their geochemistry, UNK7 could be a Peggy dyke sample, and UNK6 can be either from the Speckled dyke or the Georgette dyke (Figs. 5.1, 5.2 and 5.3).
- Unknown 8 and 9 are possibly the same unnamed dyke as they are geochemically similar (Figs, 5.1, 5.2 and 5.3) and were sampled close together (Fig. 2.2).

From a structural point of view the dykes can also be grouped according to strike. The fact that the positions and strikes are inferred from borehole data means it is often difficult to determine the exact strike of a dyke from a mine plan. In addition, dykes are not perfectly linear, resulting in a gentle oscillation of the strike. McCarthy *et al.* (1990) overcame the problem of oscillating strikes by dividing strike directions into 15° intervals. Table 5.1 shows the grouping of the dykes according to the three plots, as well as according to strike. The largest group in the Zr/P v P/Ti plot encompasses three strike groups which, for the sake of clarity, were placed in the table consecutively. Therefore, the strike intervals do not appear in exact numerical order. Unknown 1, 2, 3, 5, 6 and 7 and the Ventersdorp lava sample were excluded from the table as they cannot be linked to a specific strike and the links between the unknown samples and known dykes have already been discussed in the previous paragraph. Unknown 4, 8 and 9 were included as they are unnamed dykes and not samples with an unknown origin.

When the grouping in the plots is compared to the strike grouping, a very good correlation is found between geochemistry and strike (Table 5.1). This may indicate that dykes with the same strike were possibly formed as a result of the same magmatic event, agreeing well with the conclusions drawn by McCarthy *et al.* (1990). However, when confronted with such a long period of time (Ventersdorp to Karoo), one should be careful of drawing such conclusions as later magmas may have intruded into weak areas created by earlier tectonic regimes. If the results regarding

dyke strikes in the ERPM mine from McCarthy *et al.,* (1990) are applied to this study, the Lib and Jeans dyke can be classified as Ventersdorp dykes. Ilmenite diabase dykes as well as Loraine and Jeanette dykes may all have strikes varying between 105° and 165°. Dykes from this study that may be classified as ilmenite diabase dykes are, the Bank, CLA, Brazil, Ken, Amigo and Soll dykes. It is doubtful as to whether the 90 – 105° strike of the Peggy, Georgette and Speckled dykes classifies them as belonging to either the Loraine or Jeanette Formations of the Ventersdorp Supergroup.

Table 5.1. Grouping of dyke samples according to the three plots and approximate strike derived from the locality maps in Chapter 2.

<table>
<tr><th>Strike In degrees(°)</th><th>Grouping according to Strike</th><th>Grouping according to TiO_2 v Zr (Fig. 4.1)</th><th>Grouping according to Zr/P v P/Ti (Fig. 4.2)</th><th>Grouping according to Linton's discriminant plot (Fig. 4.3)</th></tr>
<tr><td>0 - 15°</td><td>Kudu, Skelm, Unknown 4</td><td>Skelm 1 and 3, Unknown 4</td><td rowspan="3">Speckled, Peggy, Georgette, Unknown 4, 8 and 9, FRI4, SOL3, Kudu, Sill1, Skelm, Twin</td><td>Skelm 1 and 3, Unknown 4, FRI4.</td></tr>
<tr><td>60 – 75°</td><td>Twin, Unknown 8 and 9</td><td>Unknown 8 and 9, Peggy, Kudu, CLA, GEOR3, Soll, Skelm 5</td><td>Unknown 8 and 9, Peggy, Kudu, SOL3, Skelm 5, JEA2</td></tr>
<tr><td>90 – 105°</td><td>Peggy, Georgette, Speckled</td><td>Speckled, Georgette, Sill1, Twin</td><td>Speckled, Georgette, Sill1, Twin</td></tr>
<tr><td>15 – 30°</td><td>Sill, Friday, PE, Little Tumi, Swannie</td><td rowspan="2">Friday, PE, Jeans, Swannie, Sill2, Skelm 2, Amigo</td><td rowspan="2">Jeans, Friday, PE, Sill2, Swannie, Amigo 1 and 2, SKE2</td><td>CLA, Soll</td></tr>
<tr><td>30 – 45°</td><td>Lib, Jeans</td><td>Friday, Jeans, PE, Sill2, Swannie, Skelm 2, Amigo 1 and 2</td></tr>
<tr><td>150–165°</td><td>Bank, CLA, Brazil, Ken, Amigo, Soll</td><td>Bank, Brazil, Ken</td><td>CLA, Ken, Brazil, Soll, Bank, Amigo 3 and 5</td><td>Bank, Brazil, Ken, Amigo 3 and 5</td></tr>
</table>

None of the dykes sampled in this study can be classified as epidiorites, as no dykes with 120° strike were sampled. McCarthy *et al*., (1990) did, however, not include any Bushveld, Pilanesberg or Karoo dykes in their study. This prevents any definite conclusions, regarding dyke ages based on strike, to be made at this stage in the study. The similarity in strike of the Jeans and Lib dykes is not reflected in their geochemistry. The Lib dyke never plots close to the Jeans dyke in any of the three plots used (Figs. 5.1, 5.2 and 5.3), but is chemically similar to the Little Tumi dyke. If the two dykes do share a common origin, it seems plausible that one of them was emplaced in a re-activated weak zone created by tectonism in the Witwatersrand rocks.

5.2 Classification According to Literature Data

As was previously mentioned, the dykes in the Carletonville mines, as in the ERPM mine (McCarthy *et al.,* 1990), are related to a number of igneous events. Although a cumulate effect can be found in dykes, resulting in the enrichment of mantle-compatible elements such as Cr and Ni, their chemistry should be similar to the lavas for which they acted as feeder channels (McCarthy *et al.*, 1990). In an attempt to correlate the dykes with other igneous events, geochemical data from literature were collected for the following:

- Ventersdorp Supergroup (Bowen, 1984a),
- The Hekpoort lavas (Oberholzer, 1995) and the Bushy Bend lavas (Eriksson, 1994),
- Tholeiites and basalts from the Marginal Zone and sills of the Bushveld Complex (Davies and Tredoux, 1985),
- Marginal Rocks from the Eastern Bushveld Complex (Harmer and Sharpe, 1985),
- The Losberg Complex (Danchin and Ferguson, 1970) and Bushveld-aged sills in the Vredefort Dome (Coetzee *et al.*, 2006) and Fochville areas (Cawthorn *et al.*, 1981).
- Karoo dolerites (Erlank, 1984, Sweeney, *et al.*, 1994 and Elburg and Goldberg, 2000).

Sufficient data for the Pilanesberg alkaline complex is unavailable, but these rocks should be easily recognisable from their geochemical characteristics, as alkali rocks usually contain very small amounts of compatible elements such as MgO, CaO, TiO_2, Ni and Cr and unusually high concentrations of K_2O, N_2O, Zr, Y and REEs (Gerasimovsky, 1974).

The geochemical data of all these igneous events, excluding Pilanesberg, were plotted on the same plots used for the mine data, namely TiO_2 v Zr, Zr/P v P/Ti (Bowen, 1984a), and Linton's discriminant plot (1992) (Fig. 5.4). As these plots employ only incompatible elements, they cannot be affected by the cumulate effect previously mentioned.

In the TiO_2 v Zr plot (Fig. 5.4A) it is possible to distinguish between Bushveld samples, high-Ti-Zr Karoo basalts and most of the Klipriviersberg rocks. As expected, the Losberg rocks (Danchin and Ferguson, 1970) and Vredefort tholeiites (Coetzee *et al.*, 2006) group with the Bushveld rocks. The Lorraine-Edenville rocks form a separate small group within the Bushveld field. Very little separation is found between the Hekpoort lavas and the Bushveld rocks, as well as between the Lesotho formation basalts, the Bushy Bend lavas and the Alberton and Orkney Formation.

In the Zr/P v P/Ti plot (Fig. 5.4B) very little separation is found between many of the groups, excluding the Makwassie Formation and the Goedgenoeg and Rietgat Formations. This plot is therefore not useful for determining to which igneous provinces the dykes are related.

On Linton's discriminant plot (1992) (Fig. 5.4C), essentially the same kind of separation is achieved as in the TiO_2 v Zr plot (Fig. 5.4A). Using the literature data on the plots, fields can be derived that can in turn be used to classify the Carletonville mine samples.

The Loraine-Edenville rocks are indistinguishable from the Bushveld rocks on these plots. In order to obtain a better separation between the two groups, principle component analysis (Le Maitre, 1968) was attempted. Principle component analysis defines a new set of orthogonal axes, or eigenvectors, which gives the maximum spread of the data in the direction of these vectors. Each eigenvector has an

associated eigenvalue which indicates the proportion of total variance represented by the vector (Table 5.2).

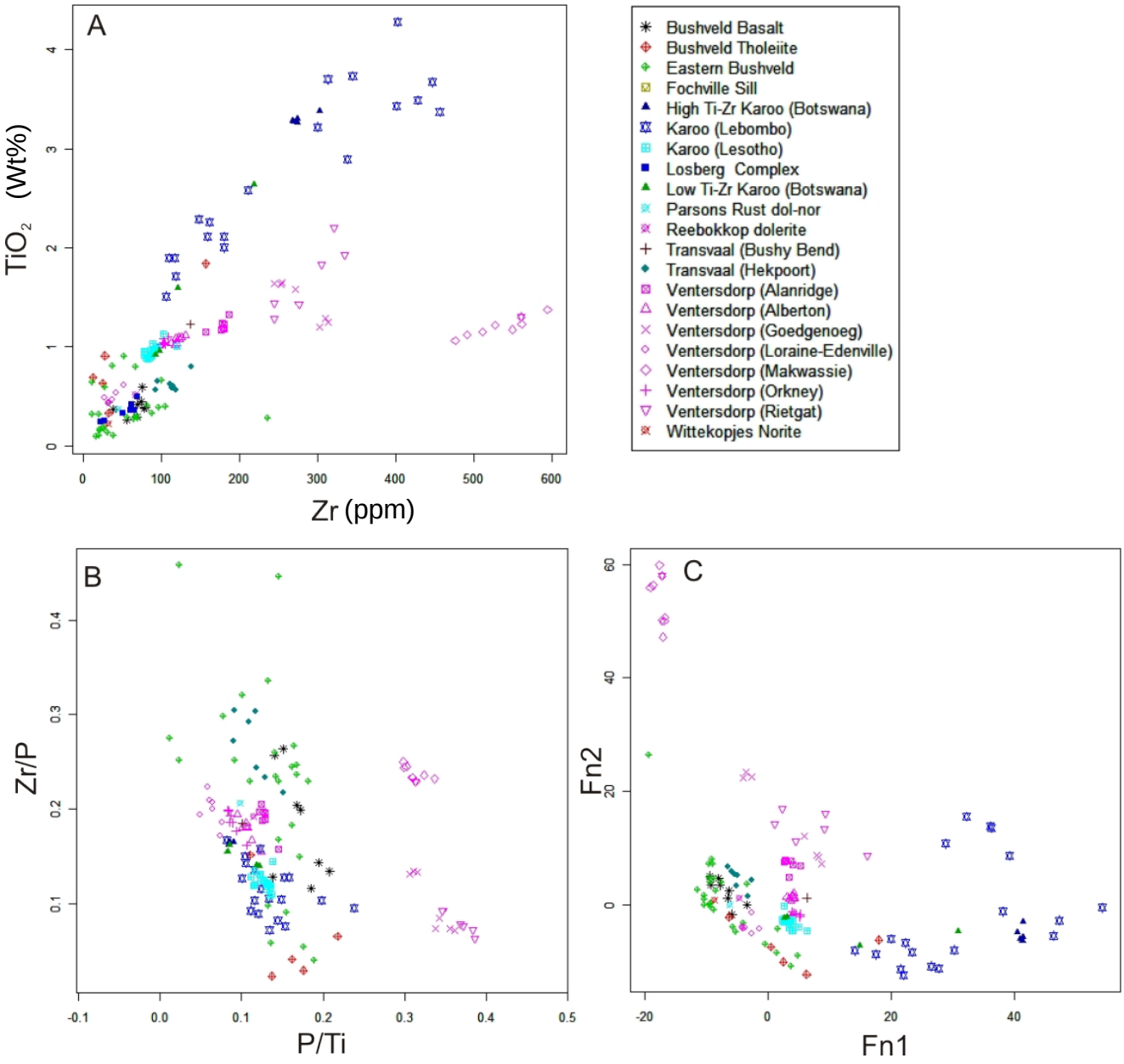

Figure 5.4. Data from various igneous provinces with possible relevance to the study area on, A: TiO_2 (wt%) v Zr (ppm); B: Zr/P v P/Ti; C: disciminant plots. A and B is derived from (Bowen, 1984a) and C from Linton, 1992). Fn1=0.0172Y-0.06078Zr+20.8084TiO_2-11.4636 and Fn2=-0.24892Y+0.16017Zr-11.7088TiO_2-0.07079.

The number of vectors equals the number of variables, and each variable is assigned a coefficient (Table 5.3). The sum of the squares of these coefficients equals 1. The first eigenvector will contain the most information, with subsequent functions containing less (Le Maitre, 1968 and Rolllinson, 1993). Principle

component analysis was executed in GCDkit (Janousek *et al.,* 2007). The best separation was obtained when Rb, Sr and SiO_2 were used, although SiO_2 only occurs in the third component, and therefore only Rb and Sr were plotted.

Table 5.2. The importance of the components, including the proportion of variance and cumulative proportion of each component. All values were rounded to three decimals. Values were generated by GCDkit (Janousek *et al.*, 2007).

	Component 1	Component 2	Component 3
Standard deviation	144.591	59.511	3.665
Proportion of Variance	0.855	0.145	0.000
Cumulative Proportion	0.855	0.999	1.000

Table 5.3. The coefficients of each variable used in principle component analysis, generated by GCDkit (Janousek *et al.*, 2007).

	Component 1	Component 2	Component 3
SiO2			1.00
Rb	-0.813	-0.583	
Sr	0.583	-0.813	

This plot, however, still does not separate the groups perfectly (Fig. 5.5). The Eastern BIC (Harmer and Sharpe, 1985) rocks and, to a certain extent, tholeiitic rocks (Davies and Tredoux, 1985) from the Marginal Zone of the BIC can be separated from the Loraine-Edenville rocks (Bowen, 1984a), but there is still significant overlap between the Loraine-Edenville rocks and the basaltic Bushveld rocks (Davies and Tredoux, 1985). It should also be mentioned that Rb and Sr are potentially not reliable, due to their mobility; this plot should therefore be used with circumspection where altered rocks, such as those encountered in this study, are concerned.

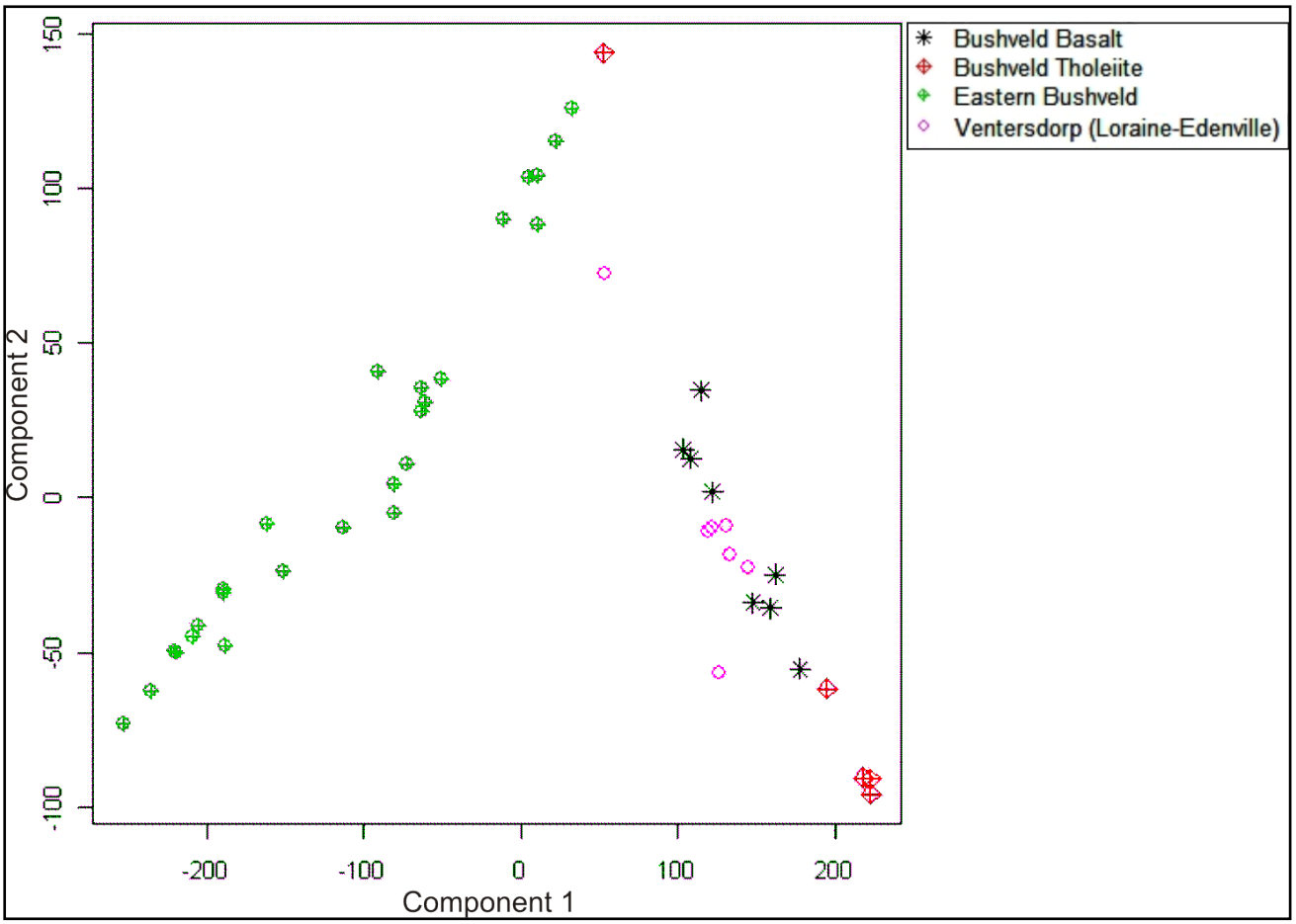

Figure 5.5. The separation of Bushveld (Harmer and Sharpe, 1985 and Davies and Tredoux, 1985) and Loraine-Edenville (Bowen, 1984a) rocks achieved by principle component analysis (Le Maitre, 1968).

Chemical compositions from dykes from ERPM mine that have already been grouped according to the stratigraphy (McCarthy *et al.*, 1990) were also plotted on the same systems for the purpose of comparison. When the geochemistry of the dykes from ERPM (McCarthy *et al.*, 1990) are plotted on TiO2 v Zr (Fig. 4.6) the Bushveld 1, 2 and 3 type dykes, as well as the Loraine and Jeanette dykes plot in the Bushveld and Loraine-Edenville fields and are chemically indistinguishable. The Alberton Formation dykes plot in the Ventersdorp field, but the Westonaria and Orkney Formation dykes enlarge this field, causing it to overlap with the fields of the Hekpoort and Lesotho Formations. The ilmenite diabase, epidiorite and Bushveld 4 dykes form three separate groups that encroach into the Lebombo basalt field (Fig. 5.6).

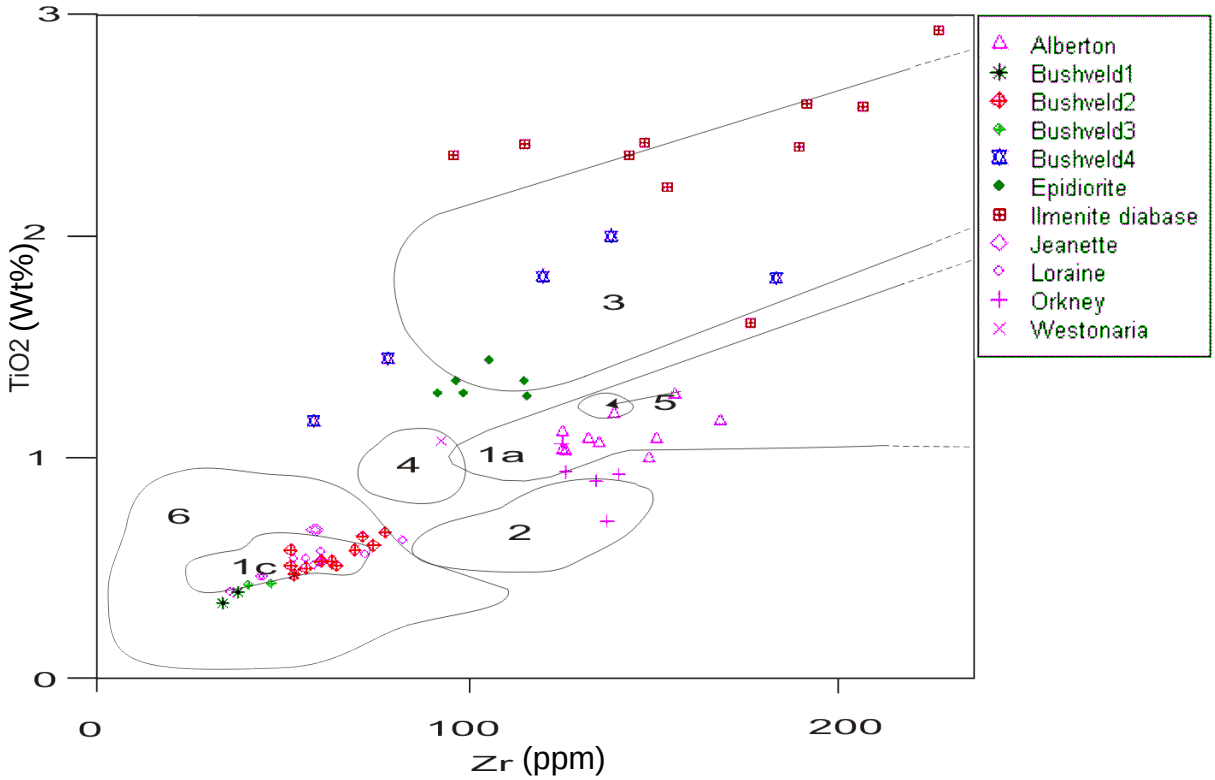

Figure 5.6. The geochemistry of dykes from ERPM compared to literature data fields derived from Fig. 5.4A. 1a: Alberton, Rietgat, Goedgenoeg, Orkney and Alanridge Formations (Ventersdorp Supergroup); 1c: Loraine-Edenville Formation (Ventersdorp Supergroup); 2: Lesotho Formation (Karoo); 3: Lebombo Basalts (Karoo); 4: Hekpoort Lavas (Transvaal Supergroup); 5: Bushy Bend Lavas (Transvaal Supergroup); 6: Bushveld Igneous Complex.

On Linton's discriminant plot (1992) (Fig. 5.7), the Alberton, Orkney and Westonaria Formation dykes all plot in the Ventersdorp field. The Bushveld 1, 2 and 3 and Loraine and Jeanette dykes form a tight group that mostly coincides with the Bushveld field. The ilmenite diabase and Bushveld 4 dykes once again form two separate groups that overlap with the Lebombo basalt field. The epidiorite dykes do not plot in any of the fields.

When the mine samples are plotted on the TiO_2 v Zr plot (Fig. 4.8), the Georgette, Twin and Speckled dykes as well as Unknown 6 are classified as Lorraine-Edenville rocks, with SIL1 plotting in the Bushveld field. The PE, Friday, Swannie, Skelm, Jeans, Soll, some Peggy samples and Unknown 1, 2 and 4. Apart from the Ventersdorp lava sample, Unknown 7, JEA 3, Unknown3 and two Peggy samples are grouped as Klipriviersberg rocks, with 3 of the other Peggy samples plotting in the Lebombo Basalt field and one as an Epidiorite. Unknown 3, 8 and 9 and SKE5 plot as Ventersdorp dykes. The CLA dyke is classified as a Type 4 Bushveld dyke,

but the Soll dyke and GEOR3 plot very close to this field, although SOL3 plots away from the other two Soll dyke samples. The Brazil, Ken and Amigo dykes form their own separate field, and the Lib and Little Tumi samples are separated from all other samples and fields as a result of their high Zr, but moderate TiO_2 contents. The rest of the dyke samples all plot as Lebombo Basalts.

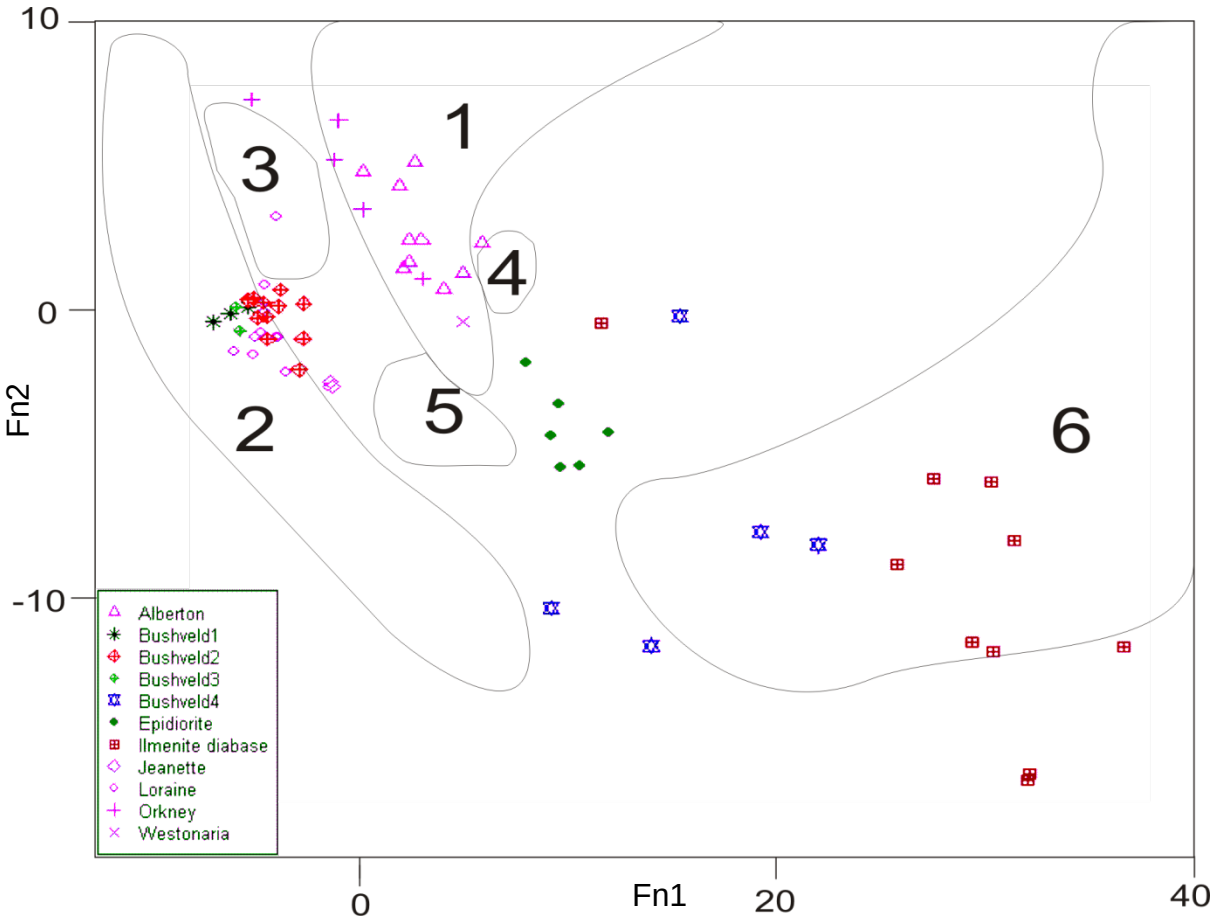

Figure 5. 7. The geochemistry of dykes from ERPM (McCarthy *et al.,* 1990) compared to literature data fields derived from Fig. 4.4C. 1: Ventersdorp Supergroup; 2: Bushveld Igneous Complex; 3: Hekpoort Formation; 4: Bushy Bend Lavas; 5: Lesotho Formation Basalts; 6: Lebombo Basalts.

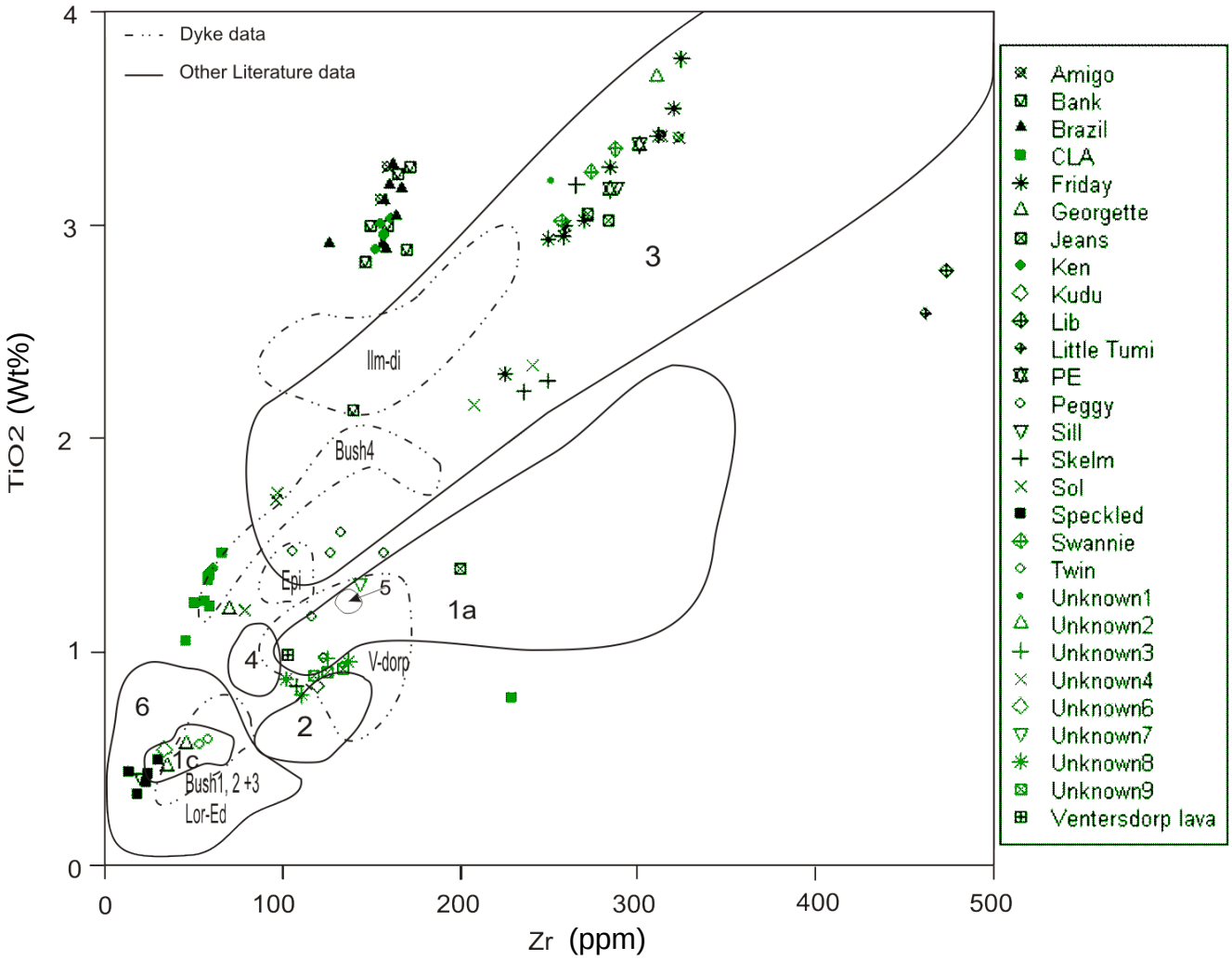

Figure 5.8. The geochemistry of dykes from the study area compared to all literature data fields on TiO_2 (wt%) v Zr (ppm). 1: Ventersdorp Supergroup; 2: Bushveld Igneous Complex; 3: Hekpoort Formation; 4: Bushy Bend Lavas; 5: Lesotho Formation Basalts; 6: Lebombo Basalts. ERPM dyke data (McCarthy *et al.,* 1990): "V-dorp": Ventersdorp; "Lor-Ed": Loraine-Edenville: "Bush": Bushveld Type; "Epi": Epidiorite; "Ilm-di": Ilmenite-diabase.

In Linton's discriminant plot (Fig. 5.9), the Speckled dyke and SIL1 are classified as either Lorraine-Edenville or Bushveld rocks, with the Georgette and twin dykes and UNK6 sample plotting in the Bushveld/Loraine-Edenville dyke field. Unknown 8 and 9, the Ventersdorp lava sample, the Kudu dyke and Unknown 4 are classified as Ventersdorp rocks. The Friday, Amigo, Jeans, PE and Swannie dykes are classified as high Ti-Zr Karoo dolerites, along with Unknown 1 and 2 and the CLA dyke and Ken 1 and 4 are classified as Type 4 Bushveld dykes, and SOL 1 and 2 could be either Bushveld rocks or high-Ti-Zr Karoo dolerite. The Brazil, Ken, Amigo and Bank dykes plot in a field of their own, except for two Bank dyke samples and one Brazil dyke sample that plot in the Ilmenite-Diabase field. The Lib and Little Tumi Dykes once again plot away from the other fields.

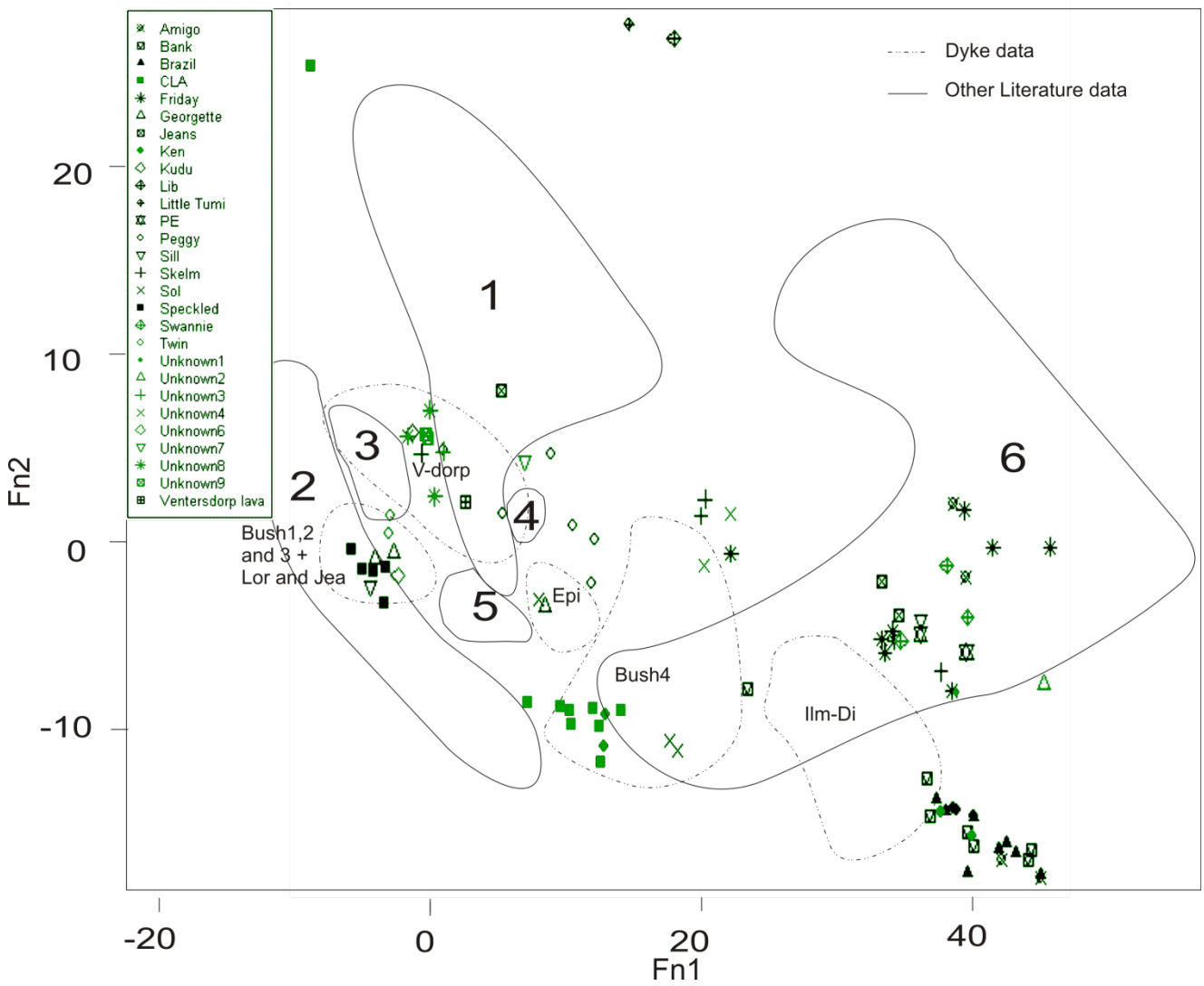

Figure 5.9. The geochemistry of dykes from the study area compared to all literature data fields on Linton's (1992) discriminant plot. 1: Ventersdorp Supergroup; 2: Bushveld Igneous Complex; 3: Hekpoort Formation; 4: Bushy Bend Lavas; 5: Lesotho Formation Basalts; 6: Lebombo Basalts. ERPM dyke data (McCarthy *et al.,* 1990): "V-dorp": Ventersdorp; "Lor-Ed": Loraine-Edenville: "Bush": Bushveld Type; "Epi": Epidiorite; "Ilm-di": Ilmenite-diabase.

5.3 Rare Earth Elements

The Rare Earth Elements (REEs) all have very similar chemical and physical properties as they all form stable trivalent ions of similar size. The differences in chemical behaviour result from the small but steady decrease in size with increase in atomic number. These small differences cause REEs to become fractionated relative to each other (Rollinson, 1993). The light REEs (LREEs) are incompatible in the mantle and become concentrated in melts during partial melting. Consequently, the mantle becomes LREE depleted (White, 2007). For this reason rocks containing olivine and ortho- and clinopyroxene are more enriched in the

heavy REEs. However, the REEs are all incompatible in these minerals in basaltic and andesitic liquids, and are only slightly fractionated. Extreme depletion of the HREE could indicate the presence of garnet in the source. The middle REEs, Sm to Ho, are highly compatible in hornblende and even a moderate amount of this mineral can cause enrichment of these elements. Clinopyroxene has a similar effect on the MREEs although the effect is not so pronounced (Rollinson, 1993). The REEs are highly insoluble and immobile and REE patterns generally remain unchanged during low-grade metamorphism and weathering. As a result it is possible to derive the pre-metamorphic history of rocks from REE patterns (White, 2007).

5.3.1 Discussion of REE Patterns

REE concentrations were normalised using the C1 chondrite values published by Anders and Grevesse (1989). REE with even atomic numbers are more stable, and therefore more abundant than REE with odd atomic numbers. This will result in a zigzag pattern when “raw” REE data is plotted according to increasing atomic number. It is for this reason that REE data has to be normalised. The REE concentrations of chondritic meteorites are the most popular choice for normalising values for two reasons. The first is that they are thought to be relatively unfractionated samples of the solar system, and normalising with chondrite values will not only eliminate the variation between odd and even atomic number elements, but will also allow the identification of any REE fractionation relative to chondritic meteorites. The second reason is that element concentrations can be determined by analysis rather than by estimation, as is the case with primitive mantle values (Rollinson, 1993).

The dykes show a variety of REE patterns (Fig. 5.10). At a first glance it seems that the dykes can be divided into three groups based on their LREE content: The CLA, and Unkown 6 dykes and the SIL1 have either virtually no LREE enrichment or a slight depletion, others have intermediate LREE content (Ventersdorp lava and the Twin, Georgette, Amigo and Soll dykes), and a third group is highly enriched by LREEs (the Little Tumi and Lib dykes). The CLA and Unknown 6 dykes, as well as the sill have an almost chondritic pattern with the CLA dyke having a very slight

negative Eu anomaly. The implications of these flat patterns will be discussed subsequently.

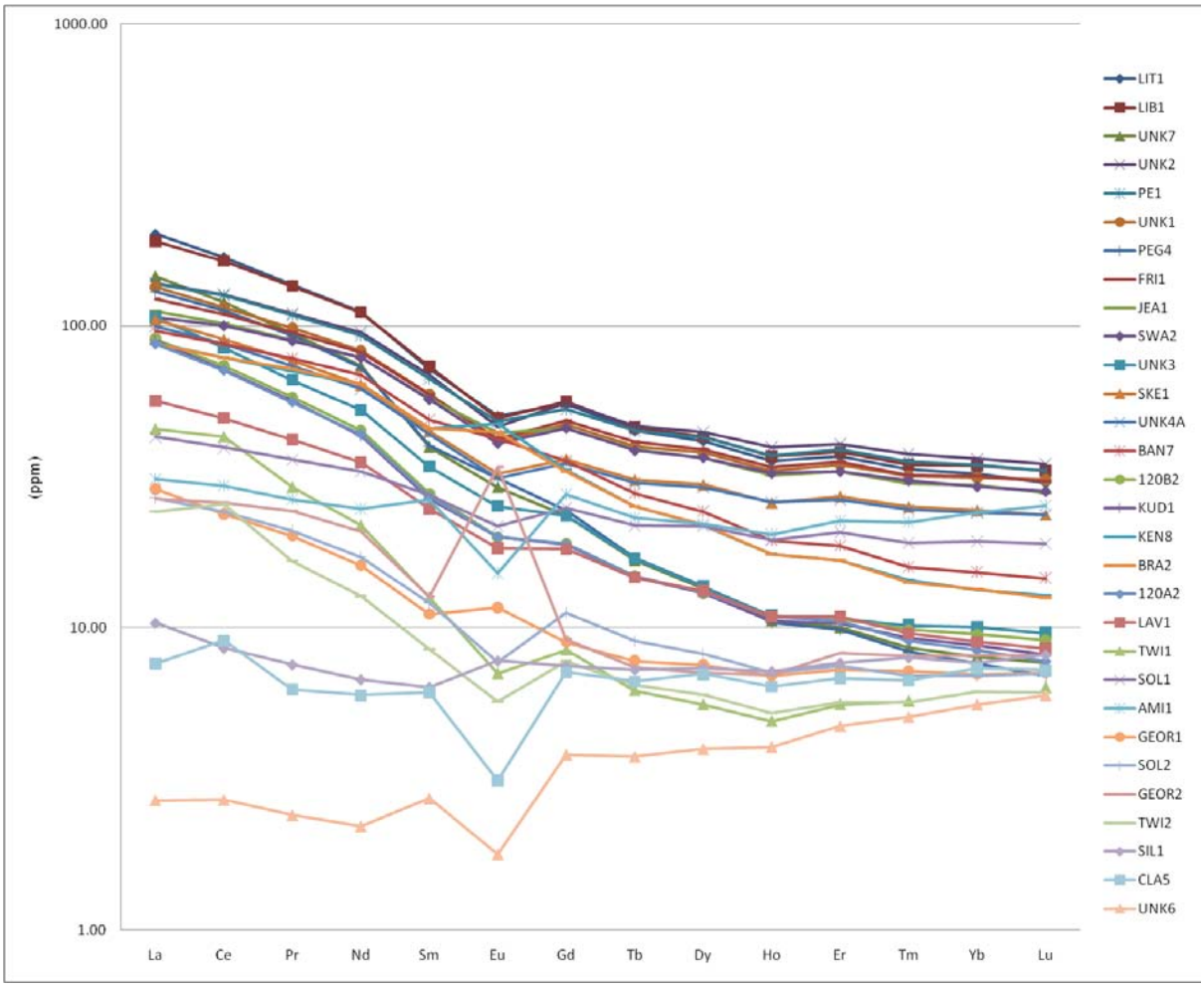

Figure 5.10. The REE patterns of the dykes. REE data normalised to C1 chondrite after Anders and Grevesse (1989).

The two Georgette dyke samples have very similar patterns. Both show some enrichment in the LREEs, but GEOR2 has a very large positive Eu anomaly, reflecting the large amount of plagioclase in the sample (Fig. 3.10) (Rollinson, 1993). This Eu anomaly is not accompanied by unusually high CaO, Na_2O or K_2O concentrations, but all three element oxides were shown to have been mobile (Fig. 4.9 E, F and H) and may therefore have been removed from the sample. Eu, on the other hand is immobile (White, 2007) and would not have been removed. In numerous cases the REE patterns overlap to such an extent that the different samples become indistinguishable from one another. These include, PE1 and Unknown 2; Kudu, Unknown8 and 9(120A) and (120B); and, to a lesser extent, Ken

and Brazil. The most variation is found on the LREE side of the diagram with the least fractionation having taken place in the HREEs.

5.3.2 Classification of dykes according to REE data from literature

REE data for the Ventersdorp Supergroup, specifically from the Alberton, Orkney and Loraine-Edenville formations (Marsh, *et al.*, 1992), Bushveld-aged dykes and sills (Maier and Barnes, 1998) and both high and low Ti-Zr Karoo basalts (Elburg and Goldberg, 2000) were collected for the purpose of comparison with data from this study. The data were chondrite normalised using the values published by Anders and Grevesse (1989), plotted, and converted to fields that cover a range of REE data for each igneous province (Fig. 5.11), by tracing the highest and lowest values for each element. Dotted lines indicate the absence of element data.

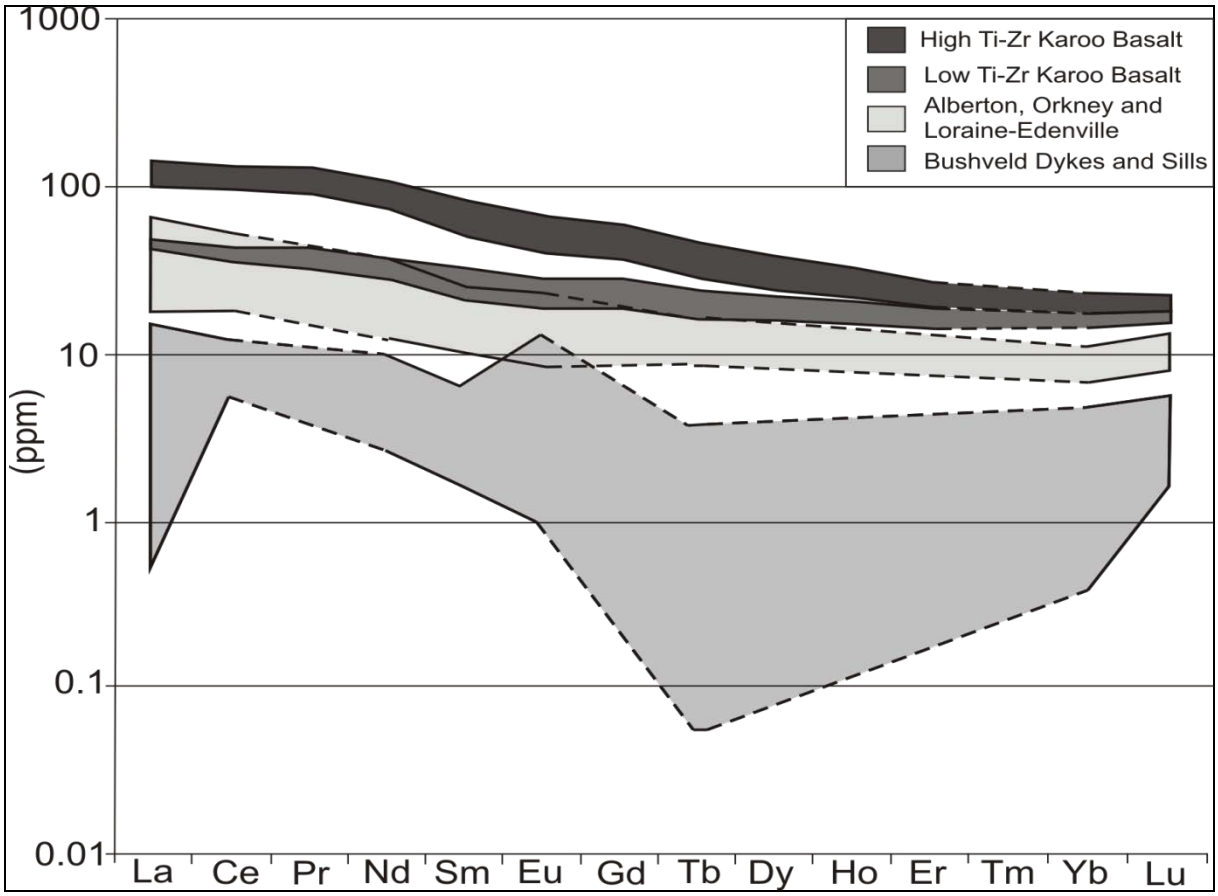

Figure 5.11. Fields derived from REE data for the Ventersdorp (Marsh *et al.*, 1992), Bushveld (Maier and Barnes, 1998) and Karoo (Elburg and Goldberg, 2000), mafic rocks.

The REE data from this study was then plotted over these fields in order to obtain a classification (Fig. 5.12).

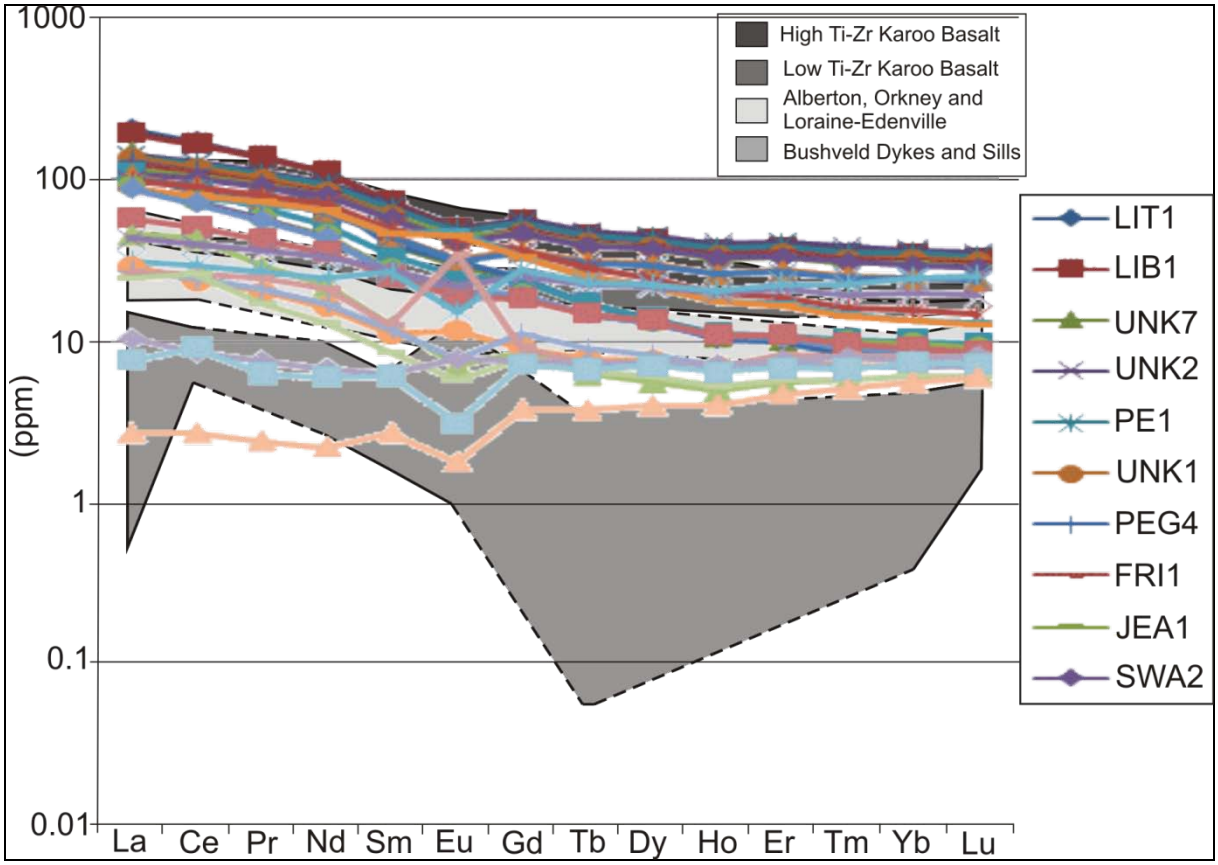

Figure 5.12. Dyke REE data from this study compared to literature REE data. Karoo (Elburg and Goldberg, 2000), Ventersdorp (Marsh *et al.*, 1992) and Bushveld (Maier and Barnes, 1998).

When REE data from this study are compared to literature data (Fig. 5.11 and 5.12), CLA5, SIL1 and UNK6 are classified as Bushveld intrusives, confirming the classification of both the TiO_2 v Zr and Linton discriminant plots. Although AMI1 is over all more enriched in REEs than CLA dyke, it has a pattern very similar to that of the Bushveld intrusives (Fig. 5.13).

LAV1 plots in the Ventersdorp field and corresponds exactly to the Alberton Formation REE pattern (Fig. 5.12). The greatest variation in REE content in the different volcanic formations in the Ventersdorp Supergroup is found in the LREEs, with very little variation in HREEs. For the Allanridge, Goedgenoeg, Rietgat and Makwassie Formations only La, Ce and Nd data are available (Bowen, 1984a), but this is adequate to show that these rocks are considerably more LREE enriched than the Loraine-Edenville, Orkney and Alberton Formations. LAV1 shows a very slight negative Eu anomaly. The data from Marsh *et al*. (1992) does not include Gd, making it difficult to draw any conclusions about the presence of Eu anomalies from

their data. However, it is probably safe to assume that such an anomaly is present to a greater or lesser extent in all the mafic Ventersdorp rocks. When these criteria are used in the identification of Ventersdorp-age dykes, the Little Tumi, Lib, PE, Friday, Jeans, Swannie, Skelm, Kudu and Unknown 8 and 9 dykes, as well as the Unknown 1, 2, and 4 samples are classified as Ventersdorp dykes (Fig. 5.14).

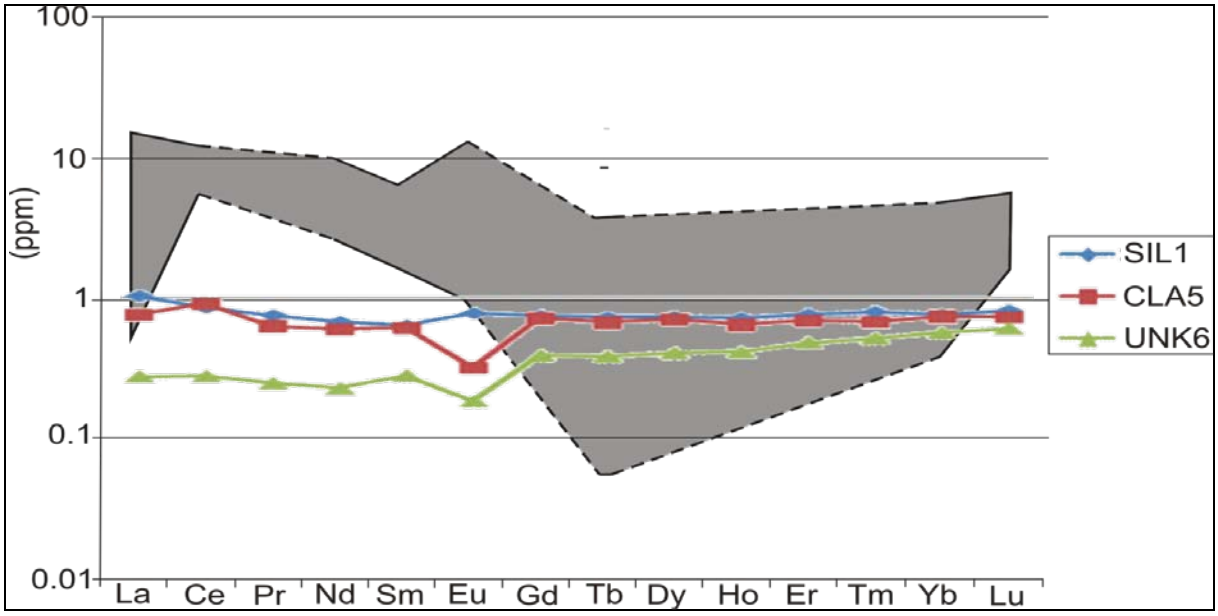

Figure 5. 13. REE patterns of the CLA dyke, SIL1 and UNK6 compared to Busveld REE data (Maier and Barnes, 1998).

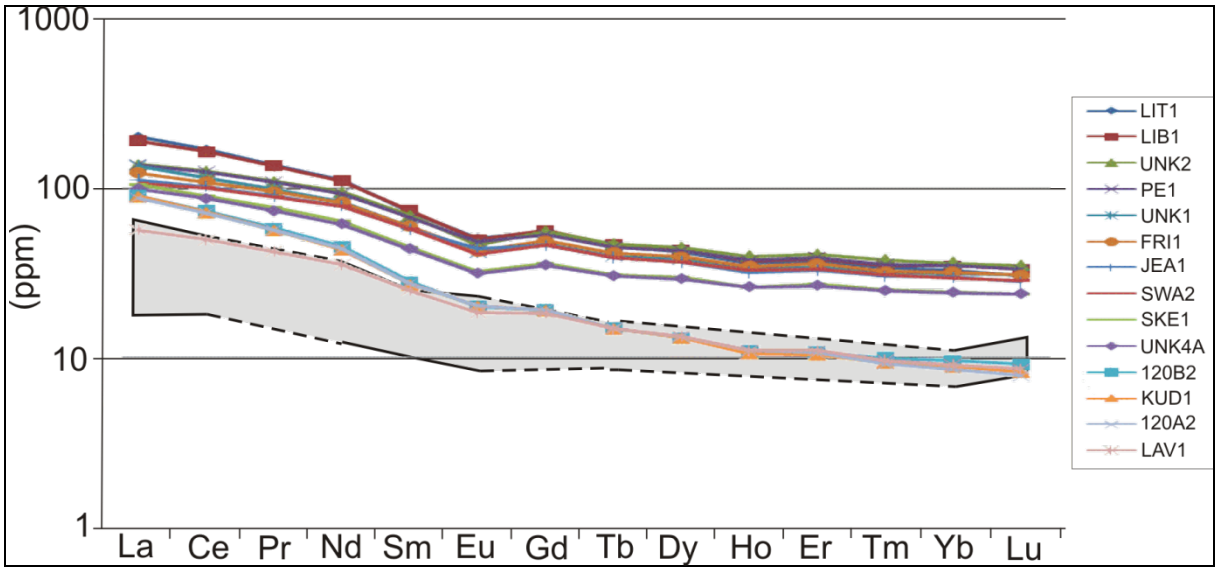

Figure 5.14. Dykes with similar (likely Ventersdorp) REE patterns compared to data from Marsh *et al.* (1992).

The Soll dyke's REE pattern matches that of the low-Ti-Zr Karoo basalt, although SOL1 does not fit exactly into the low-Ti-Zr basalt field and SOL2 plots completely outside of this field (Fig. 5.15). None of the samples fit the high-Ti-Zr Karoo basalt field.

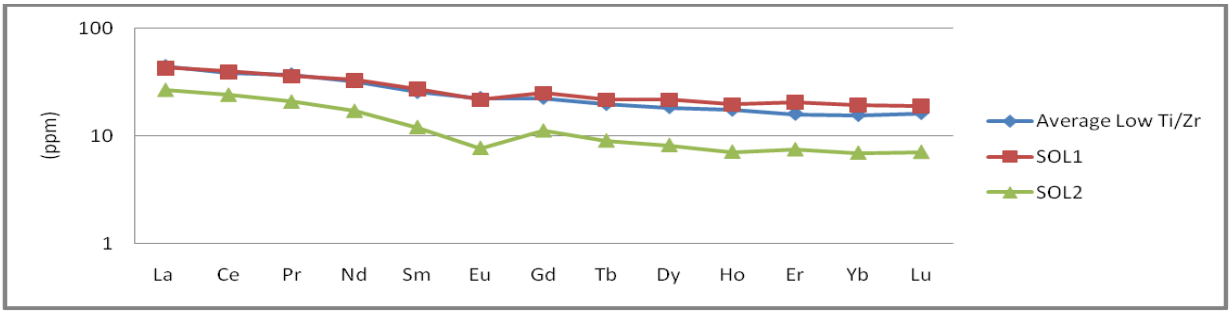

Figure 5.15. REE patterns from the Soll dyke compared to the average REEs in low Ti/Zr Karoo basalt (Elburg and Goldberg, 2000).

The remaining 10 samples seem to belong to three different groups (Fig. 5.16). The Brazil, Bank and Ken samples plot below the high-Ti-Zr Karoo Basalt field, but run almost perfectly parallel to it, and it seems likely that they may belong to this group. The Peggy dyke and its two matching Unknown samples, UNK 3 and 7 are difficult to place. Lenhard (1988) identified the Peggy dyke as being of Ventersdorp age, but its REE pattern is considerably steeper than that of the other Ventersdorp dykes. However, these samples do not fit in any of the other fields, and the other element plots (Figs. 5.8 and 5.9) classify the Peggy dyke as having a Ventersdorp, or close to Ventersdorp, chemical composition. It is therefore likely that Lenhard's classification (1988) of the Peggy dyke is correct.

The two Twin and Georgette dyke samples clearly fall in a group of their own. The only remaining mafic igneous event in the region, other than those which have been considered up until now, is the Pilanesberg Alkaline Complex and its related intrusives. Comparison of dyke samples with Pilanesberg geochemistry is hindered by the aparent lack of available data. In order to test the possibility of the Twin and Georgette dykes belonging to the Pilanesberg Complex, REE data from two syenite dykes from the Noqui Alkaline Province in the Democratic Republic of Congo (Makutu *et al.*, 2004), as well as one syenite sample from the Palabora Complex in South Africa, NIM-S (Govindaraju, 1994), were used to derive an REE field for syenites (Fig. 5.17). Apart from the large positive Eu anomaly in GEOR2, the Twin

and Georgette dykes fit the syenite field perfectly. This classification is a “best-fit” for the data available and should not be seen as a definite classification.

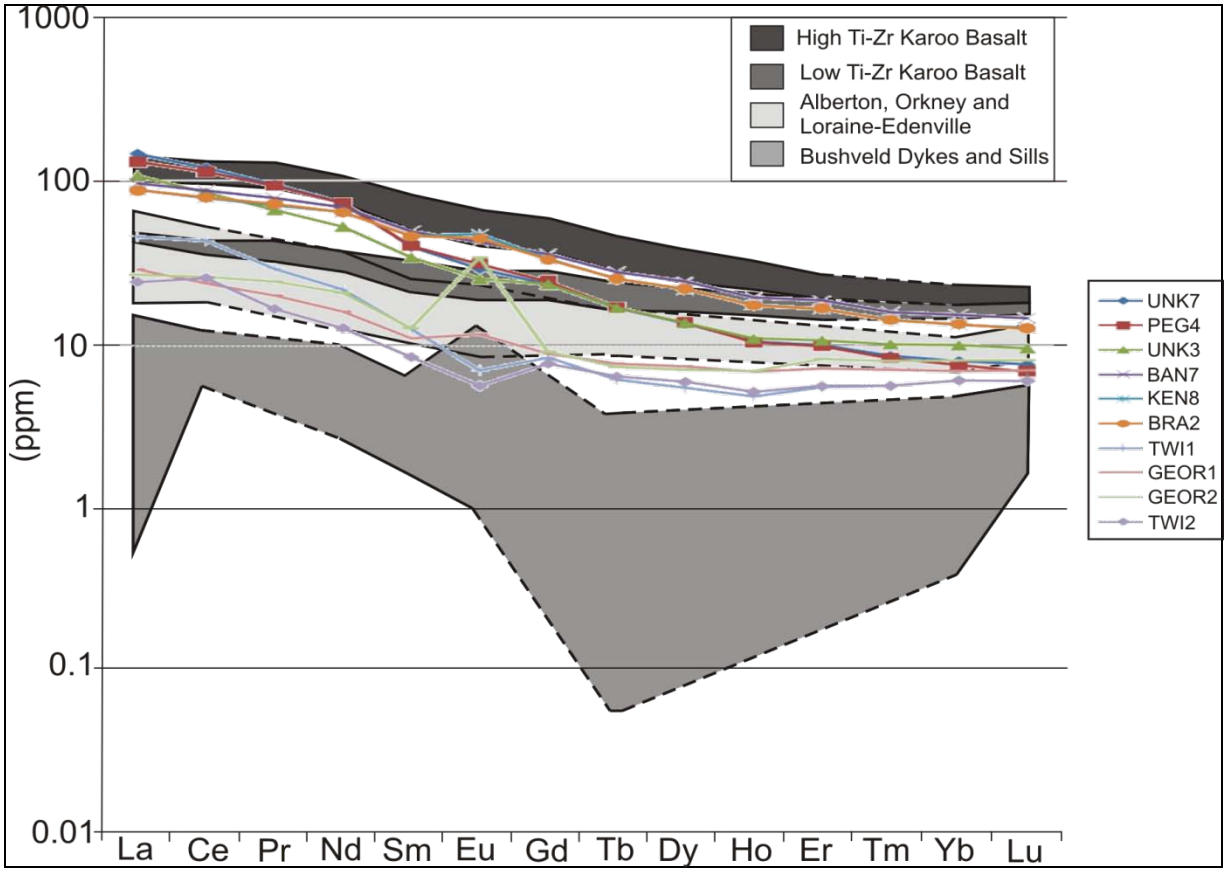

Figure 5.16. REE patterns of the, hitherto, unclassified dykes compared to the REE fields of Ventersdorp (Marsh *et al.*, 1992) and Bushveld (Maier and Barnes, 1998) and Karoo rocks (Elburg and Goldberg, 2000).

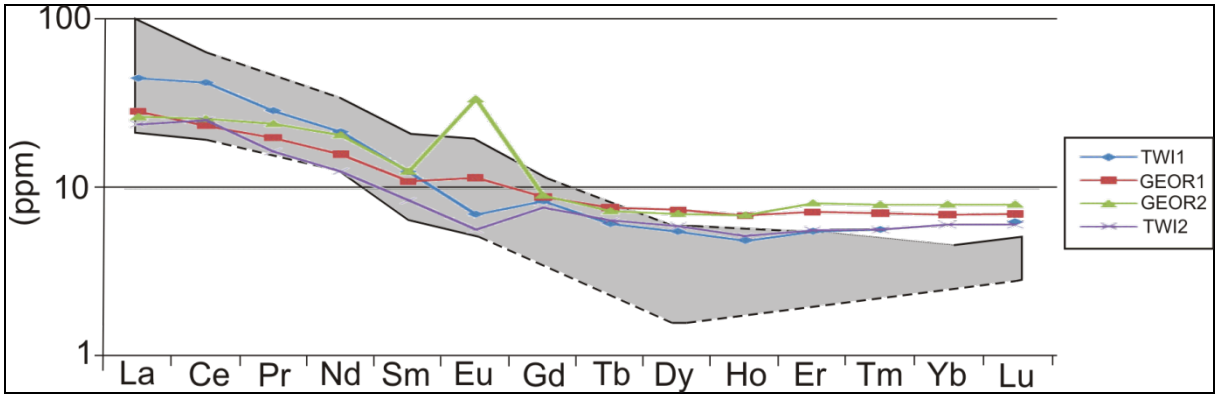

Figure 5. 17. A comparison of the unclassified dykes with an REE field derived from syenites from the Democratic Republic of Congo (Makutu *et al.*, 2004) and the Palabora Complex, South Africa (Govindaraju, 1994).

5.4 Discussion

Differences in geochemistry between dykes of the same age, or even samples from the same dyke, could be the result of differences in grade of metamorphism and alteration conditions between dykes or in different locations along one dyke, an argument which is strengthened by the variations in mineralogy discussed in Chapter 3. In order to understand how such differences in alteration could have come about, one needs to take a closer look at fluid flow in the Witwatersrand Supergroup.

Various types of fluids that contributed to metamorphism and alteration were present during the diagenesis and metamorphism of the Witwatersrand Supergroup. These are: connate waters that were trapped in pore spaces and bound in clay minerals, and were expelled during compaction and diagenesis; metamorphic fluids produced when hydrous minerals are broken down at higher temperatures and pressures; retrograde fluids that are present after peak metamorphism; meteoric or surface waters that invade the basin along permeable horizons; and magmatic fluids from the intrusives (Phillips *et al*., 1990).

Connate water from the original Witwatersrand sediments can be disregarded when one considers the influence of fluids on the dykes, as, during compaction, this water would have moved to the margin of the basin towards areas of lower pressure (Phillips *et al*., 1990). The movement of metamorphic fluid is controlled by deformation zones, and especially by microscopic and even sub-microscopic dislocations along grain boundaries. Meteoric waters can invade the Witwatersrand Basin at any time, especially in areas where it crops out (Phillips *et al*., 1990). Meteoric water influx and movement occurs along permeable horizons and may be channelled parallel to impermeable lithologies. Dykes that extend all the way to the surface can therefore act as conduits for meteoric water to enter the lower parts of the basin. The role of retrograde fluids is negligible, as mineralogical studies indicate that only minimal retrograde metamorphism has occurred both in the Witwatersrand rocks themselves and in the intrusives (Phillips *et al*., 1990). The extent of the effect of magmatic fluids is debatable. The majority of the magmas that intruded into the Witwatersrand Supergroup were mafic, and could therefore not have had high water contents. As a result, the influence of magmatic fluids was very localised and concentrated around the intrusives (Phillips *et al*., 1990). For the

magmatic water of an intrusive to have any effect on an older intrusive, the two must be situated very close together, or even cut each other. Magmatic fluids could therefore be responsible for the alteration of a small part of a dyke, but leave most of it intact (Phillips *et al*., 1990).

According to Onstott *et al.*, (2006) the fracture water in the Witwatersrand Basin represents a mixture of paleo-meteoric water and 2.0 – 2.3 Ga old hydrothermal fluid. The hydrothermal fluid was highly saline and had temperatures of 250 - 300°C. The meteoric water had a low salinity, high CO_2 content, and was approximately 10k – >1.5 Ma old. Mixing of these two components has probably been occurring for at least the past 100 Ma (Onstott *et al.*, 2006).

The misclassification of some dyke samples as other dykes and the reasons there for have been discussed. However, a simple misnaming during logging or sampling cannot always account for scatter. While the chemical differences between samples from the "same" dyke that were taken a considerable distance apart could be explained by them being, in reality, from more than one intrusive, it still does not explain cases such as the Ken and CLA dykes where samples were taken close to one another. For that, one needs to look at possible element mobility.

Even though the HFSEs, that include Ti, Zr, Y and the REEs, are generally regarded as being mobile, it has been found in numerous studies on the weathering and metasomatism of igneous rocks that this is not always the case. One such a study was conducted on weakly altered to completely kaolinitised andesites and dacites from the Erenler Dağı Volcanics in Konya, Turkey (Karakaya, 2009). These rocks were weakly to highly altered by hydrothermal fluids and then weathered by surface conditions. It was found that Zr and Y remain immobile in weakly to moderately altered rocks, but that their concentrations decreased significantly in the kaolinitised rocks. The Light and Middle REE contents were found to decrease slightly with weak to moderate alteration, but would increase in the completely weathered rock, but in general REE patterns of moderately altered rocks were sub-parallel to that of the parent rock, but with a slight overall depletion.

Experimental and field data has shown that HFSE can occur in a wide range of temperature and pressure conditions. Zr and Ti solubility is largely enhanced with increasing P and T (Jiang *et al.*, 2005). High temperature alteration at the Strange

Lake peralkaline complex of North-Eastern Canada resulted in a depletion of HFSE and HREE, while these elements were significantly enriched in areas of low temperature alteration (Salvi and Williams-Jones, 1996). Both very high and very low pH conditions can result in the mobilisation of Ti and Zr. Furthermore, the presence of F^- and OH^- can result in the formation of Zr-F-OH complexes that lead to the solubility of Zr over much wider pH ranges (Jiang *et al.,* 2005). Onstott *et al.* (2006) reported very low (µM) F concentrations in the Witwatersrand fracture water, but the F concentrations may have been significantly higher before large-scale mixing with meteoric water occured. In extreme pH conditions, both Ti and Zr can become mobile in low temperature fluids (270-300°C) (Jiang *et al*., 2005). The mobility of HFSEs in such high pH environments can likely be due to hydroxy and carbonatohydroxo complexing. Sulphate can also act as a complexing agent, but the only data available are from high temperature and pressure environments and more experimental work is needed to test the significance of the influence of sulphate on HFSE mobility (Jiang *et al.,* 2005).

The exact role of complexing ions and their effect on the intrusives in the Witwatersrand Supergroup is difficult to assess. The Witwatersrand Supergroup is made up of a number of different lithologies, and the geochemistry and mineralogy of each will influence the chemistry of the fluids in contact with them to a certain extent. This, in turn, could result in different effects on the intrusives. According to Phillips *et al.* (1990), metamorphic fluids in general had temperatures in excess of 200°C and a neutral to moderately acidic pH. They state that the absence of evaporate minerals mean that chloride and sulphate were not significant, but that fluid inclusion studies confirm the presence of CO_2 and CH_4 (Phillips *et al.*, 1990). However, one should not exclude the possibility that the highly saline, ancient hydrothermal fluids (Onstott *et al.*, 2006) may have had some effect on at least the older dykes before being diluted gradually by meteoric water. The absence of evaporate minerals may possibly be attributed to the later influx of the meteoric water. Whether more extreme pH conditions than those reported by Phillips *et al.* (1990) could have been present on small scale would require a very detailed investigation of the Witwatersrand rocks which is beyond the scope of this study.

The relatively small differences in geochemistry in e.g. the Peggy dyke are possibly the result of element mobility, as the origin of these samples is reasonably certain

and the scatter is more than what one would expect for incompatible elements in a single mafic intrusive, especially compared to other intrusives such as the Friday, Bank and Brazil dykes. Whether large differences in geochemistry over large distances, such as those found in the Jeans dyke, are the result of element mobility or of the sampling of two different intrusives will only become clear if more sampling is done at closer distances along the dyke. The anomalous geochemistry of CLA9 cannot be attributed to either element mobility or distance as all other CLA dyke samples are chemically similar to each other and CLA9 was taken from the same section of drill core as CLA4 and 5. It is, however from the chill zone of the dyke and the most plausible explanation for its anomalous geochemistry would be contamination by the country rock. No other intrusive cuts or comes close enough to the CLA dyke in this particular location for contamination by another dyke to be considered a possibility (Fig 2.4). There is no clear reason why the chemistry of KEN1 and 4 are similar to that of the CLA dyke and further sampling is required in for this issue to be resolved.

The Soll dyke offers proof for the mobilisation of HFSEs by fluids. SOL3 was sampled in a fault, which would act as a conduit for fluids, and is slightly depleted in TiO_2, Zr and Y relative to SOL1 and 2. If these elements were mobile it becomes increasingly possible that the REEs could have been mobile as well. As REE mobility tends to result in a general depletion of REEs while preserving the inherent REE pattern (Karakaya, 2009), this should not affect the allocation of dykes to igneous provinces, although it would influence the allocation of Ventersdorp-age dykes to the different formations within the Supergroup. A small possibility of HREE enrichment exists (Salvi and Williams-Jones, 1996), but as no other HFSEs seem to be significantly enriched, the importance of HREE enrichment is minimal. The well constrained geochemistry of the Brazil, Bank and (to a somewhat lesser extent) Ken dykes, indicates a lesser presence of fluids. The fresh appearance of the Brazil dyke confirms this. This is an indication that these dykes are the youngest of the intrusives. Although Onstott *et al.* (2006) state that the dykes with a north-south strike, of which the Bank dyke is one, belong to the Pilanesberg Complex, they do not provide reasons for this statement.

5.5 Conclusion

The absence of data concerning the strike of dykes other than those of the epidiorites, ilmenite-diabases and early Ventersdorp aged dykes hinder the classification of dykes by the use of strike. The fact that dykes with different origins may have the same strike, due to the intrusion of younger magmas into older weak zones, is an additional problem.

The use of the HFSE Ti, Zr and Y, and the REEs was moderately successful in firstly grouping the dykes among themselves, and secondly in grouping them with other igneous events. Dykes from the Ventersdorp Supergroup (Peggy, Unknown 8 and 9, Kudu and Skelm dykes, and the Jeans dyke in Mponeng, Bushveld Igneous Complex (Speckled and CLA dykes and the sill) and Karoo Igneous Province (Brazil, Bank, Ken and possibly Soll dykes) are present, with the possibility of the Twin and Georgette dykes belonging to the Pilanesberg Complex. Some classifications remain inconclusive, e.g. the Friday and Swannie dykes, that are classified as Ventersdorp dykes in the REE plots, but as high-Ti-Zr Karoo basalts in the other HFSE plots. The variable alteration of the dykes is, in some cases, reflected in their geochemistry, and proof was found that the HFSEs are not entirely immobile. This mobility makes the classification of the dykes more difficult as it causes scatter between samples from the same dyke, and less adherence to the geochemistry of their allocated igneous provinces. The extreme variation in geochemistry between some samples from the same dyke that were taken a considerable distance apart warrants sampling in between in order to determine if the samples are, in reality, from the same dyke.

Chapter 6: The Engineering Aspects of the Dykes

6.1 Introduction

The preceding chapters have, to a greater extent, been purely academic. In practise, the presence of a dyke poses problems during mining. Not only do they impede the rate of mining due to displacement of the ore body, but larger dykes require haulages traversing them to be given special treatment, as they are susceptible to rock bursts (Brink, 1979). According to Gill *et al.* (1993) "a rockburst is a sudden rock failure characterised by the breaking up and expulsion of rock from its surroundings, accompanied by a violent release of energy". Gill *et al.* (1993) defined two broad classes of rock bursts: Type I, resulting from fault-slip events, and Type II, resulting from the failure of the rock mass itself, which includes strain bursts and pillar bursts (Gill *et al.*, 1993). Most of the large seismic events in the mines are recorded close to geological structures. Of these structures, the dykes are considered to be the most hazardous (Chichowicz, 1997). These events are completely random and are very seldom related to blasting (pers. comm. H. Moller, 2009).

6.2 The Dangers Posed by Dykes

The reasons for seismic activity in these areas are related to stress changes in the area, rock properties (particularly rock strength), and the challenges posed by mining in very hard rock such as the dykes (Table 6.1). The deep mine environment is a high stress environment, and the excavations made during mining introduce additional, tensional stresses. In some cases the stresses are not transferred well across major geological structures, causing amplification of stress between the structure and the face. This, in turn leads to a high probability of seismic activity.

Table 6.1. The compressional strength of the three most common lithologies in Tau Tona and Mponeng (supplied by H. Moller, AngloGold Ashanti).

Material	Strength (uni-axial compressive tests)
Dyke	300MPa (or higher)
Quartzite	200MPa
Shale	150MPa

Of all the many different properties of country rock and dykes which can result in different strain rates in the same time window during mining, different rock strengths are the most important (pers. comm. H. Moller, 2009). When a dyke and adjacent country rock are subjected to the same change in stress, they behave differently and so doing, create a mechanism to shear free from each other, resulting in a Type I rock burst (Gill *et al.*, 1993). The nature of the contact between country rock and dyke also determines the size of the seismic event will take place. Two very different types of contacts can both result in seismic events: A welded contact will be broken when stress applied exceeds its strength, and a soft contact with a wavy form that will not allow free movement, will require rock material to be sheared off before movement can take place. During the mining process, the highest stress environment is found immediately ahead of the advancing face. Under normal circumstances, this will induce fracturing in the rock which aids in the redistribution of stresses ahead of the mining face. Most dykes are very hard which means that they will not fracture easily. This results in the build-up of extremely high stress ahead of the mining face, up to the point where the rock fails. The freedom offered by the nearby excavation causes the rock to buckle and burst into the working area (pers. comm. H. Moller, 2009). Jeffery (1975) found that the thickness of the dyke is a contributing factor, and that dykes with thicknesses of ±15m or more are more likely to cause rockbursts than smaller dykes.

The intrusion of dykes altered areas in the surrounding Witwatersrand quartzite and shales by means of contact metamorphism, resulting in a hardened, brittle rock. This rock is blocky and makes it difficult to support the roof of the excavation. The major concern in such an area is fall of ground induced by gravity and seismic activity. Similar blocky conditions are created in dykes as they respond to the stress changes induced by mining. These blocks are usually much larger than in the case of metamorphosed country rock and fall of ground occurrences are generally much more severe (pers. comm. H. Moller, 2009).

6.3 A Case Study

The physical properties of rocks are affected by their degree of alteration, and therefore by their mineralogy and chemistry. A study by Moon and Jayawardane (2004) investigated the relationship between chemistry, mineralogy and

geomechanical characteristics very comprehensively, using rocks from an abandoned basalt quarry at Karamu, near Hamilton, New Zealand. The quarry provided a complete weathering sequence from fresh to completely weathered basalt and the authors identified five weathering zones: fresh, slightly weathered, moderately weathered, highly weathered and completely weathered. At an early stage of weathering a significant decrease in CaO, MgO, FeO, Na_2O, K_2O, Rb and Sr took place, accompanied by a significant relative increase in Fe_2O_3 and Zr.

Very little textural change took place between fresh and moderately weathered basalt, and indeed very little mineralogical change occurred between fresh and slightly altered rocks, with the formation of clay minerals, such as smectite, kaolinite and illite, only becoming significant in moderately weathered rocks. However, the greatest decrease in dry density and increase in porosity, and the accompanying decrease in strength, occurred between fresh and slightly weathered rock. The authors attributed this dramatic loss of intact strength to microfractures that develop due to cation substitution. The loss of Ca^{2+}, Fe^{2+}, and Mg^{2+} and their substitution by the significantly smaller H^{+} and Al^{3+} cations creates imbalances in the crystal lattices, which in turn leads to the formation of microfractures. Surface weathered rocks can therefore lose strength before any mineralogical changes become apparent (Moon and Jayawardane, 2004).

6.4 Dykes from this Study

The minerals formed in the dykes because of the greenschist metamorphic environment of the Witwatersrand basin are considerably different from those formed in the surface weathering environment studied by Moon and Jayawardane (2004). However, the chloritisation and saussuritisation of primary mafic minerals will result in the same style of weakening of the rocks by reducing the cohesion between primary minerals as secondary minerals form along crystal boundaries (Pusch, 1995). Dykes that have lost a significant amount of strength in fact are less problematic than those that appear to be perfectly intact.

Detailed mineralogy has been discussed in Chapter 2 and will not be repeated here, except to remind the reader that the dykes can be broadly divided into three groups based on their degree of alteration: completely altered - where all primary minerals

have been altered, mostly altered but still containing some primary minerals (specifically pyroxenes), and largely unaltered. The Brazil dyke is the only dyke in this study to belong to the last group. The only significant alteration in this dyke is found close to veins and fractures and very few of these are present. During sample preparation it was found that the rock is very hard compared to the other dykes and does not break easily. However, if the findings of Moon and Jayawardane (2004) are taken into account, the very slight alteration observed in some of the Brazil dyke samples would already have reduced the strength of the rock significantly. A chemical trend similar to that found by Moon and Jayawardane (2004) is seen in the Brazil dyke, especially regarding Ca and Sr concentrations. These elements are significantly depleted in the two slightly weathered samples (BRA2 and 3) compared to the fresh (BRA 4) sample. Fe_2O_3 shows a slight enrichment in these samples (Fig. 6.1). The strength of the Brazil dyke would therefore be variable.

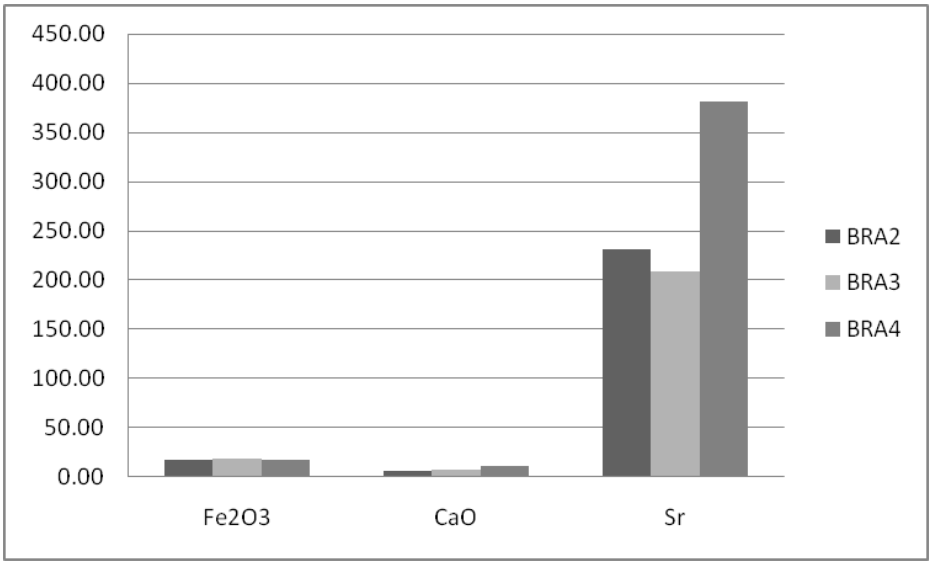

Figure 6.1. Comparison of Fe_2O_3, CaO and Sr concentrations in BRA2, 3 and 4 indicating a depletion in CaO and Sr, and a slight apparent enrichment in Fe_2O_3 in BRA2 and 3 relative to BRA4. Fe_2O_3 and CaO concentrations are given in wt% and Sr is given in ppm)

Dykes in the second group include the CLA, Ken and Amigo dyke. As the primary pyroxenes occur either as small scattered remains or as clusters, it is unlikely that they will affect rock strength significantly, and these rocks will likely have properties similar to that of the completely altered dykes. All the other dykes in the study are completely weathered.

The Jeans dyke should be mentioned in particular as it contains large patches of calcite. Such a rock may react differently under the stresses than one that consists dominantly of chlorite and quartz. Both minerals have low hardness and excellent cleavage – the result of weak atomic cohesion (Wenk and Bulakh, 2004) – but calcite is more brittle than chlorite. The calcite crystals are also considerably larger than the chlorite crystals with larger cleavage planes. This nature of the calcite crystals would likely make the rock more susceptible to Griffith-type failure, depending on the orientation of the crystals. Griffith cracks can form from microscopic or even sub-microscopic defects under tensional stress. When such stress exists for a prolonged period of time, these microscopic cracks can grow until they intersect lower order discontinuities (i.e. larger cracks and joints), resulting in a significant reduction of rock strength (Pusch, 1995). The time required for significant Griffith cracks to form is probably much longer than that taken to negotiate dykes during mining and they would likely not reduce the strength of the dyke to an extent where the risk of a rock burst is diminished. It could, however, become significant in the already excavated dyke and may contribute to the formation of the blocky conditions previously mentioned, creating stability problems. The extent of the contribution of calcite towards instability depends on the distribution of calcite in the rock. This would only be possible to assess if more, closely spaced samples of the dyke are examined.

During mining operations, the problem of rock bursts is overcome partly by the preconditioning technique. This involves the drilling of a single row of additional, longer holes that are blasted in conjunction with the usual blast holes. This serves to weaken the rock ahead of the face, decreasing the risk of rock bursts (pers. comm. H. Moller, 2009). The parts of the Jeans dyke containing calcite should respond very well to preconditioning, and even normal blasting should contribute to the weakening of the rock, as rock around blasted areas is damaged to several tens of centimetres from the blast (Pusch, 1995).

Another important feature of the dykes, from an engineering perspective, is veining. Veins are filled with a variety of minerals, namely quartz, epidote, calcite, mixtures of quartz and chlorite and, less commonly, sulphides and iron oxides/hydroxides (see Chapter 3). These veins are classified as 4^{th} order discontinuities (Pusch, 1995) and are responsible for the bulk hydraulic conductivity of the rock and provided

pathways for hydrothermal fluids. These discontinuities can expand and soften, creating unstable wedges or block sliding. These joints would generally contribute significantly to the weakening of the rock, but pure quartz veins can be welded and behave very much the same as unfractured rock (Pusch, 1995). The Twin dyke is the only case in this study where a pure quartz vein was found. In all other instances quartz occurred in combination with chlorite, calcite, epidote or sulphides. Veins in the Skelm dyke consist almost exclusively of epidote, which has also been fractured. The orientation of the joints and veins will, however, be a major factor in the weakening of the rock, regardless of their composition.

6.5 Concluding Remark

It has been shown in this study that dyke alteration is heterogeneous and it would be dangerous to assign properties to dykes on the basis of only a few samples. Gill *et al.* (1993) confirmed that using data from areas in which the geology is considered comparable to the area in question can lead to the inaccurate evaluation of the mechanical properties of the rock mass. It is therefore essential to assess each case on its own merit. Dyke – country rock contacts have not been included in this study, but since the dykes themselves have been subjected to a variety of conditions, resulting in the varying mineralogy, it should be safe to assume that the dyke contacts are also not the same everywhere, especially since the dykes passed through more than one lithology during intrusion.

Chapter 7: Conclusions and Recommendations

7.1 Conclusion

The mineralogical investigation of the dykes in Tau Tona and Mponeng revealed that most dykes, with the exception of the Brazil dyke, are altered. The most abundant minerals are chlorite, actinolite, epidote, quartz and albitised and/or saussuritised feldspar, corresponding to a greenschist metamorphic facies mineral composition. In the Jeans dyke feldspars were converted to calcite. The most common vein minerals are quartz, calcite, epidote and chlorite, with sulphides and Fe oxides occurring occasionally. Veins usually consist of a combination of these minerals, but veins in the Skelm dyke consist almost exclusively of epidote. Often, dyke alteration is very heterogeneous with different samples from the same dyke containing different minerals, e.g. primary pyroxene may be present in some samples, but not in others. This heterogeneity is similar to that reported by Winter, (1995) for the Alberton Formation and is likely due to the different lithologies traversed by the dykes, resulting in differences in fluid flow.

Similar heterogeneity is found in the chemistry of the dykes, notably in the more mobile elements such as Ca, Na, Mg, Rb and Sr, resulting in a wide range of element concentrations in some of the dykes. Evidence was also found for the mobility of traditionally immobile elements such as Ti, Zr and Y. In the Peggy dyke, the scatter produced on plots employing these elements can only be explained by their mobility, as Ti, Zr and Y are mantle incompatible and not greatly affected by the primary magmatic processes in basaltic magmas. Further evidence for their mobility is found in the Soll dyke, where a sample taken from a fault was significantly depleted in these elements. It is uncertain whether large differences in chemistry between samples from the same dyke, such as those found in the Jeans and Skelm dyke, are the result of element mobility or of the sampling of different dykes, and more, closely spaced sampling is required in order to resolve this issue.

A different type of heterogeneity was found where both chill- and central zones of dykes were sampled from the same drill core. It was found that the mantle compatible elements Cr and Ni are significantly enriched in the chill zones. Exceptions are found in the Speckled dyke and in Unknown 8 and 9, where the central zones are enriched in Cr and Ni. This may be the result of flow

differentiation during dyke intrusion, which resulted in the migration of first-formed, chill zone crystals to the centre of the dyke, but more detailed sampling of the dykes in question is required in order to determine if this enrichment of the central zone is present everywhere these dykes.

Bowen's (1984a) TiO_2 v Zr and Zr/P v P/Ti plots as well as Linton's (1992) discriminant plot proved useful in dividing the dykes into groups according to chemistry. These groups correlated reasonably well with groups formed by dykes with similar strike, which may indicate that dykes with similar strike may share a common origin. However, dykes with different ages and origins may have the same strike due to the intrusion of younger dykes into older weak zones and conclusions regarding the relationship between strike and origin cannot be made until more detailed work has been done. The Lib and Little Tumi dykes that are chemically similar to each other, but different from all the other dykes in the study, do not strike in the same direction, and either one may have intruded into a weak zone created by earlier tectonic events.

Geochemical data for igneous rocks from the Ventersdorp Supergroup, Transvaal Supergroup, Bushveld Igneous Complex and Karoo Supergroup, as well as for dykes from the ERPM mine were collected and plotted on the same three plots employed for the geochemical separation of the dykes from this study. However, the Zr/P v P/Ti plot was unable to separate the data from different igneous provinces in a satisfactory way, and was discarded. The Loraine-Edenville rocks proved to be chemically indistinguishable from most of the Bushveld rocks even when principal component analysis was attempted, with the Loraine-Edenville rocks forming a group of their own within the Bushveld field.

Over all, the classifications in the TiO_2 v Zr and discriminant plots correlate well. The Georgette, Twin and Speckled dykes as well as Unknown 6 and SIL1 are classified as Loraine-Edenville/Bushveld dykes. The CLA dyke is classified as a Bushveld Type 4 dyke. The PE, Friday, Swannie, Skelm, Jeans, Soll, and Unknown 1, 2 and 4 plot as Lebombo basalts. The Brazil, Ken, Amigo and Bank dykes plot in a field of their own, and the Little Tumi and Lib dykes always plot away from the other samples in their own group. Unknown 3, 7, 8 and 9, JEA3, and two Peggy samples

are grouped as Ventersdorp dykes, although the Peggy samples do show some scatter. This is likely due to the mobility of the elements used for classification.

The heterogeneity of dyke composition should be taken into account for rock engineering purposes as this could cause different sections of the same dyke to have different physical properties. It would therefore be dangerous to assign specific properties to dykes based on only a few samples.

7.2 Recommendations

It is important to note that, due to the nature of the sampling, this study by no means gives a complete account of either the mineralogy or geochemistry of the dykes. It is therefore recommended that dykes be sampled at closer intervals in order to obtain a more complete picture of both their mineralogy and geochemistry. Such sampling can be done routinely during core logging.

8: References

Anders, E. and Grevesse, N. (1989). Abundances of the elements: meteoritic and solar. *Geochimica et Cosmochimica Acta*, **53**, 197 – 214.

Anhaeusser, C.R. (2006). Ultramafic and Mafic intrusions of the Kaapvaal Craton. *In:* Johnson, M.R., Anhaeusser, C.R, and Thomas, R.J. (Eds.), *The Geology of South Africa.* Geological Society of South Africa. 95 – 134.

Barker, D.S. (1983). *Igneous Rocks*. Prentice-Hall, Englewood Cliffs, NJ, 417pp.

Bhattacharji, S. (1967). Mechanics of flow differentiation in ultramafic and mafic sills. *Journal Geology*, **75**, 101 – 112.

Bowen T.B. (1984a). *The Geochemical stratigraphy of the volcanic rocks of the Witwatersrand triad in the Klerksdorp area, Transvaal.* M.Sc. dissertation, (unpubl.), Rhodes University, Grahamstown. 223pp.

Bowen M.P. (1984b). *The Petrogenesis of the Volcanic rocks of the Witwatersrand Triad*. M.Sc. dissertation (unpubl.). Rhodes University, Grahamstown. 204pp.

Brink, A.B.A. (1979). *Engineering Geology of Southern Africa. Volume 1.* Building Publications, Pretoria. 319 pp.

Burger, A.J. and Coertze, F.J. (1973-1974). Age determinations – April 1972 to March 1974. *Annals of the Geological Survey, South Africa,* **10**, 135 – 141.

Cawthorn, R.G., Davies, G., Clubley-Armstrong, A, and McCarthy, T.S. (1981). Sills associated with the Bushveld Complex, South Africa: an estimate of the parental magma composition. *Lithos*, **14**, 1 – 15.

Cawthorn, R.G., Eales, H.V., Walraven, F., Uken, R., and Watkeys, M.K. (2006). The Bushveld Complex. *In:* Johnson, M.R., Anhaeusser, C.R, and Thomas, R.J. (Eds.), *The Geology of South Africa.* Geological Society of South Africa. 261 – 282.

Chichowicz, A. (1997). *Develop a more reliable means of assessing safety risk due to rockbursts and rockfalls as a managerial decision support technique.* Safety in Mines Advisory Research Committee. 48pp.

Coetzee, M.S., Beukes, G.J., De Bruiyn, H., Bisschoff, A.A. (2006). Geochemistry and petrogenesis of tholeiitic intrusions of possible Bushveld-age in the Vredefort Dome, South Africa. *Journal of African Earth Sciences*, **45**, 213 – 235.

Danchin, R.V. and Ferguson, J. (1970). The Geochemistry of the Losberg Intrusion, Fochville, Transvaal, *In: Symposium on the Bushveld Igneous Complex and Other Layered Intrusions.* The Geological Society of South Africa Special Publication 1. 689 – 714pp.

Davies, G. and Tredoux, M. (1985). The Platinum-Group Element and Gold Contents of the Marginal Rocks and Sills of the Bushveld Complex. *Economic Geology*, **80**, 838 – 848.

De Bruiyn, H., Schoch, A.E., Van der Westhuizen, W.A., and Myburgh, C.A. (2000). Picrite from the Katse area, Lesotho: evidence for flow differentiation. *Journal of African Earth Sciences*, **31,** 657 – 666.

De La Roche, H. Leterrier, J. Grandclaude, P. and Marchal, M. (1980). A classification of volcanic and plutonic rocks using R1-R2 – diagram and major element analyses - its relationships with current nomenclature. *Chemical Geology*, **29**,183 – 210.

Duncan, A.R. and Marsh, J.S. (2006). The Karoo Igneous Province. *In:* Johnson, M.R., Anhaeusser, C.R, and Thomas, R.J. (Eds.), *The Geology of South Africa.* Geological Society of South Africa. 501 – 520.

Elburg, M. and Goldberg, A. (2000). Age and geochemistry of Karoo dolerite dykes from northeast Botswana. *Journal of African Earth Sciences*, **31**, 539 – 554.

Eriksson, P.G., Engelbrecht, J.P., Res, M. and Harmer, R.E. (1994). The Bushy Bend lavas, a new volcanic member of the Pretoria Group, Transvaal Sequence. *South African Journal of Geology*, **91**, 1 – 7.

Eriksson, P.G. Altermann, W. and Hartzer, F.J. (2006). The Transvaal Supergroup and its Precursors. *In:* Johnson, M.R., Anhaeusser, C.R, and Thomas, R.J. (Eds.), *The Geology of South Africa.* Geological Society of South Africa. 237 – 260.

Erlank, A.J. (Ed.) (1984). *The Petrology of the Volcanic Rocks of the Karoo Province*. Geological Society of South Africa. 395pp.

Fumerton, S.L. (1975). *The felsic sills on the ERPM Boksburg.* M.Sc. dissertation (unpubl.), University of the Witwatersrand, Johannesburg. 103pp.

Gerasimovsky, V.I. (1974). Trace Elements in Selected Groups of Alkaline Rocks. *In:* Sørensen, H. (Ed.), *The Alkaline Rocks.* Wiley-Interscience, 622pp.

Gill, D.E., Aubertin, M. and Simon, R. (1993). A practical engineering approach to the evaluation of rockburst potential. In: Young, R.P. (Ed.) *Rockbursts and Seismicity in Mines*. Balkema, Rotterdam, 449pp.

Govindaraju, K. (Ed.) (1994). Special issue of the Geostandards Newsletter. *Geostandards Newsletter*, **18**, 158pp.

Greeff, M.T. (1988a*). Petrographic Description of various dykes from Western Deep Levels.* Anglo American Research Laboratories.

Greeff, M.T. (1988b) *Some Implications resulting from the petrographic examination of Western Deep Levels dykes.* Anglo American Research Laboratories Project No. R/87/296 Report No. 1.

Harmer, R.E. and Sharpe, M.R. (1985). Field relations and Strontium Isotope Systematics of the Marginal Rocks of the Eastern Bushveld Complex. *Economic Geology*, **80**, 813 – 837.

Harris, C. and Watkins, R.T. (1990). Fluid interaction in the Witwatersrand gold fields: oxygen isotope geochemistry of Ventersdorp-age dolerite intrusions. *South African Journal of Geology*, **93**, 611 – 615.

Irvine, T.N. and Baragar, W.R.A. (1971) A guide to the chemical classification of the common volcanic rocks. *Canadian Journal of Earth Sciences,* **8**, 523 – 548.

Janousek, V., Farrow, C., Erban, V., and Smid, J. (2007). GCDkit for Win 2.2.

Jeffery, D.G. (1975). *Structural discontinuity in the Witwatersrand Group on the ERPM Mine: their geology, geochemistry and rock mechanics behavior.* M.Sc. dissertation (unpubl.), University of the Witwatersrand, Johannesburg. 108pp.

Jensen, L.S. (1976). A new cation plot for classifying subalkaline volcanic rocks. *Ontario Division of Mines*, *Miscellaneous Paper,* **66**.

Jiang, S.-Y., Wang, R.-C., Xu, X.-S., Zhao, K.-D. (2005). Mobility of high field strength elements (HFSE) in magmatic-, metamorphic-, and submarine-hydrothermal systems. *Physics and Chemistry of the Earth*, **30**, 1020 – 1029.

Karakaya, N. (2009). REE and HFS element behaviour in the alteration facies of the Erenler Dağı Volcanics (Konya, Turkey) and kaolinite occurrence. *Journal of Geochemical Exploration*, **101**, 185 – 208.

Le Maitre, R.W. (1968). Chemical Variation within and between Volcanic Rock Series – A Statistical Approach. *Journal of Petrology*, **9**, 220 – 252.

Lenhard, W.A. (1988). *Some observations regarding the influence of geology on mining induced seismicity at Western Deep Levels, Ltd.* Sangorm Symposium: Rock mechanics in Africa.

Linton, P.L. (1992). *The geochemical Stratigraphy of the Klipriviersberg group along the western margin of the Witwatersrand basin.* M.Sc. dissertation (unpubl.), Univ. Witwatersrand, Johannesburg. 276pp.

Maier, W.D., and Barnes, S.-J. (1998). Concentrations of rare earth elements in silicate rocks of the Lower, Critical and Main Zones of the Bushveld Complex. *Chemical Geology*, **105**, 85 – 103.

Makutu, M.N., Kanika, M., Bwanga, N., Nguangu, K. and Mpoyi, K. (2004). Petrology and geochemistry of igneous rocks of the Noqui Alkaline Province (Bas-Congo, Democratic Republic of Congo). *Bulletin du Centre de Recherches Géologiques et Minières*, **5**, 28-39.

Marsh, J.S., Bowen, M.P., Rogers, N.W. and Bowen, T.B. (1992). Petrogenesis of Late Archaean Flood-Type Basic Lavas from the Klipriviersberg Group, Ventersdorp Supergroup, South Africa. *Journal of Petrology*, **33**, 817 – 847.

McCarthy, T.S., McCallum, K., Myers, R.E., and, Linton, P. (1990). Stress states along the northern margin of the Witwatersrand Basin during Klipriviersberg Group volcanism. *South African Journal of Geology*, **93**, 245 – 260.

McCarthy, T.S. (2006). The Witwatersrand Supergroup. *In:* Johnson, M.R., Anhaeusser, C.R, and Thomas, R.J. (Eds.), *The Geology of South Africa.* Geological Society of South Africa. 155 – 186.

Meier, D.L., Heinrich, C.A., and Watts, M.A. (2009). Mafic dikes displacing Witawatersrand gold reefs: Evidence against metamorphic-hydrothermal ore formation. *Geology*, **37**, 607 – 610.

Middlemost, E.A.K. (1989) Iron oxidation ratios, norms and the classification of volcanic rocks. *Chemical Geology*, **7**, 19 – 26.

Miyashiro, A. (1994). *Metamorphic Petrology*. University College, London. 404pp.

Moon, V. and Jayawardane, J. (2004). Geomechanical and geochemical changes during early stages of weathering of Karamu Basalt, New Zealand. *Engineering Geology*, **74**, 57 – 72.

Nesse, W.D. (2004). *Introduction to Optical Mineralogy*. Oxford University Press. 348pp.

Norrish, K., and Hutton, J.T. (1969). An accurate X-ray spectrographic method for the analysis of a wide range of geological samples*. Geochimica et Cosmochimica Acta*, **33**, 431 – 453.

Oberholzer, J.D., (1995). *Die Geologie van die piroklastiese gesteentes in die Hekpoort Formasie, Transvaal Opeenvolging.* M.Sc. dissertation (unpubl.), University of Pretoria. 120pp.

Onstott, T.C., Lin, L.-H., Davidson, M., Mislowack, B., Borcsik, M., Hall, J., Slater, G., Ward, J., Sherwood Lollar, B., Lippmann-Pipke, J., Boice, E., Pratt, L.M., Pfiffner, S., Moser, D., Gihring, T., Kieft, T.L., Phelps, T.J., Van Heerden, E., Litthauer, D., Deflaun, M., Rothmel, R., Wanger, G., Southam, G. (2006). The Origin and Age of Biogeochemical Trends in Deep Fracture Water of the Witwatersrand Basin, South Africa. *Geomicrobiology Journal*, **23**, 369 – 414.

Palmer, K.J., Spencer, R.M., Hewitt, T. and McCarthy, T.S. (1986). The geochemical stratigraphy of the Klipriviersberg lavas as a stratigraphic guide in the Witwatersrand Basin. *Abstracts of the Geocongress '86*, Geological Society of South Africa, Johannesburg, 171 – 174.

Pearce, J.A. and Cann, J.R. (1973). Tectonic setting of basic volcanic rocks determined using trace element analyses. *Earth and Planetary Science Letters*, **19,** 290 – 300.

Pearce, T.H., Gorman, B.E., and Birkett, T.C. (1977). The relationship between major element chemistry and tectonic environment of basic and intermediate volcanic rocks. *Earth and Planetary Science Letters*, **36**, 121 – 132.

Phillips, G.N., Law, J.D.M., and Myers, R.E. (1990). The role of fluids in the evolution of the Witwatersrand Basin. *South African Journal of Geology*, **93**, 54 – 69.

Pusch, R. (1995). *Rock Mechanics on a Geological Base*. Elsevier, Amsterdam. 498pp.

Rezcko, B.F.F., Oberholzer, J.D., Res, M., Eriksson, P.G. and Schreiber, U.M. (1995). A re-evaluation of the volcanism of the Palaeoproterozoic Pretoria Group (Kaapvaal craton) and a hypothesis on basin development. *Journal of African Earth Sciences*, **21**, 505 – 519.

Robb, L.J. (2005). *Introduction to ore-forming processes.* Blackwell Science. 373pp.

Robinson, D and Bevins, R. E. (1999). Patterns of regional low-grade metamorphism in metabasites. *In:* (Eds.) Frey, M. and Robinson, D., *Low-Grade Metamorphism* Blackwell Science. 313pp.

Rollinson, H.R. (1993). *Using Geochemical data: evaluation, presentation, interpretation.* Longman Scientific and technical. 352pp.

Rompel, A.K.K. (1995). Tectonic history of the central Welkom Goldfield, with particular reference to President Brand Mine Ph.D. Thesis (Unpubl.) University of the Witwatersrand, Johannesburg. 241pp.

SACS Task Group for the Witwatersrand Supergroup (2006). A revised stratigraphic framework for the Witwatersrand Supergroup. *Lithostratigraphic Series of the South African Committee for Stratigraphy,* **42**.

Salvi, S. and Williams-Jones, A.E. (1996). The role of hydrothermal processes in concentrating high-field strength elements in the Strange Lake peralkaline complex, northeastern Canada. *Geochimica et Cosmochimica Acta*, **60**, 1917 – 1932.

Schiffman, P. and Day, H.W. (1999). Petrological methods for the study of very low-grade metabasites, *In:* (Eds.) Frey, M. and Robinson, D., *Low-Grade Metamorphism* Blackwell Science. 313pp.

Sun, S.-S., Nesbitt, R.W., McCulloch, M.T. (1989). Geochemistry and petrogenesis of Archaean and early Proterozoic siliceous high-magnesium basalts. In: Crawford, A.J. (Eds.), *Boninites.* Unwin Hyman, London, 148–173.

Sweeney, R.J., Duncan, A.R. and Erlank, A.J. (1994). Geochemistry and Petrogenesis of Central Lebombo Basalts of the Karoo Igneous Province. *Journal of Petrology*, **35**, 95 – 125.

Van der Westhuizen, W.A., De Bruiyn, H., Meintjies, P.G. (2006). The Ventersdorp Supergroup. *In:* Johnson, M.R., Anhaeusser, C.R, and Thomas, R.J. (Eds.), *The Geology of South Africa.* Geological Society of South Africa. 187 – 209.

Verwoerd, W.J. (2006). The Pilanesberg Alkaline Province *In:* Johnson, M.R., Anhaeusser, C.R, and Thomas, R.J. (Eds.), *The Geology of South Africa.* Geological Society of South Africa. 381 – 395.

Verzani, J. (2005). *Using R for introductory statistics*. Chapman and Hall/CRC, 414pp.

Wenk, H.-R. and Bulakh, A. (2004). *Minerals: Their Constitution and origin.* Cambridge University Press, 646pp.

White, W.M. (2007). *Geochemistry* Electronic Textbook available from www.geo.cornell.edu/geology/classes/geo455/Chapters.HTML.

Winchester, J.A. and Floyd, P.A. (1977). Geochemical discrimination of different magma series and their differentiation products using immobile elements. *Chemical Geology*, **20**, 325-343.

Winter, H. de la R. (1976). A lithostratigraphic classification of the Ventersdorp succession. *Transactions of the Geological Society of South Africa*, **79,** 31 – 48.

Winter, F. (1995). The stratigraphy and geochemistry of the Alberton formation, Ventersdorp Supergroup, Southwest of Klerksdorp. M.Sc. dissertation (unpubl.) Univ. of the Free State, Bloemfontein. 267pp.

www.anglogoldashanti.com accessed on 18 June 2009

www.mining-technology.com accessed on 18 June 2009

Yardley, B.W.D. (1989). An introduction to Metamorphic Petrology. Pearson. 248 pp.

Appendix A: Sampling Localities

Table A - 1. Sample names and localities

Sample	Dyke Name	Mine	Borehole	Depth
AMI1	Amigo	Tau Tona	DPH 3887	
AMI2	Amigo	Tau Tona	DPH 3887	
AMI3	Amigo	Tau Tona	LIB TT 2002	315
AMI5	Amigo	Tau Tona	DPH 3923	391.8
BAN1	Bank	Tau Tona	DPH 3885	
BAN3	Bank (chill)	Tau Tona	DPH 3885	28.4
BAN4	Bank	Tau Tona	DPH 3880	67.7
BAN5	Bank (chill)	Tau Tona	DPH 3880	41
BAN6	Bank (chill)	Tau Tona	DPH 3880	71.1
BAN7	Bank	Tau Tona	DPH 3885	35.2
BAN8	Bank (chill)	Tau Tona	DPH 3885	52.7
BRA1	Brazil (chill)	Tau Tona	DPH 3881	184.3
BRA2	Brazil	Tau Tona	DPH 3881	187.2
BRA3	Brazil (chill)	Tau Tona	DPH 3884	195.65
BRA4	Brazil	Tau Tona	DPH 3884	195
BRA5	Brazil (chill)	Tau Tona	DPH 3881	186.75
BRA6	Brazil (chill)	Tau Tona	DPH 3884	192.37
BRA7	Brazil (chill)	Tau Tona	Underground Sampling	104
BRA8	Brazil	Tau Tona	Underground Sampling	104
CLA1	CLA (chill)	Tau Tona	DPH 3883	196.9
CLA2	CLA (chill)	Tau Tona	DPH 3883	162
CLA3	CLA	Tau Tona	DPH 3883	177.7
CLA4	CLA	Tau Tona	DPH 3884	90.36
CLA5	CLA	Tau Tona	DPH 3884	97.9
CLA6	CLA (chill)	Tau Tona	DPH 3882	85.45
CLA7	CLA	Tau Tona	DPH 3882	76.55
CLA8	CLA	Tau Tona	DPH 3884	87.77
CLA9	CLA (chill)	Tau Tona	DPH 3884	83.33
FRI1	Friday	Tau Tona	DPH 3887	230
FRI2	Friday	Tau Tona	DPH 3887	234
FRI3	Friday	Tau Tona	LIB TT 2002	210
FRI4	Friday	Tau Tona	LIB 120	730
FRI5	Friday	Tau Tona	DPH 3887	
FRI6	Friday (chill)	Tau Tona	DPH 3887	
FRI7	Friday	Tau Tona	DPH 3923	203.82
FRI8	Friday (chill)	Tau Tona	DPH 3923	193.85
FRI9	Friday (chill)	Tau Tona	DPH 3923	206.5
GEOR1	Georgette	Mponeng	DBH 1890	11
GEOR2	Georgette	Mponeng	DBH 1890	48

GEOR3	Georgette	Mponeng	GBH 2928	110.55
JEA1	Jeans	Tau Tona	LIB TT 2002	505
JEA2	Jeans	Mponeng	GBH 2919	27
JEA3	Jeans	Tau Tona	LIB TT 2002	
KEN1	Ken	Tau Tona	DPH 3883	200.45
KEN2	Ken	Tau Tona	DPH 3884	223.65
KEN3	Ken	Tau Tona	DPH 3884	223.35
KEN4	Ken	Tau Tona	DPH 3883	203.9
KEN5	Ken	Tau Tona	Underground sampling	104 level
KEN6	Ken	Tau Tona	Underground sampling	104 level
KEN7	Ken	Tau Tona	Underground sampling	104 level
KUD1	Kudu	Tau Tona	LIB TT 2002	870
LAV1	Lava sample	Mponeng	DBH 1884	16
LIB1	LIB	Mponeng	GBH 2919	33.8
LIT1	Little Tumi	Mponeng	GBH 2919	103.5
PE1	PE	Mponeng	GBH 2922	103.5
PE2	PE (chill)	Mponeng	GBH 2922	31
PEG1	Peggy	Tau Tona	UD36	2871
PEG2	Peggy (Maggie)	Tau Tona	DPH 3964A	
PEG3	Peggy (Chill zone)	Tau Tona	DPH 3964A	2909
PEG4	Peggy	Tau Tona	UD 36	2623
PEG5	Peggy	Mponeng	DBH 1884	70
PEG6	Peggy	Mponeng	DBH 1884	21
SIL1	Sill	Tau Tona	LIC 118	47
SIL2	Sill	Tau Tona	LIB 120	282
SKE1	Skelm	Tau Tona	LIB TT 2002	
SKE2	Skelm	Tau Tona	DPH 3905	90
SKE3	Skelm	Tau Tona	LIB TT 2002	420
SKE5	Skelm	Tau Tona	LIC 118	850
SOL1	Soll	Tau Tona	DPH3935	
SOL2	Soll	Tau Tona	DPH 3935	242
SOL3	Soll	Tau Tona	DPH 3961	115
SPE1	Speckled	Tau Tona	DPH 3867	157.5
SPE2	Speckled	Tau Tona	DPH3867	161.3
SPE3	Speckled (chill)	Tau Tona	GBH 3997	
SPE4	Speckled	Tau Tona	GBH 3997	88
SPE5	Speckled (chill)	Tau Tona	GBH 3997	90
SWA1	Swannie (chill)	Tau Tona	GBH 3994A	63
SWA2	Swannie	Tau Tona	GBH 3994A	50
SWA3	Swannie (chill)	Tau Tona	GBH 3994A	44
TWI1	Twin	Tau Tona	DPH 3924	288.4
TWI2	Twin	Tau Tona	DPH 3924	287.9

UNK1	Unknown1	Tau Tona	LIC 118	130
UNK2	Unknown2	Mponeng	GBH 2919	63
UNK3	Unknown3	Mponeng	GBH 2939	1.8
UNK4A	Unknown4	Mponeng	GBH 2918	0.5
UNK4B	Unknown4 (chill)	Mponeng	GBH 2918	1.3
UNK6	Unknown6	Tau Tona/Mponeng	GBH 3953	74.1
UNK7	Unknown7	Tau Tona/Mponeng	DPH 3964A	204.64
120A1	LIB120(1) chill	Tau Tona	LIB120	594
120A2	LIB120(1)mid	Tau Tona	LIB120	600
120A3	LIB120(1) chill	Tau Tona	LIB120	606
120B1	LIB120(2) chill	Tau Tona	LIB120SE2	348
120B2	LIB120(2) mid	Tau Tona	LIB120SE2	351
120B3	LIB120(2) chill	Tau Tona	LIB120SE2	356

Appendix B: Mineralogy

X-ray Diffraction Scans

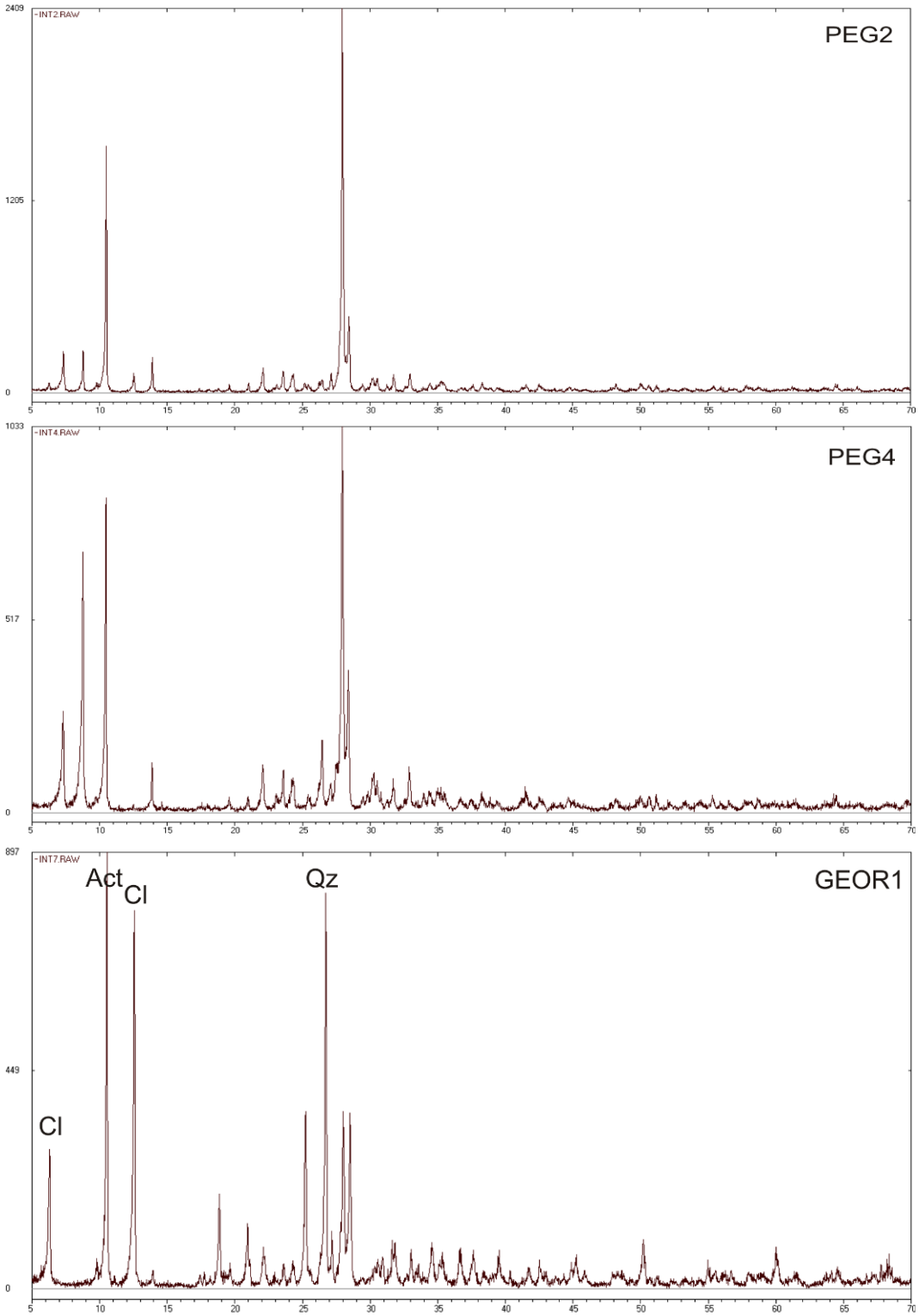

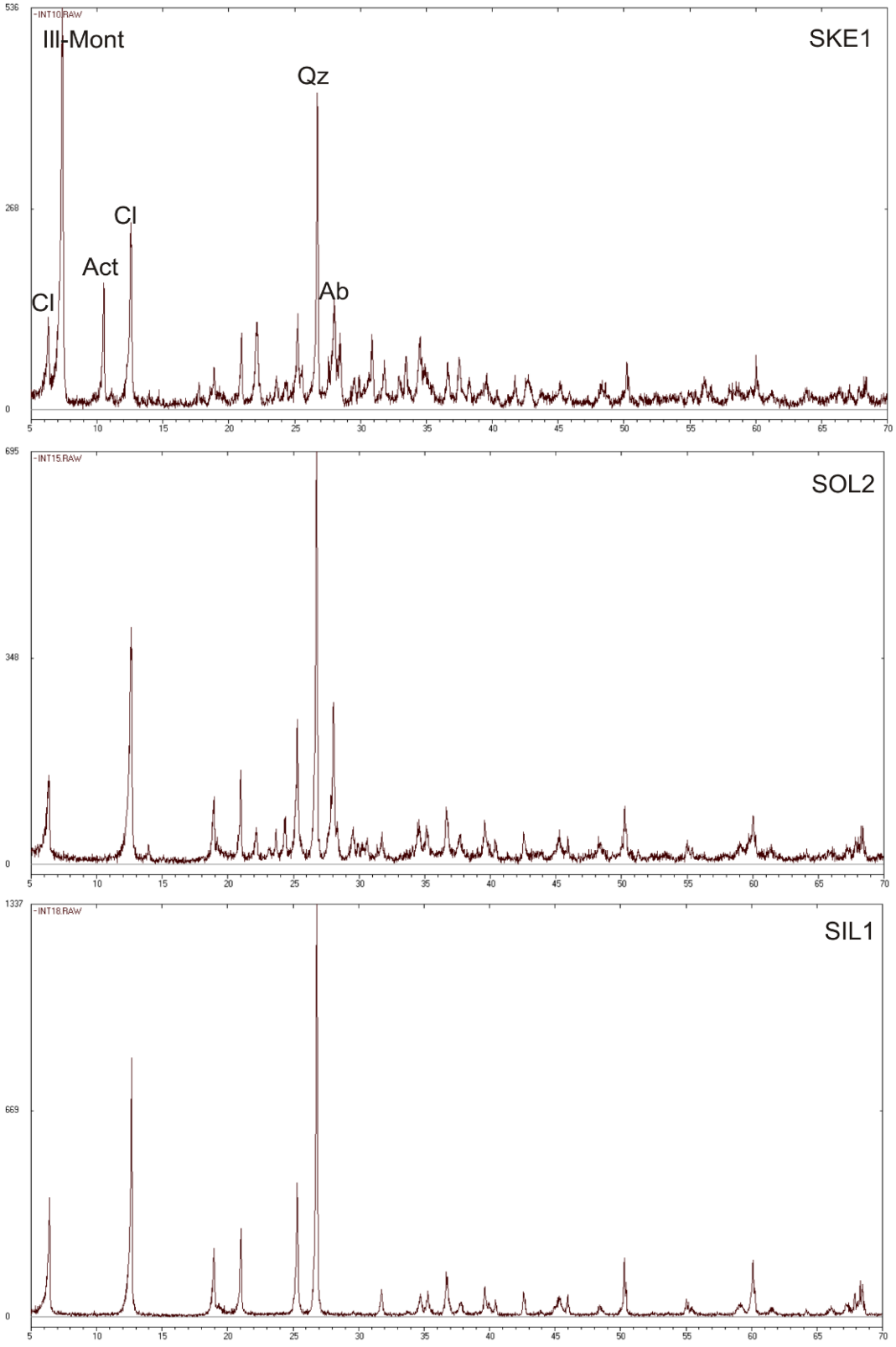
INT10.RAW
Ill-Mont
SKE1
Qz
Cl
Act
Cl
Ab
536
268
0
INT15.RAW
SOL2
695
348
0
INT18.RAW
SIL1
1337
669
0
5
10
15
20
25
30
35
40
45
50
55
60
65
70

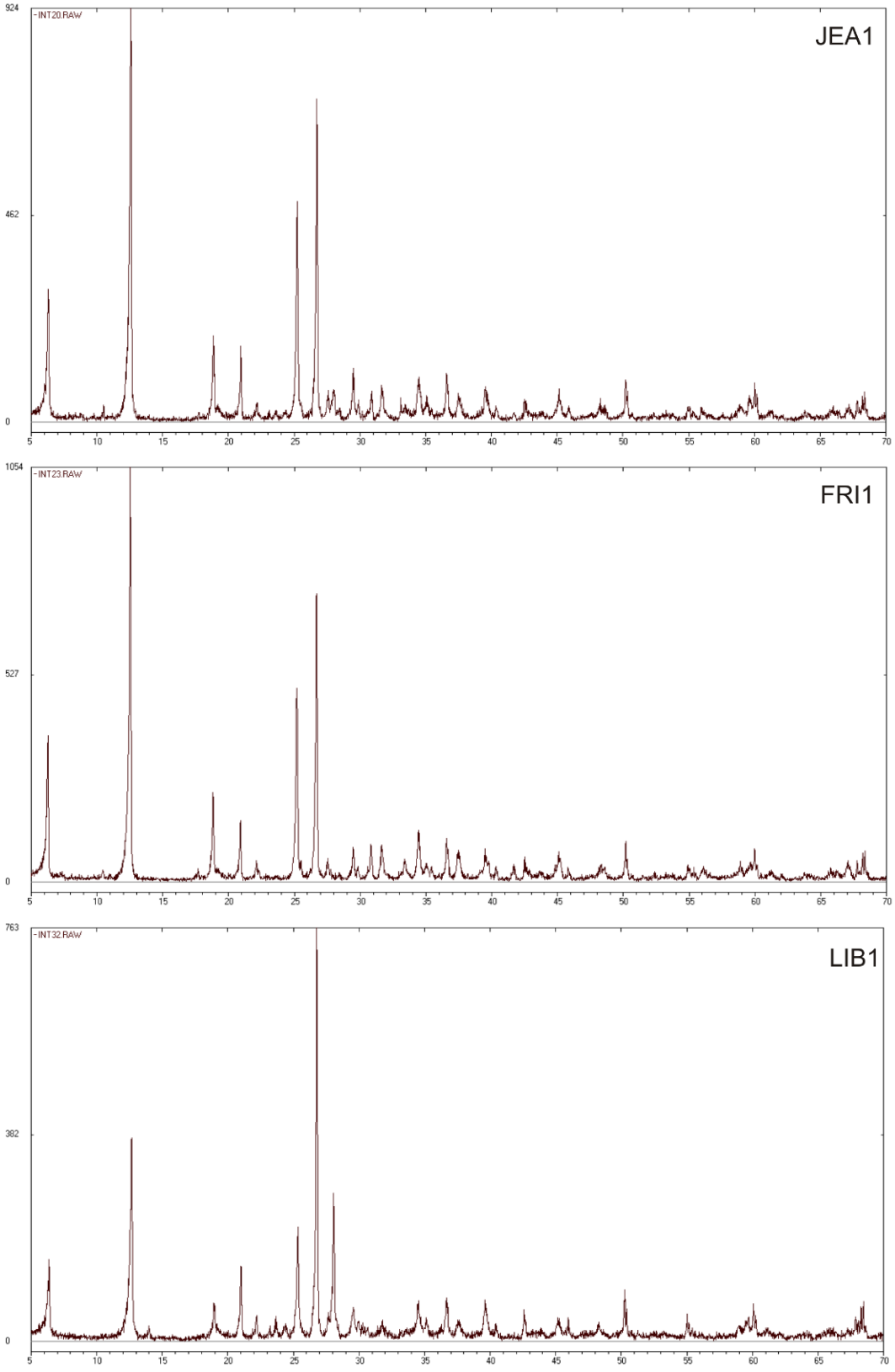
- INT20.RAW
JEA1
924
462
0
- INT23.RAW
FRI1
1054
527
0
- INT32.RAW
LIB1
763
382
0
5
10
15
20
25
30
35
40
45
50
55
60
65
70

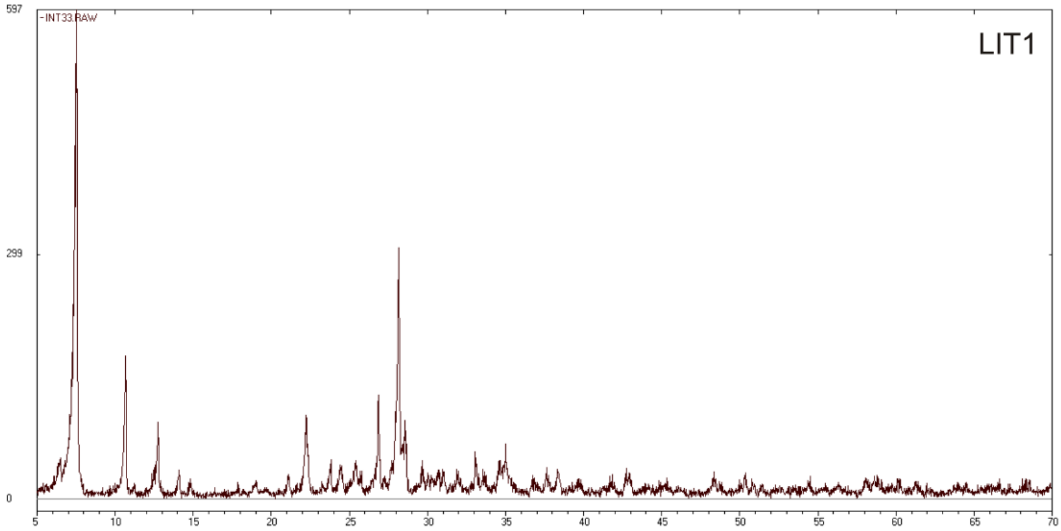
INT33.RAW
LIT1
597
299
0
5
10
15
20
25
30
35
40
45
50
55
60
65
70

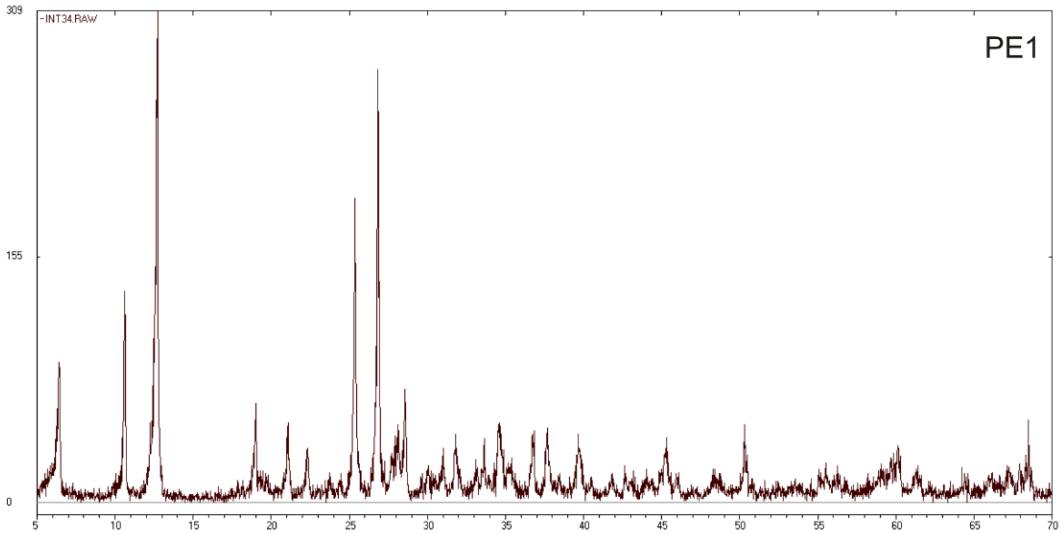
INT34.RAW
PE1
309
155
0
5
10
15
20
25
30
35
40
45
50
55
60
65
70

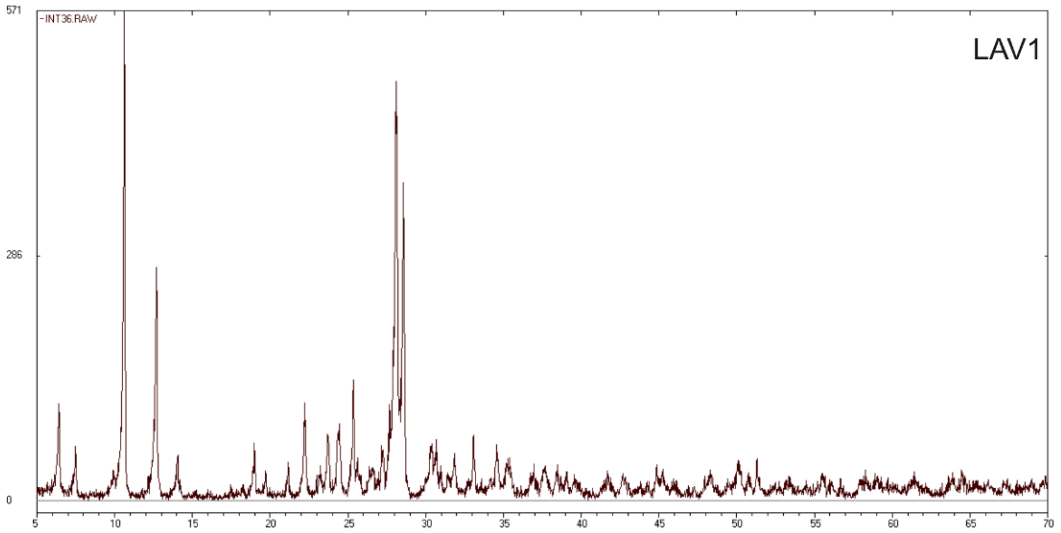
INT36.RAW
LAV1
571
286
0
5
10
15
20
25
30
35
40
45
50
55
60
65
70

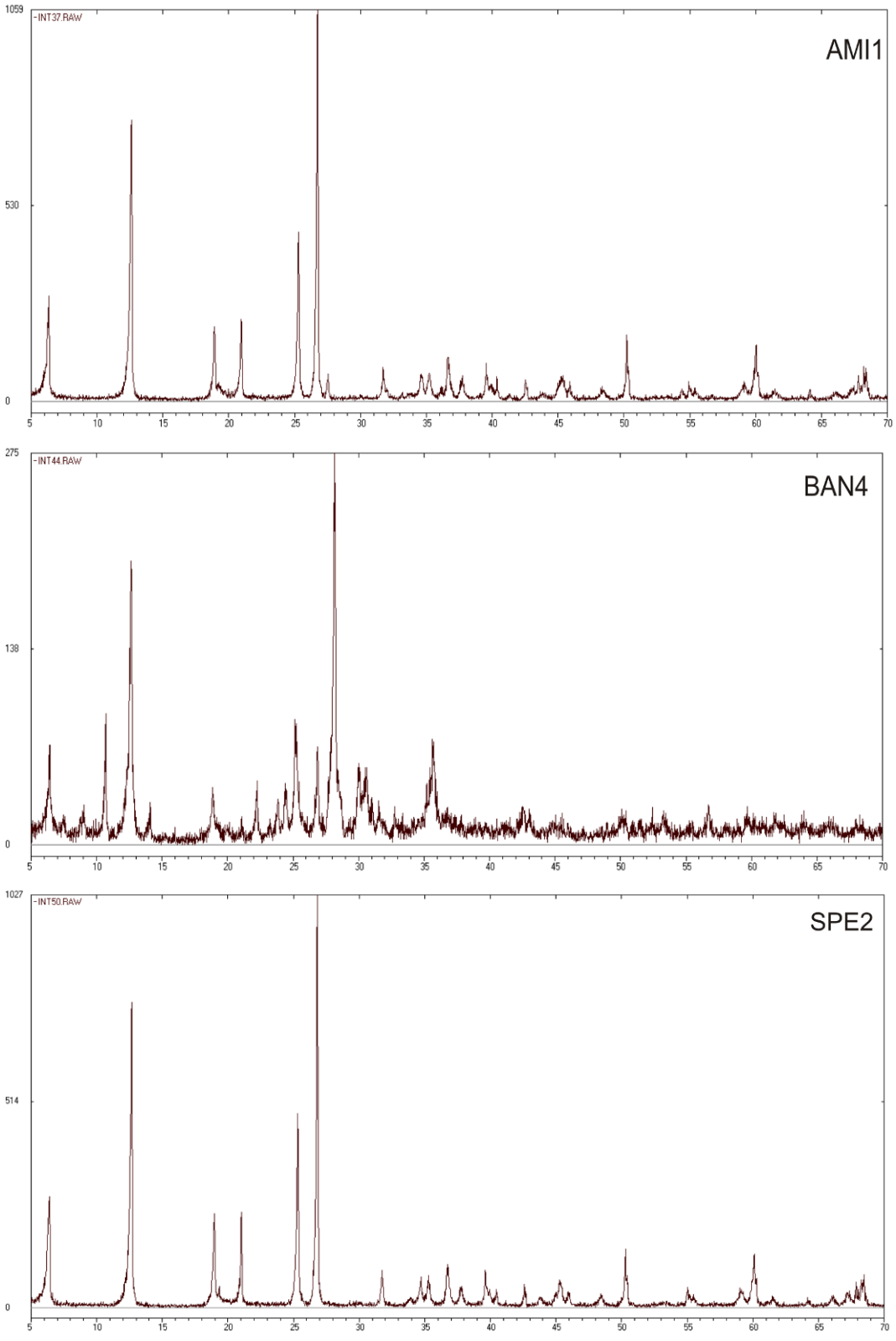
INT37.RAW
AMI1
1059
530
0
INT44.RAW
BAN4
275
138
0
INT50.RAW
SPE2
1027
514
0
5
10
15
20
25
30
35
40
45
50
55
60
65
70

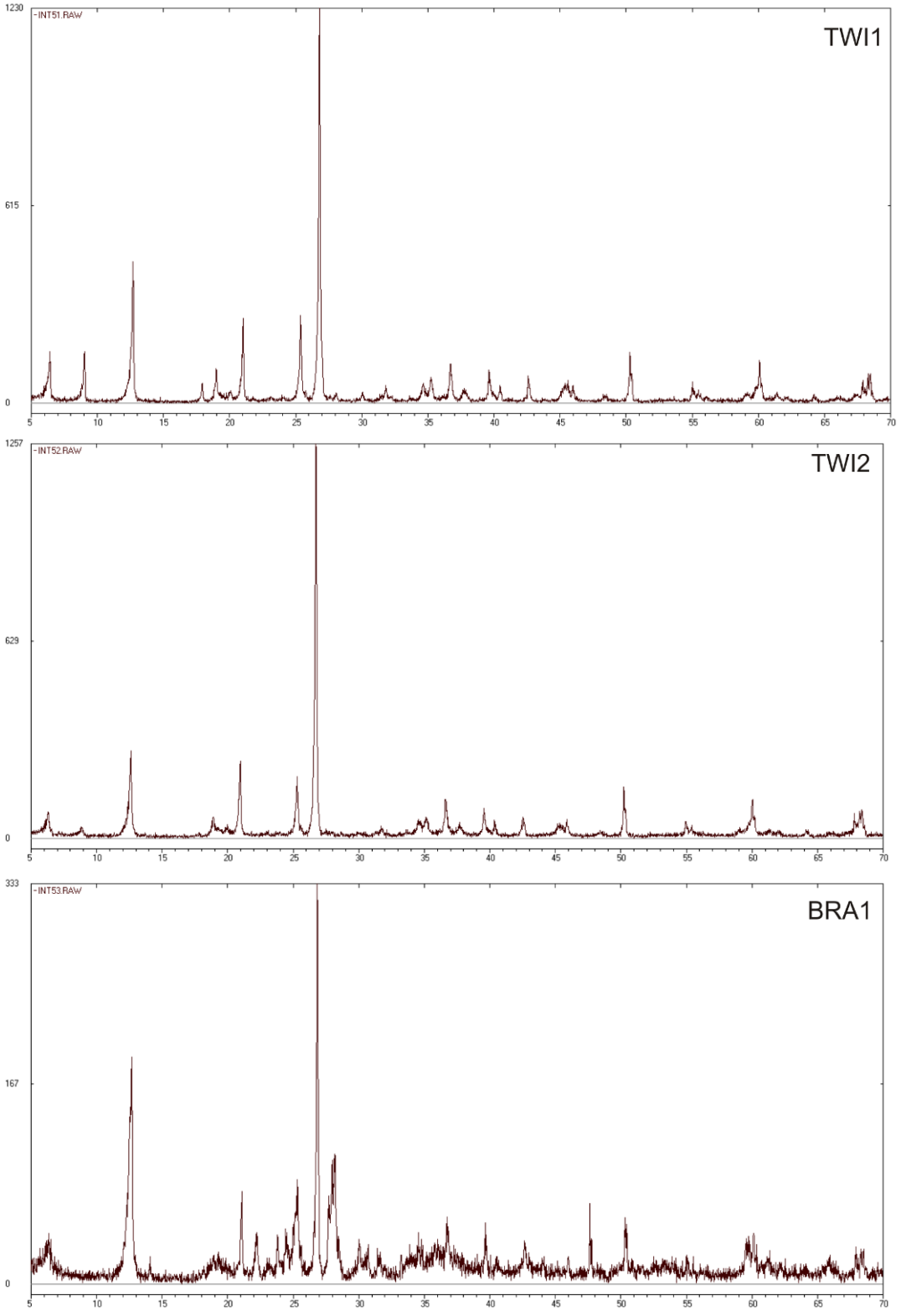
INT51.RAW
TWI1
1230
615
0
INT52.RAW
TWI2
1257
629
0
INT53.RAW
BRA1
333
167
0
5
10
15
20
25
30
35
40
45
50
55
60
65
70

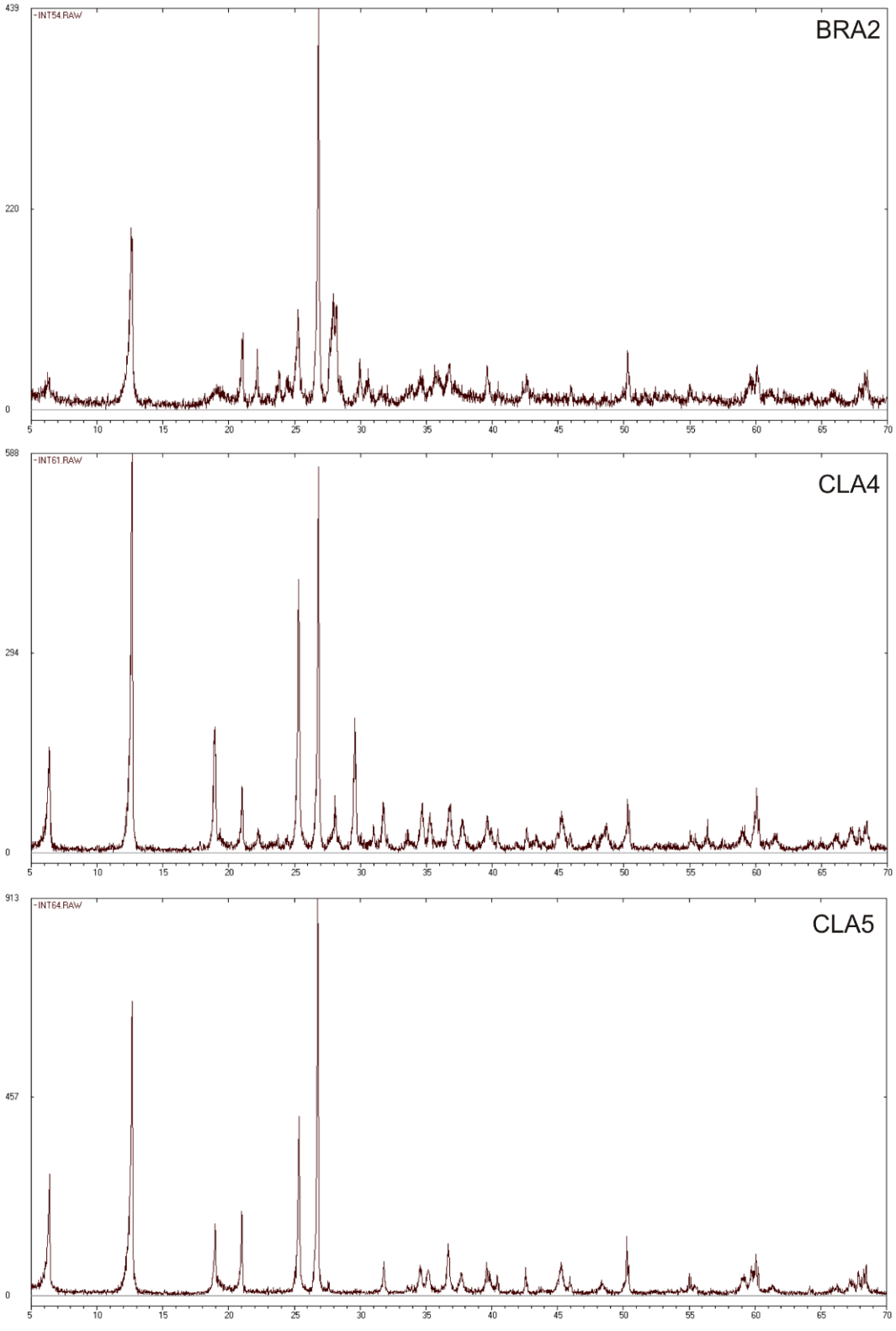
INT54.RAW
BRA2
439
220
0
INT61.RAW
CLA4
588
294
0
INT64.RAW
CLA5
913
457
0
5
10
15
20
25
30
35
40
45
50
55
60
65
70

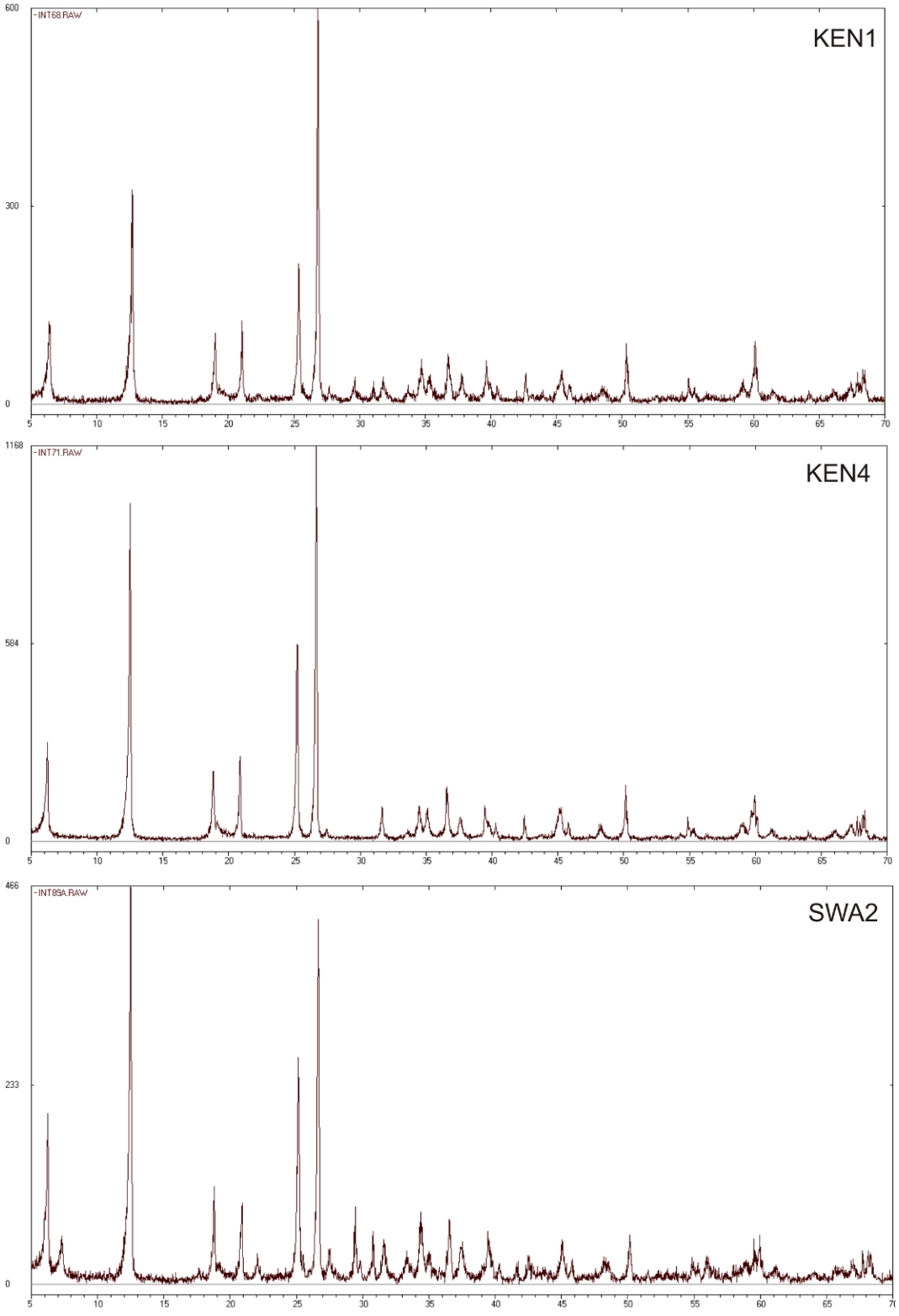
INT68.RAW
KEN1
600
300
0
INT71.RAW
KEN4
1168
584
0
INT89A.RAW
SWA2
466
233
0
5
10
15
20
25
30
35
40
45
50
55
60
65
70

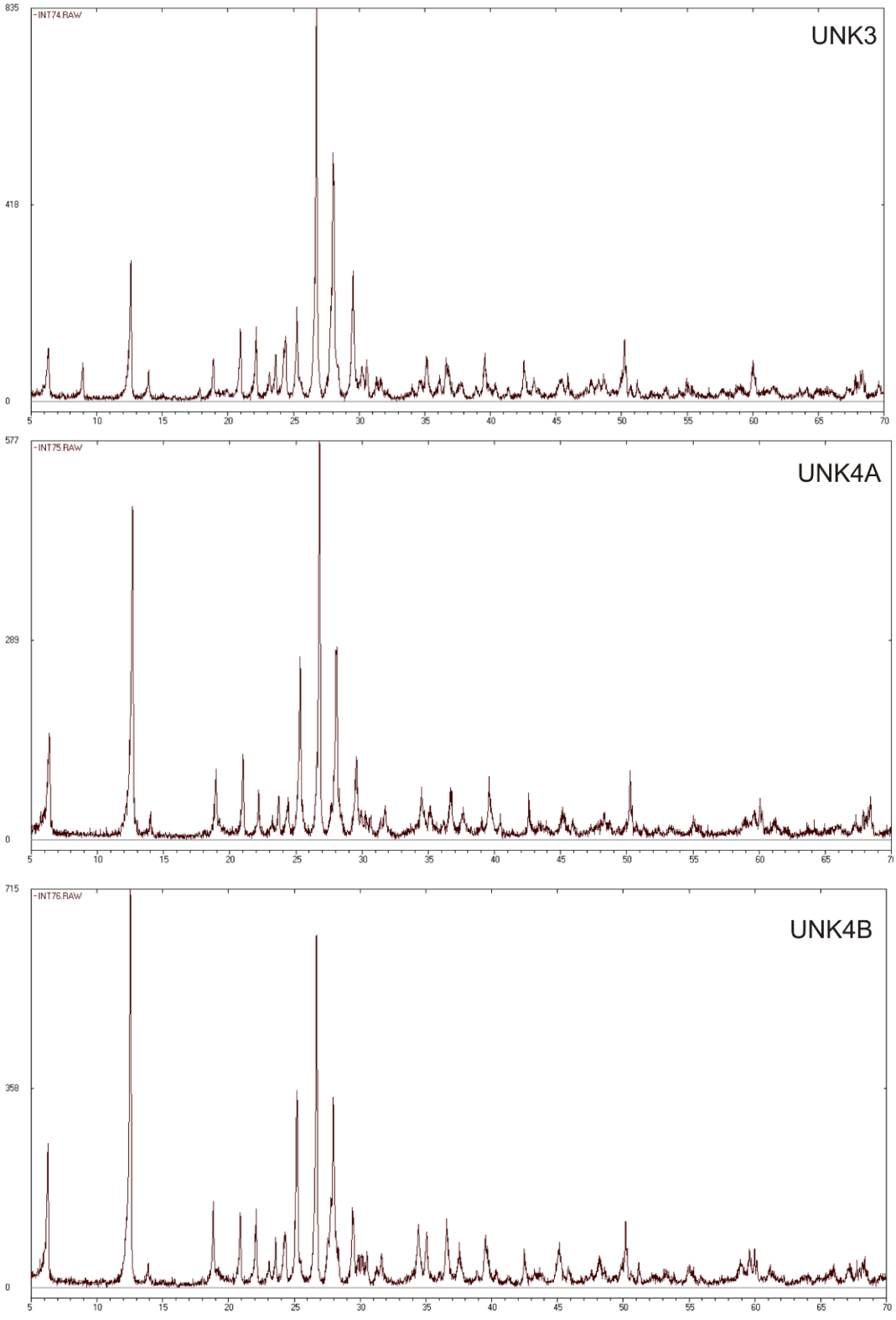
835
418
0
INT74.RAW
UNK3
5
10
15
20
25
30
35
40
45
50
55
60
65
70
577
289
0
INT75.RAW
UNK4A
715
358
0
INT76.RAW
UNK4B

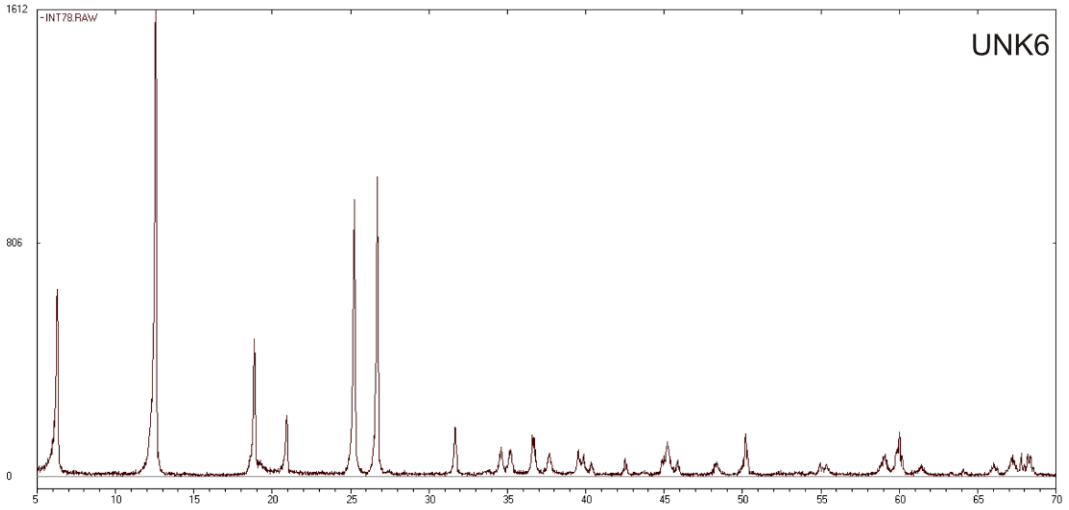
INT78.RAW
UNK6
1612
806
0
5
10
15
20
25
30
35
40
45
50
55
60
65
70

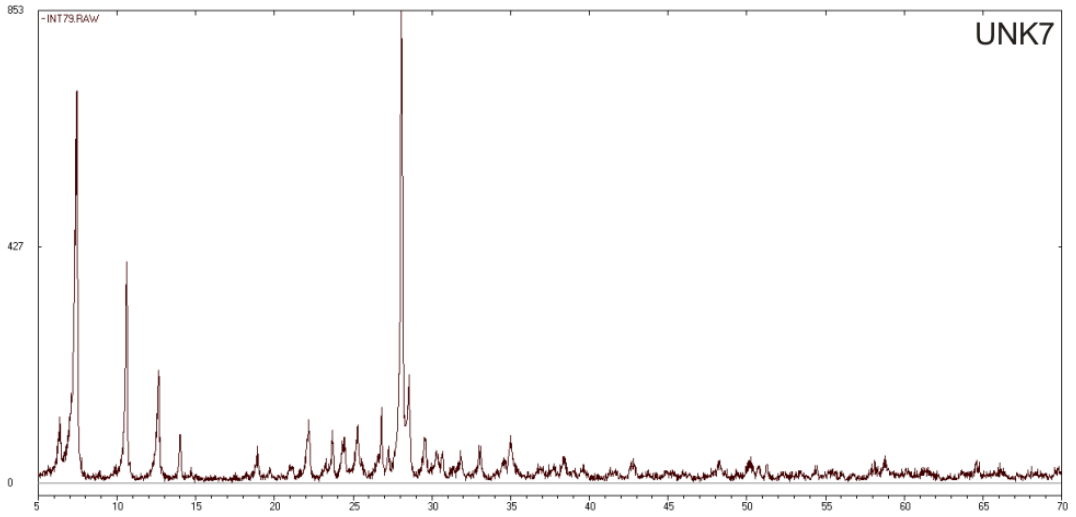
INT79.RAW
UNK7
853
427
0
5
10
15
20
25
30
35
40
45
50
55
60
65
70

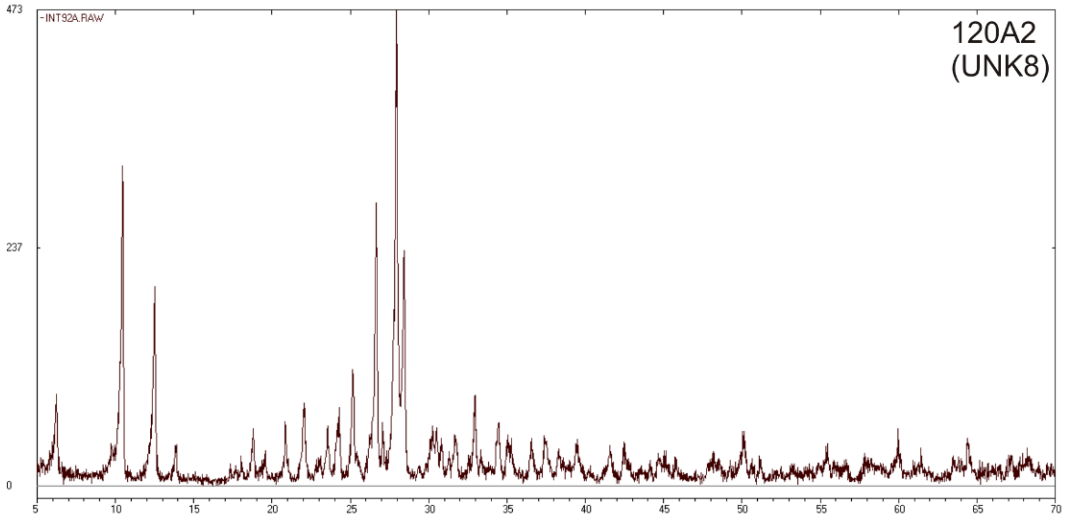
INT92A.RAW
120A2
(UNK8)
473
237
0
5
10
15
20
25
30
35
40
45
50
55
60
65
70

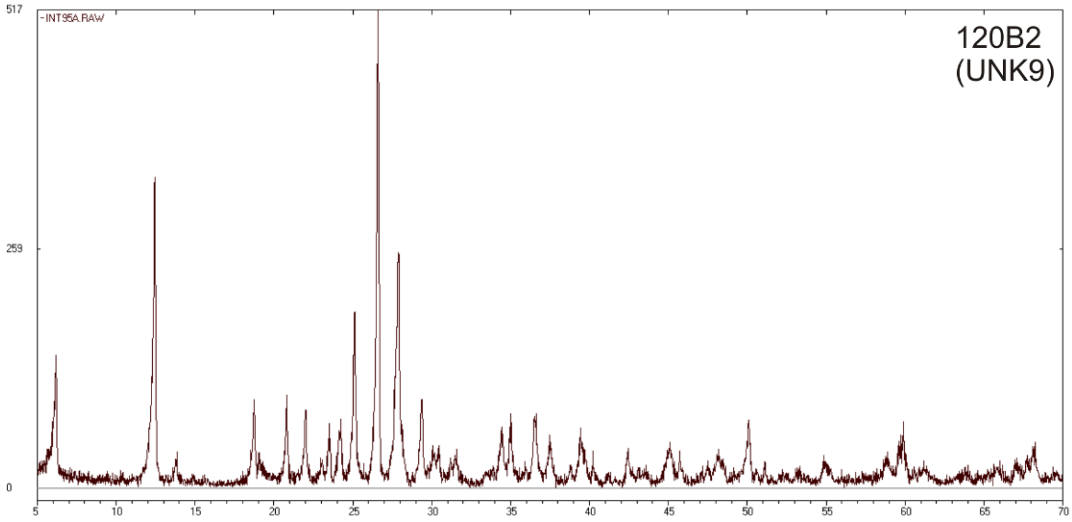

Table B.1. Approximate modal mineral quantities.

	PEG2	PEG4	GEOR1	SKE1	SOL2	SIL1	JEA1
>40%	Albite	Albite	Actinolite	Illite-Mont.		Quartz Chlorite	Chlorite
20 – 40%	Actinolite	Actinolite	Chlorite		Albite Chlorite		Quartz
10 – 20%	Illite-Mont. Biotite		Epidote Quartz	Albite Chlorite Actinolite			
5 – 10%	Epidote Chlorite	Illite-Mont. Epidote		Quartz	Quartz Opaque minerals	Opaque minerals	Calcite Epidote
<5%	Sphene		Opaque minerals Sphene	Opaque minerals Sphene	Opaque minerals		Opaque minerals Sphene

Table B.1 (Continued).

	FRI1	LIB1	LIT1	PE1	LAV1	AMI1	BAN4
>40 %	Chlorite		Illite-Mont.		Actinolite	Quartz Chlorite	
20 – 40%		Chlorite Albite	Albite	Chlorite Quartz	Albite		Albite
10 – 20%	Quartz	Quartz	Quartz Actinolite Chlorite	Actinolite	Chlorite		Chlorite Actinolite
5 – 10%	Prehnite Epidote Opaque minerals	Opaque minerals		Epidote	Hydrobiotite		Hydrobiotite Illite-Mont.
<5%	Sphene		Opaque minerals	Opaque minerals		Opaque minerals	Opaque minerals

Table B.1 (Continued).

	SPE2	TWI1	TWI2	BRA1+2	CLA3	CLA5	KEN1
>40%	Quartz Chlorite	Quartz	Quartz			Quartz Chlorite	Quartz Chlorite
20 – 40%				Albite	Quartz Chlorite		
10 – 20%		Chlorite Illite-Mont.	Illite-Mont.	Chlorite Pigeonite Quartz	Albite		
5 – 10%			Chlorite	Actinolite	Epidote	Sphene	
<5%	Opaque minerals	Opaque minerals	Opaque minerals	Opaque minerals	Sphene		Opaque minerals

Table B.1 (Continued).

	KEN4	SWA2	UNK3	UNK4	UNK6	UNK7	UNK8	UNK9
>40%	Quartz Chlorite	Chlorite			Chlorite Quartz	Albite	Albite	
20 – 40%		Quartz	Quartz Albite	Albite Chlorite Quartz		Illite-Mont.	Actinolite	Quartz Chlorite
10 – 20%			Chlorite			Chlorite Actinolite	Quartz Illite-Mont.	Albite
5 – 10%		Illite-Mont.	Illite-Mont.	Epidote Opaque minerals			Chlorite	Chalco-pyrite
<5%	Opaque minerals	Opaque minerals Sphene		Sphene	Opaque minerals	Sphene	Sphene	Opaque minerals

CIPW Norms

Table B - 2. CIPW norms

	PEG1	PEG2	PEG3	PEG4	PEG5	PEG6
Quartz	2.60	0.57	0.10	1.81	3.24	1.59
Corundum	0.00	0.00	0.00	0.00	0.00	0.00
Orthoclase	8.33	3.61	7.15	11.17	8.45	8.81
Albite	22.85	43.24	35.37	32.07	40.87	41.21
Anorthite	12.64	8.28	14.34	9.90	9.40	12.35
Diopside	26.97	17.08	20.55	17.09	11.95	14.99
Hypersthene	20.34	21.36	17.56	21.84	20.25	16.82
Olivine	0.00	0.00	0.00	0.00	0.00	0.00
Magnetite	2.86	2.62	2.23	2.70	2.47	1.96
Ilmenite	2.81	2.83	2.28	2.98	2.81	1.92
Apatite	0.62	0.43	0.45	0.45	0.57	0.36

Table B - 2 (Continued).

	GEOR1	GEOR2	GEOR3	SKE1	SKE5	SKE2	SKE3
Quartz	15.95	14.25	51.37	11.60	15.45	9.39	10.84
Corundum	0.00	0.00	6.44	0.00	0.00	0.00	0.00
Orthoclase	0.18	0.00	0.00	0.71	0.00	0.00	0.59
Albite	14.39	7.70	0.00	13.71	25.13	4.23	13.12
Anorthite	28.41	32.72	3.03	29.13	25.44	33.56	29.64
Diopside	8.74	2.51	0.00	10.64	7.15	8.58	12.37
Hypersthene	29.03	39.74	34.78	25.99	22.86	33.34	25.42
Olivine	0.00	0.00	0.00	0.00	0.00	0.00	0.00
Magnetite	1.93	1.93	2.00	3.13	1.97	3.39	3.09
Ilmenite	1.20	1.01	2.34	4.28	1.69	5.93	4.18
Apatite	0.19	0.17	0.21	0.83	0.38	1.73	0.76

Table B - 2 (Continued).

	SOL1	SOL2	SOL3	KUD1	SIL1	SIL2
Quartz	27.86	14.99	60.08	20.44	38.23	7.80
Corundum	15.46	3.96	7.80	0.00	11.33	0
Orthoclase	0.00	0.00	0.00	0.06	0.00	1.24
Albite	0.00	16.50	0.00	16.75	0.00	10.75
Anorthite	0.22	22.84	0.23	30.54	2.24	29.56
Diopside	0.00	0.00	0.00	2.70	0.00	17.93
Hypersthene	48.79	35.26	27.34	25.44	45.14	21.94
Olivine	0.00	0.00	0.00	0.00	0.00	0
Magnetite	4.00	2.74	2.07	2.00	2.22	3.13
Ilmenite	3.33	3.27	2.34	1.69	0.91	5.91
Apatite	0.50	0.50	0.33	0.38	0.14	1.78

Table B - 2 (Continued).

	LIB1	LIT1	PE1	PE2	LAV1	JEA1	JEA2	JEA3
Quartz	16.73	7.541	10.72	13.155	5.125	12.611	19.066	12.20
Corundum	0	0	0	1.3	0.549	0	12.029	0
Orthoclase	0	4.078	0	0	6.619	0	0	0
Albite	10.323	21.154	5.585	8.039	34.608	3.892	8.885	4.15
Anorthite	29.941	22.157	32.809	30.199	24.967	33.571	7.487	34.15
Diopside	1.279	8.363	5.02	0	0	7.405	0	6.21
Hypersthene	30.784	26.653	34.643	35.975	23.958	32	46.62	32.72
Olivine	0	0	0	0	0	0	0	0
Magnetite	3.378	3.277	3.523	3.175	1.87	3.262	2.436	3.36
Ilmenite	5.206	4.845	5.89	6.27	1.957	5.681	2.679	5.62
Apatite	2.037	1.99	1.895	1.966	0.355	1.658	0.829	1.71

Table B - 2 (Continued).

	FRI1	FRI2	FRI3	FRI4	FRI5	FRI6	FRI7	FRI8	FRI9
Quartz	13.49	26.73	13.98	11.37	19.75	14.42	12.42	15.26	25.96
Corundum	0	14.127	0	0	10.22	0	0	12.15	14.48
Orthoclase	0	0	0	0	0	0	0	0	0
Albite	0	0	0	10.66	0	0.25	0.68	0	0
Anorthite	35.28	0.66	35.83	34.35	10.86	35.99	35.14	9.72	0.57
Diopside	10.99	0	6.75	1.55	0	4.63	11.26	0	0
Hypersthene	29.89	46.34	33.23	33.82	47.29	34.21	29.89	49.24	46.52
Olivine	0	0	0	0	0	0	0	0	0
Magnetite	3.35	4.05	3.31	3.22	4.16	3.38	3.38	4.71	4.12
Ilmenite	5.49	6.35	5.47	4.33	6.08	5.59	5.62	6.99	6.57
Apatite	1.68	1.99	1.61	0.81	1.87	1.68	1.73	2.18	1.99

Table B - 2 (Continued).

	AMI1	AMI2	AMI3	AMI5
Quartz	32.07	34.86	15.23	11.96
Corundum	15.08	14.67	3.32	2.51
Orthoclase	0	0	0	0.12
Albite	0	0	12.52	12.78
Anorthite	0.42	0.44	24.67	27.20
Diopside	0	0	0	0
Hypersthene	40.99	39.12	34.45	35.18
Olivine	0	0	0	0
Magnetite	3.19	3.00	3.13	3.23
Ilmenite	6.35	6.33	5.80	6.08
Apatite	2.13	1.8	0.88	0.95

Table B - 2 (Continued).

	BAN1	BAN3	BAN4	BAN5	BAN6	BAN7	BAN8
Quartz	2.43	3.56	2.69	11.11	12.54	2.52	5.78
Corundum	0	0	0	0	0.59	0	0
Orthoclase	2.66	0.65	3.96	0.95	0.12	3.19	2.31
Albite	19.46	17.18	20.82	9.48	12.27	19.97	14.39
Anorthite	28.10	27.10	24.96	33.60	32.12	26.91	28.90
Diopside	14.62	16.80	14.35	1.55	0	14.77	13.41
Hypersthene	25.30	25.60	26.20	33.21	32.50	25.76	27.35
Olivine	0	0	0	0	0	0	0
Magnetite	2.71	3.03	3.20	3.19	2.87	3.12	3.12
Ilmenite	4.09	5.28	5.59	6.02	6.08	5.38	5.59
Apatite	0.69	0.81	0.69	0.92	0.95	0.76	0.88

Table B - 2 (Continued).

	SPE1	SPE2	SPE3	SPE5	TWI1	TWI2
Quartz	13.93	28.35	48.33	40.89	41.34	45.90
Corundum	1.53	12.88	10.10	12.11	14.70	13.77
Orthoclase	0	0	0	0	10.17	13.53
Albite	0	0	0	0	1.02	1.52
Anorthite	27.24	0.63	0.27	0.50	0.16	0.27
Diopside	0	0	0	0	0	0
Hypersthene	53.77	53.92	38.54	43.16	28.93	21.88
Olivine	0	0	0	0	0	0
Magnetite	2.62	3.07	2.06	2.54	2.29	1.75
Ilmenite	1.00	1.06	0.78	0.87	1.24	1.197
Apatite	0.14	0.17	0.12	0.14	0.21	0.19

Table B - 2 (Continued).

	BRA1	BRA2	BRA3	BRA4	BRA5	BRA6	BRA7	BRA8
Quartz	14.53	17.87	10.93	4.51	3.85	21.40	2.05	4.70
Corundum	4.599	3.569	0.994	0	0	3.786	0	0
Orthoclase	0.06	0	0	0.36	0.77	0	3.49	3.37
Albite	14.3	10.15	14.05	16.08	16.42	13.37	16.16	13.03
Anorthite	19.56	23.81	28.77	27.58	27.36	21.51	25.73	27.89
Diopside	0	0	0	16.104	17.263	0	17.206	16.249
Hypersthene	36.55	34.16	35.24	25.67	24.84	29.69	25.67	25.44
Olivine	0	0	0	0	0	0	0	0
Magnetite	3.42	3.19	3.23	3.10	3.06	2.86	3.22	3.07
Ilmenite	6.10	5.80	5.93	5.43	5.38	5.89	5.66	5.43
Apatite	0.95	0.90	0.90	0.81	0.83	0.92	0.85	0.83

Table B - 2 (Continued).

	CLA1	CLA2	CLA3	CLA4	CLA5	CLA6	CLA7	CLA8	CLA9
Quartz	19.61	21.95	5.99	10.68	20.56	1.99	3.16	9.58	47.14
Corundum	17.97	17.15	0	0	15.17	0	0	0	11.35
Orthoclase	0	0	0	0	0	0	0	0	0
Albite	0	0	4.57	0	6.26	14.55	12.69	0	0
Anorthite	0.36	0.49	40.39	42.05	0.44	35.45	35.64	43.47	0.38
Diopside	0	0	5.89	3.16	0	9.84	7.92	7.44	0
Hypersthene	55.43	53.77	38.57	37.73	51.46	33.28	35.18	33.30	36.67
Olivine	0	0	0	0	0	0	0	0	0
Magnetite	4.06	3.76	2.58	2.54	4.22	2.54	2.45	2.41	2.99
Ilmenite	2.62	2.81	2.41	2.39	2.58	2.62	2.36	2.07	1.60
Apatite	0.36	0.38	0.33	0.31	0.38	0.38	0.33	0.28	0.02

Table B - 2 (Continued).

	KEN1	KEN2	KEN3	KEN4	KEN5	KEN6	KEN7
Quartz	7.70	3.02	13.08	4.64	7.68	7.96	6.36
Corundum	2.99	0	0	11.50	0	0	0
Orthoclase	0	0	0.06	0	0.77	0.77	0.71
Albite	17.6	17.01	0	27.33	10.07	10.83	12.44
Anorthite	25.61	28.33	37.27	0.36	31.11	31.20	30.05
Diopside	0	16.82	10.96	0	12.40	10.69	14.24
Hypersthene	42.70	25.18	28.03	52.96	28.51	28.96	26.81
Olivine	0	0	0	0	0	0	0
Magnetite	2.78	2.90	2.99	3.9	3.13	3.10	3.06
Ilmenite	2.64	5.61	5.38	2.68	5.49	5.64	5.51
Apatite	0.36	0.88	0.85	0.36	0.85	0.88	0.85

Table B - 2 (Continued).

	UNK1	UNK2	UNK3	UNK4A	UNK4B	UNK6	UNK7
Quartz	7.66	2.30	20.62	7.59	25.90	3.98	5.73
Corundum	0	0.41	0	0	3.35	9.22	0
Orthoclase	0	0	5.73	0	0	0	4.61
Albite	8.12	4.74	14.47	24.12	0	31.57	32.24
Anorthite	31.41	37.61	33.14	24.10	31.4	0.19	11.29
Diopside	12.87	0	8.29	12.60	0	0	10.08
Hypersthene	28.97	42.03	11.81	24.32	28.23	54.73	29.55
Olivine	0	0	0	0	0	0	0
Magnetite	3.34	4.13	0.96	2.97	2.52	3.18	2.71
Ilmenite	5.97	6.84	1.92	4.07	4.41	1.16	2.57
Apatite	1.80	2.08	0.43	0.76	0.83	0.17	0.45

Table B - 2 (Continued).

	120A1	120A2	120A3	120B1	120B2	120B3
Quartz	20.92	12.33	18.73	24.53	17.78	32.23
Corundum	2.70	0	0	0.74	1.06	11.94
Orthoclase	0	0	13.48	12.29	0	9.34
Albite	30.63	26.49	0.68	1.44	17.69	1.52
Anorthite	18.62	22.76	32.34	32.13	29.22	4.35
Diopside	0	13.41	14.29	0	0	0
Hypersthene	22.95	21.12	16.65	24.90	30.14	35.85
Olivine	0	0	0	0	0	0
Magnetite	1.94	1.97	1.70	1.77	2.06	2.54
Ilmenite	1.9	1.62	1.75	1.81	1.79	1.84
Apatite	0.43	0.33	0.40	0.40	0.38	0.40

Appendix C: Chemistry

Major Elements

Table C – 1. Major Element Concentrations (wt%). Bdl = below detection limit.

Sample	SiO2	Al2O3	Fe2O3	MnO	MgO	CaO	Na2O	K2O	TiO2	P2O5	LOI	Sum
AMI1	50.13	14.15	15.65	0.04	7.96	1.18	bdl	bdl	3.10	0.84	4.97	97.88
AMI2	53.46	14.19	15.19	0.03	8.02	1.04	bdl	bdl	3.20	0.73	5.21	100.52
AMI3	49.02	13.89	15.53	0.18	5.46	5.12	1.39	bdl	2.87	0.35	5.74	99.55
AMI5	47.98	14.19	16.21	0.20	5.55	5.69	2.54	0.02	3.03	0.38	4.76	100.55
BAN1	49.89	14.43	14.41	0.20	5.66	9.64	2.09	0.53	2.12	0.29	1.68	100.94
BAN3	48.51	13.24	15.98	0.22	5.63	9.99	1.96	0.19	2.77	0.34	1.06	99.90
BAN4	49.02	13.37	16.29	0.22	4.86	8.50	3.18	0.64	2.82	0.28	1.80	100.99
BAN5	49.77	14.10	16.60	0.17	5.43	7.54	1.54	0.15	3.11	0.39	2.76	101.57
BAN6	50.08	14.28	14.67	0.15	5.79	6.79	2.22	0.02	3.09	0.38	3.19	100.67
BAN7	48.86	13.81	15.87	0.21	5.01	9.05	2.84	0.52	2.73	0.31	1.55	100.76
BAN8	49.25	13.43	16.07	0.21	5.44	9.28	1.96	0.38	2.86	0.36	1.40	100.64
BRA1	49.28	13.91	17.27	0.18	5.60	4.27	1.57	0.01	3.07	0.38	4.24	99.78
BRA2	51.49	13.95	16.48	0.17	5.40	5.18	1.74	bdl	2.99	0.37	3.66	101.45
BRA3	48.39	13.49	16.22	0.21	5.62	5.94	1.46	0.00	2.93	0.36	4.11	98.73
BRA4	49.55	13.40	16.51	0.23	5.52	9.96	2.30	0.06	2.88	0.34	2.03	102.80
BRA5	49.52	13.46	16.29	0.21	5.55	10.21	2.23	0.13	2.86	0.35	1.83	102.65
BRA6	54.34	14.06	14.86	0.14	4.79	4.78	2.15	bdl	3.06	0.38	3.47	102.02
BRA7	46.61	12.69	16.34	0.24	5.18	9.41	1.46	0.57	2.86	0.34	3.44	99.13
BRA8	47.73	12.94	15.74	0.22	5.31	9.67	1.43	0.55	2.77	0.34	2.24	98.94
CLA1	46.66	17.35	20.55	0.18	9.80	0.26	bdl	bdl	1.32	0.14	5.86	101.74
CLA2	48.40	16.65	19.05	0.31	10.06	0.30	bdl	bdl	1.42	0.16	5.86	101.94
CLA3	46.74	14.59	12.66	0.19	8.55	9.09	0.39	bdl	1.18	0.13	7.07	100.49
CLA4	47.01	14.32	12.48	0.17	7.86	8.75	1.16	bdl	1.17	0.12	3.96	96.92
CLA5	49.58	15.98	21.53	0.22	7.78	0.29	bdl	bdl	1.32	0.15	5.33	101.87
CLA6	47.98	15.15	12.86	0.18	7.72	9.35	1.13	bdl	1.32	0.15	7.23	102.97
CLA7	49.30	15.24	12.74	0.17	8.46	9.14	1.84	bdl	1.21	0.14	2.65	100.80
CLA8	48.84	15.58	12.41	0.16	7.68	10.50	1.50	bdl	1.07	0.12	3.00	100.77
CLA9	63.65	11.07	15.23	0.14	5.51	0.09	bdl	bdl	0.81	0.01	4.04	100.07
FRI1	48.39	12.61	17.24	0.21	5.28	10.42	bdl	bdl	2.82	0.69	4.35	101.78
FRI2	49.05	13.85	20.65	0.27	7.52	1.19	bdl	bdl	3.22	0.81	4.91	101.03
FRI3	48.48	12.78	17.06	0.22	5.82	9.57	0.13	0.01	2.80	0.66	3.60	101.13
FRI4	49.62	14.17	16.57	0.22	4.86	7.55	1.30	bdl	2.22	0.33	3.85	100.68
FRI5	46.17	13.47	21.07	0.32	7.25	3.11	bdl	bdl	3.06	0.75	5.12	100.26
FRI6	47.60	12.62	17.20	0.31	5.36	8.97	0.31	bdl	2.82	0.68	5.29	101.15
FRI7	47.05	12.52	17.36	0.24	5.13	10.47	0.09	bdl	2.86	0.71	4.46	100.90
FRI8	42.39	15.02	24.05	0.59	6.53	3.06	0.12	bdl	3.56	0.88	5.05	101.26
FRI9	47.94	14.17	21.14	0.40	7.27	1.17	0.05	bdl	3.36	0.82	5.01	101.32

Sample	SiO2	Al2O3	Fe2O3	MnO	MgO	CaO	Na2O	K2O	TiO2	P2O5	LOI	Sum
GEOR1	57.74	13.10	10.11	0.14	7.48	7.89	1.84	0.03	0.62	0.08	2.39	101.43
GEOR2	53.08	12.61	9.50	0.15	9.91	6.84	1.28	bdl	0.50	0.07	7.99	101.89
GEOR3	69.95	7.39	10.38	0.12	8.16	0.71	bdl	bdl	1.20	0.09	3.81	101.58
JEA1	47.36	12.35	16.30	0.21	5.54	8.96	0.12	bdl	2.83	0.67	5.35	99.64
JEA2	51.82	15.87	12.36	0.13	11.42	1.90	1.71	bdl	1.36	0.34	5.37	102.26
JEA3	47.49	12.73	17.02	0.21	5.30	8.91	0.62	bdl	2.83	0.68	4.60	100.33
KEN1	50.69	14.97	13.92	0.34	8.54	5.08	bdl	bdl	1.31	0.15	6.28	100.99
KEN2	47.33	13.29	14.91	0.21	5.92	9.97	2.25	bdl	2.86	0.36	4.58	101.64
KEN3	47.68	13.21	15.25	0.23	5.53	10.27	1.36	0.01	2.73	0.35	3.02	99.63
KEN4	48.28	16.00	19.45	0.37	9.06	0.26	bdl	bdl	1.33	0.14	5.68	100.14
KEN5	48.83	13.29	16.32	0.21	5.69	9.57	1.37	0.13	2.85	0.36	3.17	101.78
KEN6	48.55	13.30	15.98	0.22	5.56	9.10	1.60	0.10	2.89	0.36	2.87	100.53
KEN7	48.36	13.25	15.84	0.21	5.55	9.73	1.43	0.12	2.83	0.35	2.69	100.36
KUD1	58.63	14.17	10.35	0.14	4.82	6.88	2.47	0.01	0.87	0.16	3.15	101.65
LAV1	56.73	17.73	9.94	0.13	4.32	5.26	5.38	1.13	1.03	0.15	1.16	102.96
LIB1	50.59	12.47	17.13	0.20	3.47	7.18	1.60	bdl	2.63	0.83	5.22	101.23
LIT1	50.97	12.78	17.07	0.22	3.52	7.43	2.86	0.68	2.51	0.82	2.78	101.63
PE1	47.50	12.71	18.04	0.20	5.53	8.61	0.92	bdl	3.01	0.78	3.39	100.65
PE2	48.06	13.29	15.99	0.23	6.13	6.85	1.33	bdl	3.15	0.79	4.13	99.91
PEG1	51.70	10.24	14.61	0.18	5.24	9.06	4.11	1.36	1.43	0.25	3.38	101.56
PEG2	55.39	11.99	13.74	0.15	4.58	5.95	5.73	0.61	1.47	0.18	1.25	101.04
PEG3	55.37	13.55	11.88	0.14	4.86	8.16	4.45	1.22	1.21	0.19	0.79	101.81
PEG4	55.01	11.81	14.36	0.16	4.50	6.42	3.66	1.95	1.58	0.20	1.18	100.82
PEG5	56.87	12.87	12.98	0.13	3.61	5.04	5.68	1.43	1.47	0.24	0.87	101.19
PEG6	56.99	14.06	10.31	0.14	4.10	6.26	5.03	1.48	1.01	0.15	0.75	100.28
SIL1	57.65	10.99	10.59	0.24	10.17	0.48	bdl	bdl	0.44	0.06	5.12	95.21
SIL2	44.53	11.94	15.06	0.16	4.04	10.19	1.29	0.19	2.82	0.68	9.09	99.98
SKE1	51.61	13.24	16.28	0.23	3.95	8.71	1.78	0.12	2.21	0.34	2.99	101.46
SKE2	45.86	12.43	16.98	0.23	5.96	9.27	0.67	bdl	2.96	0.69	5.56	100.53
SKE3	51.36	13.32	16.11	0.22	4.17	9.20	1.84	0.10	2.17	0.32	2.93	101.74
SKE5	58.33	13.97	10.24	0.16	4.77	6.95	4.03	bdl	0.87	0.16	1.39	100.83
SOL1	51.10	14.98	20.39	0.17	7.69	0.31	bdl	bdl	1.69	0.20	5.40	101.52
SOL2	51.77	14.75	13.73	0.18	6.17	4.63	2.52	bdl	1.63	0.20	5.78	101.32
SOL3	72.07	7.63	10.58	0.02	5.07	0.22	bdl	bdl	1.19	0.13	3.24	99.93
SPE1	49.63	10.43	12.53	0.52	12.06	5.06	bdl	bdl	0.46	0.06	9.82	100.20
SPE2	54.25	12.37	15.36	0.18	11.45	0.21	bdl	bdl	0.53	0.07	5.66	99.79
SPE3	66.88	9.85	10.52	0.13	8.82	0.11	bdl	bdl	0.40	0.05	4.34	100.55
SPE4	34.71	10.48	13.90	1.09	15.70	9.62	bdl	bdl	0.43	0.05	15.08	100.48
SPE5	58.50	11.20	12.22	0.12	8.68	0.17	bdl	bdl	0.42	0.06	4.78	95.45
SWA1	46.10	13.25	20.93	0.34	7.73	1.11	bdl	bdl	3.05	0.77	5.44	97.95
SWA2	47.35	12.18	18.16	0.21	5.00	9.94	bdl	bdl	2.85	0.70	4.73	100.81

Sample	SiO2	Al2O3	Fe2O3	MnO	MgO	CaO	Na2O	K2O	TiO2	P2O5	LOI	Sum
SWA3	46.67	13.03	23.11	0.24	6.70	1.07	bdl	bdl	3.00	0.74	5.26	99.82
TWI1	62.91	16.65	11.98	0.05	4.71	0.14	0.08	1.70	0.65	0.09	3.97	102.93
TWI2	66.49	16.50	9.19	0.04	3.60	0.15	0.18	2.27	0.62	0.08	3.58	102.72
UNK1	44.95	12.20	16.43	0.26	5.19	9.71	0.90	bdl	2.92	0.70	7.34	100.60
UNK2	40.23	14.11	20.42	0.25	5.59	8.16	0.52	bdl	3.36	0.82	6.51	99.98
UNK3	55.89	15.06	4.73	0.11	3.72	8.44	4.09	0.91	0.95	0.17	7.56	101.63
UNK4A	50.61	12.84	14.90	0.20	4.00	7.87	2.31	bdl	2.03	0.31	6.53	101.55
UNK4B	51.43	14.14	12.71	0.14	4.55	6.46	3.30	bdl	2.20	0.33	6.09	101.29
UNK6	51.84	14.52	15.84	0.10	11.54	0.12	bdl	bdl	0.57	0.06	5.74	99.92
UNK7	55.12	11.02	14.02	0.19	5.95	4.86	4.50	0.76	1.32	0.19	4.28	102.21
120A1	58.88	14.76	9.77	0.09	3.51	3.81	5.01	bdl	0.95	0.17	2.69	99.56
120A2	57.50	13.27	10.28	0.14	5.29	7.90	3.51	bdl	0.84	0.14	1.70	100.55
120A3	53.19	13.24	8.20	0.33	4.15	9.36	0.01	2.09	0.85	0.15	9.33	100.91
120B1	56.97	14.20	8.81	0.39	4.47	6.33	0.26	1.96	0.90	0.16	7.09	101.54
120B2	54.99	14.30	10.21	0.16	5.75	5.74	3.52	bdl	0.89	0.15	5.10	100.72
120B3	58.47	15.15	13.05	0.25	6.67	1.08	0.10	1.55	0.95	0.17	4.09	101.53

Major Element Summary

Amigo

	n	NA	Mean	SD	Min	Max
SiO2	4	0	53.19	2.23	50.68	55.86
TiO2	4	0	3.23	0.14	3.05	3.34
Al2O3	4	0	14.96	0.20	14.80	15.23
Fe2O3	4	0	16.61	0.52	15.90	17.12
MnO	4	0	0.12	0.10	0.03	0.21
MgO	4	0	7.16	1.53	5.82	8.57
CaO	4	0	3.46	2.64	1.09	6.01
Na2O	2	2	1.50	0.02	1.48	1.51
K2O	1	3	0.02	NA	0.02	0.02
P2O5	4	0	0.61	0.26	0.37	0.9

Bank

	n	NA	Mean	SD	Min	Max
SiO2	7	0	50.65	0.75	49.38	51.86
TiO2	7	0	2.85	0.36	2.12	3.20
Al2O3	7	0	14.16	0.48	13.39	14.77
Fe2O3	7	0	16.05	0.97	14.36	16.97
MnO	7	0	0.20	0.02	0.16	0.23
MgO	7	0	5.56	0.33	5.06	6.00
CaO	7	0	8.85	1.11	7.00	9.96
Na2O	7	0	1.92	0.51	1.12	2.46
K2O	7	0	0.33	0.24	0.02	0.67
P2O5	7	0	0.34	0.05	0.29	0.40

Brazil

	n	NA	Mean	SD	Min	Max
SiO2	8	0	50.83	2.26	48.51	55.14
TiO2	8	0	3.00	0.14	2.83	3.21
Al2O3	8	0	13.83	0.56	13.21	14.56
Fe2O3	8	0	16.62	0.87	15.08	18.08
MnO	8	0	0.21	0.04	0.14	0.25
MgO	8	0	5.49	0.30	4.86	5.86
CaO	8	0	7.59	2.58	4.47	10.13
Na2O	8	0	1.68	0.25	1.20	1.94
K2O	5	3	0.27	0.28	0.01	0.59
P2O5	8	0	0.37	0.02	0.34	0.40

CLA

	n	NA	Mean	SD	Min	Max
SiO2	9	0	51.95	5.33	48.66	66.04
TiO2	9	0	1.26	0.19	0.84	1.48
Al2O3	9	0	15.76	1.84	11.49	18.10
Fe2O3	9	0	16.17	3.92	12.69	22.31
MnO	9	0	0.20	0.05	0.15	0.33
MgO	9	0	8.52	1.41	5.72	10.47
CaO	9	0	5.55	5.05	0.09	10.74
Na2O	4	5	1.13	0.57	0.54	1.72
K2O	0	9	NA	NA	NA	NA
P2O5	9	0	0.13	0.05	0.01	0.16

Friday

	n	NA	Mean	SD	Min	Max
SiO2	9	0	49.36	2.07	44.33	51.49
TiO2	9	0	3.07	0.41	2.28	3.68
Al2O3	9	0	13.99	0.97	12.93	15.71
Fe2O3	9	0	19.78	2.79	17.04	24.91
MnO	9	0	0.31	0.12	0.22	0.6
MgO	9	0	6.4	1.12	5.05	7.8
CaO	9	0	6.34	4.07	1.22	10.74
Na2O	3	6	0.46	0.7	0.03	1.26
K2O	0	9	NA	NA	NA	NA
P2O5	9	0	0.73	0.17	0.34	0.92

Georgette

	n	NA	Mean	SD	Min	Max
SiO2	3	0	62.23	8.07	56.78	71.50
TiO2	3	0	0.80	0.38	0.53	1.23
Al2O3	3	0	11.43	3.36	7.55	13.49
Fe2O3	3	0	10.34	0.24	10.17	10.61
MnO	3	0	0.14	0.02	0.12	0.16
MgO	3	0	8.84	1.57	7.57	10.60
CaO	3	0	5.34	4.01	0.73	7.98
Na2O	2	1	1.31	0.56	0.91	1.70
K2O	1	2	0.03	NA	0.03	0.03
P2O5	3	0	0.08	0.01	0.07	0.09

Jeans

	n	NA	Mean	SD	Min	Max
SiO2	3	0	51.20	2.32	49.69	53.87
TiO2	3	0	2.45	0.90	1.41	2.99
Al2O3	3	0	14.29	1.92	13.06	16.50
Fe2O3	3	0	15.96	2.71	12.85	17.81
MnO	3	0	0.19	0.05	0.14	0.22
MgO	3	0	7.76	3.57	5.54	11.87
CaO	3	0	6.92	4.29	1.97	9.47
Na2O	3	0	0.67	0.33	0.46	1.05
K2O	0	3	NA	NA	NA	NA
P2O5	3	0	0.59	0.21	0.35	0.72

Ken

	n	NA	Mean	SD	Min	Max
SiO2	7	0	50.24	1.61	48.77	53.52
TiO2	7	0	2.48	0.74	1.39	2.97
Al2O3	7	0	14.41	1.38	13.50	16.94
Fe2O3	7	0	16.52	1.91	14.70	20.59
MnO	7	0	0.27	0.08	0.21	0.39
MgO	7	0	6.81	1.72	5.69	9.60
CaO	7	0	7.94	3.82	0.27	10.63
Na2O	6	1	1.88	0.76	1.19	3.23
K2O	4	3	0.10	0.06	0.01	0.13
P2O5	7	0	0.30	0.11	0.15	0.37

Kudu

	n	NA	Mean	SD	Min	Max
SiO2	1	0	59.84	NA	59.84	59.84
TiO2	1	0	0.89	NA	0.89	0.89
Al2O3	1	0	14.46	NA	14.46	14.46
Fe2O3	1	0	10.57	NA	10.57	10.57
MnO	1	0	0.14	NA	0.14	0.14
MgO	1	0	4.92	NA	4.92	4.92
CaO	1	0	7.02	NA	7.02	7.02
Na2O	1	0	1.98	NA	1.98	1.98
K2O	1	0	0.01	NA	0.01	0.01
P2O5	1	0	0.16	NA	0.16	0.16

Lib

	n	NA	Mean	SD	Min	Max
SiO2	1	0	52.69	NA	52.69	52.69
TiO2	1	0	2.74	NA	2.74	2.74
Al2O3	1	0	12.98	NA	12.98	12.98
Fe2O3	1	0	17.84	NA	17.84	17.84
MnO	1	0	0.21	NA	0.21	0.21
MgO	1	0	3.62	NA	3.62	3.62
CaO	1	0	7.47	NA	7.47	7.47
Na2O	1	0	1.22	NA	1.22	1.22
K2O	0	1	NA	NA	NA	NA
P2O5	1	0	0.86	NA	0.86	0.86

Little Tumi

	n	NA	Mean	SD	Min	Max
SiO2	1	0	51.77	NA	51.77	51.77
TiO2	1	0	2.55	NA	2.55	2.55
Al2O3	1	0	12.98	NA	12.98	12.98
Fe2O3	1	0	17.33	NA	17.33	17.33
MnO	1	0	0.22	NA	0.22	0.22
MgO	1	0	3.58	NA	3.58	3.58
CaO	1	0	7.55	NA	7.55	7.55
Na2O	1	0	2.5	NA	2.5	2.5
K2O	1	0	0.69	NA	0.69	0.69
P2O5	1	0	0.84	NA	0.84	0.84

PE

	n	NA	Mean	SD	Min	Max
SiO2	2	0	49.69	1.00	48.98	50.40
TiO2	2	0	3.20	0.14	3.10	3.30
Al2O3	2	0	13.52	0.58	13.11	13.93
Fe2O3	2	0	17.69	1.29	16.77	18.60
MnO	2	0	0.23	0.02	0.21	0.24
MgO	2	0	6.07	0.52	5.70	6.43
CaO	2	0	8.03	1.20	7.18	8.87
Na2O	2	0	0.81	0.21	0.66	0.95
K2O	0	2	NA	NA	NA	NA
P2O5	2	0	0.82	0.02	0.80	0.83

Peggy

	n	NA	Mean	SD	Min	Max
SiO2	6	0	55.69	1.47	53.47	57.38
TiO2	6	0	1.37	0.22	1.01	1.57
Al2O3	6	0	12.52	1.26	10.60	14.15
Fe2O3	6	0	13.07	1.74	10.37	15.11
MnO	6	0	0.15	0.02	0.14	0.18
MgO	6	0	4.54	0.61	3.63	5.42
CaO	6	0	6.86	1.58	5.06	9.37
Na2O	6	0	4.25	0.90	2.70	5.11
K2O	6	0	1.34	0.42	0.61	1.89
P2O5	6	0	0.20	0.04	0.15	0.26

Sill

	n	NA	Mean	SD	Min	Max
SiO2	2	0	56.41	10.39	49.06	63.76
TiO2	2	0	1.80	1.86	0.48	3.11
Al2O3	2	0	12.65	0.71	12.15	13.15
Fe2O3	2	0	14.16	3.46	11.71	16.60
MnO	2	0	0.22	0.06	0.17	0.26
MgO	2	0	7.85	4.79	4.46	11.24
CaO	2	0	5.88	7.57	0.53	11.23
Na2O	1	1	1.27	NA	1.27	1.27
K2O	1	1	0.21	NA	0.21	0.21
P2O5	2	0	0.41	0.49	0.06	0.75

Skelm

	n	NA	Mean	SD	Min	Max
SiO2	4	0	53.09	4.56	48.39	59.33
TiO2	4	0	2.12	0.92	0.89	3.12
Al2O3	4	0	13.58	0.46	13.12	14.21
Fe2O3	4	0	15.32	3.34	10.42	17.91
MnO	4	0	0.21	0.04	0.16	0.24
MgO	4	0	4.85	1.02	4.02	6.29
CaO	4	0	8.77	1.19	7.07	9.79
Na2O	4	0	1.66	1.01	0.50	2.97
K2O	2	2	0.11	0.01	0.10	0.12
P2O5	4	0	0.39	0.24	0.16	0.73

Soll

	n	NA	Mean	SD	Min	Max
SiO2	3	0	60.69	11.98	53.01	74.50
TiO2	3	0	1.57	0.29	1.23	1.75
Al2O3	3	0	12.99	4.42	7.88	15.54
Fe2O3	3	0	15.52	5.19	10.94	21.15
MnO	3	0	0.13	0.10	0.02	0.19
MgO	3	0	6.57	1.37	5.24	7.97
CaO	3	0	1.81	2.66	0.23	4.88
Na2O	1	2	1.95	NA	1.95	1.95
K2O	0	3	NA	NA	NA	NA
P2O5	3	0	0.19	0.04	0.14	0.21

Speckled

	n	NA	Mean	SD	Min	Max
SiO2	5	0	57.25	10.95	40.45	69.25
TiO2	5	0	0.49	0.06	0.41	0.56
Al2O3	5	0	11.86	1.09	10.20	13.11
Fe2O3	5	0	14.12	2.24	10.89	16.29
MnO	5	0	0.46	0.49	0.14	1.27
MgO	5	0	12.46	3.69	9.13	18.30
CaO	5	0	3.46	4.92	0.12	11.21
Na2O	0	5	NA	NA	NA	NA
K2O	0	5	NA	NA	NA	NA
P2O5	5	0	0.06	0.01	0.05	0.07

Swannie

	n	NA	Mean	SD	Min	Max
SiO2	3	0	49.37	0.20	49.14	49.51
TiO2	3	0	3.14	0.16	2.96	3.28
Al2O3	3	0	13.56	0.82	12.64	14.23
Fe2O3	3	0	21.94	2.86	18.84	24.49
MnO	3	0	0.28	0.07	0.22	0.36
MgO	3	0	6.86	1.57	5.19	8.30
CaO	3	0	4.22	5.29	1.14	10.32
Na2O	0	3	NA	NA	NA	NA
K2O	0	3	NA	NA	NA	NA
P2O5	3	0	0.78	0.05	0.73	0.82

Twin

	n	NA	Mean	SD	Min	Max
SiO2	2	0	65.32	2.49	63.56	67.08
TiO2	2	0	0.64	0.01	0.63	0.65
Al2O3	2	0	16.73	0.13	16.64	16.82
Fe2O3	2	0	10.69	2.01	9.27	12.11
MnO	2	0	0.05	0.01	0.04	0.06
MgO	2	0	4.20	0.80	3.63	4.76
CaO	2	0	0.16	0.01	0.15	0.16
Na2O	2	0	0.15	0.04	0.12	0.18
K2O	2	0	2.01	0.40	1.72	2.29
P2O5	2	0	0.09	0.01	0.08	0.09

Unknown1

	n	NA	Mean	SD	Min	Max
SiO2	1	0	48.24	NA	48.24	48.24
TiO2	1	0	3.14	NA	3.14	3.14
Al2O3	1	0	13.09	NA	13.09	13.09
Fe2O3	1	0	17.63	NA	17.63	17.63
MnO	1	0	0.27	NA	0.27	0.27
MgO	1	0	5.57	NA	5.57	5.57
CaO	1	0	10.42	NA	10.42	10.42
Na2O	1	0	0.96	NA	0.96	0.96
K2O	0	1	NA	NA	NA	NA
P2O5	1	0	0.76	NA	0.76	0.76

Unknown2

	n	NA	Mean	SD	Min	Max
SiO2	1	0	43.08	NA	43.08	43.08
TiO2	1	0	3.6	NA	3.6	3.6
Al2O3	1	0	15.11	NA	15.11	15.11
Fe2O3	1	0	21.86	NA	21.86	21.86
MnO	1	0	0.27	NA	0.27	0.27
MgO	1	0	5.99	NA	5.99	5.99
CaO	1	0	8.74	NA	8.74	8.74
Na2O	1	0	0.56	NA	0.56	0.56
K2O	0	1	NA	NA	NA	NA
P2O5	1	0	0.88	NA	0.88	0.88

Unknown3

	n	NA	Mean	SD	Min	Max
SiO2	1	0	59.42	NA	59.42	59.42
TiO2	1	0	1.01	NA	1.01	1.01
Al2O3	1	0	16.01	NA	16.01	16.01
Fe2O3	1	0	5.03	NA	5.03	5.03
MnO	1	0	0.11	NA	0.11	0.11
MgO	1	0	3.95	NA	3.95	3.95
CaO	1	0	8.97	NA	8.97	8.97
Na2O	1	0	1.71	NA	1.71	1.71
K2O	1	0	0.97	NA	0.97	0.97
P2O5	1	0	0.18	NA	0.18	0.18

Unknown4

	n	NA	Mean	SD	Min	Max
SiO2	2	0	53.65	0.53	53.27	54.02
TiO2	2	0	2.23	0.13	2.14	2.32
Al2O3	2	0	14.19	0.95	13.52	14.86
Fe2O3	2	0	14.52	1.65	13.35	15.68
MnO	2	0	0.18	0.04	0.15	0.21
MgO	2	0	4.50	0.40	4.21	4.78
CaO	2	0	7.54	1.05	6.79	8.28
Na2O	1	1	2.85	NA	2.85	2.85
K2O	0	2	NA	NA	NA	NA
P2O5	2	0	0.34	0.02	0.32	0.35

Unknown6

	n	NA	Mean	SD	Min	Max
SiO2	1	0	55.05	NA	55.05	55.05
TiO2	1	0	0.61	NA	0.61	0.61
Al2O3	1	0	15.42	NA	15.42	15.42
Fe2O3	1	0	16.81	NA	16.81	16.81
MnO	1	0	0.1	NA	0.1	0.1
MgO	1	0	12.25	NA	12.25	12.25
CaO	1	0	0.13	NA	0.13	0.13
Na2O	1	0	3.73	NA	3.73	3.73
K2O	0	1	NA	NA	NA	NA
P2O5	1	0	0.07	NA	0.07	0.07

Unknown7

	n	NA	Mean	SD	Min	Max
SiO2	1	0	56.28	NA	56.28	56.28
TiO2	1	0	1.35	NA	1.35	1.35
Al2O3	1	0	11.25	NA	11.25	11.25
Fe2O3	1	0	14.32	NA	14.32	14.32
MnO	1	0	0.19	NA	0.19	0.19
MgO	1	0	6.08	NA	6.08	6.08
CaO	1	0	4.96	NA	4.96	4.96
Na2O	1	0	3.81	NA	3.81	3.81
K2O	1	0	0.78	NA	0.78	0.78
P2O5	1	0	0.19	NA	0.19	0.19

Unknown8

	n	NA	Mean	SD	Min	Max
SiO2	3	0	59.41	2.06	58.04	61.78
TiO2	3	0	0.92	0.08	0.85	1.00
Al2O3	3	0	14.47	1.00	13.49	15.48
Fe2O3	3	0	9.88	0.81	8.95	10.44
MnO	3	0	0.20	0.14	0.09	0.36
MgO	3	0	4.53	0.85	3.68	5.37
CaO	3	0	7.41	3.16	3.99	10.21
Na2O	3	0	2.28	1.92	0.08	3.62
K2O	1	2	2.28	NA	2.28	2.28
P2O5	3	0	0.16	0.02	0.14	0.18

Unknown9

	n	NA	Mean	SD	Min	Max
SiO2	3	0	59.60	1.01	58.46	60.38
TiO2	3	0	0.95	0.02	0.94	0.97
Al2O3	3	0	15.27	0.25	15.05	15.54
Fe2O3	3	0	11.19	2.05	9.34	13.39
MnO	3	0	0.28	0.13	0.17	0.42
MgO	3	0	5.89	1.07	4.73	6.84
CaO	3	0	4.63	3.07	1.10	6.70
Na2O	3	0	0.81	1.11	0.17	2.09
K2O	2	1	1.83	0.35	1.58	2.08
P2O5	3	0	0.17	0.01	0.16	0.17

Ventersdorp lava

	n	NA	Mean	SD	Min	Max
SiO2	1	0	56.43	NA	56.43	56.43
TiO2	1	0	1.03	NA	1.03	1.03
Al2O3	1	0	17.64	NA	17.64	17.64
Fe2O3	1	0	9.89	NA	9.89	9.89
MnO	1	0	0.12	NA	0.12	0.12
MgO	1	0	4.3	NA	4.3	4.3
CaO	1	0	5.23	NA	5.23	5.23
Na2O	1	0	4.09	NA	4.09	4.09
K2O	1	0	1.12	NA	1.12	1.12
P2O5	1	0	0.15	NA	0.15	0.15

Trace Elements

Table C – 2. Trace Element Concentrations (ppm). Bdl = below detection limit.

Sample	S	Sc	V	Cr	Co	Ni	Cu	Zn	Ga	Ge
AMI1	861.37	31.45	279.35	54.30	13.85	44.85	75.96	92.53	21.27	bdl
AMI2	168.25	29.78	305.35	127.90	10.86	48.17	49.89	93.21	19.21	bdl
AMI3	345.66	26.94	389.19	89.85	40.34	54.65	103.84	111.10	20.03	0.39
AMI5	49.02	24.02	390.74	93.89	23.85	49.69	74.83	95.07	21.59	bdl
BAN1	495.32	31.90	274.87	23.41	33.04	40.22	92.66	110.19	24.92	0.86
BAN3	565.24	27.57	310.19	37.85	37.61	42.84	87.47	112.24	22.27	0.99
BAN4	528.33	28.60	308.03	20.51	31.02	30.20	117.62	119.00	24.10	1.21
BAN5	902.06	28.28	399.84	83.97	40.97	54.26	92.51	118.22	22.34	bdl
BAN6	931.61	29.52	395.58	86.72	46.94	50.73	89.82	104.78	21.86	bdl
BAN7	470.26	30.46	307.84	17.51	36.73	35.21	78.65	127.23	26.30	1.01
BAN8	612.27	32.10	323.89	28.73	35.09	43.45	88.77	111.58	23.09	0.02
BRA1	701.91	29.03	345.22	26.31	27.80	43.01	96.52	123.90	23.86	0.86
BRA2	845.00	31.94	333.13	17.66	33.56	41.76	90.48	113.18	22.99	0.32
BRA3	437.86	24.63	387.75	78.02	33.23	51.07	88.25	120.02	23.22	bdl
BRA4	482.95	29.24	320.08	25.17	34.54	36.70	88.11	113.11	23.54	0.42
BRA5	522.54	30.97	310.39	18.50	36.58	38.52	88.12	110.67	23.52	0.05
BRA6	1339.72	27.88	346.32	21.11	25.86	42.03	95.46	106.29	23.42	1.20
BRA7	432.80	27.14	359.47	92.27	43.24	48.85	85.45	107.96	23.10	bdl
BRA8	334.53	26.85	301.89	63.44	35.22	39.82	75.56	85.30	18.06	0.04
CLA1	61.69	21.45	237.48	66.11	35.00	209.51	55.61	166.88	18.61	bdl
CLA2	442.33	34.84	270.93	77.56	32.91	135.54	345.58	522.63	17.73	0.01
CLA3	180.55	32.36	196.26	58.97	37.65	126.38	78.21	126.77	15.16	bdl
CLA4	308.56	36.49	221.74	79.91	38.60	122.85	62.12	88.69	14.96	0.64
CLA5	55.90	30.63	252.93	66.23	25.32	155.15	28.87	169.24	17.46	0.99
CLA6	176.28	37.76	226.15	66.18	34.75	102.66	61.70	107.83	13.84	0.33
CLA7	289.05	31.69	210.96	82.78	42.15	130.73	64.67	85.14	14.85	1.09
CLA8	276.08	31.88	205.16	84.62	39.65	164.73	56.84	82.07	15.89	1.00
CLA9	51.64	11.37	118.69	1040.05	28.51	271.15	36.30	101.23	13.36	bdl
FRI1	137.15	30.90	249.78	30.70	30.83	62.59	70.68	131.76	19.05	1.26
FRI2	116.39	32.16	275.84	31.60	26.43	77.82	48.95	449.00	22.18	0.22
FRI3	131.65	32.29	252.15	33.62	35.16	65.53	65.05	153.76	17.50	0.26
FRI4	406.56	26.95	274.63	14.83	43.06	52.47	117.03	174.24	18.87	bdl
FRI5	687.51	33.02	292.52	33.01	39.37	56.03	62.23	382.08	21.42	bdl
FRI6	508.71	28.87	254.68	29.95	36.68	58.78	69.41	255.83	19.07	0.58
FRI7	320.27	28.53	237.98	29.06	31.37	55.20	65.66	149.05	18.82	0.82
FRI8	91.30	36.57	328.04	38.38	4.37	143.75	86.64	425.45	23.87	0.24
FRI9	67.10	37.51	306.08	31.87	22.54	75.72	26.54	846.40	22.49	0.14
GEOR1	420.52	30.46	159.84	185.80	44.93	223.31	93.39	77.50	13.10	1.10
GEOR2	16.44	29.72	162.07	159.46	34.29	192.55	50.89	63.82	12.12	0.08
GEOR3	2021.17	15.48	127.85	252.67	56.55	618.93	190.82	319.79	11.01	0.62
JEA1	228.53	34.02	289.09	24.97	30.38	61.65	79.75	149.89	19.36	0.44
JEA2	9.26	24.41	164.73	192.59	33.29	355.94	21.54	108.05	18.94	0.90
JEA3	620.26	34.15	305.95	25.91	34.31	61.87	73.28	123.06	19.46	bdl
KEN1	44.56	30.63	225.98	61.00	35.25	117.47	59.00	217.15	17.34	bdl
KEN2	469.21	30.24	334.73	17.49	28.97	43.24	87.56	117.51	22.45	0.27
KEN3	653.60	29.74	321.93	23.28	34.62	44.25	99.44	108.37	22.41	bdl
KEN4	862.69	36.95	261.94	65.96	31.72	127.20	198.52	345.40	17.68	bdl

Sample	S	Sc	V	Cr	Co	Ni	Cu	Zn	Ga	Ge
KEN5	368.29	30.24	376.90	88.43	38.62	47.79	89.14	104.49	21.62	0.04
KEN6	206.16	29.53	382.03	81.89	40.93	50.18	85.94	108.05	22.10	0.61
KEN7	939.79	28.41	380.67	74.79	46.86	47.67	87.17	105.01	20.98	bdl
KUD1	37.37	23.18	155.50	27.57	35.31	92.29	90.01	70.19	17.41	bdl
LAV1	15.51	23.51	159.71	36.16	37.00	110.35	40.82	85.20	19.07	bdl
LIB1	662.40	36.73	137.78	9.65	28.77	29.44	54.80	119.97	20.35	0.78
LIT1	478.53	32.85	146.22	9.08	28.26	32.36	52.51	144.51	20.14	0.23
PE1	1338.16	30.75	216.86	28.11	36.18	52.94	98.45	153.41	19.31	0.34
PE2	2297.68	26.59	241.83	36.27	37.37	42.67	122.11	255.93	17.54	0.12
PEG1	64.76	16.86	127.99	139.09	56.67	167.21	252.59	112.03	14.45	bdl
PEG2	130.19	17.29	113.53	27.09	39.82	140.23	325.98	106.68	16.70	0.18
PEG3	78.17	18.30	133.81	23.74	38.52	117.88	159.44	93.79	18.36	0.79
PEG4	147.04	11.98	108.51	20.12	38.24	126.03	381.11	110.12	17.10	0.44
PEG5	93.97	7.51	73.23	15.64	30.21	88.74	255.31	96.85	17.78	0.14
PEG6	7.97	20.05	143.59	21.80	34.79	100.82	35.35	86.31	15.71	0.15
SIL1	55.98	32.14	193.28	585.37	58.51	437.63	138.79	174.84	10.61	bdl
SIL2	223.63	36.83	291.57	118.55	39.94	66.16	77.74	53.51	14.73	bdl
SKE1	84.96	33.19	285.37	7.55	28.00	43.28	117.89	154.22	18.73	0.87
SKE2	455.55	35.41	237.73	25.45	33.03	58.67	71.03	152.17	17.73	1.10
SKE3	102.20	35.16	291.25	9.84	32.27	48.42	121.85	134.20	19.89	1.52
SKE5	48.68	22.86	187.39	185.51	42.40	110.71	99.47	77.74	14.28	bdl
SOL1	258.65	33.48	275.84	22.75	34.47	68.90	590.40	299.69	18.23	0.90
SOL2	311.60	29.47	253.96	22.46	35.10	63.60	81.97	81.00	16.71	0.29
SOL3	2888.86	20.15	138.72	276.35	68.77	1015.77	314.85	77.36	15.01	0.64
SPE1	155.04	28.22	207.29	2904.30	42.64	497.45	61.78	120.38	9.61	bdl
SPE2	1859.48	36.31	197.16	546.01	58.52	365.20	146.85	208.69	13.45	bdl
SPE3	11.15	20.43	152.46	1769.71	40.98	316.74	21.66	89.27	10.14	0.20
SPE4	61.18	31.80	185.83	2912.73	79.86	457.54	52.81	94.70	8.74	bdl
SPE5	7.39	21.60	186.99	2144.68	36.82	389.70	18.66	90.40	10.92	0.53
SWA1	384.86	27.52	286.85	137.93	31.37	74.02	186.66	369.80	18.75	0.76
SWA2	54.63	28.27	248.23	102.05	37.76	64.57	62.33	121.59	16.83	bdl
SWA3	1775.56	26.31	288.89	117.14	64.55	159.98	328.54	375.13	16.74	bdl
TWI1	134.67	33.94	210.16	136.51	53.65	214.55	142.97	95.93	16.16	0.39
TWI2	51.27	29.45	196.22	125.20	34.05	149.93	51.73	72.84	15.36	bdl
UNK1	129.11	34.07	263.83	98.84	38.20	48.44	52.31	180.25	16.91	0.16
UNK2	61.34	34.01	319.18	118.47	41.36	59.58	55.33	146.45	19.29	bdl
UNK3	121.38	25.87	137.00	8.45	20.56	60.30	248.66	40.36	12.96	bdl
UNK4A	476.54	33.13	281.66	16.05	30.35	39.40	143.16	123.18	17.27	0.15
UNK4B	276.47	35.41	311.79	20.47	28.97	43.79	69.31	83.60	19.26	0.18
UNK6	155.26	29.60	212.40	609.04	63.89	370.36	33.43	150.14	15.28	0.74
UNK7	247.91	8.94	105.60	32.50	42.29	151.34	310.56	118.92	16.05	bdl
120A1	1293.05	18.26	171.69	34.71	50.11	63.60	137.89	80.15	15.51	bdl
120A2	33.36	25.32	193.35	224.40	53.43	132.85	83.45	75.13	15.31	bdl
120A3	65.46	18.86	143.60	31.36	27.47	57.10	184.38	180.06	12.75	bdl
120B1	100.22	22.81	188.39	61.50	34.60	74.04	93.85	217.30	15.51	bdl
120B2	123.79	18.55	185.70	134.19	43.03	92.27	66.11	71.53	14.19	bdl
120B3	52.39	21.98	209.50	130.84	44.34	108.30	85.58	186.77	17.35	0.33

Sample	Rb	Sr	Y	Zr	Nb	Sb	Ba	Hf	Ta	Pb
AMI1	1.10	8.81	51.09	312.76	19.87	48.88	bdl	5.96	7.54	0.02
AMI2	0.45	8.05	41.69	321.81	18.42	bdl	bdl	bdl	9.41	4.13
AMI3	5.27	95.86	29.58	164.78	14.72	bdl	0.94	6.51	10.48	6.17
AMI5	3.49	231.92	28.42	168.34	14.30	bdl	64.52	2.20	12.41	3.31
BAN1	16.46	413.79	28.12	151.02	13.66	43.86	320.54	6.78	4.54	3.74
BAN3	3.16	360.67	27.78	157.03	15.24	46.63	176.25	7.57	8.57	4.56
BAN4	28.42	288.77	31.43	168.75	15.56	61.80	225.10	6.79	2.42	6.26
BAN5	5.12	296.71	29.84	174.00	15.25	bdl	155.45	bdl	7.01	5.05
BAN6	1.39	294.53	30.52	180.68	15.47	bdl	87.11	11.06	6.17	8.10
BAN7	20.04	448.63	31.35	178.89	16.66	52.66	257.19	4.70	2.37	5.02
BAN8	10.89	336.62	28.85	160.10	15.47	48.61	245.51	3.82	4.67	2.46
BRA1	0.75	183.80	29.19	171.16	16.35	49.10	47.16	2.19	3.70	15.22
BRA2	1.90	231.02	28.91	167.27	16.02	39.45	53.17	7.52	4.80	30.08
BRA3	0.86	207.65	28.14	169.84	14.05	bdl	66.62	4.18	8.49	28.86
BRA4	1.52	381.54	28.98	166.41	15.10	54.38	131.78	5.08	6.40	2.38
BRA5	4.17	390.98	28.80	167.56	14.86	49.43	190.96	3.48	3.75	5.98
BRA6	1.63	250.93	30.73	175.86	16.42	56.25	54.72	6.80	1.98	10.29
BRA7	23.39	455.04	29.05	173.10	13.16	bdl	358.61	4.30	5.90	6.18
BRA8	17.15	336.95	23.93	138.15	12.11	bdl	254.58	3.88	9.05	4.79
CLA1	0.67	3.96	29.82	75.67	7.02	61.71	bdl	bdl	0.98	1.55
CLA2	0.02	4.02	17.95	81.53	6.93	42.84	bdl	0.37	9.87	8.38
CLA3	0.31	256.14	22.27	73.09	6.52	55.29	bdl	5.42	2.74	14.66
CLA4	bdl	226.86	22.48	67.65	5.82	49.82	5.60	bdl	5.84	2.38
CLA5	0.44	4.45	18.61	74.22	7.29	64.50	bdl	4.09	6.33	1.77
CLA6	0.23	299.06	22.22	75.38	6.09	52.99	bdl	2.87	2.34	7.61
CLA7	0.62	272.73	24.71	75.46	6.57	40.56	6.40	1.47	7.68	2.27
CLA8	0.21	320.01	22.88	63.09	6.09	45.14	0.26	2.02	4.96	2.97
CLA9	0.19	2.45	9.08	234.12	10.58	bdl	bdl	6.04	9.84	bdl
FRI1	1.28	397.28	51.92	260.93	17.97	55.21	27.78	6.29	5.95	10.91
FRI2	0.12	10.96	35.41	310.79	19.87	53.89	bdl	4.21	8.13	8.05
FRI3	1.12	351.29	50.24	252.91	16.64	43.02	3.71	4.08	6.17	11.62
FRI4	1.43	283.99	42.83	230.50	15.27	43.40	33.61	2.95	6.13	8.43
FRI5	0.22	8.23	64.15	285.40	19.85	50.26	bdl	10.11	3.20	17.37
FRI6	0.57	323.02	50.83	262.30	17.46	49.16	bdl	8.99	7.39	9.05
FRI7	0.88	471.47	54.15	272.43	18.20	48.66	1.22	8.76	8.42	18.20
FRI8	1.01	11.46	35.09	323.05	21.60	53.05	bdl	7.48	4.26	7.62
FRI9	0.44	10.13	42.82	318.86	20.70	53.44	bdl	0.09	16.00	10.98
GEOR1	3.57	314.85	12.24	62.78	5.57	50.18	166.53	2.41	0.68	2.84
GEOR2	0.87	119.23	11.72	52.59	4.88	37.23	17.01	2.02	5.06	27.36
GEOR3	0.25	14.04	10.33	85.64	15.07	43.55	bdl	1.11	6.70	15.43
JEA1	1.99	397.27	50.35	273.67	16.54	48.33	bdl	9.95	9.32	6.02
JEA2	0.75	117.35	33.78	206.73	13.59	48.27	1.94	4.93	7.89	3.66
JEA3	0.76	438.06	51.35	284.35	16.46	48.66	bdl	5.73	6.59	6.90
KEN1	0.43	138.17	25.58	74.69	6.61	51.18	bdl	1.05	7.51	95.45
KEN2	0.88	298.57	29.39	164.96	16.65	48.67	39.59	2.25	2.98	9.08
KEN3	2.86	363.98	27.88	162.07	15.88	54.08	75.78	9.95	3.13	5.84
KEN4	0.79	4.70	19.18	77.18	6.92	58.24	bdl	bdl	9.26	12.85
KEN5	5.31	329.98	27.55	166.99	14.59	bdl	407.39	2.94	12.14	3.92
KEN6	5.42	339.08	27.57	170.17	14.05	bdl	337.04	5.01	10.51	3.28
KEN7	4.96	343.79	27.60	167.15	13.96	bdl	415.46	4.30	8.38	4.75
KUD1	bdl	777.98	18.58	131.53	8.24	46.59	38.30	3.28	5.57	7.30

Sample	Rb	Sr	Y	Zr	Nb	Sb	Ba	Hf	Ta	Pb
LAV1	15.05	778.25	16.81	115.91	7.85	46.54	722.83	0.23	7.16	4.03
LIB1	0.34	334.10	60.62	462.27	24.68	45.31	bdl	9.05	2.27	bdl
LIT1	77.85	642.24	59.58	451.25	23.70	51.37	637.23	9.66	5.16	2.88
PE1	bdl	269.08	56.83	285.70	18.81	51.57	bdl	9.22	11.60	7.82
PE2	0.12	143.85	60.93	300.74	20.01	47.93	bdl	7.41	4.07	16.67
PEG1	62.60	579.55	15.94	139.22	17.54	bdl	452.02	6.51	12.87	7.03
PEG2	27.53	1284.80	14.79	119.37	17.79	53.69	593.32	7.81	5.31	6.62
PEG3	24.18	856.08	19.72	128.68	19.58	49.10	587.45	4.14	3.23	7.03
PEG4	73.10	674.11	17.93	144.27	20.47	54.59	406.56	4.60	2.93	0.85
PEG5	47.18	718.15	18.49	167.03	22.48	52.45	528.18	3.87	6.76	3.84
PEG6	35.25	972.05	19.09	135.00	10.74	46.78	595.86	6.06	5.46	1.90
SIL1	0.91	7.65	11.22	39.36	4.21	42.77	bdl	2.31	6.84	250.68
SIL2	15.56	601.14	55.37	289.02	17.64	bdl	243.10	2.20	8.96	6.49
SKE1	18.11	394.59	46.99	252.80	15.94	57.13	613.87	4.33	6.22	6.57
SKE2	0.47	348.12	52.50	267.96	16.80	49.76	bdl	4.92	bdl	23.52
SKE3	14.86	296.00	44.72	240.27	16.22	37.61	453.76	10.60	7.93	10.52
SKE5	0.21	938.84	16.21	120.83	6.24	bdl	66.14	9.38	7.73	8.71
SOL1	bdl	4.23	32.33	110.64	8.43	52.40	bdl	1.34	6.62	0.42
SOL2	0.49	111.10	31.21	109.54	8.51	41.75	4.99		3.11	4.46
SOL3	0.43	11.28	14.00	93.98	16.31	37.78	bdl	3.66	6.28	54.87
SPE1	bdl	26.89	9.57	42.56	4.30	bdl	bdl	1.89	11.00	5.26
SPE2	0.40	4.12	9.34	48.33	4.79	48.65	bdl	0.50	4.98	2.29
SPE3	0.09	4.09	5.56	37.09	3.24	bdl	bdl	bdl	6.50	0.60
SPE4	0.76	62.44	9.52	32.95	3.23	bdl	bdl	1.98	9.31	1.26
SPE5	0.35	3.39	10.39	41.85	3.23	bdl	bdl	bdl	7.69	1.01
SWA1	0.52	17.76	46.52	288.38	16.90	bdl	bdl	3.80	9.08	35.27
SWA2	4.01	357.44	48.19	259.99	15.54	bdl	115.40	10.46	8.26	9.75
SWA3	0.65	15.79	32.19	275.92	16.14	bdl	bdl	12.45	17.22	80.58
TWI1	48.59	17.13	11.31	74.64	5.72	45.08	379.04	2.59	7.21	bdl
TWI2	63.09	17.64	12.62	69.77	5.13	44.33	471.15	2.19	2.45	bdl
UNK1	0.11	295.01	47.38	254.77	14.29	bdl	bdl	4.56	12.64	37.04
UNK2	0.55	335.10	59.33	309.81	17.51	bdl	bdl	5.79	15.65	4.17
UNK3	39.77	278.75	20.45	136.72	8.79	43.68	220.82	2.52	3.33	1.22
UNK4A	0.83	305.71	41.43	214.48	14.72	48.06	0.93	10.71	3.06	3.83
UNK4B	0.36	256.94	41.78	245.33	16.18	52.42	bdl	6.46	6.95	1.43
UNK6	0.61	2.76	10.68	51.44	4.92	39.76	bdl	bdl	3.44	0.97
UNK7	48.02	457.16	17.97	154.41	21.27	46.27	788.53	4.46	6.34	4.63
120A1	0.54	255.36	19.51	148.40	8.39	bdl	17.90	3.50	5.13	2.13
120A2	1.75	631.22	16.31	123.66	6.84	bdl	184.78	6.52	7.56	9.85
120A3	66.12	126.77	20.67	115.53	7.02	bdl	760.80	4.87	9.59	20.48
120B1	77.28	100.52	19.52	136.65	8.10	bdl	1014.34	3.51	9.12	19.64
120B2	0.33	245.79	16.25	129.68	7.39	bdl	29.19	1.65	9.93	3.56
120B3	56.78	26.50	24.28	145.67	7.62	bdl	667.33	7.21	5.87	51.52

Sample	Bi	Th	U
AMI1	4.50	9.79	1.44
AMI2	2.95	9.52	bdl
AMI3	4.60	8.30	bdl
AMI5	3.04	6.60	bdl
BAN1	3.42	9.45	bdl
BAN3	3.13	11.28	bdl
BAN4	2.92	10.53	bdl
BAN5	4.01	7.67	bdl
BAN6	4.81	4.62	bdl
BAN7	5.78	10.97	0.65
BAN8	2.67	8.28	bdl
BRA1	4.68	10.45	bdl
BRA2	6.31	9.83	0.57
BRA3	6.34	6.76	bdl
BRA4	3.97	9.69	bdl
BRA5	5.06	10.42	bdl
BRA6	2.95	10.59	bdl
BRA7	4.61	7.76	bdl
BRA8	3.89	5.48	bdl
CLA1	2.52	9.75	0.3
CLA2	5.37	10.11	bdl
CLA3	4.35	7.57	bdl
CLA4	4.52	9.26	bdl
CLA5	5.85	9.46	0.18
CLA6	3.29	7.74	bdl
CLA7	3.99	7.33	bdl
CLA8	4.06	8.41	bdl
CLA9	2.89	14.28	bdl
FRI1	3.33	11.05	0.85
FRI2	5.07	12.92	bdl
FRI3	1.94	8.40	bdl
FRI4	2.53	12.71	bdl
FRI5	2.69	13.56	bdl
FRI6	4.01	10.01	bdl
FRI7	5.81	10.12	bdl
FRI8	1.07	14.42	bdl
FRI9	1.37	14.11	bdl
GEOR1	2.40	8.20	0.40
GEOR2	1.49	9.87	bdl
GEOR3	2.41	11.74	0.73
JEA1	5.16	9.74	0.63
JEA2	4.31	12.59	bdl
JEA3	3.83	8.93	bdl
KEN1	4.25	8.80	bdl
KEN2	4.08	14.10	bdl
KEN3	1.69	11.11	bdl
KEN4	1.83	10.56	bdl
KEN5	5.10	8.62	bdl
KEN6	4.82	5.74	bdl
KEN7	5.08	7.41	0.59

Sample	Bi	Th	U
KUD1	3.44	7.91	0.81
LAV1	3.82	7.16	0.73
LIB1	4.52	12.29	1.70
LIT1	4.55	13.22	1.66
PE1	5.64	11.48	0.99
PE2	2.99	10.81	bdl
PEG1	6.67	6.39	bdl
PEG2	4.25	9.46	bdl
PEG3	3.58	10.19	bdl
PEG4	2.46	11.26	0.62
PEG5	3.44	10.99	bdl
PEG6	4.30	7.84	bdl
SIL1	7.15	7.79	0.26
SIL2	11.07	7.56	bdl
SKE1	4.07	10.86	0.93
SKE2	4.12	12.00	bdl
SKE3	6.13	10.91	bdl
SKE5	3.45	3.48	bdl
SOL1	4.13	11.21	bdl
SOL2	4.85	9.91	0.27
SOL3	3.10	11.29	0.77
SPE1	4.55	8.75	bdl
SPE2	2.02	9.96	bdl
SPE3	5.15	6.06	bdl
SPE4	3.44	6.22	bdl
SPE5	3.64	6.95	bdl
SWA1	4.57	10.36	bdl
SWA2	4.21	7.76	0.85
SWA3	2.64	9.22	bdl
TWI1	1.39	9.31	0.60
TWI2	3.39	8.98	0.55
UNK1	5.14	5.47	0.90
UNK2	4.45	7.24	1.03
UNK3	2.71	11.01	0.95
UNK4A	4.10	11.81	0.96
UNK4B	5.67	11.49	bdl
UNK6	0.92	10.44	0.49
UNK7	4.08	13.61	0.67
120A1	2.54	9.34	bdl
120A2	4.51	6.27	0.82
120A3	1.31	8.33	bdl
120B1	2.73	11.40	bdl
120B2	3.56	8.48	0.86
120B3	4.52	7.85	bdl

Summary of Selected Trace Elements

Amigo

	n	NA	Mean	Std dev	Min	Max
S	4	0	356	358	49	861
Sc	4	0	28	3	24	31
V	4	0	341	57	279	391
Cr	4	0	91	30	54	128
Co	4	0	22	13	11	40
Ni	4	0	49	4	45	55
Cu	4	0	76	22	50	104
Zn	4	0	98	9	93	111
Rb	4	0	3	2	0	5
Sr	4	0	86	106	8	232
Y	4	0	38	11	28	51
Zr	4	0	242	87	165	322
Hf	3	1	5	2	2	7

Bank

	n	NA	Mean	Std dev	Min	Max
S	7	0	644	192	470	932
Sc	7	0	30	2	28	32
V	7	0	331	48	275	400
Cr	7	0	43	30	18	87
Co	7	0	37	5	31	47
Ni	7	0	42	8	30	54
Cu	7	0	92	12	79	118
Zn	7	0	115	7	105	127
Rb	7	0	12	10	1	28
Sr	7	0	349	63	289	449
Y	7	0	30	1	28	31
Zr	7	0	167	11	151	181
Hf	6	1	7	3	4	11

Brazil

	n	NA	Mean	Std dev	Min	Max
S	8	0	637	328	335	1340
Sc	8	0	28	2	25	32
V	8	0	338	28	302	388
Cr	8	0	43	30	18	92
Co	8	0	34	5	26	43
Ni	8	0	43	5	37	51
Cu	8	0	88	6	76	97
Zn	8	0	110	12	85	124
Rb	8	0	6	9	1	23
Sr	8	0	305	100	184	455
Y	8	0	28	2	24	31
Zr	8	0	166	12	138	176
Hf	8	0	5	2	2	8

CLA

	n	NA	Mean	Std dev	Min	Max
S	9	0	204.7	135.5	51.64	442.33
Sc	9	0	29.83	8.35	11.37	37.76
V	9	0	215.6	43.27	118.69	270.93
Cr	9	0	180.3	322.54	58.97	1040.1
Co	9	0	34.95	5.4	25.32	42.15
Ni	9	0	157.6	52.51	102.66	271.15
Cu	9	0	87.77	97.81	28.87	345.58
Zn	9	0	161.2	139.49	82.07	522.63
Rb	8	1	0.34	0.22	0.02	0.67
Sr	9	0	154.4	145.25	2.45	320.01
Y	9	0	21.11	5.67	9.08	29.82
Zr	9	0	91.13	53.87	63.09	234.12
Hf	7	2	3.18	2.09	0.37	6.04

Friday

	n	NA	Mean	Std dev	Min	Max
S	9	0	274.07	219.61	67.1	687.51
Sc	9	0	31.87	3.55	26.95	37.51
V	9	0	274.63	29.64	237.98	328.04
Cr	9	0	30.34	6.41	14.83	38.38
Co	9	0	29.98	11.5	4.37	43.06
Ni	9	0	71.99	28.33	52.47	143.75
Cu	9	0	68.02	24.72	26.54	117.03
Zn	9	0	329.73	230.63	131.76	846.4
Rb	9	0	0.79	0.47	0.12	1.43
Sr	9	0	207.54	194.07	8.23	471.47
Y	9	0	47.49	9.38	35.09	64.15
Zr	9	0	279.69	32.13	230.5	323.05
Hf	9	0	5.88	3.29	0.09	10.11

Georgette

	n	NA	Mean	Std dev	Min	Max
S	3	0	819.4	1060.2	16.44	2021.2
Sc	3	0	25.22	8.44	15.48	30.46
V	3	0	149.9	19.15	127.85	162.07
Cr	3	0	199.3	48.05	159.46	252.67
Co	3	0	45.26	11.13	34.29	56.55
Ni	3	0	344.9	237.79	192.55	618.93
Cu	3	0	111.7	71.74	50.89	190.82
Zn	3	0	153.7	144	63.82	319.79
Rb	3	0	1.56	1.77	0.25	3.57
Sr	3	0	149.4	152.65	14.04	314.85
Y	3	0	11.43	0.99	10.33	12.24
Zr	3	0	67	16.92	52.59	85.64
Hf	3	0	1.85	0.67	1.11	2.41

Jeans

	n	NA	Mean	Std dev	Min	Max
S	3	0	286.02	309.53	9.26	620.26
Sc	3	0	30.86	5.59	24.41	34.15
V	3	0	253.26	77.13	164.73	305.95
Cr	3	0	81.16	96.51	24.97	192.59
Co	3	0	32.66	2.04	30.38	34.31
Ni	3	0	159.82	169.84	61.65	355.94
Cu	3	0	58.19	31.9	21.54	79.75
Zn	3	0	127	21.2	108.05	149.89
Rb	3	0	1.17	0.71	0.75	1.99
Sr	3	0	317.56	174.58	117.35	438.06
Y	3	0	45.16	9.87	33.78	51.35
Zr	3	0	254.92	42.07	206.73	284.35
Hf	3	0	6.87	2.7	4.93	9.95

Ken

	n	NA	Mean	Std dev	Min	Max
S	7	0	506	332	45	940
Sc	7	0	31	3	28	37
V	7	0	326	62	226	382
Cr	7	0	59	28	17	88
Co	7	0	37	6	29	47
Ni	7	0	68	37	43	127
Cu	7	0	101	45	59	199
Zn	7	0	158	92	104	345
Rb	7	0	3	2	0	5
Sr	7	0	260	136	5	364
Y	7	0	26	3	19	29
Zr	7	0	140	44	75	170
Hf	6	1	4	3	1	10

Kudu

	n	NA	Mean	Std dev	Min	Max
S	1	0	37.37	NA	37.37	37.37
Sc	1	0	23.18	NA	23.18	23.18
V	1	0	155.5	NA	155.5	155.5
Cr	1	0	27.57	NA	27.57	27.57
Co	1	0	35.31	NA	35.31	35.31
Ni	1	0	92.29	NA	92.29	92.29
Cu	1	0	90.01	NA	90.01	90.01
Zn	1	0	70.19	NA	70.19	70.19
Rb	0	1	NaN	NA	NA	NA
Sr	1	0	777.98	NA	777.98	777.98
Y	1	0	18.58	NA	18.58	18.58
Zr	1	0	131.53	NA	131.53	131.53
Hf	1	0	3.28	NA	3.28	3.28

Lib

	n	NA	Mean	Std dev	Min	Max
S	1	0	662.4	NA	662.4	662.4
Sc	1	0	36.73	NA	36.73	36.73
V	1	0	137.8	NA	137.78	137.78
Cr	1	0	9.65	NA	9.65	9.65
Co	1	0	28.77	NA	28.77	28.77
Ni	1	0	29.44	NA	29.44	29.44
Cu	1	0	54.8	NA	54.8	54.8
Zn	1	0	120	NA	119.97	119.97
Rb	1	0	0.34	NA	0.34	0.34
Sr	1	0	334.1	NA	334.1	334.1
Y	1	0	60.62	NA	60.62	60.62
Zr	1	0	462.3	NA	462.27	462.27
Hf	1	0	9.05	NA	9.05	9.05

Little Tumi

	n	NA	Mean	Std dev	Min	Max
S	1	0	478.53	NA	478.53	478.53
Sc	1	0	32.85	NA	32.85	32.85
V	1	0	146.22	NA	146.22	146.22
Cr	1	0	9.08	NA	9.08	9.08
Co	1	0	28.26	NA	28.26	28.26
Ni	1	0	32.36	NA	32.36	32.36
Cu	1	0	52.51	NA	52.51	52.51
Zn	1	0	144.51	NA	144.51	144.51
Rb	1	0	77.85	NA	77.85	77.85
Sr	1	0	642.24	NA	642.24	642.24
Y	1	0	59.58	NA	59.58	59.58
Zr	1	0	451.25	NA	451.25	451.25
Hf	1	0	9.66	NA	9.66	9.66

PE

	n	NA	Mean	Std dev	Min	Max
S	2	0	1818	678.48	1338.2	2297.7
Sc	2	0	28.67	2.94	26.59	30.75
V	2	0	229.3	17.66	216.86	241.83
Cr	2	0	32.19	5.77	28.11	36.27
Co	2	0	36.77	0.84	36.18	37.37
Ni	2	0	47.8	7.26	42.67	52.94
Cu	2	0	110.3	16.73	98.45	122.11
Zn	2	0	204.7	72.49	153.41	255.93
Rb	1	1	0.12	NA	0.12	0.12
Sr	2	0	206.5	88.55	143.85	269.08
Y	2	0	58.88	2.9	56.83	60.93
Zr	2	0	293.2	10.63	285.7	300.74
Hf	2	0	8.31	1.28	7.41	9.22

Peggy

	n	NA	Mean	Std dev	Min	Max
S	6	0	87	50	8	147
Sc	6	0	15	5	8	20
V	6	0	117	25	73	144
Cr	6	0	41	48	16	139
Co	6	0	40	9	30	57
Ni	6	0	123	28	89	167
Cu	6	0	235	123	35	381
Zn	6	0	101	10	86	112
Rb	6	0	45	20	24	73
Sr	6	0	847	255	580	1285
Y	6	0	18	2	15	20
Zr	6	0	139	16	119	167
Hf	6	0	5	2	4	8

Sill

	n	NA	Mean	Std dev	Min	Max
S	2	0	139.8	118.55	55.98	223.63
Sc	2	0	34.49	3.316	32.14	36.83
V	2	0	242.4	69.502	193.28	291.57
Cr	2	0	352	330.09	118.55	585.37
Co	2	0	49.23	13.131	39.94	58.51
Ni	2	0	251.9	262.67	66.16	437.63
Cu	2	0	108.3	43.169	77.74	138.79
Zn	2	0	114.2	85.793	53.51	174.84
Rb	2	0	8.235	10.359	0.91	15.56
Sr	2	0	304.4	419.66	7.65	601.14
Y	2	0	33.3	31.219	11.22	55.37
Zr	2	0	164.2	176.54	39.36	289.02
Hf	2	0	2.255	0.078	2.2	2.31

Skelm

	n	NA	Mean	Std dev	Min	Max
S	4	0	173	190	49	456
Sc	4	0	32	6	23	35
V	4	0	250	48	187	291
Cr	4	0	57	86	8	186
Co	4	0	34	6	28	42
Ni	4	0	65	31	43	111
Cu	4	0	103	23	71	122
Zn	4	0	130	36	78	154
Rb	4	0	8	9	0	18
Sr	4	0	494	299	296	939
Y	4	0	40	16	16	52
Zr	4	0	220	67	121	268
Hf	4	0	7	3	4	11

Soll

	n	NA	Mean	Std dev	Min	Max
S	3	0	1153	1503.5	258.65	2888.9
Sc	3	0	27.7	6.839	20.15	33.48
V	3	0	222.8	73.667	138.72	275.84
Cr	3	0	107.2	146.5	22.46	276.35
Co	3	0	46.11	19.624	34.47	68.77
Ni	3	0	382.8	548.21	63.6	1015.8
Cu	3	0	329.1	254.51	81.97	590.4
Zn	3	0	152.7	127.33	77.36	299.69
Rb	2	1	0.46	0.042	0.43	0.49
Sr	3	0	42.2	59.77	4.23	111.1
Y	3	0	25.85	10.275	14	32.33
Zr	3	0	104.7	9.317	93.98	110.64
Hf	2	1	2.5	1.64	1.34	3.66

Speckled

	n	NA	Mean	Std dev	Min	Max
S	5	0	418.85	807.54	7.39	1859.48
Sc	5	0	27.67	6.73	20.43	36.31
V	5	0	185.95	20.64	152.46	207.29
Cr	5	0	2055.49	977.69	546.01	2912.73
Co	5	0	51.76	17.73	36.82	79.86
Ni	5	0	405.33	72.31	316.74	497.45
Cu	5	0	60.35	51.9	18.66	146.85
Zn	5	0	120.69	50.8	89.27	208.69
Rb	4	1	0.4	0.28	0.09	0.76
Sr	5	0	20.19	25.64	3.39	62.44
Y	5	0	8.88	1.9	5.56	10.39
Zr	5	0	40.56	5.83	32.95	48.33
Hf	3	2	1.46	0.83	0.5	1.98

Swannie

	n	NA	Mean	Std dev	Min	Max
S	3	0	738.4	913.3	54.63	1775.6
Sc	3	0	27.37	0.99	26.31	28.27
V	3	0	274.7	22.91	248.23	288.89
Cr	3	0	119	18.02	102.05	137.93
Co	3	0	44.56	17.6	31.37	64.55
Ni	3	0	99.52	52.57	64.57	159.98
Cu	3	0	192.5	133.2	62.33	328.54
Zn	3	0	288.8	144.87	121.59	375.13
Rb	3	0	1.73	1.98	0.52	4.01
Sr	3	0	130.3	196.69	15.79	357.44
Y	3	0	42.3	8.8	32.19	48.19
Zr	3	0	274.8	14.23	259.99	288.38
Hf	3	0	8.9	4.53	3.8	12.45

Twin

	n	NA	Mean	Std dev	Min	Max
S	2	0	92.97	58.97	51.27	134.67
Sc	2	0	31.7	3.17	29.45	33.94
V	2	0	203.19	9.86	196.22	210.16
Cr	2	0	130.85	8	125.2	136.51
Co	2	0	43.85	13.86	34.05	53.65
Ni	2	0	182.24	45.69	149.93	214.55
Cu	2	0	97.35	64.52	51.73	142.97
Zn	2	0	84.39	16.33	72.84	95.93
Rb	2	0	55.84	10.25	48.59	63.09
Sr	2	0	17.39	0.36	17.13	17.64
Y	2	0	11.96	0.93	11.31	12.62
Zr	2	0	72.2	3.44	69.77	74.64
Hf	2	0	2.39	0.28	2.19	2.59

Unknown1

	n	NA	Mean	Std dev	Min	Max
S	1	0	129.1	NA	129.11	129.11
Sc	1	0	34.07	NA	34.07	34.07
V	1	0	263.8	NA	263.83	263.83
Cr	1	0	98.84	NA	98.84	98.84
Co	1	0	38.2	NA	38.2	38.2
Ni	1	0	48.44	NA	48.44	48.44
Cu	1	0	52.31	NA	52.31	52.31
Zn	1	0	180.3	NA	180.25	180.25
Rb	1	0	0.11	NA	0.11	0.11
Sr	1	0	295	NA	295.01	295.01
Y	1	0	47.38	NA	47.38	47.38
Zr	1	0	254.8	NA	254.77	254.77
Hf	1	0	4.56	NA	4.56	4.56

Unknown2

	n	NA	Mean	Std dev	Min	Max
S	1	0	61.34	NA	61.34	61.34
Sc	1	0	34.01	NA	34.01	34.01
V	1	0	319.18	NA	319.18	319.18
Cr	1	0	118.47	NA	118.47	118.47
Co	1	0	41.36	NA	41.36	41.36
Ni	1	0	59.58	NA	59.58	59.58
Cu	1	0	55.33	NA	55.33	55.33
Zn	1	0	146.45	NA	146.45	146.45
Rb	1	0	0.55	NA	0.55	0.55
Sr	1	0	335.1	NA	335.1	335.1
Y	1	0	59.33	NA	59.33	59.33
Zr	1	0	309.81	NA	309.81	309.81
Hf	1	0	5.79	NA	5.79	5.79

Unknown3

	n	NA	Mean	Std dev	Min	Max
S	1	0	121.4	NA	121.38	121.38
Sc	1	0	25.87	NA	25.87	25.87
V	1	0	137	NA	137	137
Cr	1	0	8.45	NA	8.45	8.45
Co	1	0	20.56	NA	20.56	20.56
Ni	1	0	60.3	NA	60.3	60.3
Cu	1	0	248.7	NA	248.66	248.66
Zn	1	0	40.36	NA	40.36	40.36
Rb	1	0	39.77	NA	39.77	39.77
Sr	1	0	278.8	NA	278.75	278.75
Y	1	0	20.45	NA	20.45	20.45
Zr	1	0	136.7	NA	136.72	136.72
Hf	1	0	2.52	NA	2.52	2.52

Unknown4

	n	NA	Mean	Std dev	Min	Max
S	2	0	376.5	141.47	276.47	476.54
Sc	2	0	34.27	1.61	33.13	35.41
V	2	0	296.73	21.31	281.66	311.79
Cr	2	0	18.26	3.13	16.05	20.47
Co	2	0	29.66	0.98	28.97	30.35
Ni	2	0	41.59	3.1	39.4	43.79
Cu	2	0	106.23	52.22	69.31	143.16
Zn	2	0	103.39	27.99	83.6	123.18
Rb	2	0	0.59	0.33	0.36	0.83
Sr	2	0	281.32	34.49	256.94	305.71
Y	2	0	41.6	0.25	41.43	41.78
Zr	2	0	229.91	21.81	214.48	245.33
Hf	2	0	8.59	3.01	6.46	10.71

Unknown6

	n	NA	Mean	Std dev	Min	Max
S	1	0	155.3	NA	155.26	155.26
Sc	1	0	29.6	NA	29.6	29.6
V	1	0	212.4	NA	212.4	212.4
Cr	1	0	609	NA	609.04	609.04
Co	1	0	63.89	NA	63.89	63.89
Ni	1	0	370.4	NA	370.36	370.36
Cu	1	0	33.43	NA	33.43	33.43
Zn	1	0	150.1	NA	150.14	150.14
Rb	1	0	0.61	NA	0.61	0.61
Sr	1	0	2.76	NA	2.76	2.76
Y	1	0	10.68	NA	10.68	10.68
Zr	1	0	51.44	NA	51.44	51.44
Hf	0	1	NaN	NA	NA	NA

Unknown7

	n	NA	Mean	Std dev	Min	Max
S	1	0	247.91	NA	247.91	247.91
Sc	1	0	8.94	NA	8.94	8.94
V	1	0	105.6	NA	105.6	105.6
Cr	1	0	32.5	NA	32.5	32.5
Co	1	0	42.29	NA	42.29	42.29
Ni	1	0	151.34	NA	151.34	151.34
Cu	1	0	310.56	NA	310.56	310.56
Zn	1	0	118.92	NA	118.92	118.92
Rb	1	0	48.02	NA	48.02	48.02
Sr	1	0	457.16	NA	457.16	457.16
Y	1	0	17.97	NA	17.97	17.97
Zr	1	0	154.41	NA	154.41	154.41
Hf	1	0	4.46	NA	4.46	4.46

Unknown8

	n	NA	Mean	Std dev	Min	Max
S	3	0	464	718	33	1293
Sc	3	0	21	4	18	25
V	3	0	170	25	144	193
Cr	3	0	97	110	31	224
Co	3	0	44	14	27	53
Ni	3	0	85	42	57	133
Cu	3	0	135	51	83	184
Zn	3	0	112	59	75	180
Rb	3	0	23	38	1	66
Sr	3	0	338	262	127	631
Y	3	0	19	2	16	21
Zr	3	0	129	17	116	148
Hf	3	0	5	2	4	7

Unknown9

	n	NA	Mean	Std dev	Min	Max
S	3	0	92	36	52	124
Sc	3	0	21	2	19	23
V	3	0	195	13	186	210
Cr	3	0	109	41	62	134
Co	3	0	41	5	35	44
Ni	3	0	92	17	74	108
Cu	3	0	82	14	66	94
Zn	3	0	159	77	72	217
Rb	3	0	45	40	0	77
Sr	3	0	124	112	26	246
Y	3	0	20	4	16	24
Zr	3	0	137	8	130	146
Hf	3	0	4	3	2	7

Ventersdorp lava

	n	NA	Mean	Std dev	Min	Max
S	1	0	15.51	NA	15.51	15.51
Sc	1	0	23.51	NA	23.51	23.51
V	1	0	159.7	NA	159.71	159.71
Cr	1	0	36.16	NA	36.16	36.16
Co	1	0	37	NA	37	37
Ni	1	0	110.4	NA	110.35	110.35
Cu	1	0	40.82	NA	40.82	40.82
Zn	1	0	85.2	NA	85.2	85.2
Rb	1	0	15.05	NA	15.05	15.05
Sr	1	0	778.3	NA	778.25	778.25
Y	1	0	16.81	NA	16.81	16.81
Zr	1	0	115.9	NA	115.91	115.91
Hf	1	0	0.23	NA	0.23	0.23

Rare Earth Elements

Table C – 3. Rare Earth Element Concentrations (ppm).

	La	Ce	Pr	Nd	Sm	Eu	Gd	Tb	Dy	Ho
PEG4	30.43	67.81	8.28	32.82	5.90	1.75	4.82	0.62	3.34	0.58
GEOR1	6.77	14.3	1.80	7.28	1.63	0.65	1.77	0.28	1.83	0.39
GEOR2	6.28	15.69	2.17	9.44	1.87	1.91	1.80	0.27	1.73	0.39
SKE1	24.60	54.28	6.82	28.76	6.60	1.81	7.12	1.12	7.23	1.44
SOL1	10.07	23.85	3.22	14.87	4.03	1.22	4.91	0.79	5.27	1.09
SOL2	6.31	14.60	1.86	7.75	1.78	0.43	2.20	0.33	1.99	0.40
KUD1	20.97	43.34	5.03	19.55	3.95	1.12	3.71	0.53	3.15	0.58
SIL1	2.44	5.17	0.67	3.05	0.94	0.44	1.47	0.26	1.79	0.40
JEA1	26.26	61.68	8.00	35.54	8.43	2.48	9.01	1.41	8.86	1.77
FRI1	28.75	65.63	8.45	37.01	8.70	2.37	9.51	1.49	9.45	1.90
LIB1	44.79	99.28	12.10	50.18	10.79	2.77	11.02	1.67	10.41	2.06
LIT1	47.20	101.70	12.14	50.11	10.58	2.81	10.83	1.64	10.10	1.99
PE1	32.32	75.97	9.67	42.01	9.83	2.70	10.44	1.63	10.38	2.08
LAV1	13.28	29.91	3.75	15.99	3.66	1.03	3.59	0.53	3.23	0.61
AMI1	7.29	17.82	2.37	11.21	3.90	0.85	5.43	0.84	5.36	1.13
BAN7	22.57	52.46	6.96	31.14	7.21	2.38	7.02	1.01	5.90	1.09
TWI1	10.7	25.9	2.60	9.88	1.86	0.40	1.66	0.23	1.35	0.27
TWI2	5.70	15.5	1.48	5.77	1.25	0.32	1.52	0.23	1.46	0.29
BRA2	20.5	47.6	6.43	29.2	6.75	2.50	6.51	0.92	5.35	0.97
CLA5	1.79	5.49	0.56	2.71	0.90	0.18	1.40	0.24	1.71	0.36
UNK1	31.6	69.5	8.76	37.5	8.74	2.33	9.30	1.45	9.26	1.85
UNK2	32.5	76.4	9.78	43.0	10.1	2.60	10.9	1.70	10.8	2.21
UNK3	25.0	51.0	5.89	23.8	5.03	1.42	4.63	0.62	3.33	0.61
UNK4A	23.4	52.6	6.55	27.9	6.45	1.76	6.90	1.10	7.06	1.45
UNK6	0.63	1.63	0.21	1.00	0.40	0.10	0.75	0.14	0.97	0.23
REPL	34.2	72.1	8.42	33.3	5.84	1.64	4.64	0.61	3.28	0.59
KEN8	20.5	47.3	6.31	29.0	6.75	2.65	6.57	0.92	5.30	0.98
SWA2	25.1	60.3	7.94	35.5	8.39	2.29	9.03	1.40	8.91	1.81
120A2	20.4	42.9	4.98	19.8	3.99	1.12	3.73	0.54	3.18	0.61
120B2	21.2	44.4	5.16	20.4	4.08	1.12	3.74	0.54	3.16	0.60

	Er	Tm	Yb	Lu
PEG4	1.57	0.20	1.24	0.17
GEOR1	1.16	0.17	1.14	0.17
GEOR2	1.31	0.20	1.32	0.20
SKE1	4.34	0.61	3.99	0.58
SOL1	3.30	0.46	3.14	0.46
SOL2	1.19	0.17	1.13	0.17
KUD1	1.64	0.22	1.42	0.20
SIL1	1.22	0.19	1.24	0.20
JEA1	5.23	0.73	4.82	0.68
FRI1	5.63	0.77	5.15	0.74
LIB1	6.07	0.84	5.61	0.80
LIT1	5.87	0.81	5.27	0.73
PE1	6.21	0.86	5.65	0.81
LAV1	1.74	0.23	1.46	0.21
AMI1	3.59	0.54	3.93	0.62
BAN7	2.97	0.39	2.49	0.36
TWI1	0.89	0.14	bdl	0.15
TWI2	0.90	0.14	1.00	0.15
BRA2	2.66	0.34	2.19	0.31
CLA5	1.09	0.16	1.20	0.18
UNK1	5.51	0.77	5.12	0.75
UNK2	6.45	0.91	5.89	0.85
UNK3	1.71	0.25	1.64	0.23
UNK4A	4.22	0.60	3.93	0.58
UNK6	0.75	0.12	0.91	0.15
REPL	1.60	0.21	1.31	0.19
KEN8	2.66	0.35	2.18	0.31
SWA2	5.24	0.75	4.78	0.69
120A2	1.67	0.22	1.37	0.19
120B2	1.70	0.24	1.55	0.22

Appendix D: Standards

The following standards were used during the calibration of the XRF spectrometer:

AC-E

ASK1

ASK-2

ASK-3

BE-N

BHVO-1

USGS

BR

DT-N

FK-N

GA

GH

GS-N

GSP-1

JA-1

JA2

JB1

JB1A

JB-3

JG-1

JG-2

JG-3

JP-1

JR-2

MA-N

MICA-FE

MICA-MG

NIM-G

NIM-L

NIM-N

NIM-P

NIM-S

SARM39

SARM46

SARM48

SARM51

SARM9

SY-2 and SY-3

Details concerning all standards may be found in Govindaraju (1994).

The standard used during ICP-MS analysis for REEs was BHVO2.

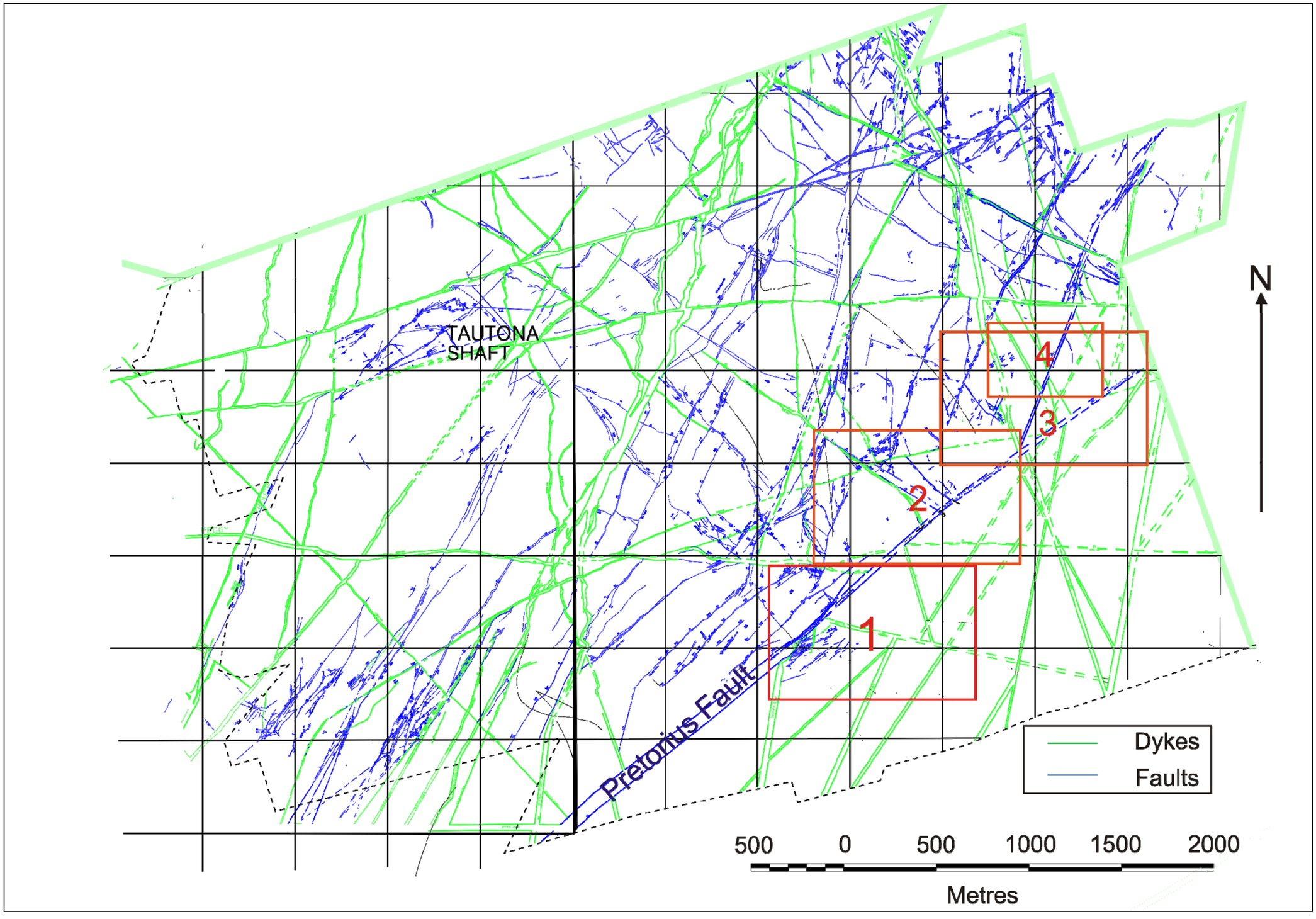

A plan of Tau Tona Mine. Numbered blocks indicate areas sampled.

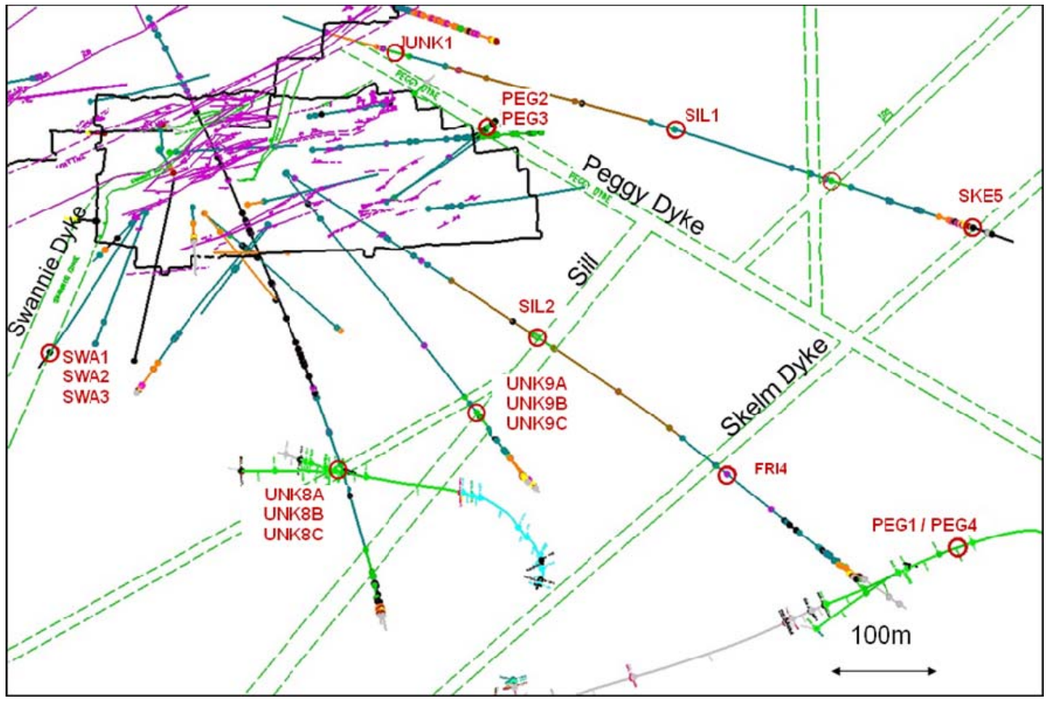

Below 120 Level localities (Block 1). Dykes are green and faults are purple.

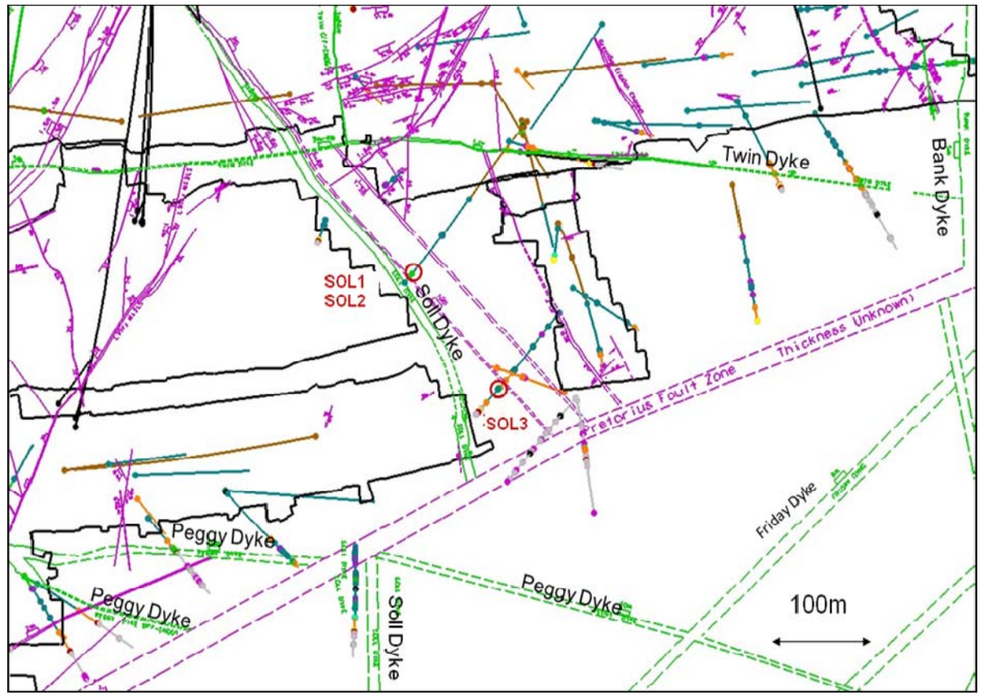

Soll 112 Level localities (Block 2).

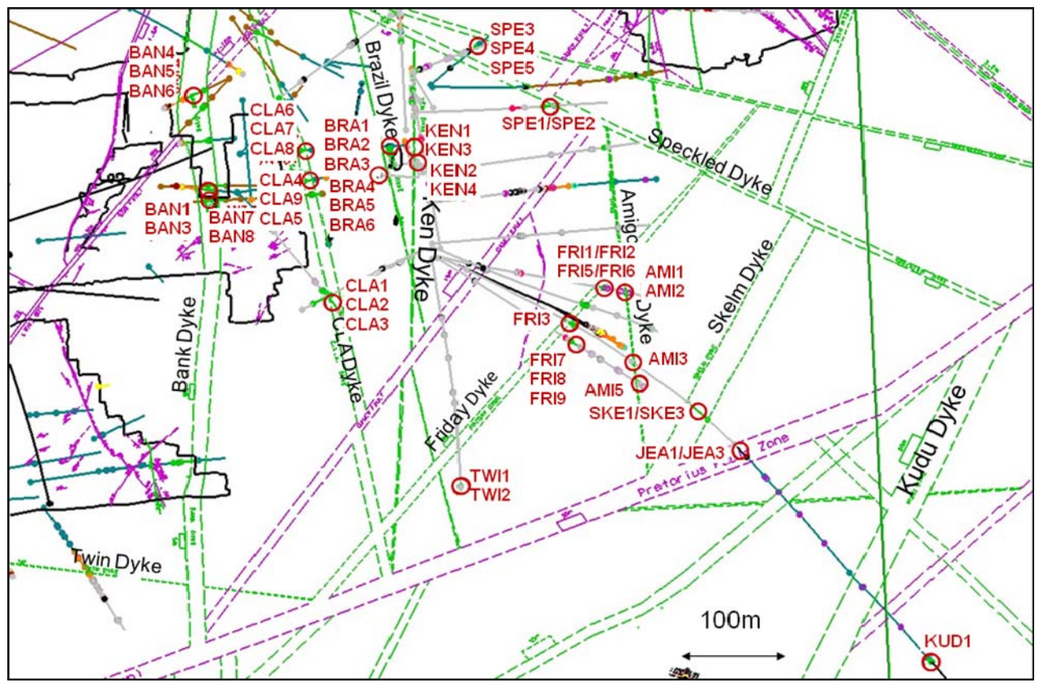

100/104 Level Localities (Block 3).

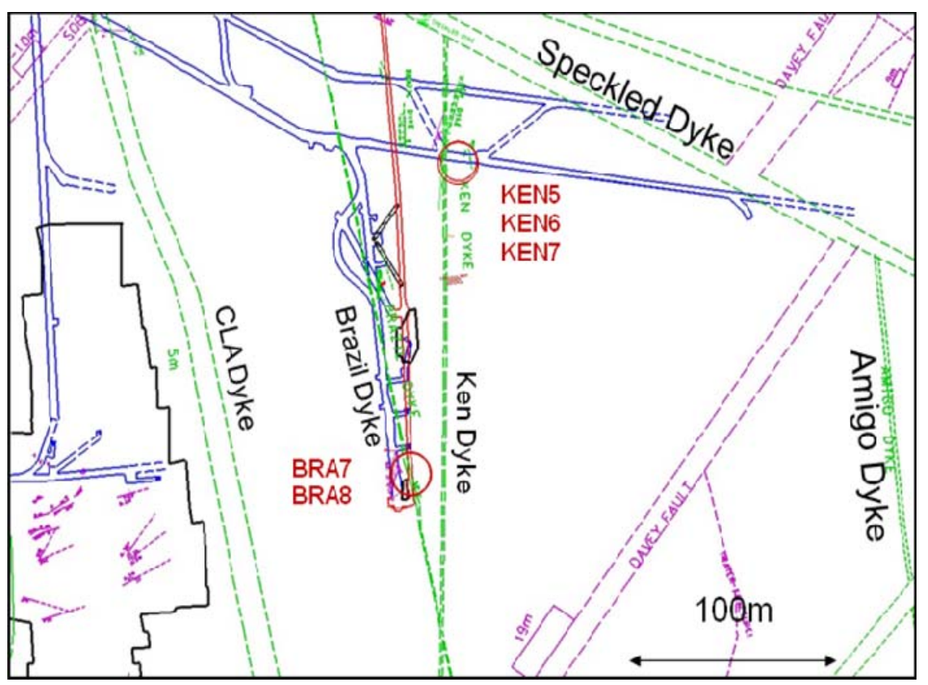

Underground Sampling on 104 level (Block 4).

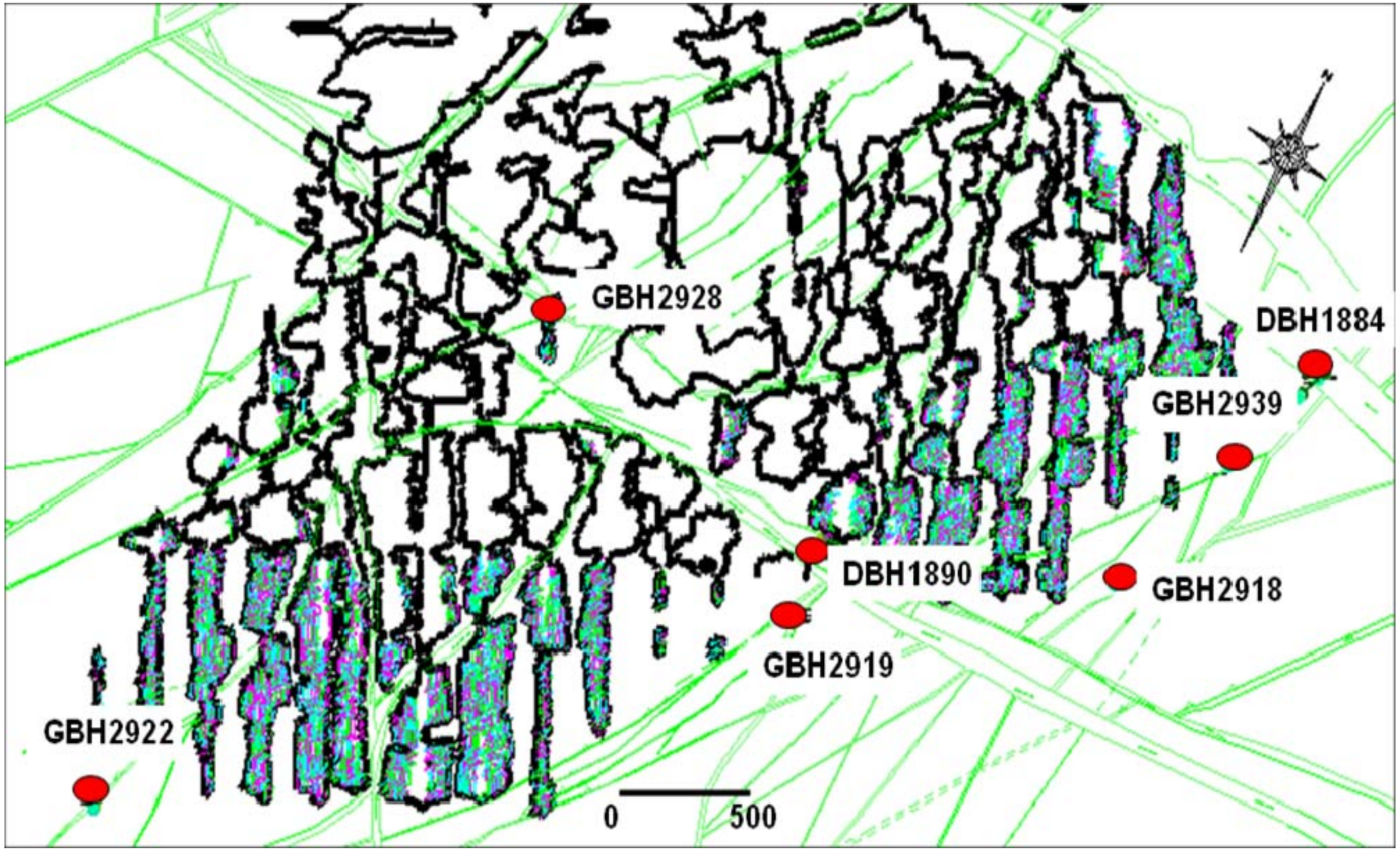

A Plan of Mponeng Mine indicating the localities of the boreholes sampled. The boreholes are represented by red dots and the dykes are (in this figure and henceforth) depicted in green.

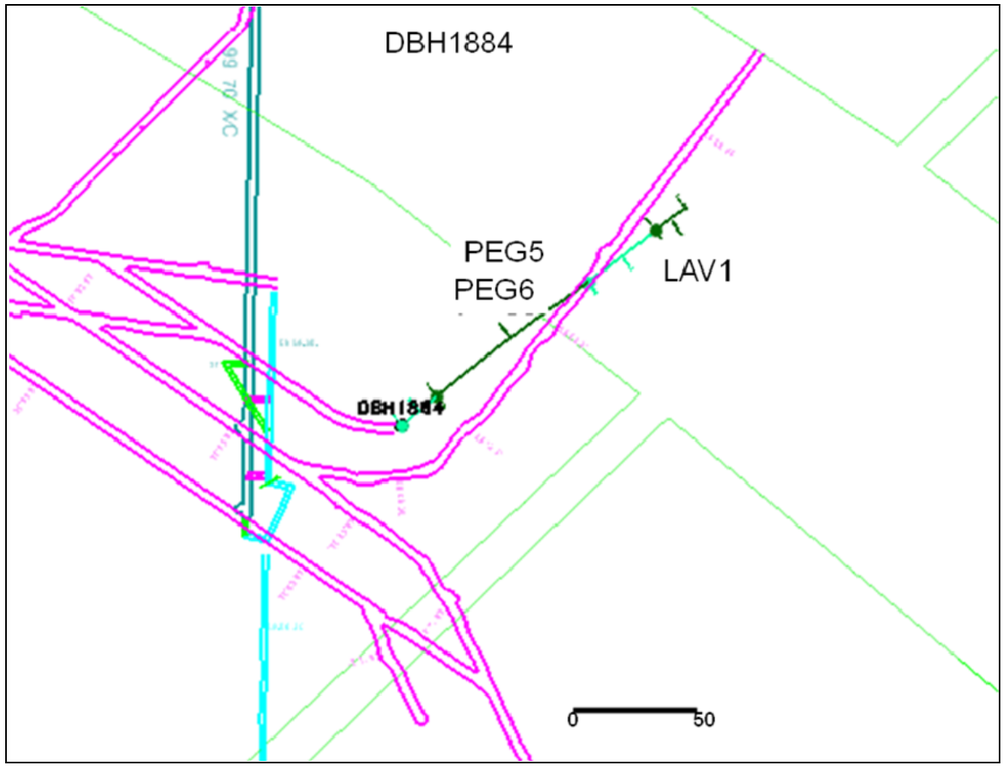

Sample localities from borehole number DBH1884.

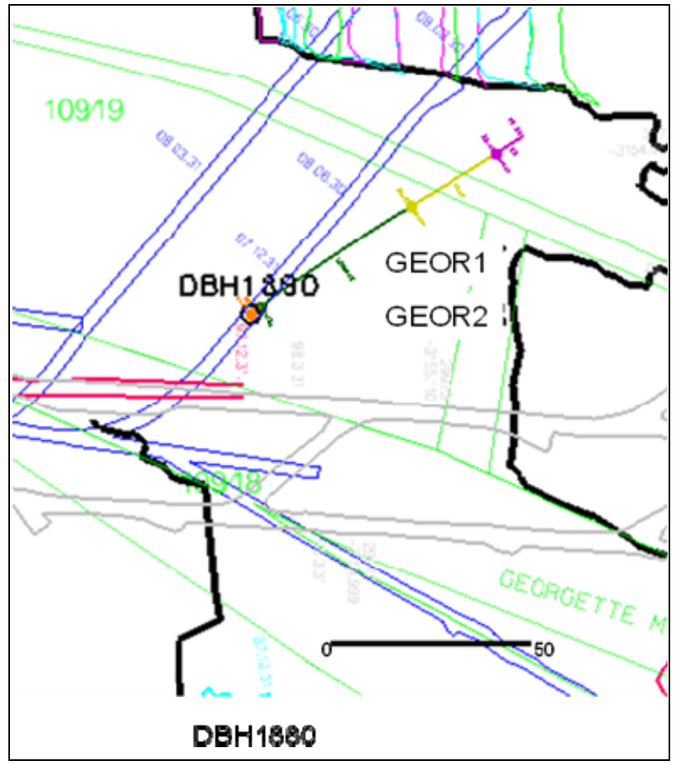

Sample localities from borehole number DBH 1880.

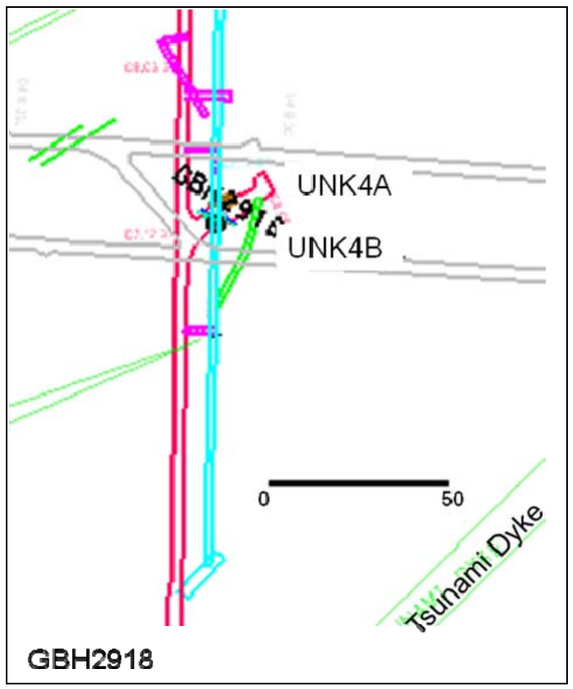

Localities of samples from borehole number GBH 2918.

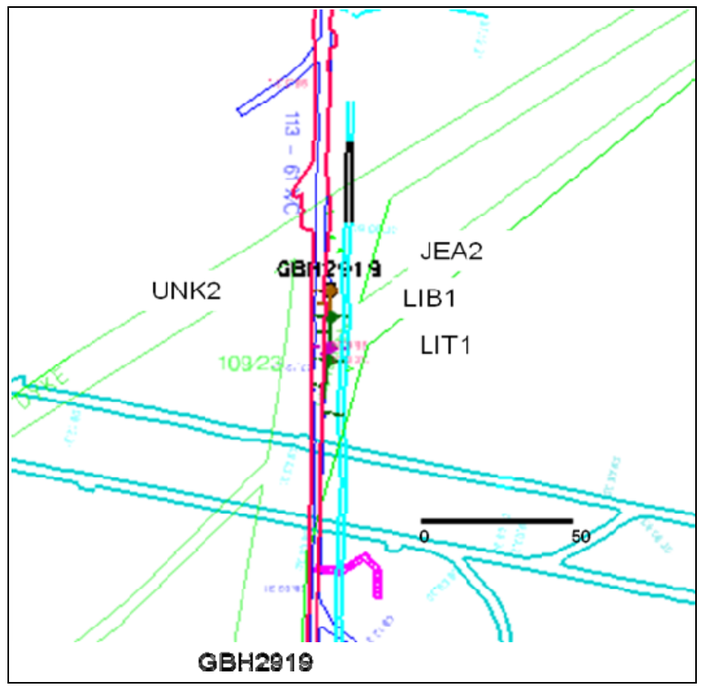

Localities of samples from borehole number GBH 2919

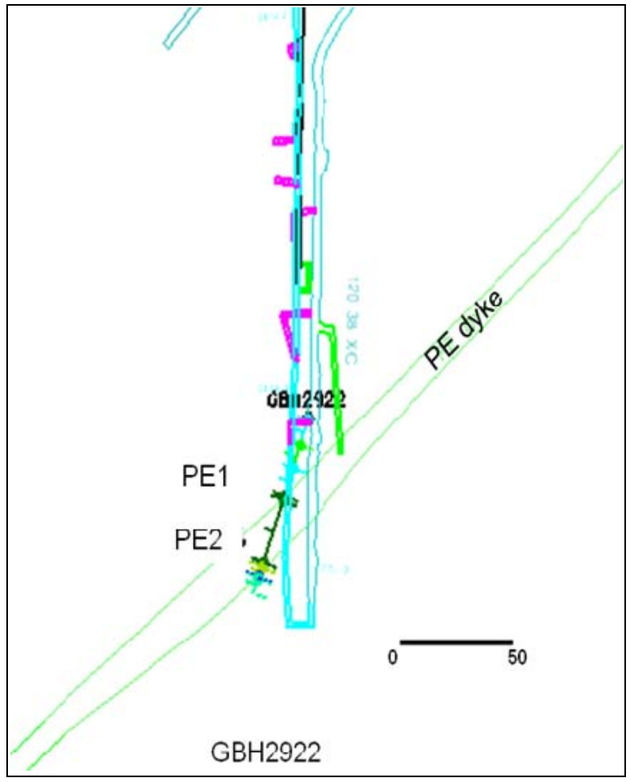

Localities of samples from borehole number GBH 2922.

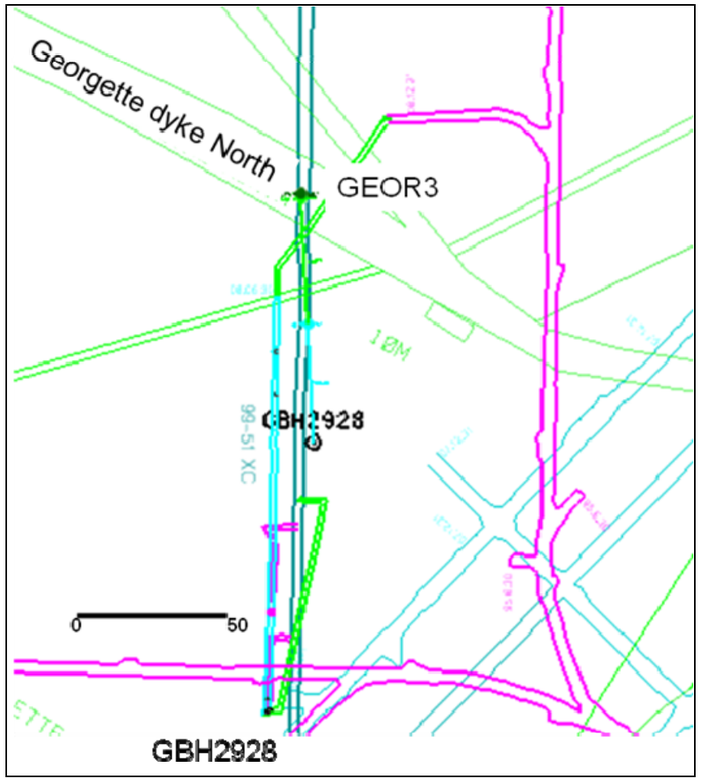

Localities of samples from borehole number GBH 2928.

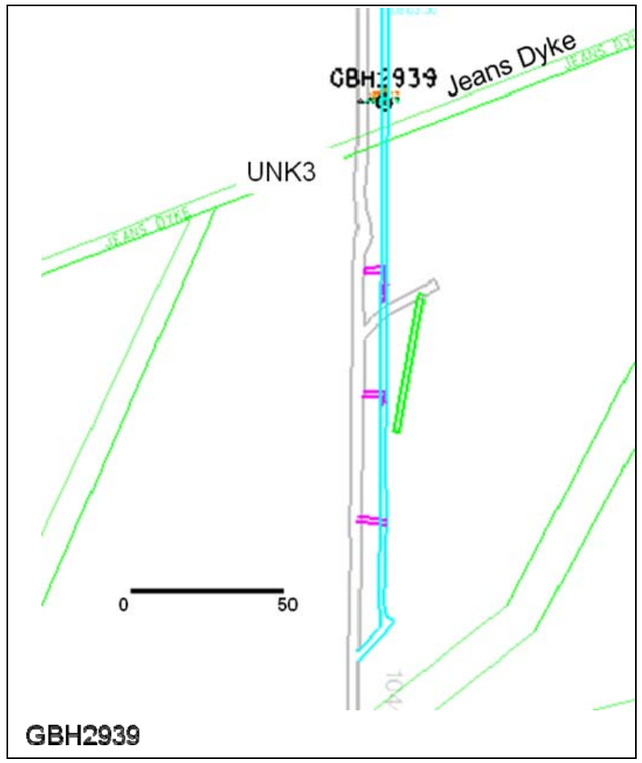

Localities of samples from borehole number GBH 2939.

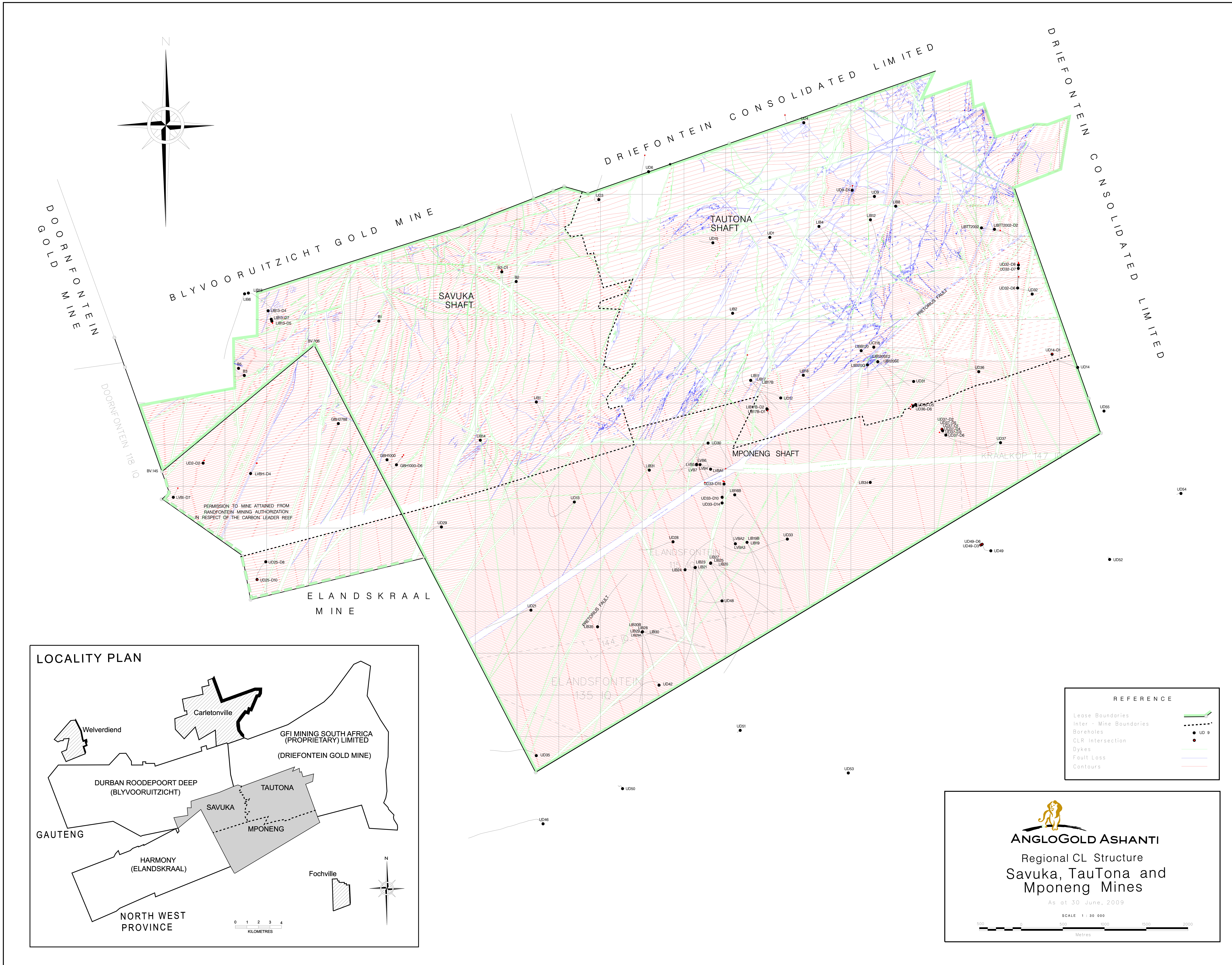

N
DRIEFONTEIN CONSOLIDATED LIMITED
BLYVOORUITZICHT GOLD MINE
DOORNFONTEIN GOLD MINE
DOORNFONTEIN 118 IQ
SAVUKA SHAFT
TAUTONA SHAFT
MPONENG SHAFT
PRETORIUS FAULT
KRAALKOP 147 IQ
ELANDSFONTEIN 115 IQ
ELANDSFONTEIN 135 IQ
ELANDSKRAAL MINE
PERMISSION TO MINE ATTAINED FROM RANDFONTEIN MINING AUTHORIZATION IN RESPECT OF THE CARBON LEADER REEF
LOCALITY PLAN
Welverdiend
Carletonville
GFI MINING SOUTH AFRICA (PROPRIETARY) LIMITED
(DRIEFONTEIN GOLD MINE)
DURBAN ROODEPOORT DEEP (BLYVOORUITZICHT)
TAUTONA
SAVUKA
MPONENG
GAUTENG
HARMONY (ELANDSKRAAL)
Fochville
NORTH WEST PROVINCE
KILOMETRES
REFERENCE
Lease Boundaries
Inter - Mine Boundaries
Boreholes
CLR Intersection
Dykes
Fault Loss
Contours
AngloGold Ashanti
Regional CL Structure
Savuka, TauTona and Mponeng Mines
As at 30 June, 2009
SCALE 1 : 30 000
Metres